European Cooperation in
Science and Technology

ESSEM

Long term changes and climatology of UV radiation over Europe

Edited by Z. Litynska, P. Koepke, H. De Backer, J. Groebner, A. Schmalwieser and L. Vuilleumier

With contributions from N. Chubarova, U. Feister, J. Kaurola, A. Kazantzidis, J. Krzyścin, A. Lindfors, P. N. den Outer, H. Slaper, H. Staiger, J. Verdebout and D. Walker

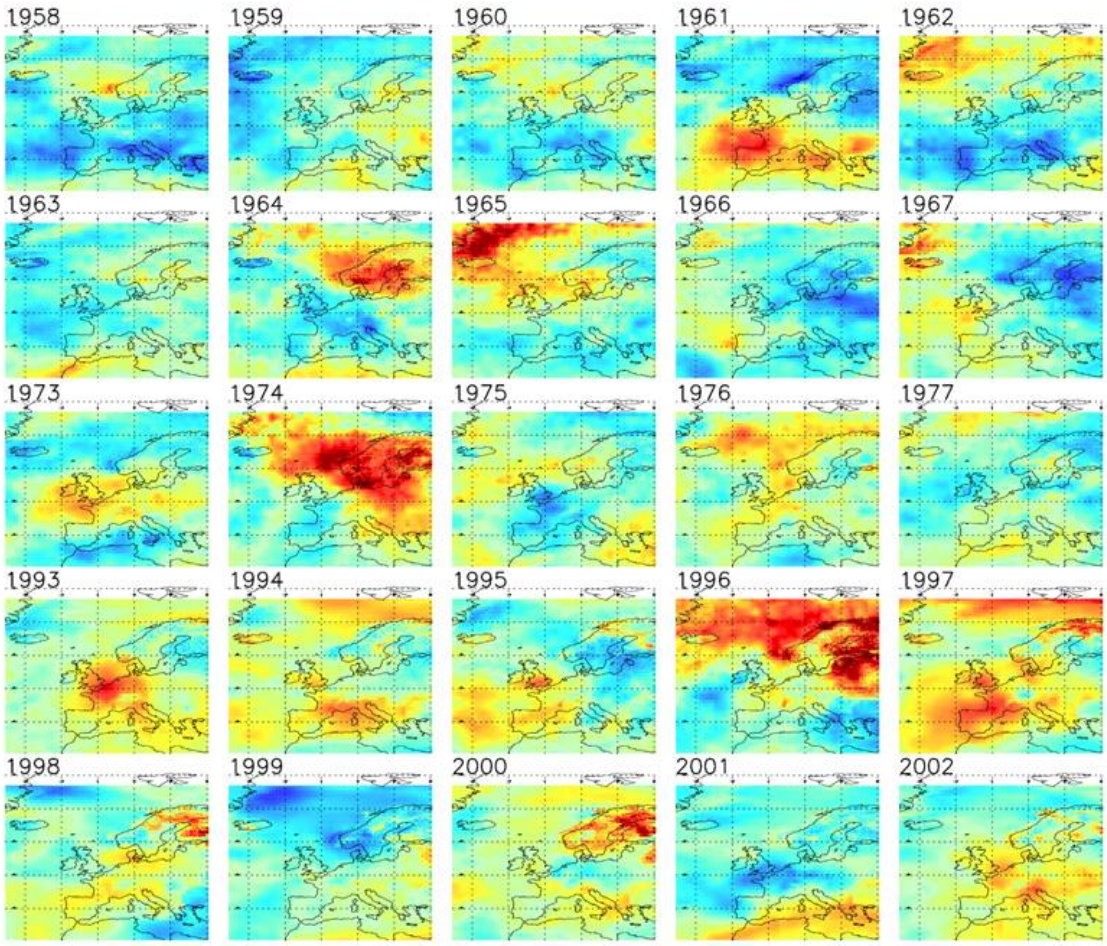

Final scientific report

COST ACTION 726

ESF provides the COST Office through an EC contract

COST is supported by the EU RTD Framework programme

COST – the acronym for European Cooperation in Science and Technology – is the oldest and widest European intergovernmental network for cooperation in research. Established by the Ministerial Conference in November 1971, COST is presently used by the scientific communities of 35 European countries to cooperate in common research projects supported by national funds.

The funds provided by COST – less than 1% of the total value of the projects – support the COST cooperation networks (COST Actions) through which, with EUR 30 million per year, more than 30 000 European scientists are involved in research having a total value which exceeds EUR 2 billion per year. This is the financial worth of the European added value which COST achieves.

A “bottom up approach” (the initiative of launching a COST Action comes from the European scientists themselves), “à la carte participation” (only countries interested in the Action participate), “equality of access” (participation is open also to the scientific communities of countries not belonging to the European Union) and “flexible structure” (easy implementation and light management of the research initiatives) are the main characteristics of COST.

As precursor of advanced multidisciplinary research COST has a very important role for the realization of the European Research Area (ERA) anticipating and complementing the activities of the Framework Programmes, constituting a “bridge” towards the scientific communities of emerging countries, increasing the mobility of researchers across Europe and fostering the establishment of “Networks of Excellence” in many key scientific domains such as: Biomedicine and Molecular Biosciences; Food and Agriculture; Forests, their Products and Services; Materials, Physical and Nanosciences; Chemistry and Molecular Sciences and Technologies; Earth System Science and Environmental Management; Information and Communication Technologies; Transport and Urban Development; Individuals, Societies, Cultures and Health. It covers basic and more applied research and also addresses issues of pre-normative nature or of societal importance.
Web: http://www.cost.esf.org

TABLE OF CONTENTS

LIST OF FIGURES

LIST OF TABLES

1 INTRODUCTION

Peter Koepke [a], Zenobia Litynska [b]
a) Meteorological Institute, L.-M.-University Munich, b) Institute of Meteorology and Water Management, Poland

Solar UV radiation plays an essential role in many biological and chemical processes, including sunburn, skin cancer and effects on the human immune system. UV radiation may be very harmful if its exposure exceeds certain limits. Since Europeans live under very different meteorological conditions and many UV-effects have a long incubation time, it is of interest to know the changes of UV radiation in space and time for Europe. Moreover, the changes of the solar UV irradiance during the last 50 years are of interest with respect to the well known evolution of the ozone layer and the general variation of climate.

Thus the COST action 726 "Long term changes and climatology of UV radiation over Europe" has been established, with the main objective to advance the understanding of UV radiation distribution under various meteorological conditions in order to determine a UV radiation climatology and assess UV changes over Europe.

This report starts with the methods which have been used for UV reconstruction (see chapter 2), i.e. model calculations using values of the atmospheric and surface constituents as input parameters that are influencing UV radiation. The question, how to get values for the input parameters, which are needed for 5 decades in the past and for the wide area of Europe, is discussed in chapter 3. Chapter 4 presents information on UV measurements, which are necessary to evaluate the quality of the modelling. The quality of the results and their uncertainty due to the uncertain or not available input parameters is presented in chapter 5. Here also results are shown which represent UV radiation modelled with other data sets. The results, the UV radiation in the past, for nearly a half century back, are the content of chapter 6. They are shown as time series for individual stations (6.1) and as maps for whole Europe (6.2), for an area between 30.5° north to 80.5° north and 25.5° west to 35.5° east, with a spatial resolution of 0.05° × 0.05°. The temporal changes of the UV irradiance in Europe are discussed in section 6.3.

As usual, the presented data for UV radiation are based on erythemal spectral weighting, i.e. they are valid for UV radiation that is responsible for sun burn and dominantly for skin cancer. With respect to temporal resolution, the data have been modelled as daily doses, which is a compromise between the temporal resolution of the available input data and that which is needed to investigate UV-processes on humans. Results with such high temporal resolution, however, may be uncertain due to the uncertainty of the atmospheric data like cloudiness (see sections 5.2 and 5.3). Thus the results are shown as monthly mean values of the daily doses. For a number of stations the results are compared with measured data, to get an idea of the quality of the results (see section 6.1) and to show the evolution with higher temporal resolution. Since UV radiation has many other biological effects besides sunburn, UV radiation is presented in section 6.4 for other biological processes besides erythemal weighting.

For distributing the huge amount of information developed by the COST action 726, an electronic atlas including all the erythemal data is available in addition to this report. Data are provided together with a computer program which enables extracting data for a certain location over a certain period. Appendix E describes how to use this program.

The results of COST action 726 give detailed information on the temporal changes of UV in Europe in nearly half a century, mainly due to changes of ozone and clouds. They give the possibility to see different behaviour in different areas and in different years. Thus, the results are a fundamental basis for further research on UV effects.

The report has been written by leader authors, but it is a result of the collective efforts of the members of the four Working Groups, coming from 22 EC COST countries and one non-COST country, and of the Management Committee. For details and further information on the action see www.cost726.org. This publication is supported by COST.

2 UV RECONSTRUCTION

Peter Koepke [a]
a) Meteorological Institute, L.-M.-University Munich.

UV radiation in the past, and at places without measurements, can only be obtained by modelling, using as input data the correct values of the parameters which affect the solar UV radiation at the surface. Consequently, a first objective of the COST action was to record the available numerical models and algorithms (Koepke et al., 2006). The needed astronomical parameters, solar elevation and solar-earth-distance, are known from geographical coordinates, date and time and thus easily available. However, detailed analysis is needed to get proper values for the atmospheric and surface parameters. This is especially valid for times four or five decades ago, when fewer parameters have been measured and stored than nowadays.

The chapter UV reconstruction starts with the basic methods of modelling, discusses the technique of biological weighting and additionally presents the methods to get UV maps.

2.1 UV MODELLING

Peter Koepke [a]
a) Meteorological Institute, L.-M.-University Munich.

Natural UV irradiance at the surface is the result of scattering and absorption of the extraterrestrial solar irradiance on its way through the atmosphere. The illuminating irradiance of the Sun at the top of the atmosphere has to take into account the earth-sun-distance, which varies through the year by about ±3 %. The use of the actual solar zenith angle (SZA) is necessary to model the processes correctly, since the SZA influences the path length of the photons through the atmosphere. The radiative effect of the different atmospheric components, like ozone, air molecules, aerosol particles or clouds, individually depends on their amount, properties and height distribution. Both, scattering and absorption must be taken into account, as well as their interaction and multiple scattering.

This results in the radiative transfer equation (RTE), which has to be solved by numerical methods because it can not be solved analytically. Different models have been developed for this purpose (Koepke et al., 1998; DeBacker et al., 2001). State of the art are one dimensional spectral multiple scattering models, which calculate the radiation field for a given atmospheric column with a processing time of a few seconds or less on current computers. They divide the atmosphere in thin layers with given mixtures of the components, i.e. with fixed scattering and absorption properties, and change these properties only vertically (one dimension). The mathematical procedures to solve the equation of radiation transfer are different, but the mathematical quality of the models is so that resulting uncertainties are negligible.

Modelling for a specific place and date is simple if the input data are available. However, to get the huge amount of data for the maps, it is not possible to model each point individually. Here the results are derived by interpolation and using look up tables (see section 2.3).

Significant uncertainties may result from the uncertainty of the values of the atmospheric components and the reflection properties of the surface. Actual values of these components often are not available or of low quality. Thus assumptions have to be made or proxy data must be used. This is especially the case for the UV climatology, which is presented here. To get the basis for modelling the UV climatology, atmospheric and surface data are needed for whole Europe with high spatial resolution and back in the past for about 50 years. Thus a big part of the activity of the COST action was to get information on the relevant input parameters, which is described in chapter 3.

Modelling of UV radiation has to be made spectrally. This is necessary, because solar irradiance is highly variable with wavelength due to the Fraunhofer lines and also the scattering and absorption properties of the atmospheric components vary spectrally. Spectral modelling of UV radiation is no problem. However, for the effects of natural solar UV radiation, of course the integral over the wavelengths has to be considered.

2.2 METHODS FOR SPECTRAL WEIGHTING

Peter Koepke [a]

a) Meteorological Institute, L.-M.-University Munich.

The solar UV radiation at the surface has spectral values that vary in their intensity between 280 and 400 nm in a range of more than one million. This holds for fixed atmospheric conditions, due to the spectral variable emission of the Sun and, more essential, the highly wavelength dependent processes in the atmosphere. The resulting spectral distribution, which changes with solar zenith angle and atmospheric conditions, is the result of the spectral modelling. However, solar UV radiation is emitted simultaneously at all wavelengths, and consequently for all applications spectral integrated values are needed. On the other hand, the biological effects of UV radiation themselves are strongly wavelength dependent, which can be taken into account by a spectral action spectrum $s_{biol}(\lambda)$. The reasons are the photons energy, which depends on wavelength, and, more essential, the specific spectral dependent absorption properties of biological molecules, which are variable for different biological UV effects. Thus, the really effective radiation for a specific process E_{proc} is given by a spectrally integrated value, where the illuminating spectral radiation $E(\lambda)$ is weighted by $s_{biol}(\lambda)$.

$$E_{biol} = \int E(\lambda) \cdot s_{biol}(\lambda) \cdot d\lambda \qquad (2.2.1)$$

The range of variable biological weighting functions is wide. Essential biological UV effects and the resulting UV irradiances are discussed in section 6.4.

Typical for all weighting functions is their low spectral resolution, which is a consequence of the limited possibilities to correlate biological effects with radiation from specific wavelengths. The illuminating UV irradiance E(λ), however, must be modelled with high spectral resolution, as mentioned above. Since the spectral properties of the atmospheric components are stable, which means that for fixed atmospheric conditions modelling at a few wavelengths is sufficient to get information for the effects at the wavelengths in between. Thus it is possible to get the complete spectrum, as necessary for biological weighting, by modelling the multiple scattering processes in the atmosphere for only 7 wavelengths. These results are spectrally interpolated and combined with the illuminating extraterrestrial solar irradiance with high spectral resolution. If the resulting spectral UV irradiances are weighted by a biological process and integrated over the wavelength, the differences against results using high resolution spectral multiple scattering are in the order of a few percent and can be neglected in comparison to the uncertainty that is resulting from the uncertainty of the used values for the atmospheric parameters.

To allow potential users to get UV irradiances for different biological weighting functions, data for the 7 wavelengths are made available on the COST web-page (www.cost726.org) together with cloud modification factors, aerosols and total ozone column.

Nevertheless, for the main body of this report, i.e. the data on erythemally weighted UV irradiances, the method with high spectral resolution and look up tables has been used.

2.3 METHODS FOR PRODUCING UV MAPS

Jean Verdebout [a]

a) European Commission Directorate General Joint Research Centre.

The daily dose maps are obtained by direct radiative transfer calculation, using the input data described in chapter 3. To produce the full map data set, about 450 billions down-welling surface irradiance calculations are needed. Running the radiative transfer code this number of times would lead to an impracticable processing time. Instead, the surface irradiance is obtained by interpolation in a Look Up Table (LUT) containing the value of the surface irradiance for combinations of the variable input parameters values.

The LUT was build using UVspec from the LibRadtran package (version 1.01) (Mayer and Kylling, 2005) (http://www.libradtran.org/doku.php). The LUT entries are: solar zenith angle, total column ozone, aerosol optical thickness at 308 nm, surface UV albedo and altitude. The choice of the input influencing

resulting LUT. For each set of input parameters, the LUT contains the erythemal dose rate (downwelling irradiance weighted by the CIE87 action spectrum (CIE, 1987)) and the downwelling irradiance at 7 discrete wavelengths (295, 300, 305, 310, 315, 330 and 360 nm) convoluted with a 5 nm FHWM triangular slit function. The values at the 7 discrete wavelengths allow computing the dose rate corresponding to a wide variety of action spectra. This required a relatively dense set of values for the total column ozone and the solar zenith angle, the two factors that most influence the spectrum. Following a series of tests, the chosen values for the LUT entries are as follow:

- Solar zenith angle: 26 values linearly scaled between 1 and 85°;
- Total column ozone: 33 values logarithmically scaled between 100 and 600 DU;
- Aerosol optical thickness at 308 nm: 8 values linearly scaled between 0 and 1.4;
- Surface albedo: 5 values linearly scaled between 0 and 1;
- Altitude: 6 values linearly scaled between 0 and 4 km.

The spectrum reconstruction tests performed with results obtained with this LUT show that the error is usually below 1 %, reaching ~3 % in the extreme cases. The tests were performed on instantaneous irradiance, daily doses and geographical averages of daily doses.

The other input parameters of UVspec (fixed) were chosen as follow:

- US standard atmospheric profiles;
- Aerosols: Angstrom coefficient = 1, single scattering albedo = 0.94, asymmetry factor = 0.75, "tropospheric aerosols – spring/summer conditions" below 2 km, background stratospheric aerosols;
- Solar extraterrestrial spectrum: Atlas plus MODTRAN at 0.5 nm resolution;
- Radiative transfer solver: disort2;
- All other UVspec parameters were left to their default values.

The maps are generated over an area extending from 25.5° W to 35.5° E and from 30.5 to 80.5° N, with a spatial resolution of 0.05° × 0.05° ("output pixel"). This spatial resolution allows to better include the effects of altitude, which would be excessively smoothed at the 1° resolution of the ERA-40 and ozone data. A single map is therefore 1 220 pixels W-E by 1 000 pixels S-N ("the output grid"). A preliminary step is to obtain the input parameters values on this grid. The solar zenith angle can easily be computed for each time and output pixel. The altitude is obtained from the GTOPO30 digital elevation model of USGS (http://edc.usgs.gov/products/elevation/gtopo30/gtopo30.html); the value attributed to each output pixel is the average altitude (GTOPO30 spatial resolution is 30'' of degree). The AOT data described in section 3.2 (at 1° spatial resolution) is corrected for altitude at the output grid resolution. The surface albedo on the output grid is generated as described in section 3.3. The total ozone data (see section 3.1) is bi-linearly interpolated on the output grid.

All produced maps contain daily doses. For each output pixel and each day, 48 times in the day are considered, separated by 30 minutes and including the local solar noon. The corresponding solar zenith angles are computed. Are considered "valid" the times for which the solar zenith angle is less than 85°. For each valid time, the dose rates are obtained by successive interpolation of the LUT respectively on total column ozone, solar zenith angle, aerosol optical thickness, altitude and surface albedo. The daily doses are obtained by temporal integration of the dose rates at the valid times, including a contribution from the angles larger than 85°, obtained by extrapolation of the dose rate / time curves. The cloudless daily doses are then corrected for the Earth-Sun distance (varying during the year). Finally, the UV–CMF (Cloud Modification Factor) is applied on all 8 doses (erythemal and the 7 wavelengths). The UV–CMF data come at the 1° spatial resolution and is applied "by blocks", i.e. the cloudless dose rates in each 20 × 20 block of output pixels are multiplied by the corresponding UV–CMF.

The produced data set consists of 8 daily dose maps (1 erythemal + at 7 wavelengths) for each day from January 1st 1958 to August 31st 2002 (16,314 days).

When kept as an array of floating point numbers in binary format, a map is a 4 880 kB file. The full data set consists of 130 512 maps for a total of 635 898 560 kB (~640 GB).

3 DATA

Hugo De Backer [a]
a) Royal Meteorological Institute of Belgium.

For the reconstruction of the past UV fields the input parameters mentioned in section 2.1 are required. The reconstruction can be done in different ways. Either it is done on station basis or on fixed grid.

The first option has the advantage of using directly the best available data but is only possible for stations with long records of the required variables. Stations with a full set of observations are very sparse, especially if you go back in time.

For the second option it is necessary to create gridded fields for each of the input parameters. By the process of spatial interpolation, the information on the day-to-day variation might be lost but the advantage is that it gives spatially resolved information.

Each of the input parameters is obtained by different observing systems. Also both the spatial and temporal variability is very different. For example the spatial scales for total ozone and aerosol are very different. Some variables, like albedo, require special attention in certain regions. Particular attention is devoted to the treatment of clouds, as they have a strong modulating effect on the UV radiation. As there are no long time series of cloud observations in the UV, this information is derived from a combination of modelled and observed global irradiation.

The next sections give a brief description of the preparation of the different input parameters used for the UV reconstruction.

3.1 OZONE

Janusz Krzyścin [a]
a) Polish Academy of Sciences, Institute of Geophysics.

Stratospheric ozone plays a key role in the physics and chemistry of the atmosphere being particularly important for the Earth radiation budget. An inverse relation with the solar UV-B radiation reaching the ground surface triggered many studies of the ozone and surface UV variability and stimulated establishing the ozone and UV global observing network. The total ozone data over Europe are available for only few ground-based stations in the pre-satellite era disallowing examination of the spatial trend variability over the whole continent. A need of having gridded ozone data for a trend analysis and input to radiative transfer models stimulated a reconstruction of the daily ozone values since January 1, 1950.

A statistical model has been proposed within the framework of the COST 726 action to reproduce past total ozone variations over Europe to be used for surface UV simulations (Krzyścin, 2008). The assimilated database of total column ozone measurements (1979–2004) from satellites covering the whole globe, known as NIWA total ozone database (named after affiliation of leading author Greg Bodeker – **N**ational **I**nstitute of **W**ater and **A**tmosphere Research, Lauder, New Zealand) is used as input to the regression model. The NIWA data were homogenized by a comparison with the ground-based Dobson spectrophotometer stations (Bodeker et al., 2005). The data from the following satellite sources contributed to NIWA: Version 8 Nimbus 7 and Earth Probe TOMS; GOME version 3.1; KNMI TOGOMI; Version 8 SBUV from NIMBUS 7, NOAA9, NOAA 11, and NOAA 16 satellite. The database was widely used in various studies of global ozone behaviour (Bodeker et al., 2001 and 2005; Fioletov et al., 2002; WMO, 2007).

The COST 726 ozone reconstruction model consists of two-step regression. The first step is a regression of the monthly means of NIWA total ozone on various explanatory variables including indices of teleconnection patterns and drivers of the global atmospheric system (QBO, ENSO, NAO, solar-cycle, effective equivalent stratospheric chlorine, vertical component of Eliasen Palm flux in the stratosphere averaged over NH mid-latitudes) and monthly means of meteorological variables (temperature and

vorticity). The drivers of the monthly total ozone are taken mostly from real measurements. The vorticity and temperature are taken from the NCEP/NCAR Reanalysis-1 database. The meteorological variables are based on global circulation model (GCM) simulations controlled by the radiosonde results, before satellite era, and the satellite results afterwards. Next is a regression of the daily departures of NIWA total ozone from the total ozone monthly means. The explanatory variables in the second regression are deviations of daily values of meteorological variables from their monthly means. Finally, the modelled daily total ozone is obtained as a sum of terms being multiplication of regression constants and pertaining explanatory variables that were selected as important regressors. The model is run independently for each grid point and 4 seasons; winter (December- February), spring (March-May), summer (June-August), and autumn (September-November). For each season the most effective set of the explanatory variables is selected using the multivariate adaptive regression splines (MARS) technique (Friedman, 1991). The ozone values are reconstructed backward to the beginning of 1950s using the regression constants, derived as a result of the model training on the NIWA data set. Following a decision by the COST 726 community only the most certain data were used. Thus, the reconstructed total ozone data are used for periods before 1979 and after the original NIWA data should be taken into account.

The COST 726 ozone database consists of daily total values since January 1, 1950 for a rectangle covering 25° W to 35° E and 31° N to 80° N (see Fig. 3.1.1 for the area) . The grid resolution is 1° × 1°. The database is available at http://private.igf.edu.pl/~jkrzys with the data reading software and files describing the data format and performance of the model.

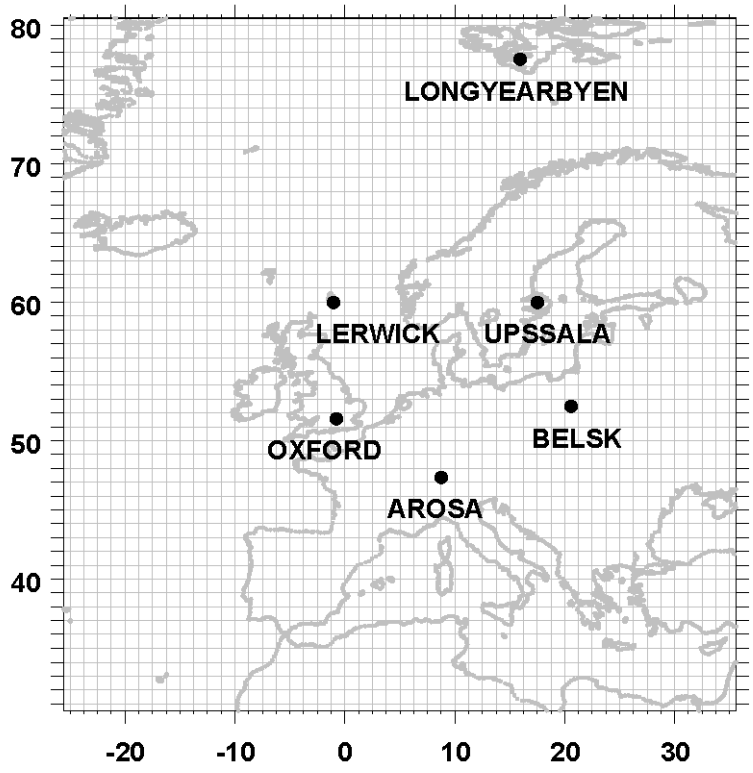

Fig. 3.1.1: The area with reconstructed COST 726 daily total ozone values for the period 1950–2004 and ground-based stations used for the validation of the model.

The quality of the COST 726 ozone database is assured by a comparison of the reconstructed total ozone with the ground-based data from several Dobson stations already in operation in the early 1950s and 1960s (see Fig. 3.1.1 for the names and location of such stations). We have two periods for the comparison: 1979-2004 (model training period) and 1950-1978 (model validation period). Figure 3.1.2 shows examples for the model/measurement comparison in the training period for two stations: Arosa

(Switzerland, one of the best station in the world with long-tradition of the ozone measurements since 1928) and Longyearbyen (Svalbard, Norway, specific weather conditions with numerous cloudy days and high noon solar zenith making weak intensity of UV signal that is used in the Dobson ozone retrieval). It is seen that the modelled total ozone values match almost perfectly the observed ones. Thus, it supports both the COST ozone model and NIWA data.

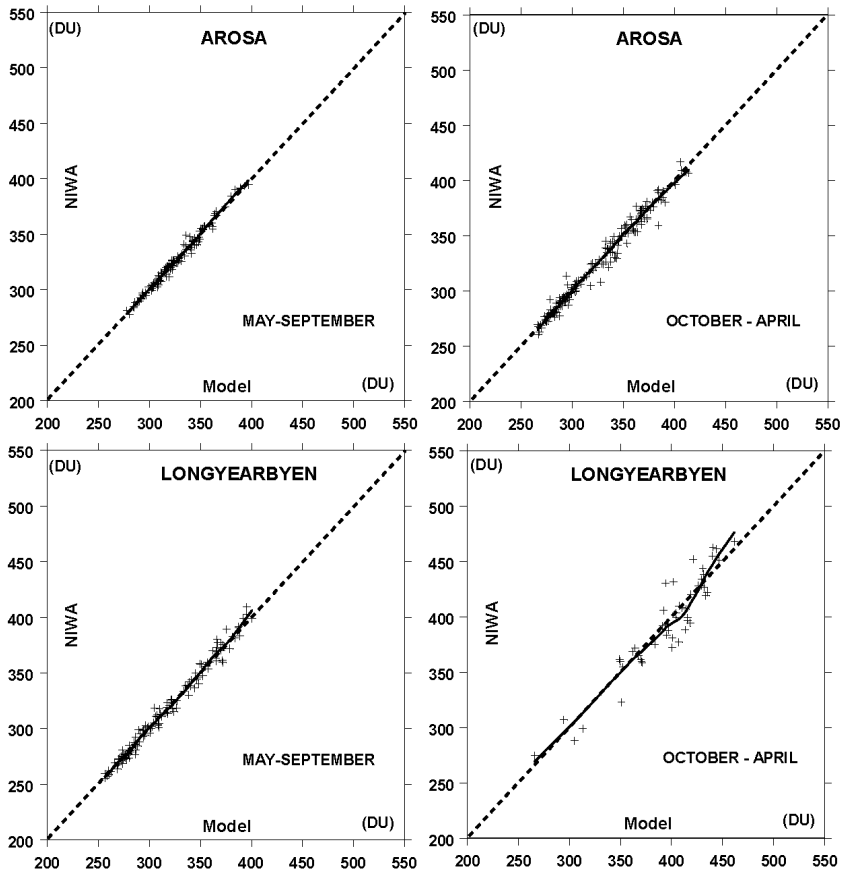

Fig. 3.1.2: NIWA monthly total ozone versus pertaining COST 726 model data for Arosa and Longyearbyean in the cold and warm sub-periods of the year. The solid curve represents a smoothed pattern from the locally weighted regression.

Figure 3.1.3 illustrates the model performance in pre-satellite era for all considered ground-based stations. The model explains 70–80 % variance of the ozone data collected before the satellite era. Bias and the long-term drift between the reconstructed and measured Dobson ozone are within a range of ±2 % (Krzyścin, 2008). It is worth mentioning that the proxies used in parameterization of the ozone dynamically driven variations in the pre-satellite era are derived from GCM model results that were normalized by the radio sounding results. Thus, the proxies have lower quality than those derived in the satellite era, especially in the early 1950s. The model/observation scatter seen in figure 3.1.3 is larger than that shown in figure 3.1.2 but still there is a correspondence between the measured and model data. It should be stressed here that the basic assumption of our model is that the relationship between total ozone and its proxies found in the satellite era can be extended back in time. It is also supported by the comparison of the reconstructed total ozone with the ground-based data for the Dobson stations operational in 1950s.

There are two databases possible for extraction of the early total ozone values over Europe: ERA-40 (since 1958) and COST 726 (since 1950). Both databases provide much better simulations of total ozone values than those taken from a simple persistent model assuming that the daily ozone in each year follows

the long-term daily mean (1979-2004) obtained using the NIWA database. The COST 726 ozone database yields smaller biases and slightly higher standard deviations when compared with the ground-based data than the same comparison with the outcome of ERA-40 model. There are basic differences between the databases; the COST 726 ozone database is derived from a statistical regression model and starts earlier but ERA-40 uses GCM simulations. The performance of these models is almost similar in the satellite era (since 1979) because the models are fed by much more reliable input than for the previous period. Recently, Krzyścin and Borkowski (2008) have examined the changes in the European total ozone since 1950 using the COST 726 ozone database.

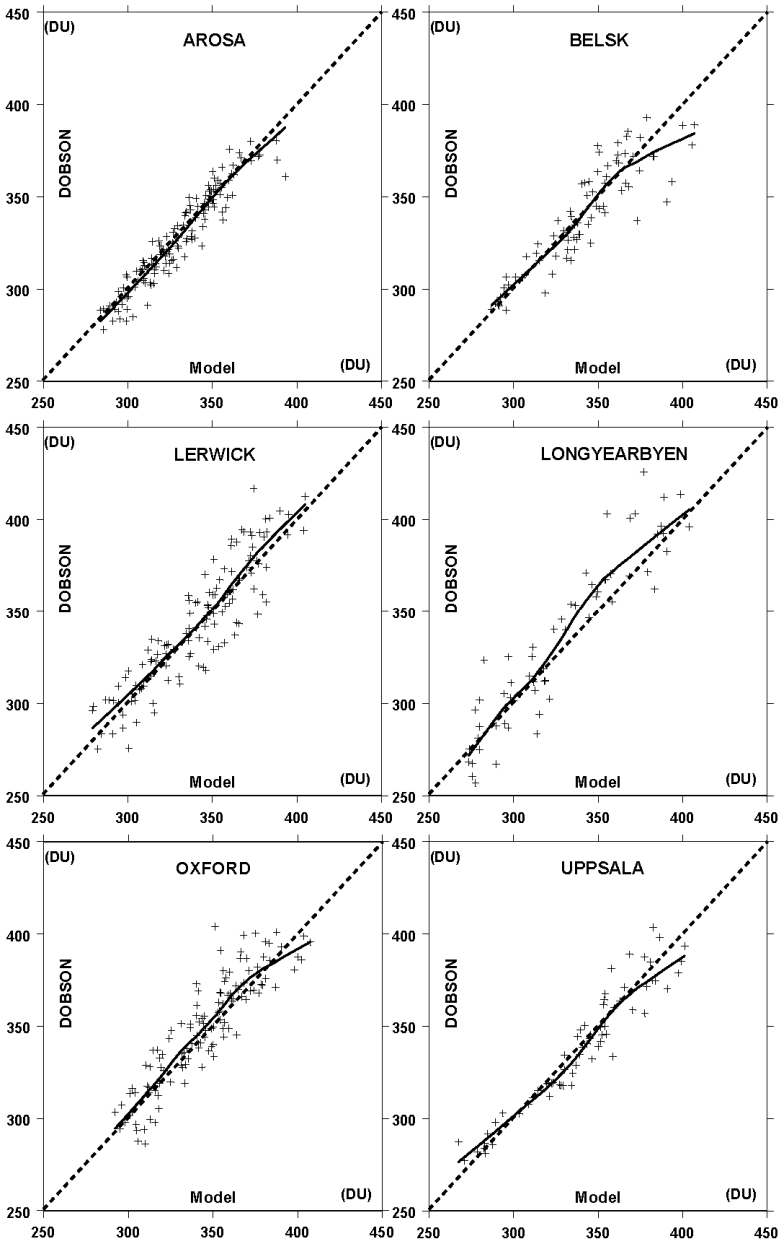

Fig. 3.1.3: Total ozone monthly means from ground-based observations in the warm sub-periods of the year versus the COST 726 model data in pre-satellite era (before 1979) for stations shown in figure 3.1.1. The solid curve represents a smoothed pattern from the locally weighted regression.

Figure 3.1.4 shows the relative daily differences between the COST model and measured total ozone at Arosa for the whole period 1950-2004. As we can see the extreme differences are ~ ±20 % that induces

at least ~20 % overestimation or underestimation of UV erythemaly weighted radiation reaching the ground-level under clear sky conditions. It is worth mentioning the long-term pattern of relative differences (see red curves) exhibit only slight and almost trendless oscillations in the cold and warm sub-periods of the year. Thus, the COST 726 ozone database is proper for an examination of averaged total ozone data rather than for analyses of extreme ozone cases. It is prepared to serve as input to UV reconstruction models. All statistics concerning UV radiation should be built by averaging daily UV data. Monthly mean UV doses seem to be unreliable if inferred from the monthly mean ozone and monthly mean cloudiness. Various comparisons with the ground-based and satellite data lead to conclusion that the COST 726 ozone database over Europe will provide valuable input values for the surface UV reconstructions there.

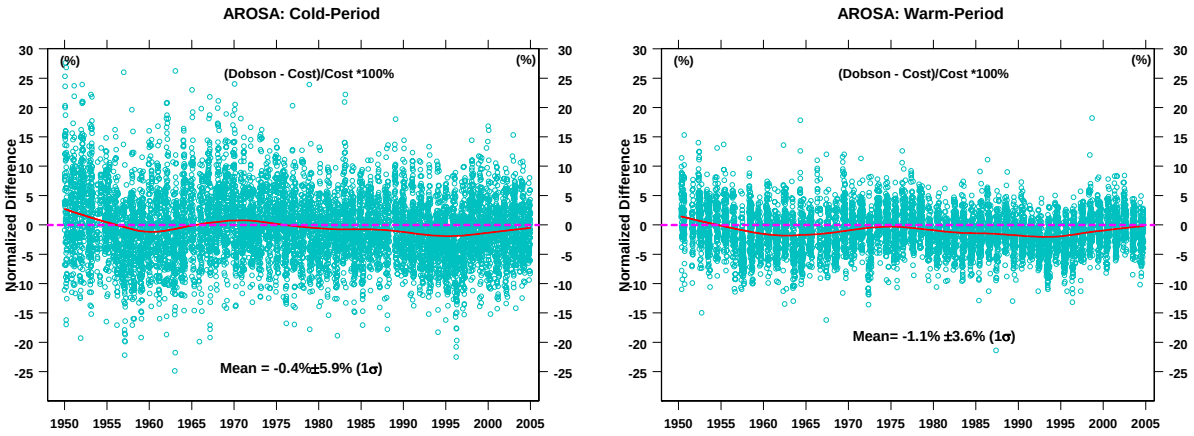

Fig. 3.1.4: Relative differences (ground-based minus COST 726) of the daily total ozone in the warm and cold periods (1950–2004) for Arosa.

3.2 AEROSOL

Natalia Chubarova [a]

a) Moscow State University, Meteorological Observatory.

Atmospheric aerosols are one of the important factors influencing solar UV irradiance. Therefore, it is necessary to have reliable spatial and temporal distribution of aerosol parameters to get proper UV estimates. For estimating the aerosol impact on UV irradiance it is necessary to know several key aerosol characteristics: the aerosol optical thickness (τ_λ), the single scattering albedo (ω_λ), the asymmetry factor (g_λ), and the Angstrom parameter (α). The development of an aerosol climatology requires long-term observations and good spatial resolution of these aerosol parameters. The approach used in this study is based on the application of the data from satellite measurements of τ_λ at 550 nm from Moderate Resolution Imaging Spectrometer (MODIS) (collection 5) combined with the aerosol products from ground-based aerosol AERONET/PHOTONS over Europe within the area of 31° – 80° N, 25° W – 35° E.

The lack of information does not allow us to account for interannual variations in aerosol optical thickness, while there is some evidence of an aerosol optical thickness negative trend at several European sites during the last decades (Ruckstuhl et al., 2008). The effects of volcanic eruption on aerosol content were also not considered due to the absence of reliable data on spatial and temporal distribution of volcanic stratospheric aerosol over Europe. However, these factors should play minor role relative to the typical aerosol optical thickness distribution.

The monthly mean MODIS τ_{550} have been taken from http://disc.sci.gsfc.nasa.gov/giovanni/ for the 2000-2008 period with 1° spatial resolution. The measurements from both TERRA and AQUA satellite platforms were used to increase the statistics and to account for possible aerosol changes during daytime.

The latest collection 5 has a good quality of data over both land and ocean, except bright surfaces (snow and desert) (Remer et al., 2008). The latter constraint does not allow us to have τ_{550} values during cold period over vast European territory with snow cover, and requires the application of additional assumptions.

In addition, the data from the ground-based AERONET/PHOTONS network (Holben et al., 1998) have been used for 1994–2006 period over the European territory, where its spatial coverage is quite satisfactory (http://aeronet.gsfc.nasa.gov/). Accurate multi-channel measurements by auto-tracking CIMEL sun/sky photometers from the UV to the near-infrared spectral region provide the data for the evaluation of the Angstrom parameter α as well as for the direct validation of the final aerosol product in the UV spectral region. In addition, the AERONET inversion algorithm provides the retrievals of the single scattering albedo and the asymmetry factor (Dubovik and King, 2000). The uncertainty of τ_λ estimates is about ±0.01 in the visible and infra-red spectral range and about ±0.02 in the UV spectral range. The quality assured measurements at level 2 (version 2) were used. Figure 3.2.1 presents the spatial distribution of the CIMEL sun/sky photometers, which provided the data for the analysis. To exclude systematic changes of aerosol parameters with surface elevation, only the data from the sites located lower than 1000 m were utilized. However, the altitude dependence of aerosol optical thickness has been applied for generating the high resolution UV maps. This dependence has been obtained on the basis of data from high altitude AERONET sites in Europe. The following correction to the aerosol optical thickness is recommended at altitudes above 1 km:

$$\tau_c = \tau \, H^{-1.65} \tag{3.2.1}$$

where H is the altitude in km.

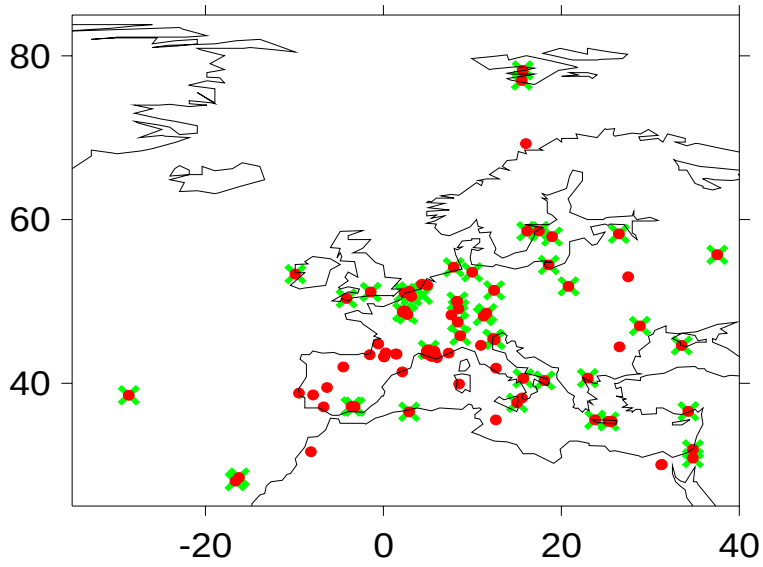

Fig. 3.2.1: Distribution of CIMEL sun/sky photometers in Europe and nearby areas. The sites, where the instrument has UV channels (340 and 380 nm), are marked with green crosses.

Although the quality of MODIS data is considered as satisfactory, several additional tests have been performed. The results show that average difference between satellite τ_{550} retrievals and ground-based data is close to zero varying within ±0.02 from month to month. However, the difference is not large and is much less than τ_{550} seasonal changes for all European regions. To get τ_λ estimates in the UV spectral range two approaches were used: by accounting for spectrally-dependent Angstrom parameter, which can be observed in some conditions (Eck et al., 1999), and with the application of a constant α value retrieved from 440–870 nm spectral range. The comparisons between the τ_{340} estimated from MODIS data using both methods and direct ground τ_{340} CIMEL measurements have revealed the same character of the difference, though with higher deviation (±0.05). The difference between the two methods is small and lies within 0.01–0.03 that is close to the uncertainty of τ_{340} estimates. At the same time, due to the much

smaller number of CIMEL instruments with UV channels (see Fig. 3.2.1) the advantages of accounting for spectral Angstrom curvature have been outweighed by the much lower statistics and, hence, larger uncertainty in the resulting Angstrom parameter spatial distribution. Finally, we have chosen the application of the constant $\alpha_{440-870}$ values. The additional analysis has revealed the presence of unrealistically high τ_{550} values (up to ~0.7–0.8) observed over some regions in the northern Arctic regions, probably, due to the existence of small spots of snow or ice within the pixel. Note, that according to the measurements at AERONET/PHOTONS sites located at high latitudes (>58° N), the average τ_{550} values are about 0.1 with the maximum monthly mean value, which does not exceed 0.2. This threshold (τ_{550}=0.2) has been chosen as an additional filter, and has been applied to the MODIS data over the northern regions (>60° N) to remove unrealistically high τ_{550}. In order to fill the gaps in aerosol loading over the bright surfaces the average monthly mean τ_λ values from the sites at LAT>58° N have been applied for snow conditions, while for desert areas the data were taken from the closest African or Arabian AERONET sites. As a result, the τ_{550} climatology over Europe has been obtained, which is used as a base for developing the UV aerosol climatology. Spatial distributions of Angstrom parameter $\alpha_{440-870}$ have been estimated using geostatistical ordinary Kriging method with a linear type of variogram model. Using these distributions the final UV aerosol (τ_{308}) climatology has been generated (Fig. 3.2.2). It is analyzed together with the spatial distribution of the precipitation and wind fields at 925 hPa (Fig. 3.2.3) from IRI/LDEO Climate Data Library (http://iridl.ldeo.columbia.edu/res) based on NOAA NCEP CPC CAMS_OPI climatology (Janoviak and Xie, 1999, Kalnay et al., 1996).

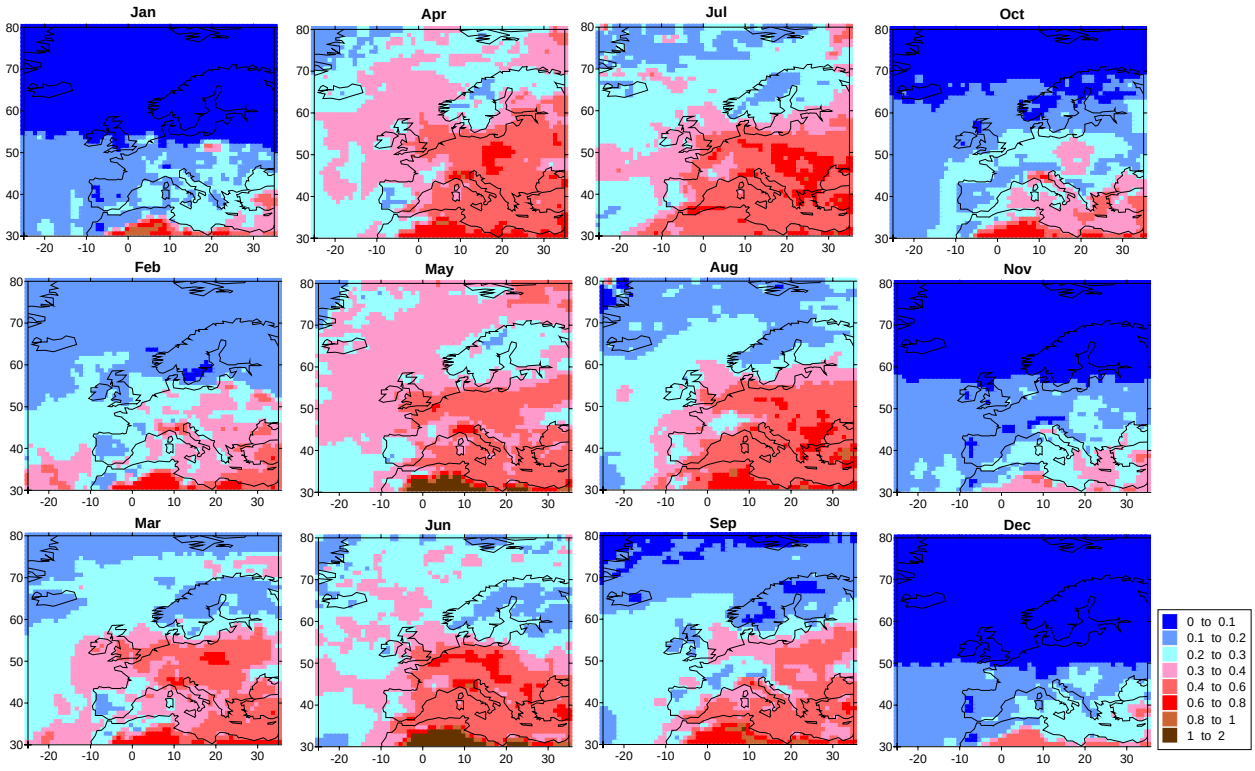

Fig. 3.2.2: Spatial distribution of τ_{308} according to MODIS/AERONET datasets.

The changes in aerosol optical thickness have a tendency to increase towards south-east, inward the continent, though with different gradients over the year. One should note the very pronounced seasonal τ_λ changes, which are sometimes higher than their difference in space. The τ_{308} values vary from ~0.05 over northern and north-western areas during cold period to $\tau_{308} \sim 0.9$ over several south, south-eastern regions. The Angstrom parameter also grows towards south-east and has noticeable seasonal changes.

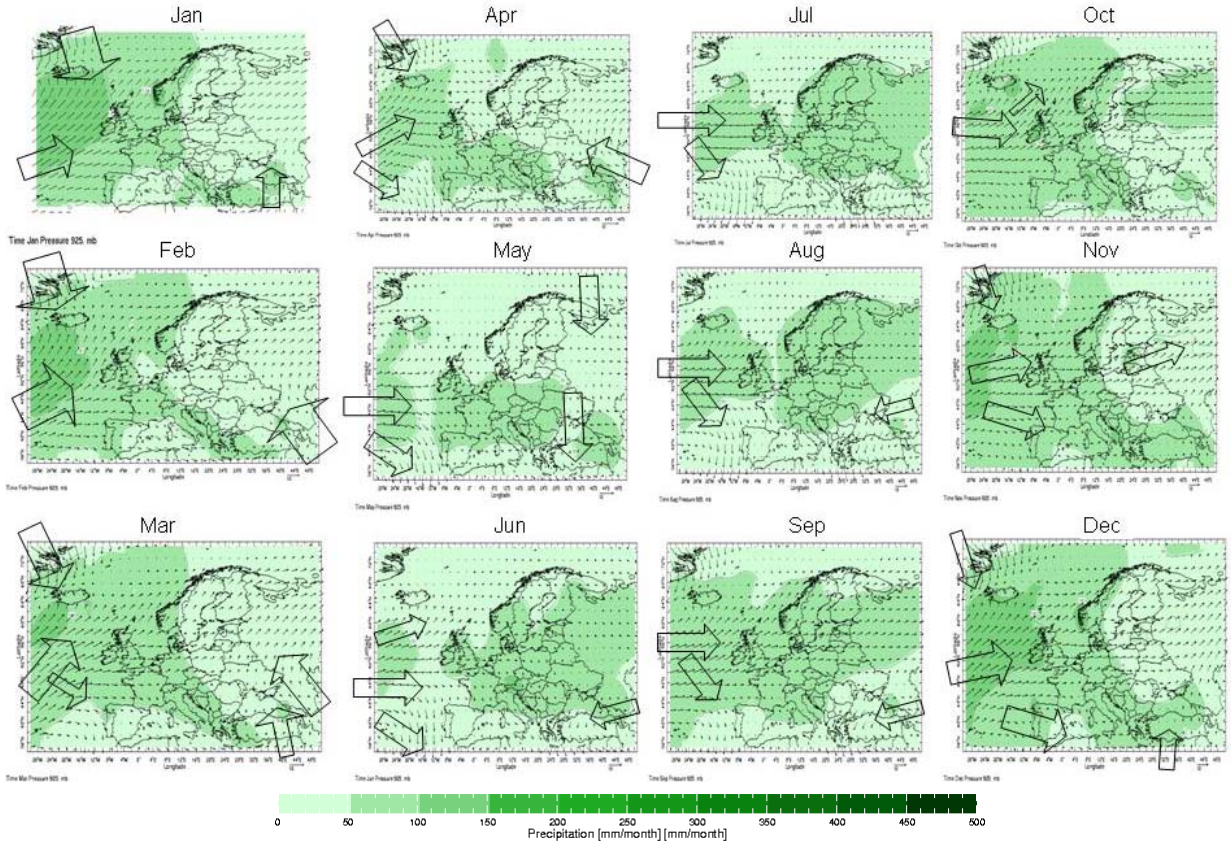

Fig. 3.2.3: Month-to-month spatial distribution of climate meteorological parameters (wind characteristics and precipitation) according to NCEP CPC CAMS_OPI data from the IRI/LDEO Climate Data Library. 1961-1990.

Figure 3.2.4 presents the examples of different seasonal τ_{340} distributions from both direct AERONET/PHOTONS measurements and the developed MODIS/AERONET climatology over the existing AERONET sites in the arctic (1), temperate (2), and subtropical (3) zones and several of their subtypes. The lowest τ_λ are observed in the Arctic zone where a maximum occurs in spring. Within a temperate zone two subtypes can be found: the area with uniform humidification with one summer τ_λ maximum (Oostende site) and the area transitional to continental type approximately eastward of ~15° E

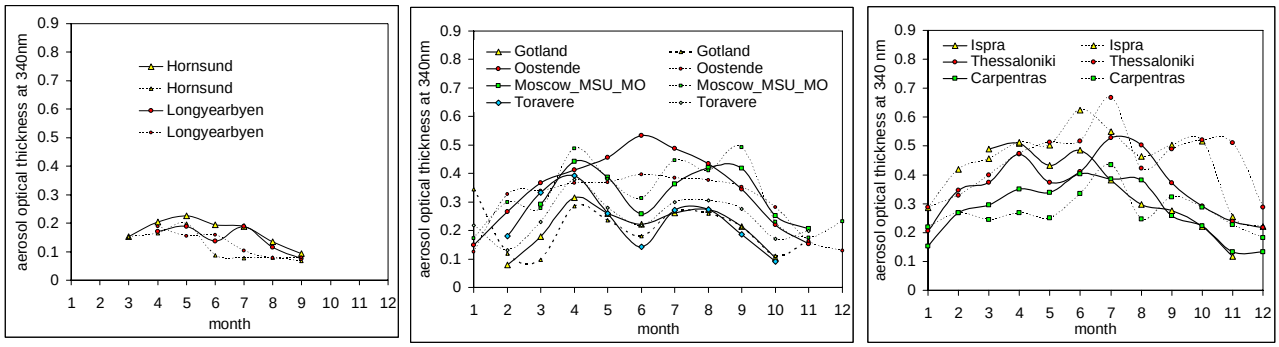

Fig. 3.2.4: Seasonal variations in τ_{340} in Arctic (1), temperate (2) and subtropical (3) climate zones. The MODIS τ_{340} retrievals are shown in solid and AERONET data by dotted lines. The coordinates of the sites: Hornsund (15.55°E, 77°N), Longyearbyen (15.649°E, 78.2°N), Gotland (19.0°E, 57.9°N), Moscow_MSU_MO (37.5°E, 55.7°N), Oostende (2.9°E, 51.2°N), Toravere (26.5°E, 58.3°N), Ispra (8.6°E, 45.8°N), Carpentras (5.1°E, 44.1°N), Thessaloniki (23.0°N, 40.6°E).

and northward of ~45° N, where the two τ_λ maxima in spring and in summer are observed, like at Gotland, Toravere and Moscow sites. In the subtropical zone there is a distinct τ_λ increase towards inner continental areas with maxima observed during warm period. At the same time the characteristics of the changes in τ_λ are much more irregular over subtropics, which can be attributed to the effects of the mineral dust aerosol advection to different Mediterranean regions from the surrounding deserts. It is necessary to note, that at some sites (for example, in Thessaloniki) the long-term τ_λ dataset obtained from Brewer measurements provides much better agreement with MODIS data than that obtained between MODIS and AERONET dataset, possibly, due to larger statistics and the application of additional clear-sky filter (Kazadzis, 2007, Koukouli et al., 2007).

Figure 3.2.2 demonstrates a permanent elevated aerosol loading due to pollution effects over several local areas: Northern Italy, the coast of Netherlands, the southern regions of Poland, and, especially in summer, over mid and low Danube lowlands. The qualitative analysis of distribution of fine mode particles PM2.5 obtained from the chemical transport model LOTOS-EUROS (Schaap et al., 2007) for 2000 (see http://home.planet.nl/~scha1378/tno/promote/) has also confirmed the existence of local maxima approximately over the same regions. The maximum monthly mean value can reach $\tau_{308} \sim 0.9$ over Northern Italy during spring- summer months, while τ_{308} is about 0.5 over nearby unpolluted area. In other polluted regions the differences are not so large and are about $\Delta\tau_{308} \sim 0.05–0.2$ with the nearby areas.

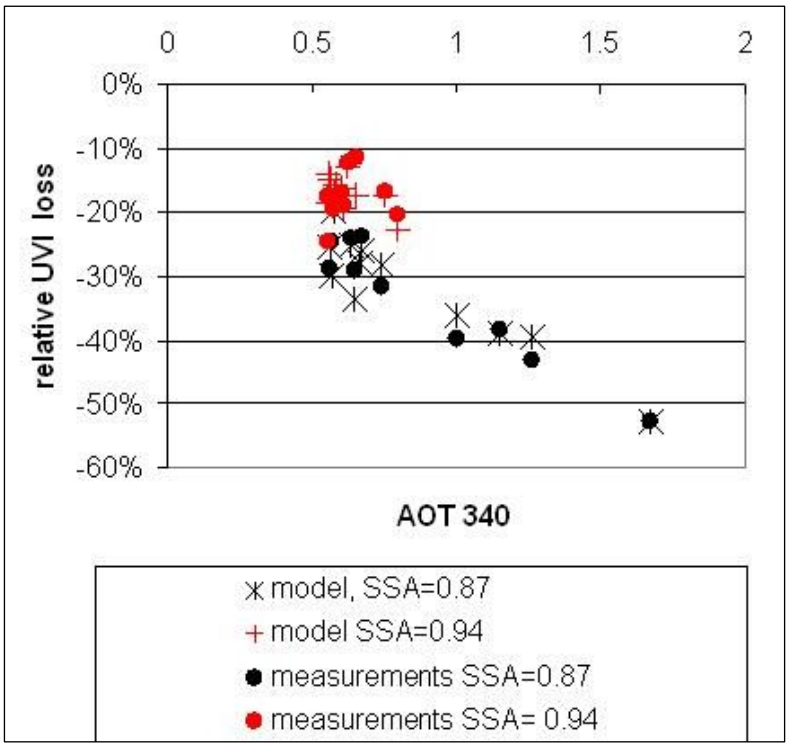

Fig. 3.2.5: Comparison between measured (dots) and modelled (crosses) UVI losses as a function of aerosol optical thickness at 340 nm at different values of single scattering albedo calculated from AERONET/PHOTONS data. Moscow, clear-sky conditions.

Single scattering albedo and asymmetry factors are retrieved through the special inversion algorithm, which has some constraints for weather conditions (Dubovik et al., 2000). The most important ones are clear sky conditions during a series of observations and high aerosol loading ($\tau_{440} > 0.4$). As a result, in winter, when τ_λ is low and cloudy conditions are dominating, the ω_λ estimates are available only from few sites over southern regions, while in summer - from approximately 50 sites. The lack of statistics and the existing uncertainty of the ω_λ retrievals ($\Delta\omega = \pm 0.03$) do not allow us to generate spatial distributions of these parameters. Instead, a study of their month-to-month variability has been conducted. No seasonal change in any of these characteristics could be detected at the 95 % confidence level. Taking into account

the ω_λ retrievals constraints, such as high aerosol loading, the absence of seasonal variations is only valid for these situations. However, it is high aerosol loading that influences significantly the solar irradiance reaching the surface, while solar irradiance is not so sensitive to the changes in ω_λ and g_λ at small aerosol optical thickness. Therefore, these retrievals can be chosen for estimating UV irradiance in Europe. In addition, it was necessary to make spectral adjustments and to re-evaluate them in UV range. This has been made with the application of Mie theory accounting for volume particle size distribution and refractive indices at 440 nm. The assumption of the same values of refractive indices in visible and UV spectra will not work properly in some cases, especially in smoke aerosol conditions (Chubarova et al., 2009). However, we can use this approximate approach due to the large statistics and the low frequency of fire smoke conditions in the overall dataset. As a result, the adjustment factors of $\Delta\omega \sim 0.01$ and of $\Delta g \sim 0.05$ have been obtained to provide the average estimates of $\omega \sim 0.94$ and of $g \sim 0.75$ in the UV region of the spectrum. These values were taken as constants within the whole UV range. The proposed method of the single scattering albedo evaluation has been tested by comparing UV irradiance relative changes in clear sky conditions with different aerosol properties. Figure 3.2.5 shows measured and modelled UV index (UVI) losses as a function of τ_{340} at different ω values obtained using the method described above. One can see a satisfactory agreement between the modelled and experimental data and a clear separation of cases with high and low values of single scattering albedo at the same aerosol optical thickness.

3.3 ALBEDO

Laurent Vuilleumier [a], Jean Verdebout [b], Daniel Walker [a,c]

a) Swiss Federal Office of Meteorology and Climatology MeteoSwiss; b) European Commission Directorate General Joint Research Centre; c) Institute for Atmospheric and Climate Science, ETH Zurich.

The surface reflectance (albedo) can strongly influence UV radiation, since it affects the amount of downwelling radiation due to multiple reflections between the earth's surface and the atmosphere. The albedo varies considerably for different surfaces and wavelength ranges. In the UV range, the majority of soils have an albedo below 10 % (Blumthaler and Ambach, 1988). The outstanding exception is snow, able to reflect up to 90 % of the incoming UV radiation, especially in case of fresh and clean snow (Ambach and Eisner, 1986).

When considering multiple reflection processes, an effective albedo should be used that characterizes the regional surface reflectance. While the local albedo can be determined by up- and downward radiation measurements, the effective albedo is more difficult to establish. Because of the binary character of the albedo in the UV (presence or absence of snow), knowledge of the regional snow cover distribution is crucial.

The relationship between albedo and the resulting UV enhancement is significant but still limited (i.e., a large change in albedo results in comparatively modest change in UV radiation). Enhancement of erythemal UV radiation can reach up to 30 % for an effective albedo of 70 % (Smolskaia et al., 2003). This amplification shows a wavelength dependency reaching a peak around 320 nm (Lenoble et al., 2004; Schwander et al., 1999).

The average effective UV albedo can be derived by different methods using observed UV radiation or information about the regional snow coverage. A common method to find the effective UV albedo is by comparing observed and modelled UV radiation (e.g. Weihs et al., 2001), either considering spectral dependencies or not: the albedo, which is an input parameter of the radiation transfer model, is adapted to match the observed UV radiation. However such techniques can lead to uncertainty up to ±0.15.

On the other hand, the average surface reflectance around a specific location can also be derived by considering the regional snow distribution. The snow information from the surrounding topography is integrated using for each pixel a distance weighted local albedo. This approach is less dependent on UV observation and modelling (c.f. Lenoble et al., 2004; Lenoble, 2000; Smolskaia et al., 2003; Weihs et al. 2001).

Finally, the snow information can be derived by remote sensing methods based on satellite observations (e.g. Foppa et al., 2007, 2004), numerical weather prediction models (e.g. Skaugen et al.,

2003) or the use of snow depth observations in (geo-) statistical approaches (e.g. Balk and Elder, 2000; Erxleben et al., 2002; Molotch et al., 2005; López-Moreno and Nogués-Bravo 2006).

Estimating the ground albedo for the COST 726 UV reconstruction represents a special challenge. For radiation transfer calculation purposes, the best ground albedo information would probably be values retrieved using satellite remote sensing in the desired wavelength range in the absence of cloud cover. However, satellite data are not available for a large fraction of the period considered. In the absence of satellite data, snow cover information can help infer the albedo in the UV range. However, even snow cover data are very scarce on the spatial extent and time period considered. The only consistent source of information for the whole period and spatial domain is the ERA-40 dataset. However, using ERA-40 to infer the presence of snow is problematic in mountainous regions because its coarse resolution hampers the representation of a realistic topography.

COST 726 UV maps are produced using a $0.05° \times 0.05°$ spatial grid. This relatively high spatial resolution allows introducing altitude effects in a reasonably realistic way. On the other hand, the ERA-40 snow cover information used for inferring albedo is only available at a coarser resolution of 1°. An empirical procedure has been developed for generating daily UV albedo maps at the higher resolution, from low resolution data, using a METEOSAT-derived UV product.

ERA-40 snow depth data (in mm water equivalent) come on a $1° \times 1°$ grid covering an area from 25.5° E to 35.5° W and 30.5° to 80.5° N[1]. The European Commission Joint Research Centre independently generated a surface UV climatology using METEOSAT to retrieve surface albedo and cloud optical thickness over Europe from 01/01/1984 to 31/08/2003, on a $0.05° \times 0.05°$ grid. The goal of the COST 726 empirical approach is to link the observed albedo range for each $0.05° \times 0.05°$ pixel to the snow depth of the corresponding ERA-40 parent cells. The pixel-dependent relationships are inferred using the common period (01/01/1984 to 31/08/2002) between the ERA-40- and METEOSAT-derived datasets. The following parameters have been determined for each high resolution pixel (i.e., one value per pixel):

- R_{max} maximum UV albedo over the whole period;
- R^S_{min} minimum snow UV albedo over the whole period (restricted to days when pixels are flagged as snow covered);
- $R_{min}(doy)$ minimum UV albedo over the whole period (irrespective of pixel snow flag), this parameter depends on day of year and is determined using a 10-days moving average;
- P^S pixel snow cover "probability" (ratio of number of days when pixel flagged as snow covered to total number of days);
- NP^S "per ERA-40 cell pixel snow cover normalized probability"; this "normalized probability" is obtained by dividing P^S by the maximum value of P^S within the parent ERA-40 cell.

In case the ERA-40 snow depth for a given day and cell is 0, the albedos of all high resolution pixels within the cell are assigned their minimum satellite-derived value $R_{min}(doy)$. In the other case, the ERA-40 snow depth (SD) for the given day and cell is normalized to the maximum value found for the same cell over the whole ERA-40 period (SD_{max}). This results in a cell-dependent normalized snow depth (NSD): $NSD=SD/SD_{max}$. Within such a cell, pixels whose snow cover normalized probability NP^S is greater than $1 - NSD^\delta$ are considered as snow covered, while the others are considered as snow free, with δ being a cell-dependent empirically-determined power factor. Then, the albedos of snow covered pixels are assigned the value $R^S_{min} + (R_{max} - R^S_{min}) \times NSD^\delta$, while the albedos of snow free pixels are assigned the values $R_{min}(doy)$ (see Fig. 3.3.1).

[1] A special treatment of pixels in ERA-40 cells identified as predominantly sea/ocean, but also including land high resolution pixels has been added to avoid that high resolution land pixels are attributed the snow depth of the parent ERA-40 sea/ocean cell (which is systematically 0). Such areas are thin strips in the south of Finland, western tips of Cornwall, Wales, Scotland, Brittany, the totality of Crete, etc.

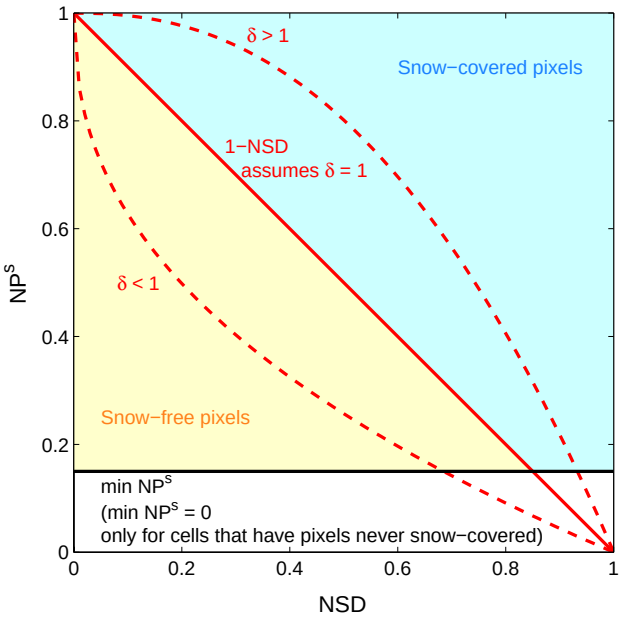

Fig. 3.3.1: Schematics of COST 726 snow cover determination.

The cell-dependent power factor δ is determined so that for each cell the average albedos as determined by the COST 726 empirical procedure and the METEOSAT dataset are equal. These average albedos are determined over the whole cell and the whole ERA-40 – METEOSAT common period, with restrictions for ensuring that totally snow-free cases are excluded. In a few cases, a solution for δ cannot be found. These correspond to ERA-40 cells that very rarely contain snow and for which the snow depth only takes a small number of distinct values (40 out of 1153 land cells). In such cases, NSD was just replaced by 0.95 × NSD.

Regarding sea ice, the ERA-40 data set gives the fractional ice cover in each cell. Within a cell, pixels are flagged as ice covered in such a number as to reproduce this value. In areas where a solid ice pack is a priori possible (within the Baltic Sea and parts of the White Sea), this choice is made in the same way as for snow over land (i.e. using the METEOSAT derived ice cover probability). Elsewhere, the ice covered pixels are chosen randomly (with a pseudo-random number generator). The UV albedo is assigned in the same way as for snow pixels; ice free pixels are assigned an albedo of 6 %.

For part of the ERA-40 area (25.5° W – 20° W and 74° N – 80.5° N) METEOSAT-derived results are not available. This includes the western half of Iceland and parts of Greenland and Svalbard. The UV albedo has then be assigned with similar laws as above but by choosing the various missing parameters on a case by case basis in order to obtain a result comparable to previously processed similar cells.

A method for estimating snow-coverage in Switzerland was independently developed using daily estimations of the snow-line altitude in five different Swiss climatic regions in combination with a high-resolution digital elevation model (gtopo30 DEM).

The snow line altitude is determined for each region by fitting a robust linear regression of snow depth against the altitudes of the measurement locations, and deducing the altitude corresponding to a snow depth threshold of 5 cm. The number of measurement stations used for this analysis is relatively constant since the beginning of the 1980's, as well as the manual measurement technique. DEM pixels whose altitude is above the snow line altitude are flagged as snow covered.

This method was cross-validated and validated against satellite snow-maps with satisfactory results. More details are given by Walker et al. (2009). The daily effective UV albedo for any Swiss area can then be derived from an empirical relationship between snow cover fraction and albedo.

These independently derived snow coverage and albedo were used to assess the uncertainties of the COST 726 equivalent quantities for two ERA-40 grid cells in Switzerland (centred on 47N-8E and 47N-9E). Verification over alpine cells is important because mountainous terrain leads to the most problematic situations in estimating the surface albedo. The Western cell (8E) encompasses mostly terrain

below 1000m a.s.l., but the fraction at elevations above 1000 m is still significant. The Eastern cell (9E) has an elevation distribution which has a majority of its terrain above 1000 m a.s.l.

For the two cells mentioned above, the COST 726 daily snow cover fractions and average albedos are compared to the equivalent quantities derived by the Swiss method in figure 3.3.2. This comparison is carried over the period 1981-2002, and is focused on extended winter seasons (November to April), because of the stronger snow signal.

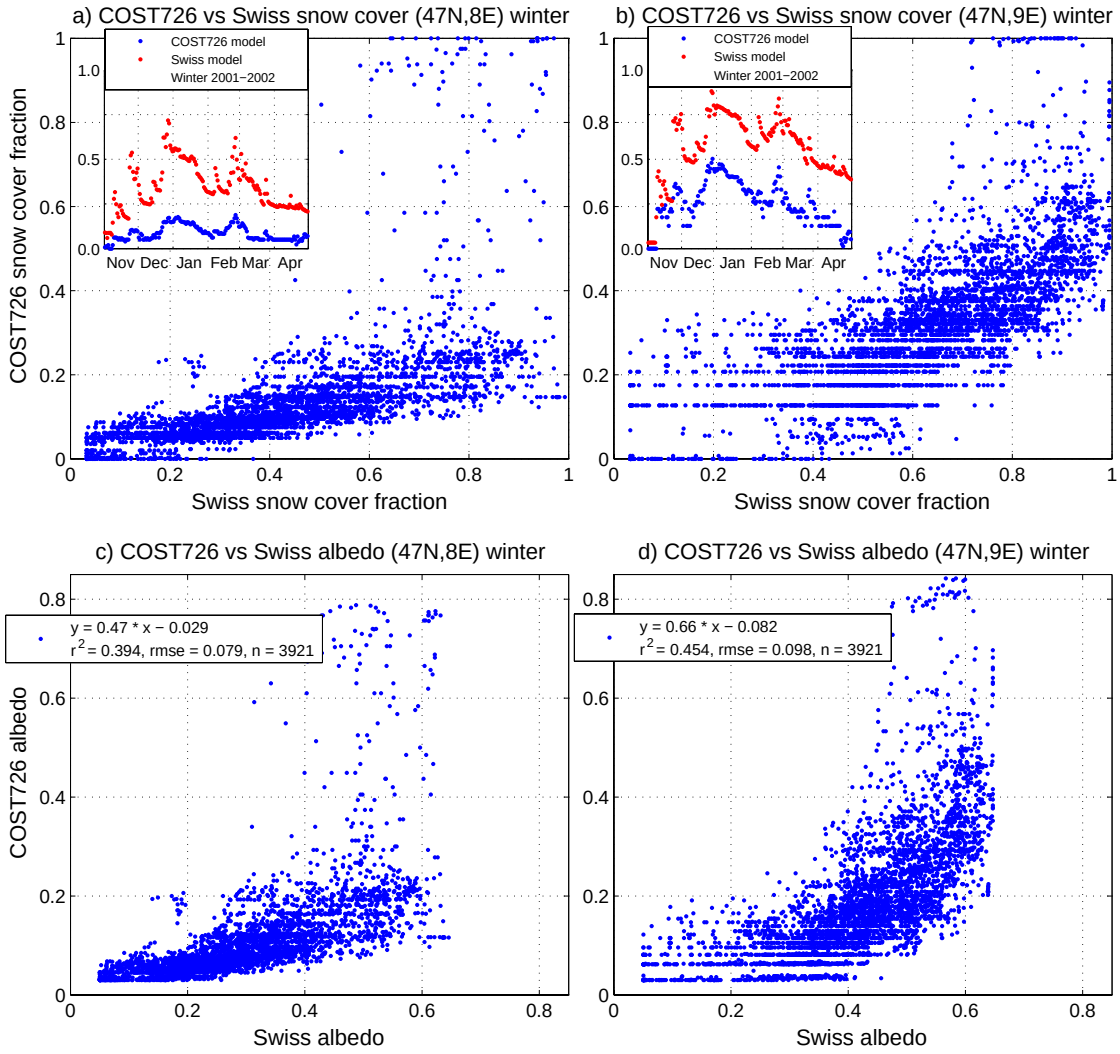

Fig. 3.3.2: COST 726-derived snow cover and albedo with respect to similar quantities derived by an independent method for two ERA-40 cells centred over Switzerland; (a and b) snow cover; (c and d) albedo.

The correlation between the parameters (albedo or snow cover) derived by the two methods is not high but still significant (r^2 on the order of 0.4 – 0.5). However, a large scatter (on the order of 0.1 for average albedo) is present. Furthermore, the COST 726-derived parameters are generally significantly lower than for the other method, except for a few exceptions. This is likely linked to the fact that the COST 726 method is based on an inferred relationship between satellite-derived albedo and model-derived snow amount, while the second method is primarily based on the absence or presence of snow. The snow cover derived from satellite remote sensing is lower than when effectively measured on the ground because elements such as forests and urban areas are relatively dark and become even darker as the snow ages. On the other hand, while the ground-measured snow-cover reflects the true amount of snow on the ground, satellite-derived albedo may be more realistic, because of the above-mentioned darkening effect.

Such comparisons show that the effective albedo is a quantity that is difficult to establish, and that uncertainties up to ±0.15 as mentioned by Weihs et al. (2001) are realistic. This may in the worst cases induce albedo-related uncertainties in the calculated UV downward radiation up to ±10 %. However, studying the time evolution of the snow cover inferred from the two methods (inserts in Fig. 3.3.2 a and b) shows that they are clearly related and follow a similar time evolution. In addition, such uncertainties specially affect difficult situations as those presented here (mountainous terrain, presence of snow). In many cases, the terrain is more uniform and snow is absent, which results in very small uncertainties linked to the albedo in the UV, especially for summer situation when UV radiation is the highest.

3.4 GLOBAL IRRADIANCE

Anders Lindfors [a]

a) Finnish Meteorological Institute.

Pyranometer measurements of global radiation (300–3000 nm) have been performed on many European locations since the International Geophysical Year 1957–58. These data contain valuable information on the influence of clouds on the radiation received at Earth's surface over the past decades. Therefore, it was chosen within COST action 726 to use these data as input for determining the Cloud Modification Factors (CMFs; see section 3.5) needed for reconstructing past UV radiation.

Pyranometer data are available from different sources. In this work, the primary data source used was the World Radiation Data Centre (WRDC; 79 sites) in St. Petersburg, which holds records of pyranometer measurements over the world since 1964, when the data centre was founded. Furthermore, some data from a server hosted by the US National Renewable Energy Laboratory (NREL; 31 sites), which mirrors an older version of the WRDC archive, were included in order to improve the coverage in the Mediterranean and the Southeastern European region. Finally, also data provided by National Meteorological and Hydrological Services (NMHS; 36 sites) and other sources (7 sites) such as universities and the Baseline Surface Radiation Network (BSRN) were used. Figure 3.4.1 provides an overview of the stations included.

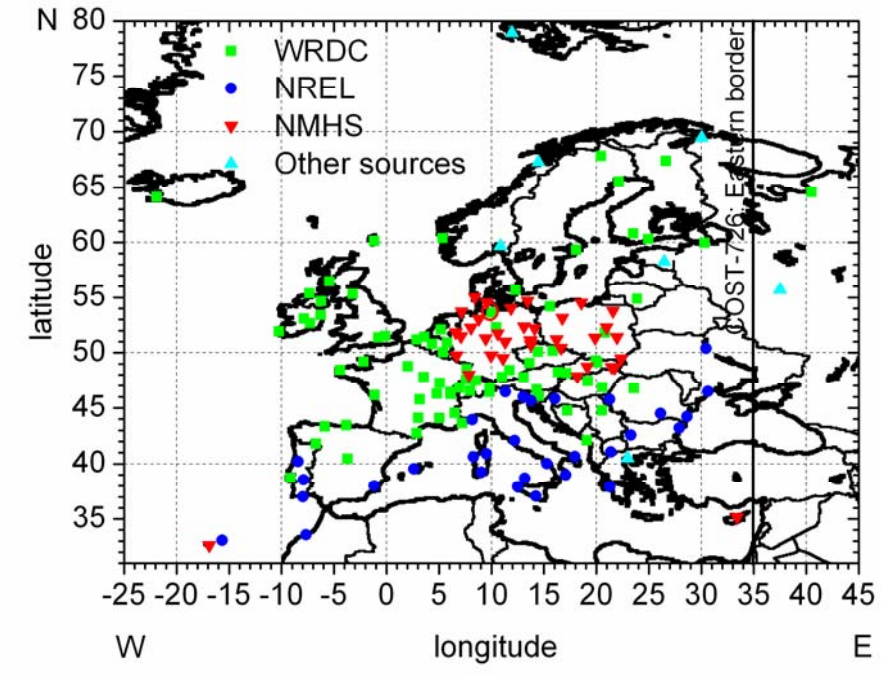

Fig. 3.4.1: Database of global radiation used in COST 726, including 79 sites from WRDC, 31 sites from NREL, 36 sites from NMHS, and 7 sites from other sources. See text for details.

The quality and the homogeneity of pyranometer measurements, which is essential for the UV reconstruction work within COST 726, depend on the efforts made to maintain the instruments in each network and at each station. Pyranometers are usually calibrated against reference instruments, which, in turn, are compared with pyrheliometers of the World Radiometric Reference (WRR). The WRR is implemented by the World Standard Group of at least four absolute pyrheliometers of different design held at the World Radiation Center in Davos, Switzerland (Fröhlich, 1991) and is accepted as representing the physical unit of total irradiance with an uncertainty of < 0.3 % (RMS).

The uncertainty and representativeness of global irradiance data have been estimated by instrument reviews and comparisons (Bener, 1950; Schieldrup Paulsen, 1968; Sonntag, 1975; Persson, 2000). Table 3.4.1 shows the overall uncertainties of hourly and daily values of global irradiance for different classes of pyranometers as defined in WMO (2006). The highest requirements to accuracy, measurement procedures, quality checks and site characteristics are put into practice at the BSRN sites, which thus provide radiation data of the best quality (BSRN, 2004). It is emphasized, however, that only four sites from the BSRN were included in this work.

Table 3.4.1: Overall uncertainty of global irradiance data achievable for different pyranometer classes according to WMO (2006).

Achievable uncertainty (%)	High quality	Good quality	Moderate quality
Hourly global irradiation	3	8	20
Daily global irradiation	2	5	10

General criteria for quality checks of global irradiance data that should be applied at the measurement site and/or at a Radiation Centre include redundancy and cross-checks with other radiation components, exceedance checks of physically impossible values (higher than extraterrestrial irradiance) and extremely rare limits, and comparison between data of neighbouring sites that are located in a comparable terrain.

All global radiation data used in this study, comprising altogether more than 1.6 million daily data points, were quality checked for exceeding the extraterrestrial limit and extremely rare values. The extraterrestrial limit was exceeded in only 73 cases, and extremely rare values exceeded in 48 cases in summer and 464 cases in winter. Figure 3.4.2 shows, as an example, the analysis performed for Copenhagen (Denmark) and Hamburg (Germany). A correction procedure to global irradiation as derived from CMFs and checks on the long-term stability of data is described in section 3.5.

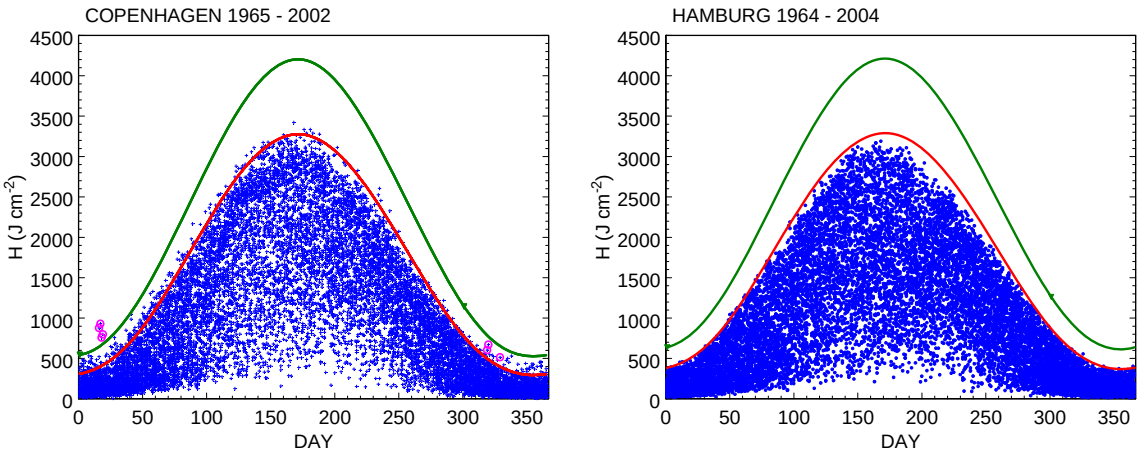

Fig. 3.4.2: Daily global irradiation (dotted) at Copenhagen (1965 – 2002) and at Hamburg (1964 – 2004). Also shown are the extraterrestrial irradiation (green; upper curve) and the extremely rare threshold (red; lower curve). The distance between the sites is 271 km.

The stations from the WRDC archive were selected during a Short-Term Scientific Mission by Anders Lindfors. The applied selection criteria were as follows: (i) the time series should be at least 20 years long; (ii) the data should be of sufficient quality according to the general quality tests performed by WRDC. The tests performed at WRDC are similar to those described above, and include, in addition, tests on the homogeneity of the time series. As some of the WRDC data had not been corrected to the WRR scale, a post-correction was carried out for those stations that had the necessary information available. At some stations, however, it was not known at which date the data in the WRDC archive started to follow the WRR scale and for these stations no post-correction could be made. This introduces an additional uncertainty of ~2 % to these stations. The same goes also for some stations from NREL, NMHS, and other sources.

3.5 CLOUD INFORMATION BY SOLAR CLOUD MODIFICATION FACTORS (SOL–CMF)

Henning Staiger [a], Jussi Kaurola [b]

a) German Meteorological Service; b) Finnish Meteorological Institute.

For cloud information, COST 726 uses daily CMF in the solar spectral range (SOL–CMF). A CMF is defined as ratio of all-sky to clear-sky down-welling irradiation at the Earth's surface. There are several algorithms available to convert SOL–CMF into UV–CMF. Data sources for SOL–CMFs are ECMWF ERA-40 fields, and observed daily sums of solar global irradiation. ERA-40 has a complete spatial and temporal coverage over the COST area. The sites are irregularly distributed, both spatially and temporally (section 3.4, Fig. 3.4.1).

The ERA-40 data (Uppala et al., 2005) makes possible to calculate SOL–CMF using the 6 hourly accumulated output of "Surface net solar radiation, clear sky" and "Surface net solar radiation" for the period 01 Jan.1958 – 31 Aug. 2002. Firstly, the ECMWF MARS post-processing software was used to interpolate original data in the N80 Quasi-regular Gaussian grid into the regular 1° × 1° latitude longitude grid used in this project. Thereafter, the 6 hourly fields were summed up to give daily totals of these two fields, and finally the daily SOL–CMFs were calculated. The SOL–CMF calculated in this way using the net radiation (downwards minus upwards) should give results very close to the SOL–CMF calculated using down-welling components apart from the distinction between direct/diffuse surface albedo. Down-welling radiation budgets are not available for clear skies in the ERA-40 data.

The SOL–CMFs calculated from the ERA-40 data were compared with the SOL–CMFs calculated from ground-based observations of daily global radiation and corresponding clear-sky values given by a radiative transfer model. The results indicated that ERA-40 SOL–CMFs have positive bias in comparison with selected ground-based data: Jokioinen +9.4 %, Norrköping +2.1 %, Bilthoven +7.4 %, Thessaloniki +3.7 %, Potsdam +11.9 %. Although the ERA-40 grid box values and in-situ measurements represent very different field-of-view such a systematic positive bias necessitates correcting the ERA-40 derived SOL–CMFs with the ground based data. The method and the results are described in the next sub-section.

SOL–CMFs are calculated dividing the observed daily sums of global irradiation by modelled clear-sky sums. Clear-sky modelling applies the ESRA clear-sky model (Rigollier et al., 2000; Scharmer and Greif, 2000, Ineichen, 2006), and a climatology of the Linke turbidity factor (Remund et al. 2003). Via ERA-40 snow depths, it is accounted for the albedo impact of snow covered surfaces. The temporal course of modelled clear-sky SOL–CMFs is in close agreement with the aerosol direct radiative effects given by Norris and Wild (2007). For the NREL retrieved sites (section 3.4) a better balanced data quality in 1964 – 1980 is achieved by "homogenisation". Gridding of "observed" SOL–CMFs has to account for outliers. Thus, a two-step cross-validation has been performed to flag possible extremes (WMO 2003 a, b, Peterson et al., 1998). For extrapolation, Shepard's gravity algorithm including a term related to the equivalence between horizontal and vertical distance is applied (Zelenka et al., 1992). For interpolation, ordinary Kriging (Wackernagel, 2003, Zelenka et al., 1992) is used based on a daily structural analysis (semi-variance). The SOL–CMF distance dependence follows the exponential variogram model type. Gridded "observed" and bias corrected ERA-40 SOL–CMFs are merged by a weighted average. The weight function for the observations is constructed such that the weight becomes 0.5 in the distance the semi-variance equals the interpolation variance in ERA-40. Figure 3.5.1 gives the long-term mean and

accuracy of merged ERA-40 and "observed" SOL-CMFs. The mean is bias free. The accuracy strongly depends on the network density available in gridding, and shows seasonal differences. Compared to independent sites 2000 and 2001, it is best for summer (16 to 18 %), worst for winter (30 to 35 %), and 24 to 25 % over the year. The scatter-plots of figure 3.5.2 assemble the daily interpolation results for independent sites in Northern (a), Western (b), and Central Europe (c), respectively. Compared are original ERA-40 (1) and COST 726 interpolated (2) SOL–CMFs. COST 726 interpolated SOL–CMFs are improved in bias and show a noticeably reduced scattering. This holds also for South-Eastern Europe, where almost no observed SOL–CMFs have been available for gridding in 2000 and 2001 (Fig. 3.5.3). Gridding implies a smoothing effect. Thus, for a given location the standard deviation of COST 726 interpolated SOL–CMFs is on principle less than that of observed SOL–CMFs.

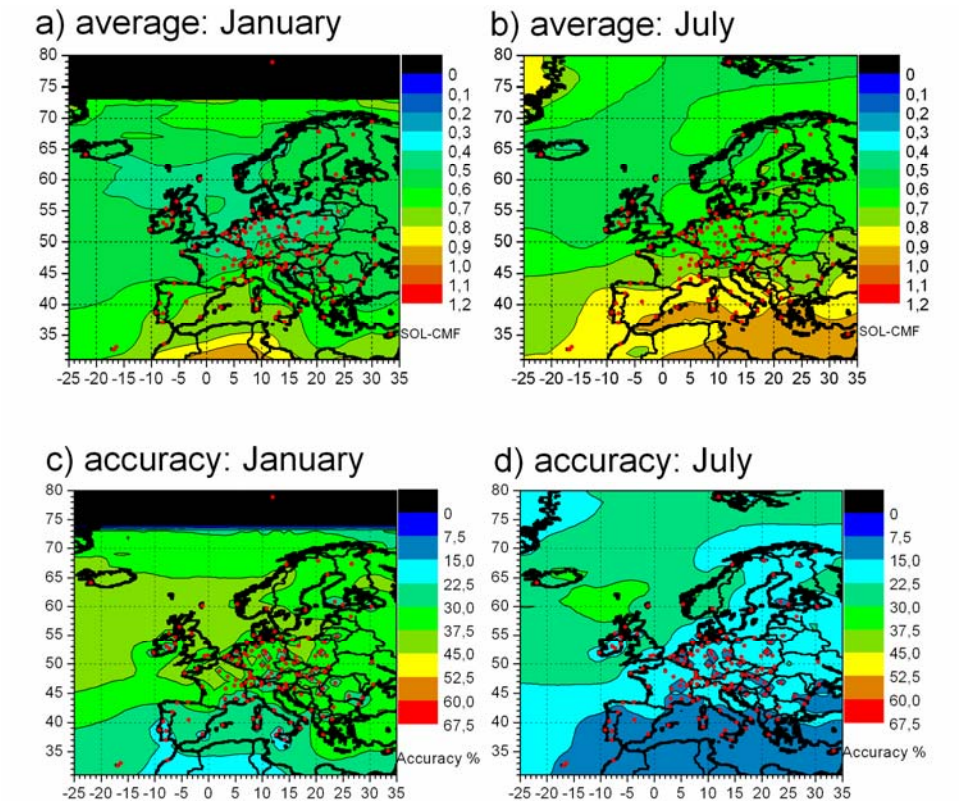

Fig. 3.5.1: Spatial distribution of SOL–CMF and its accuracy: a) 1964 – 1993 average of SOL–CMF for January; b) for July; c) 1964 – 1993 accuracy of SOL–CMF for January; d) for July.

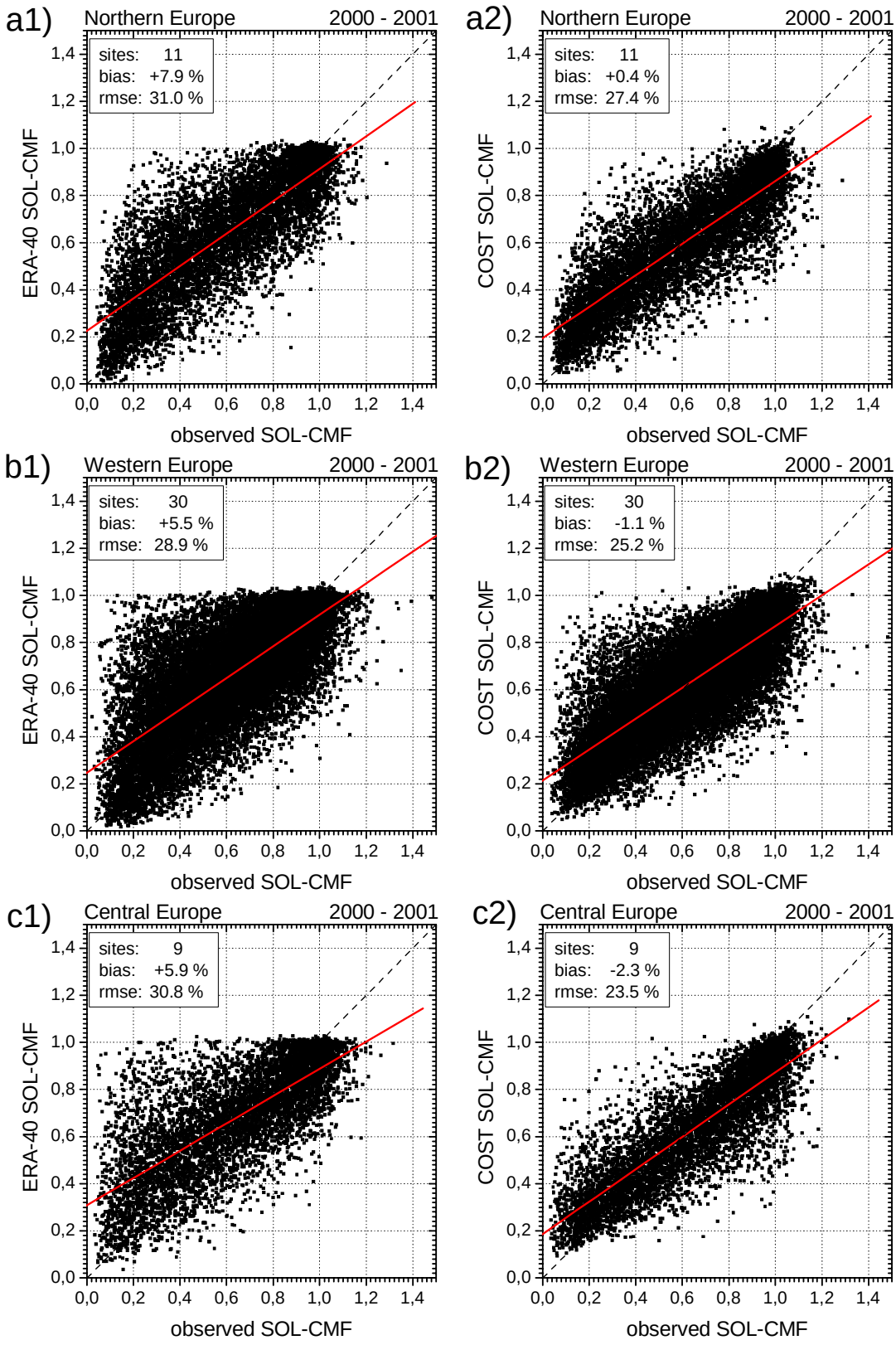

Fig. 3.5.2: ERA-40 and COST 726 interpolated SOL–CMFs compared to "observed" SOL–CMF of independent sites and the years 2000 and 2001: Northern Europe, a1) ERA-40, a2) COST, Western Europe, b1) ERA-40, b2) COST, Central Europe, c1) ERA-40, c2) COST.

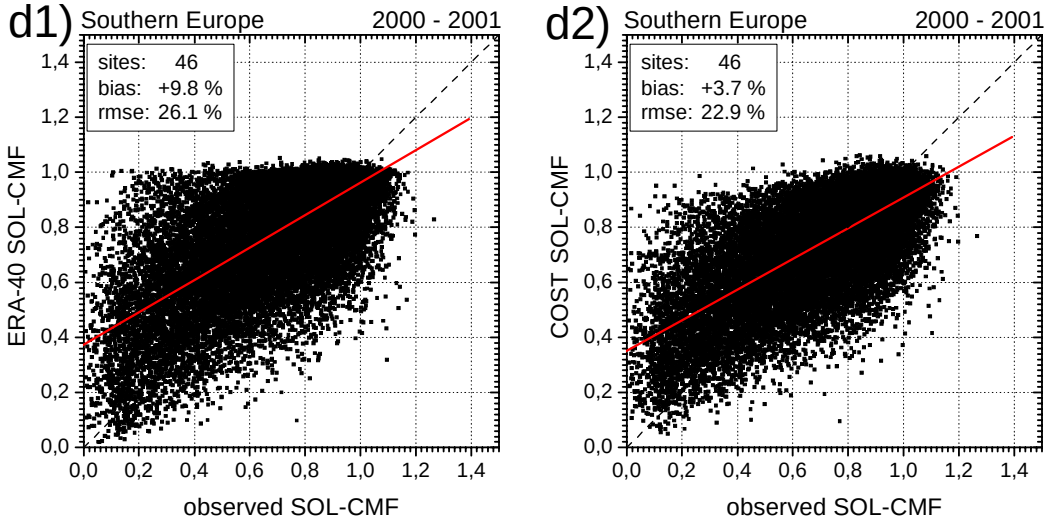

Fig. 3.5.3: As figure 3.5.2, however, for South-Eastern Europe, having almost no observed SOL–CMFs available for gridding in 2000 and 2001.

3.6 TRANSFORMING SOL–CMF INTO UV–CMF

Henning Staiger [a]

a) German Meteorological Service.

Cloud impacts on the transfer of UV radiation through the atmosphere can be assessed by using SOL–CMFs. They have proved to be a solid basis to derive CMFs for the UV radiation (UV–CMF). Observed total global irradiance includes all relevant effects for radiation transmission, such as cloud optical depth, different cloud layers, multiple reflection, as well as the distinct difference as to whether the solar disc is obscured by clouds or not. In the UV range, clouds decrease the irradiance to a lesser extent than in the visible and infrared spectral range, in particular, due to the markedly higher diffuse fraction in UV. Thus, the relationship between SOL–CMFs and UV–CMFs is not straight forward, but depend on whether, for example, the SZA and wavelength band or action spectrum in the UV have been taken into consideration (Fig. 3.6.1). Due to high SZA in winter and overall for high latitudes, the long-term average of UV–CMF increases markedly compared to SOL–CMF, and thus the relative accuracy in gridding is improved too (see Fig. 3.6.2 compared with Fig. 3.5.1). Within the COST 726 modelling exercise, several algorithms have been applied successfully in transforming observed global irradiation to UV–CMFs (Koepke et al., 2008). Models and parameterisations are discussed in more details by e.g. Curylo et al. (2007), den Outer et al. (2005), Feister et al. (2008), Krzyscin et al. (2003), Lindfors et al. (2007), Pribullova and Chmelik (2008), Rieder et al. (2008), Staiger et al. (2008). The algorithms can be classified to be of local and of generic approach, respectively. Applied in reconstruction is the generic algorithm of den Outer et al. (2005). It relates daily UV–CMFs to daily SOL–CMFs using the SZA at local noon to tune this relationship:

$$\mathrm{UV-CMF}\left(\mathrm{SZA},\mathrm{SOL-CMF}\right)=\frac{1-\left(1+p(\mathrm{SZA})\cdot\mathrm{SOL-CMF}\right)^{-0.27}}{1-\left(1+p(\mathrm{SZA})\right)^{-0.27}} \qquad (3.5.1)$$

The parameter “p” takes different values for set SZA intervals at noon and depends additionally on the wavelength (range). The uncertainty of the algorithm in terms of measured to modelled daily erythemally effective UV doses is 1.02 ± 0.09. Overall, the lesser decrease of irradiation in the UV due to clouds can be illustrated based on 101 sites in 2000 and 2001 over entire Europe by a mean observed SOL–CMF = 0.649 ± 0.275 and a corresponding mean (erythemally weighted) UV–CMF = 0.752 ± 0.230.

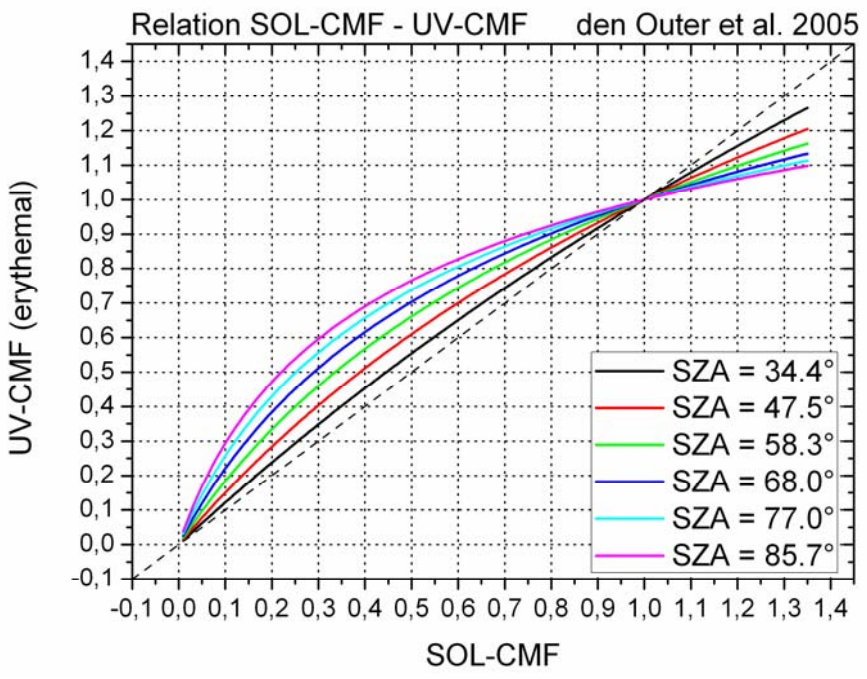

Fig. 3.6.1: Relationship between SOL–CMF and UV–CMF (erythemal weighting) from den Outer et al. (2005).

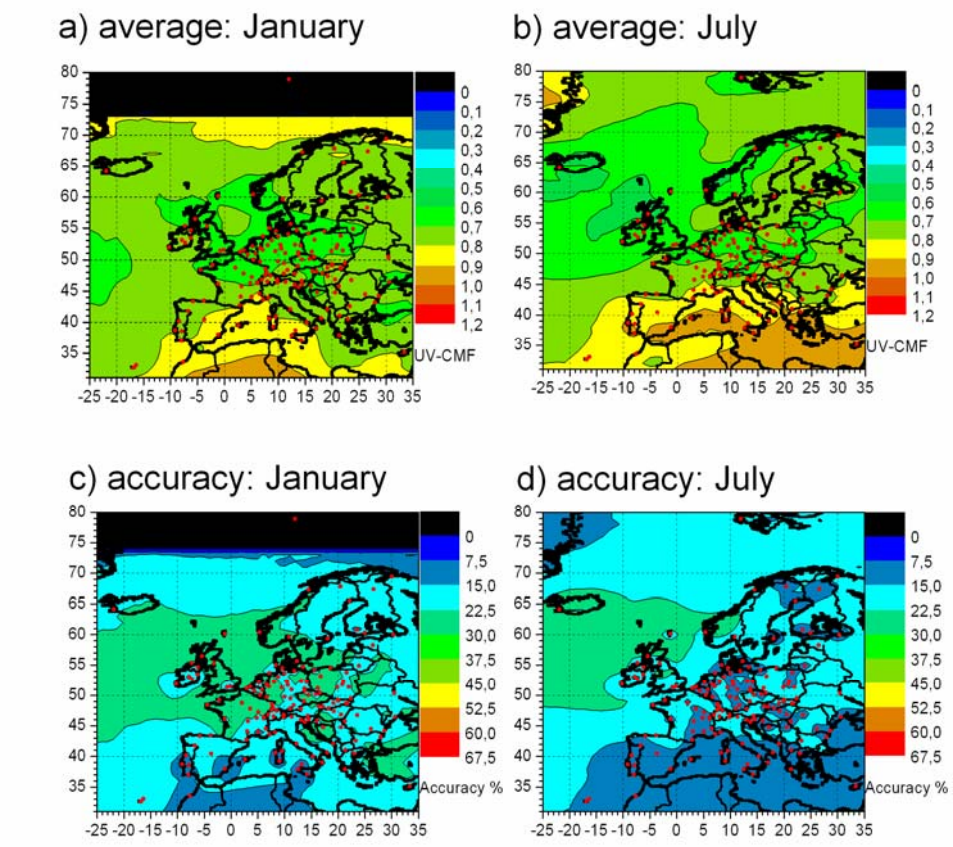

Fig. 3.6.2: Spatial distribution of (erythemally weighted) UV–CMF and its accuracy: a) 1964 – 1993 average of UV–CMF for January; b) for July; c) 1964 – 1993 accuracy of UV–CMF for January; d) for July (compare with SOL–CMF, Fig. 3.5.1)

4 SOLAR UV MEASUREMENTS

Julian Gröbner [a]
a) Physikalisch-Meteorologisches Observatorium Davos, World Radiation Center.

Solar UV irradiance is measured with spectroradiometers, broadband filter radiometers or multiband filter radiometers (MBFRs). While spectroradiometers are used as reference instruments to provide the absolute spectral UV irradiance, most networks monitoring solar UV radiation consist of filter radiometers due to their ease of use and lower purchasing costs with respect to spectroradiometers. Furthermore, the labour involved in network maintenance is considerably less than for a corresponding network of spectroradiometers.

Here, we will report on the results obtained within COST action 726 with respect to UV filter radiometers measuring erythemally weighted solar UV irradiance. These activities are a continuation of the activities initiated in COST action 713, namely the quality assurance of broadband filter radiometers measuring erythemally weighted solar irradiance. In addition, this report describes for the first time the results from an intercomparison campaign of multiband filter radiometers.

Both broadband and multiband filter radiometers are extensively used in regional and national UV monitoring networks to report solar UV irradiance levels to the public. The harmonisation of solar UV measurements across these networks was a primary goal of the activities of working group four (WG4). This activity is a necessary prerequisite for using these measurements for the validation of UV forecasting models on a European scale as well as for UV reconstruction efforts such as the ones described in this report.

The main goal of WG4 was to homogenize solar UV measurements across Europe. Three main tasks were individualised to achieve this goal:

- Provide common Quality assurance and Quality Control procedures to be implemented in all participating European regional and national UV monitoring networks.
- Perform an intercomparison and calibration campaign regrouping filter radiometers from all participating networks.
- Establish a UV irradiance reference for harmonising UV irradiance measurements on a European scale.

4.1 INTERCOMPARISON CAMPAIGNS

Julian Gröbner [a]
a) Physikalisch-Meteorologisches Observatorium Davos, World Radiation Center.

The homogeneity of solar UV measurements in Europe was ascertained by performing two separate intercomparison and calibration campaigns for broadband and multiband filter radiometers respectively. These intercomparisons provided a common UV reference to which all instruments could be compared to. The multiband filter radiometer intercomparison (FARIN) was organised by NRPA near Oslo, Norway in 2005, while the broadband filter intercomparison was held at the European UV Reference Centre (EUVC) of the Physikalisch-Meteorologisches Observatorium Davos and World Radiation Center (PMOD/WRC) in 2006. Both campaigns used reference spectroradiometers traceable to the European reference QASUME operated by the EUVC, thus essentially homogenising all participating radiometers to a common and acknowledged reference.

The results of these campaigns are described in several publications and reports and were presented at international conferences (Gröbner et al., 2007, Johnsen et al., 2008). Summary results are provided in figures 4.1.1 and 4.1.2 for the PMOD/WRC and FARIN campaigns respectively.

As shown in figure 4.1.1, broadband UV measurements between various instruments representing their respective networks differed by up to 60 % using the calibrations in use prior to the campaign. After the campaign, all instruments agreed to better than 10 % using the calibration parameters determined at the EUVC. This intercomparison showed that reliable measurements with broadband radiometers require

carefully calibrated radiometers applying the calibration and maintenance procedures described by Webb et al. (2006) and Hülsen and Gröbner (2007).

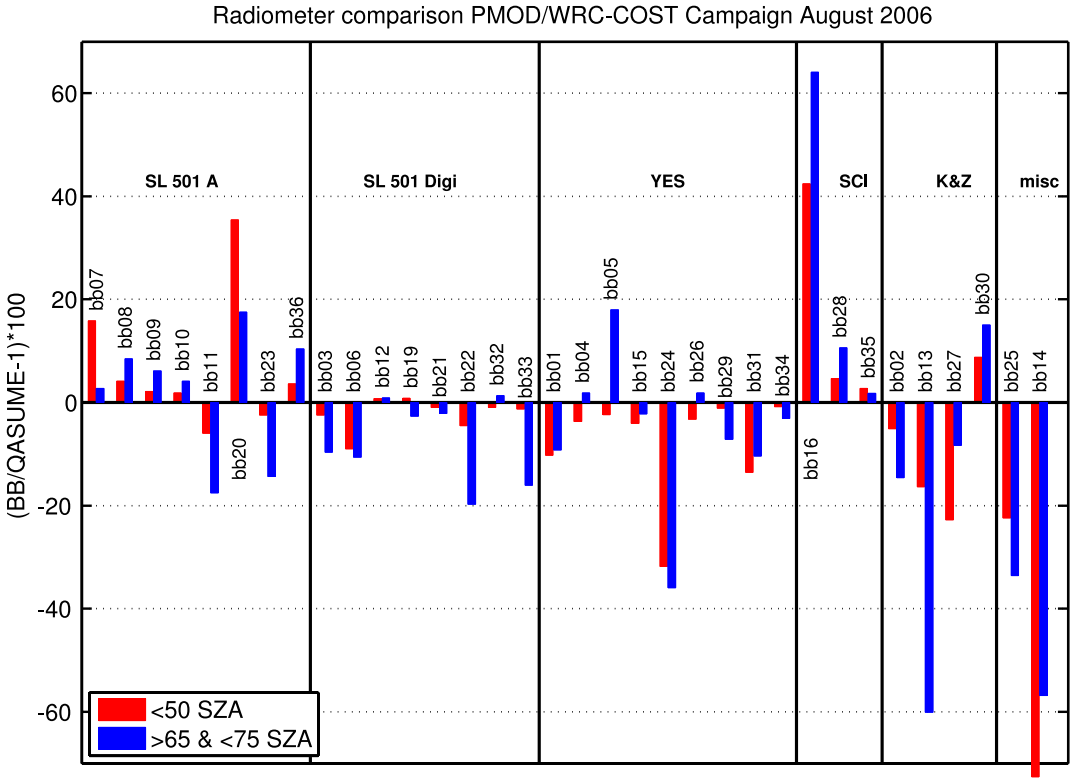

Fig. 4.1.1: Average relative differences between the broadband radiometers and the QASUME reference spectroradiometer for two solar zenith angle ranges 1) smaller than 50° (red bars) and 2) higher than 65° and lower than 75° (blue bars) using the respective calibration procedure in use by each participating institute.

The typical uncertainties of broadband radiometers measuring erythemally weighted solar irradiance were investigated using the results from this campaign. It could be shown that well maintained and stable radiometers could be calibrated with an expanded uncertainty between 7.2 % and 16 %. The largest uncertainty is due to the cosine correction function which depends significantly on the angular response of each individual radiometer, and varies between 0.9 % and 7.2 % for different types of radiometers. From the set of instruments present at the intercomparison, it was possible to derive typical cosine correction related uncertainties for the three main types of instruments:

- Kipp and Zonen, Scintec: less than 0.9 %;
- SL501: between 1.7 % and 4.3 %; and
- YES UVB-1: between 4.0 % and 7.2 %.

Thus, stable broadband radiometers with low cosine errors can measure erythemally weighted irradiances with uncertainties of the order of 7 %, while the uncertainties for instruments with larger cosine errors will be of the order of up to 16 %.

During the FARIN intercomparison, the mean ratios between participants' data and the reference were within ±5 % for 20 data sets and ±10 % for 23 data sets obtained during the core period and SZAs less than 80°. Excluding radiometers that were traceable to the same national calibration standards, 8 out of the remaining 11 sets of radiometer data were within ±5 % and 10 out of 11 sets within ±10 %. Harmonization of UVI resulted in close agreements with the reference, and the standard deviation for the collective group of 33 MBFRs operating in the same period was within ±4.6 % (2 σ) for SZA up to 80°. Corresponding standard deviation for the collective group of 26 data sets from participants was ±11.7 %.

The results demonstrated that MBFRs of type GUV, NILU-UV and UV-MFRSR-7 may provide highly accurate measurements of UV index for all realistic sky conditions and SZAs.

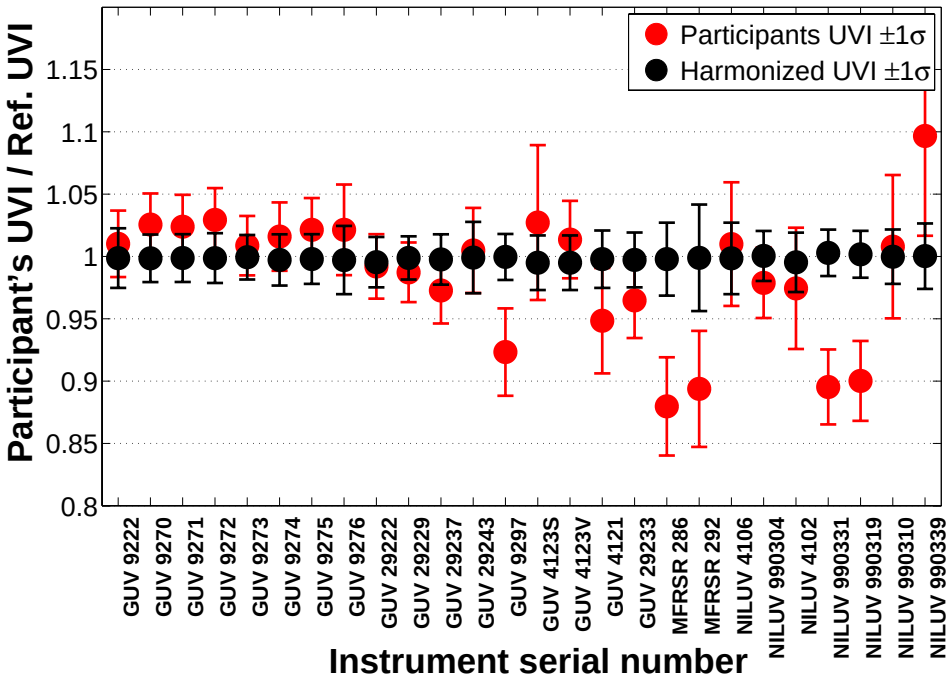

Fig. 4.1.2: Mean ratios of participants' UVI and the reference (red circles) and harmonized UVI and the reference (black circles) for 26 MBFRs operating in the core-period. X-axis: Instrument serial number. Y-axis: Relative units. Error bars indicate ±1 %, for SZA smaller than 80°. Reference in period is NRP300.

The activities of WG4 have shown the importance of following accepted quality assurance and quality control procedures to ensure that solar UV measurements are of high quality. The calibration of filter radiometers (multiband and broadband) requires well equipped calibration laboratories with fully characterised spectroradiometers used as reference instruments. As shown by Hülsen et al (2008), several calibration laboratories exist in Europe, which provide filter radiometer calibration services.

4.2 QUALITY ASSURANCE OF SOLAR UV MEASUREMENTS

Julian Gröbner [a]

a) Physikalisch-Meteorologisches Observatorium Davos, World Radiation Center.

In recent years, quality assurance and quality control procedures for UV irradiance measurements have been developed within the Global Atmosphere Watch program (GAW) of the WMO. With respect to broadband filter radiometers, a report was published which describes in detail how to perform UV measurements with these instruments and how to ascertain their respective uncertainties (Seckmeyer et al., 2007). While these documents are oriented towards expert users, their practical application at the level of network operators required the drafting of Standard Operating Procedures describing practical tasks to be implemented by each network, such as maintenance procedures, calibration procedures and data archival and backup.

This activity was accomplished by combing efforts between COST 726 and the WMO Scientific Advisory Group for UV in drafting "a practical guide to operating broadband instruments measuring erythemally weighted irradiance" (Webb et al., 2006). This document outlines the essential tasks needed to obtain reliable measurements of solar UV irradiance within a network of these instruments.

In addition, the EU-funded project Quality Assurance of spectral ultraviolet measurements in Europe through the development of a transportable unit (QASUME) is in operational use, providing Quality Assurance audits to interested parties in Europe (Gröbner et al., 2006). This activity was incorporated in the GAW regional UV calibration centre for the European region (WMO RA VI) which was established at PMOD/WRC in 2008. By its activities, the EUVC aims at improving the data quality of UV measurements in Europe and at harmonising the measurements from different stations and monitoring programs in order to ensure representative and consistent UV radiation data on a European scale.

The specific goals of the EUVC are to:

- Maintain a set of reference irradiance standards and ensure their traceability to the SI units through purchase and intercomparison of transfer standards traceable to primary irradiance standards held at National Metrological Institutes (NMIs).
- Perform intercomparisons of irradiance standards between regional calibration centres as well as UV monitoring institutes.
- Maintain and operate a transportable reference spectroradiometer for the routine quality assurance and calibration of spectroradiometers measuring spectral solar UV irradiance. Perform calibrations and quality assessments of spectroradiometers operated by UV monitoring stations through regular site visits.
- Maintain and operate a calibration centre for the characterisation and calibration of UV filter radiometers.
- Provide on-site training and expert advice to station personnel to help maintain the required data quality.

5 ASSESSMENT OF MODELLED UV RADIATION

Harry Slaper [a], Peter N. den Outer [a], Henning Staiger [b], Jean Verdebout [c].

a) Dutch National Institute for Public Health and the Environment (RIVM); b) German Meteorological Service; c) European Commission Directorate General Joint Research Centre.

UV-radiation levels at the ground can most accurately be determined by ground-based measurements with well characterized, calibrated and quality controlled spectroradiometers. However, long term measurement series are very scarce, and the time-period covered is usually restricted to 10–20 years at most. Broadband instruments measuring erythemally weighted solar irradiance can also be used to measure biologically effective UV and the day to day variation therein, but the long term stability is not easily proven and quality assurance and quality control (QA/QC) requirements are substantial.

The evaluation of effects, such as skin cancer or cataracts requires long term data on the biologically effective UV-climate and the changes and variability therein. For risk-assessments lifetime UV-radiation levels are relevant. Furthermore, long term evaluations are required in order to study the effects of environmental atmospheric changes in ozone and climate on the UV-budgets.

In view of the limited availability of ground based measured UV-data, an estimate of the European UV-climate and variability therein requires modelling of the UV-radiation budgets received at ground level. In a previous report, COST 726 has made a comparison of several modelling algorithms with ground based UV-measurements over a limited time-period at four locations in Europe. From that comparison it was found that several methods provided good agreement with the measured ground based UV-data. However, all methods are not equally suited for the calculation of UV-radiation levels all over the European continent over decades in view of the requirements for locally and specific input data.

Algorithms using ground based ozone data and global solar radiation measurements, were found to provide the best results in the comparison with UV-measurements. The methods that use satellite-derived datasets on ozone and cloud effects showed larger uncertainty than the methods using ground based input data, when compared to ground-based measurements. However, the geographical region covered by satellite-based approaches also has major advantages since ground based input is available only at a limited number of sites.

To improve the satellite derived CMFs a location dependent correction was applied using global solar radiation data from the World Radiation Data Centre (WRDC) and national meteorological stations. Thus, the COST action 726 has led to an improved reconstruction of UV-maps.

In this chapter we extend the comparison of the COST action 726 improved UV-mapping with ground-based UV measurements, both in terms of the time-period covered, as well as the number of locations included (section 5.1).

In addition, uncertainties in the use of long term reconstruction techniques come primarily from uncertainties in the long term availability and stability of the input data (sections 5.2 and 5.3).

5.1 COMPARISON OF MODELLED AND MEASURED UV

Harry Slaper [a], Peter N. den Outer [a], Natalia Chubarova [b], Andreas Kazantzidis [c,d], Uwe Feister [e].

a) Dutch National Institute for Public Health and the Environment (RIVM); b) Moscow State University, Meteorological Observatory; c) University of Patras; d) Aristotle University of Thessaloniki; e) German Meteorological Service.

Data providers: Belsk: IGFPAS, J. Krzyscin; Bergen: NRPA, B. Johnson; Bilthoven: RIVM, P. N. den Outer; Davos: MeteoSwiss, L. Vuilleumier; Hradec Kralove: CHMI, M. Janouch; Ispra: PMOD/WRC, J. Groebner; Jokioinen: FMI, J. Kaurola; Lindenberg: DWD, U. Feister; Norrköping: SHMI, W. Josefsson; Potsdam: DWD, U. Feister; Rome: URO, A. M. Siani; Sodankyla: FMI, J. Kaurola; Thessaloniki: AUTH, A. Bais; Villeneuve d'Ascq: Univ. Lille, C. Brogniez.

A systematic comparison was made between UV-data obtained from several European monitoring stations and the above mentioned selected COST action 726 methods for ground and satellite based modelling of ground based UV. Eight stations that were selected within the EU-project SCOUT-O3 are

included in the COST action 726 validation. A number of additional stations with ground based UV-data were obtained in the COST action 726.

A systematic comparison was made between UV-data obtained from several European monitoring stations and the above mentioned selected COST action 726 methods for ground and satellite based modelling of ground based UV. Eight stations that were selected within the EU-project SCOUT-O3 are included in the COST action 726 validation. A number of additional stations with ground based UV-data were obtained in the COST action 726.

Table 5.1.1: Site information

Location	Institute	Latitude N– Longitude E (deg.dec)	Instrument	Measurement period	Ground-based ancillary modelling/ dependent cloud retrieval	Station ID reference to data
Sodankylä, Finland	FMI	67.36–26.63	Brewer MKII	04/1990 – 12/2006	Yes/Yes	FIS Lakkala 2008
Jokioinen, Finland	FMI	60.81–23.49	Brewer MKIII	01/1996 – 12/2006	Yes/Yes	FIJ Lakkala 2008
Norrköping, Sweden	SMHI	58.58–16.15	Broadband	03/1983 – 12/2003	Yes/No	SEN Josefsson, 2006
Potsdam, Germany	DWD	52.37–13.08	Brewer MKII, MKIII	01/1995 - 04/2003	Yes/Yes	DEP, Feister 2008[b]
Lindenberg, Germany	DWD	52.21–14.12	Brewer MKIV, SPECTRO 320D	01/1996 – 12/2004 01/2005 – 12/2006	Yes/Yes	DEL, Feister 2008[b]
Bilthoven, The Netherlands	RIVM	52.12– 5.19	Broad band Dilor 2XY.50	02/1994 – 12/1995 02/1996 – 12/2006	Yes/Yes	NLB, Den Outer 2005
Hradec Kralove, Czech Republic	CHMI	50.18–15.83	Brewer MKIV	01/1996 – 12/2006	Yes/Yes	CRH
Thessaloniki, Greece	LAP	40.63–22.95	Broad band	08/1991 – 12/2006	Yes /Yes	GRT Kazantzidis 2006
Bergen, Norway	NRPA	60.38– 5.33	Multiband	01/1996 – 12/2002	No/Yes	NOB Johnson
Belsk, Poland	IGFPAS	51.83–20.78	Broad band Brewer MKII	05/1975 – 12/2006 01/1996 – 12/2004	No/Yes	PLB
Davos, Switzerland	PMOD/ WRC	46.81– 9.84	Broad band	01/1996 – 12/2004	No/Yes	CZD
Ispra, Italy	JRC/ ISPRA	45.80– 8.63	Brewer	01/1992 – 12/2004	No/No	ITI

The following inclusion criteria were adopted for the available datasets:

- more than 18 summer months (May-August) with at least 15 days for each month, and more than 5 years of data with at least 220 days for each year covered;
- at least one of the following three criteria should be met: the slope of modelled versus measured monthly doses in the summer should be larger than 0.75 or the correlation coefficient for modelled and measured reading for the summer months should be above 0.8 or the standard deviation in the ratio of measured to modelled yearly UV-doses is less than 0.05.

The first criterion is just to have some statistical significance, and the second set of criteria could be considered as indicative for larger data-uncertainty in the measured UV. Large uncertainty in the measured UV leads to lower slopes of modelled versus measured data and lower correlations in the monthly data. The focus on summer months is chosen, because highest doses are received in these months and the model calculations are is easier (high sun, no snow). The high year to year variability could indicate calibration uncertainties. In theory it cannot be ruled out that the larger uncertainty and variability comes from the satellite based modelling. However, the consistency observed for all other stations suggests that measurement-uncertainty is the main reason if none of the three indicating criteria are met.

All in all data from 12 stations are included in the full analysis, and for each of those stations six comparison plots are provided, comparing several aspects of the measured UV with the modelled UV from the COST-UV mapping. In addition, for all eight SCOUT-O3 stations ground based modelling results were available and also compared in a fully similar way. Table 5.1.1 summarizes the locations and available data for each of the sites used in the full statistical analysis. As can be seen the locations cover a large part of the European continent, with a latitudinal coverage from 67° N down to 40° N. The data sets cover measurement periods of 5 up to 27 years.

Comparisons are mainly based on the ratio of modelled to measured UV-doses, either using daily, monthly or yearly doses. The variability is calculated by means of the standard deviation of the ratios for the daily, monthly and yearly doses respectively.

Table 5.1.2: Summary statistics for ratios of modelled versus measured daily, monthly and yearly UV-doses for all sites and data-years

		COST 726 mapping 8 SCOUT-O3 stations	COST 726 mapping 4 additional	Ground based modelling (RIVM) 8 SCOUT-O3 stations
Year	Average ratio	1.024	1.016	1.005
	SD Site to site	0.067	0.054	0.024
	SD year to year	0.024	0.028	0.014
Monthly	Average ratio	1.058	1.046	1.028
	SD Site to site	0.083	0.058	0.046
	SD month to month	0.081	0.082	0.058
Daily	Average ratio	1.104	1.114	1.054
	SD Site to site	0.096	0.101	0.052
	SD day to day	0.25	0.31	0.16
Summer period (May-August)				
Monthly	Average ratio	1.008	0.998	0.996
	SD Site to site	0.062	0.049	0.020
	SD month to month	0.043	0.049	0.028
Daily	Average ratio	1.031	1.038	0.999
	SD Site to site	0.074	0.069	0.025
	SDday to day	0.186	0.225	0.101

Table 5.1.2 shows a few summary statistics for the ratios found for all sites and all years. We compare both, the COST 726 mapping approach and the ground based modelling method with the measurements from the eight SCOUT-O3 stations. In addition the mapping method is also compared with the four additional stations from the COST action 726. A comparison of the results for these four stations with the overall result for the 8 SCOUT-O3 sites shows that the results are similar in terms of average ratios as well as in the variations.

As expected, the modelling method using ground based cloud and ozone information provides the best results. Especially the standard deviations for the site to site variation of the average ratios and for the temporal comparisons are smaller for the modelling method using ground based input data. For the ground based modelling the average year round ratio deviates less than 1 % from the ideal ratio (1.00). The site to site variation in this ratio is 2.4 % and the temporal variation is 1.4 %. For the COST 726 mapping method the ratio for yearly sums is on average 1.024 (1.016 for 4 COST-sites). The site to site variation is 6.7 % (5.4 % for COST-sites), and the year to year variation is 2.4 % (2.8 % for COST-sites). The site to site and temporal variations increase when shorter time periods are considered. The temporal and site to site variations in the ratios are smaller in the summer months and days than in the winter period (see Table 5.1.2). In the four summer months the day to day ratio of mapped and measured daily UV-doses shows a standard deviation of around 7 % for the site to site variation, and around 20 % for the day to day variation. For the modelling using ground based input data the site to site standard deviation is no more than 2.5 % and the day to day variation is 10 %, and thus the ground based modelling provides more stable results than the mapping-method.

As described previously the CMFs used in the mapping method of this COST action 726 were adjusted on the basis of ground based solar radiation measurements. Thus, one might expect that sites where local solar radiation measurements were used to establish this correction would show better agreement than "independent" sites for which no local ground based solar radiation measurements were used in the correction of the COST 726 maps. As can be seen from table 5.1.1 for only two sites (Norrkoping and Ispra) the cloud retrieval in the mapping procedure was fully independent. For these sites the day to day variation of the ratio of mapped and measured summer UV is as large as 32–46 %, whereas for all other sites the standard deviation in the day to day ratios ranges from 10–27 % (see Table 5.1.3). However, the month to month variability for ratios of monthly sums for the summer months for these two sites is much less and fully in line with all other sites (standard deviation of around 5–5.5 %). Figure 5.1.1 summarizes the average ratios for all locations for the yearly, monthly and daily values and the variability in time and between the sites.

Site specific results for the average ratios of modelled to measured data are provided in table 5.1.3 for the UV-mapping method and in table 5.1.4 for the ground based modelling.

It should be noted that the largest deviations in the ratios occur when the irradiation levels are low: at low sun or high cloud optical thicknesses (low CMF). This is illustrated in figures 5.1.2–5.1.15 and figures 5.1.16–5.1.23 where a detailed comparison of modelled and measured data is shown for all participating sites that meet the above-mentioned criteria, including also two additional sites from COST action 726 with shorter measurement periods. Figures 5.1.2–5.1.15 provide the results for the mapping method and figures 5.1.16–5.1.23 for the ground based modelling. For each site, three comparison plots deal with the ratio of daily sums (modelled divided by measured). The first plot (left top) gives this ratio for daily sums versus day of the year, the second (left mid) versus the daily UV-sum (average of modelled and measured value) and the third (left below) versus the CMF. Also ratios of monthly sums are plotted versus day of the year to distinguish if seasonal patterns occur. The distribution of the absolute differences between measured and modelled daily UV-doses are presented in a histo plot (right top). In addition, the modelled monthly sums versus the measured sums in the summer period (months May to August) are presented in a correlation plot (right mid). Finally, year to year ratios for the yearly summed UV-doses are shown (right below) to illustrate long term stability in modelled yearly UV-doses compared to measured ones. The results show that the largest variability in the ratios occurs when the sun is low or when the CMF is low (optically thick clouds).

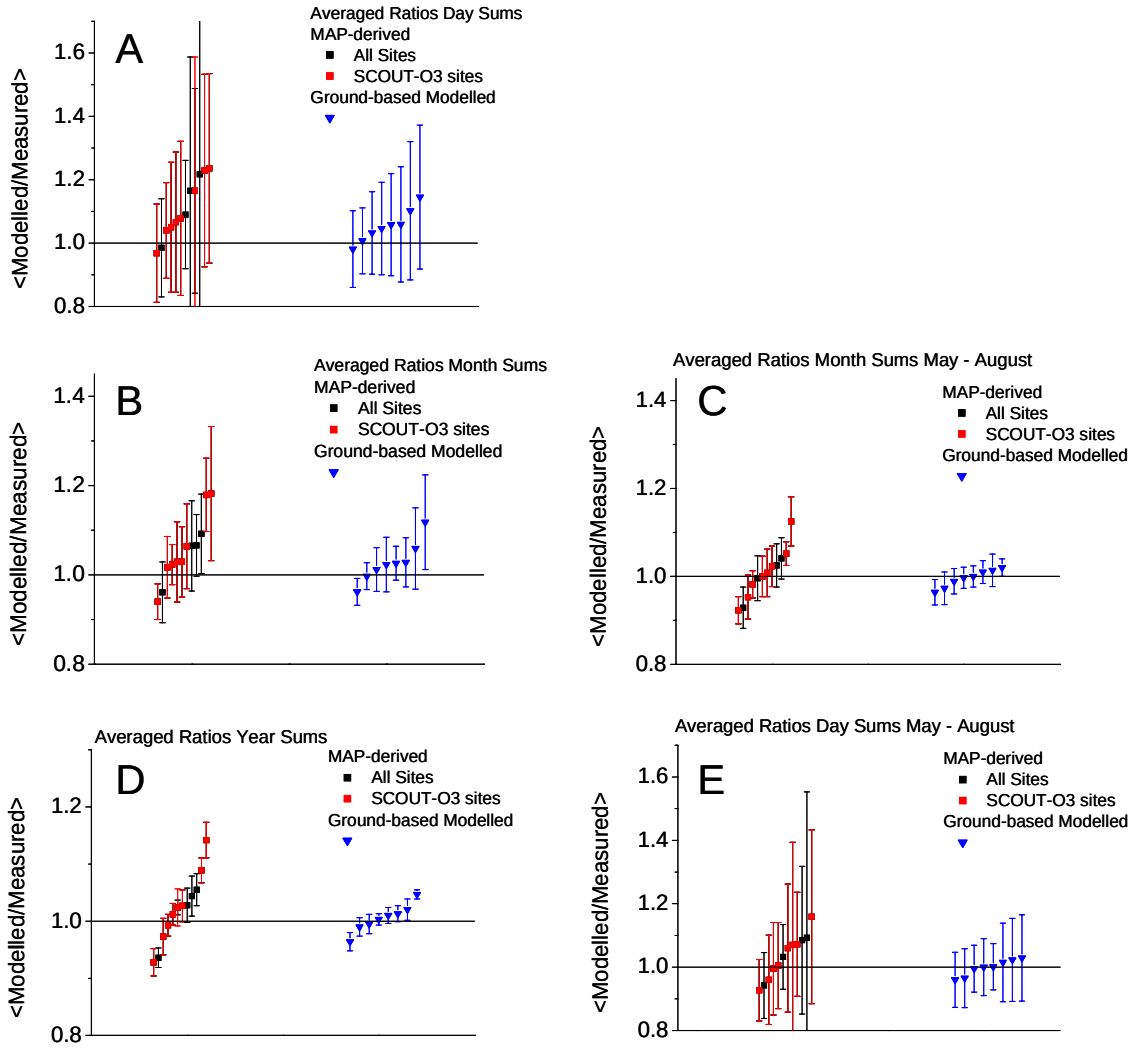

Fig. 5.1.1: Average ratio of modelled to measured UV for all sites. In each graph the red and black data on the left refer to the COST-mapping method, and the blue triangles refer to the RIVM ground based modelling. Graph A refers to the ratio of yearly UV-sums, graph B the ratio of monthly UV-sums all year round and C the summer months May to August only, D the daily ratios for all days in the year and E the daily ratios for the summer period only (months May-August). Error bars give the variability in time for each site. Results are summarised from tables 5.1.3 and 5.1.4.

Table 5.1.3: Station specific summary of modelled to measured ratio for COST-UV-mapping method and variations for daily, monthly and yearly UV-sums

Station	Day [d]	sdday [e]	Month [f]	sdmonth [g]	Year [h]	sdyear [i]
Sodankyla [a]	2382+1		88	-	12	-
Ave_Ratio [b]	1.066	0.221	1.029	0.079	1.024	0.013
Ave_Ratio_summer [c]	1.06	0.202	1.023	0.046	-	-
Jokioinen	2295+0		84	-	8	-
Ave_Ratio	1.05	0.205	1.017	0.069	0.993	0.019
Ave_Ratio_summer	0.995	0.146	0.982	0.031	-	-
Norrkoping	7111+13		234	-	20	-
Ave_Ratio	1.165	0.422	1.064	0.095	1.027	0.028
Ave_Ratio_summer	1.07	0.324	1.008	0.054	-	-
Potsdam	2177+1		76	-	7	-
Ave_Ratio	1.078	0.243	1.029	0.090	0.973	0.032
Ave_Ratio_summer	0.96	0.141	0.953	0.050	-	-
Lindenberg	1895+0		71	-	8	-
Ave_Ratio	0.968	0.155	0.94	0.040	0.928	0.024
Ave_Ratio_summer	0.927	0.097	0.923	0.031	-	-
Bilthoven	2811+2		97	-	9	-
Ave_Ratio	1.04	0.151	1.023	0.045	1.012	0.019
Ave_Ratio_summer	1.005	0.136	1	0.046	-	-
Hradec Kralove	2396+6		80	-	7	-
Ave_Ratio	1.229	0.304	1.182	0.150	1.089	0.022
Ave_Ratio_summer	1.072	0.164	1.052	0.027	-	-
Thessaloniki	3728+23		133	-	11	-
Ave_Ratio	1.236	0.299	1.179	0.082	1.142	0.031
Ave_Ratio_summer	1.159	0.274	1.125	0.056	-	-
Bergen	2156+3		72	-	7	-
Ave_Ratio	1.165	0.323	1.092	0.089	1.055	0.028
Ave_Ratio_summer	1.085	0.233	1.041	0.047	-	-
Belsk	8577+1		307	-	27	-
Ave_Ratio	1.09	0.171	1.066	0.069	1.044	0.035
Ave_Ratio_summer	1.032	0.102	1.025	0.049	-	-
Davos	2384+4		80	-	7	-
Ave_Ratio	0.985	0.155	0.961	0.068	0.936	0.017
Ave_Ratio_summer	0.942	0.104	0.929	0.047	-	-
Ispra	2795	116	100	-	8	-
Ave_Ratio	1.217	0.577	1.065	0.101	1.028	0.03
Ave_Ratio_summer	1.093	0.46	0.996	0.051	-	-

a) Total days in analysis + total days taken out of analysis because model/measured < 0.25 or model/measured > 4
b) Average Ratio: Modelled Sum / Measured Sum
c) Average Ratio: Modelled Sum / Measured Sum, May - August only
d) Daily sums
e) Standard deviation in average or difference
f) Monthly sums, data supplemented, 15 days minimum
g) Standard deviation in average or difference
h) Yearly sums, data supplemented, 220 days/year minimum, N.B. not applied to Sodankyla
i) Standard deviation in average or difference

Table 5.1.4: Station specific summary of modelled to measured ratio for ground based UV-model from RIVM and variations for daily, monthly and yearly UV-sums

Station	Day [d]	sdday [e]	Month [f]	sdmonth [g]	Year [h]	sdyear [i]
Sodankyla [a]						
Ave_Ratio [b]	1.06	0.16	1.02	0.02	1.01	
Ave_Ratio_summer [c]	1.04	0.14	1.01	0.04		
Jokioinen						
Ave_Ratio	1.06	0.18	1.03	0.06	1.013	0.014
Ave_Ratio_summer	1.02	0.17	1.01	0.026		
Norrkoping						
Ave_Ratio	1.10	0.22	1.06	0.09	1.01	0.014
Ave_Ratio_summer						
Potsdam						
Ave_Ratio	1.05	0.15	1.02	0.06	0.99	0.016
Ave_Ratio_summer	0.97	0.09	0.97	0.04		
Lindenberg						
Ave_Ratio	0.98	0.12	0.96	0.03	0.964	0.016
Ave_Ratio_summer	0.96	0.09	0.96	0.03		
Bilthoven						
Ave_Ratio	1.00	0.10	1.00	0.03	1.003	0.010
Ave_Ratio_summer	1.00	0.09	1.00	0.02		
Hradec Kralove						
Ave_Ratio	1.15	0.23	1.12	0.11	1.047	0.008
Ave_Ratio_summer	1.02	0.13	1.02	0.02		
Thessaloniki						
Ave_Ratio	1.03	0.13	1.01	0.05	0.995	0.017
Ave_Ratio_summer	0.99	0.07	0.99	0.03		

a) Total days in analysis + total days taken out of analysis because model/measured < 0.25 or model/measured > 4
b) Average Ratio: Modelled Sum / Measured Sum
c) Average Ratio: Modelled Sum / Measured Sum, May - August only
d) Daily sums
e) Standard deviation in average or difference
f) Monthly sums, data supplemented, 15 days minimum
g) Standard deviation in average or difference
h) Yearly sums, data supplemented, 220 days/year minimum, N.B. not applied to Sodankyla
i) Standard deviation in average or difference

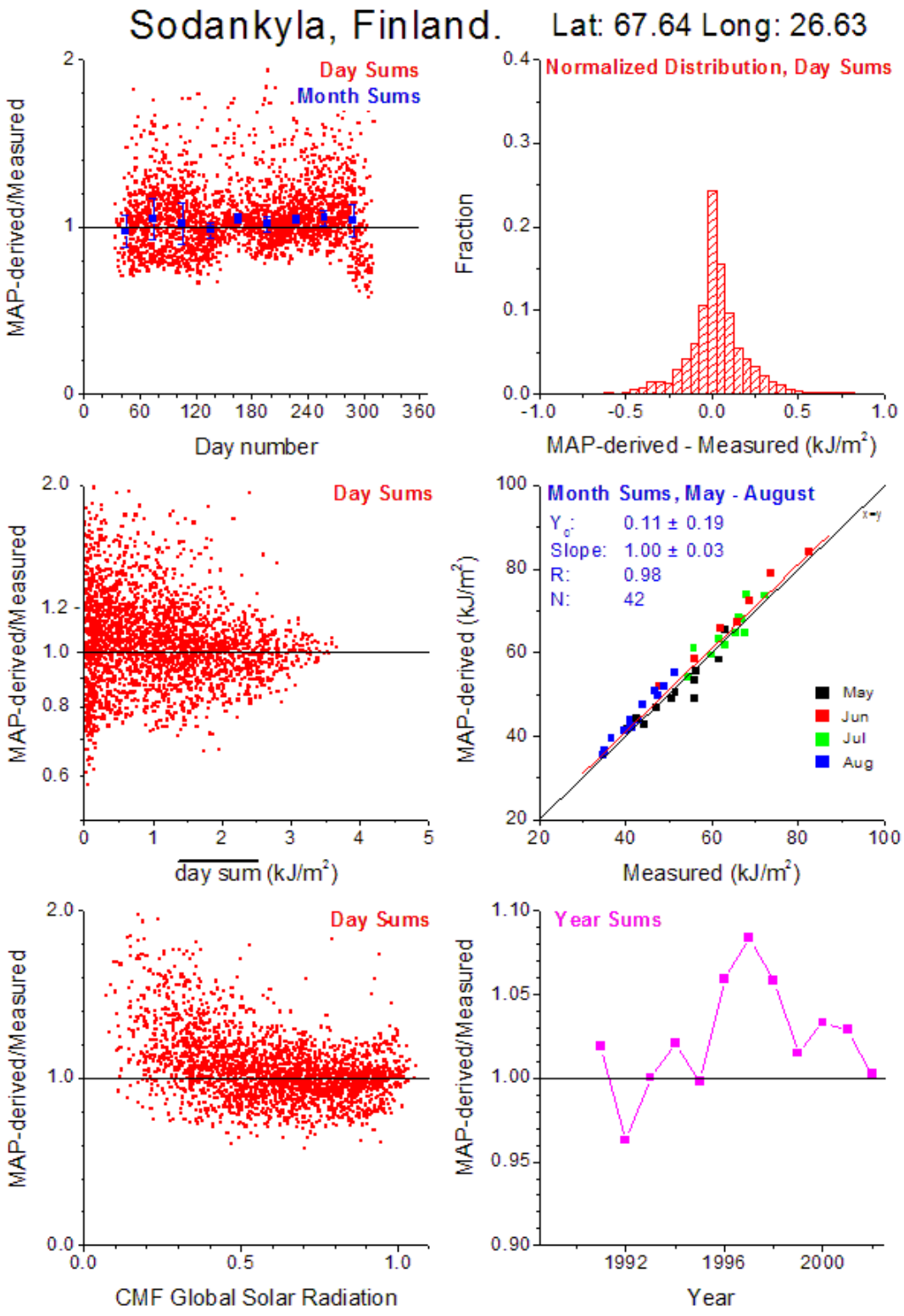

Fig. 5.1.2: Detailed results for the comparison of measured and modelled UV-doses. Results are for COST UV-mapping modelled for Sodankyla, Finland.

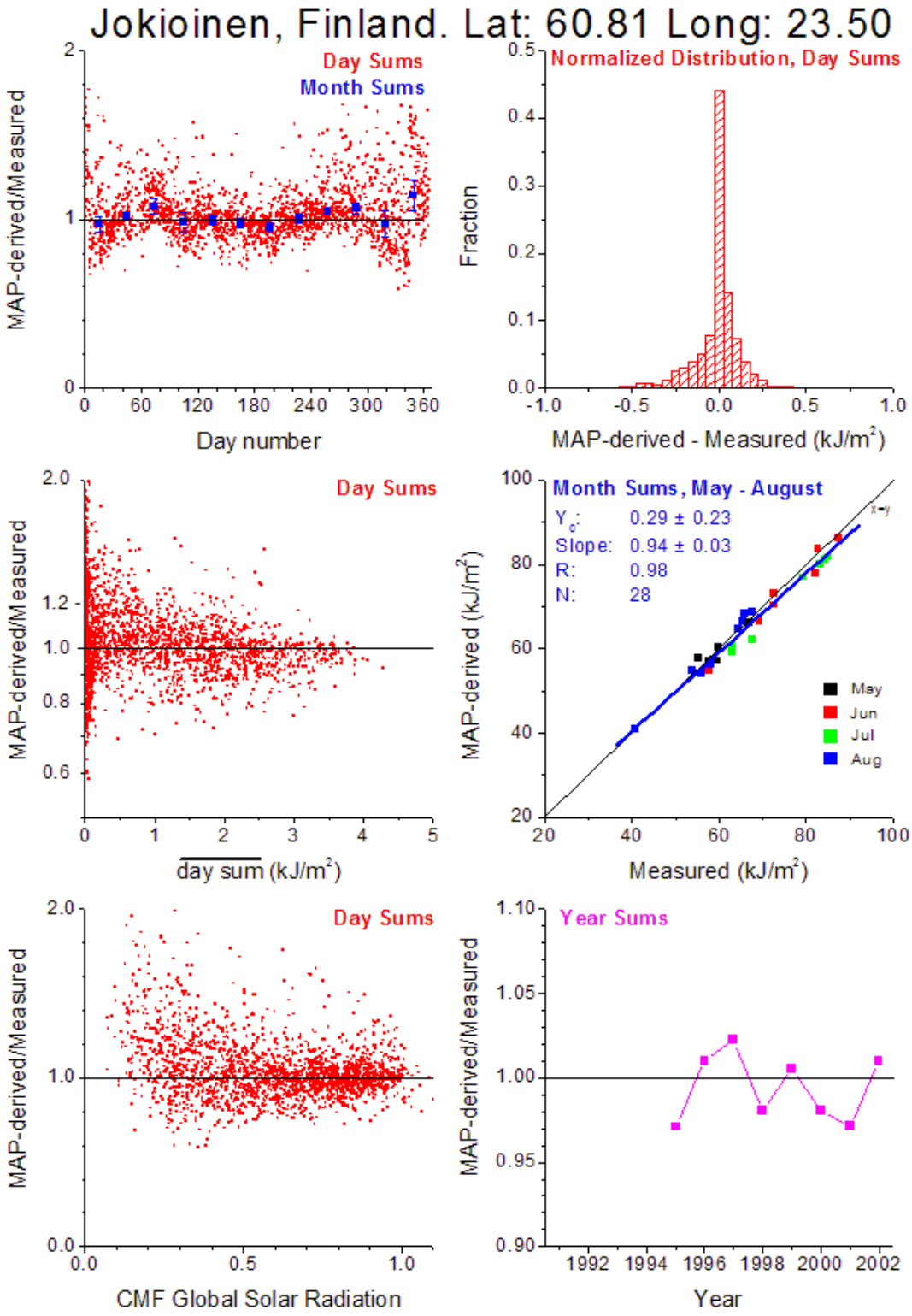

Fig. 5.1.3: Same as figure 5.1.2 for Jokioinen, Finland.

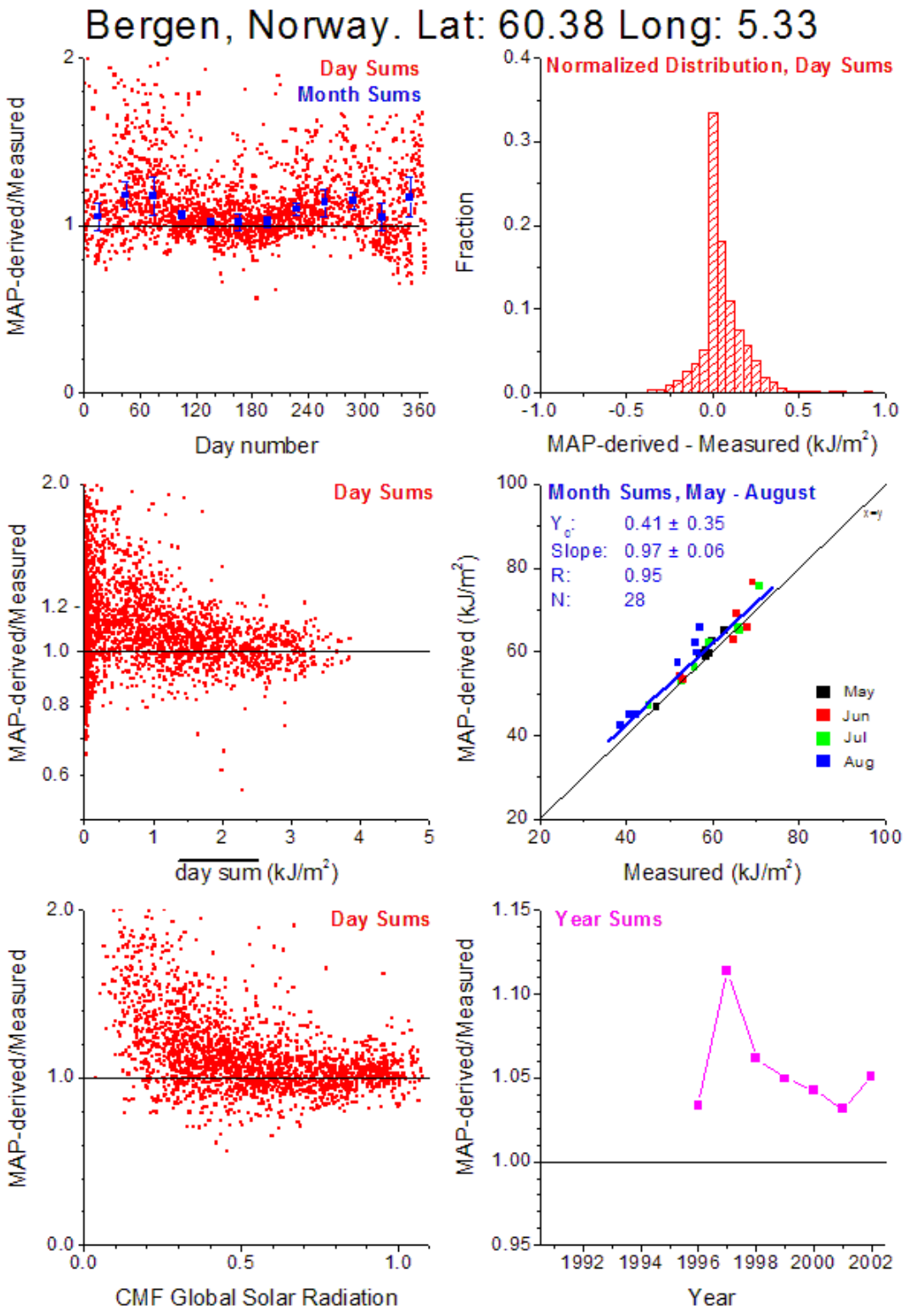

Fig. 5.1.4: Same as figure 5.1.2 for Bergen, Norway.

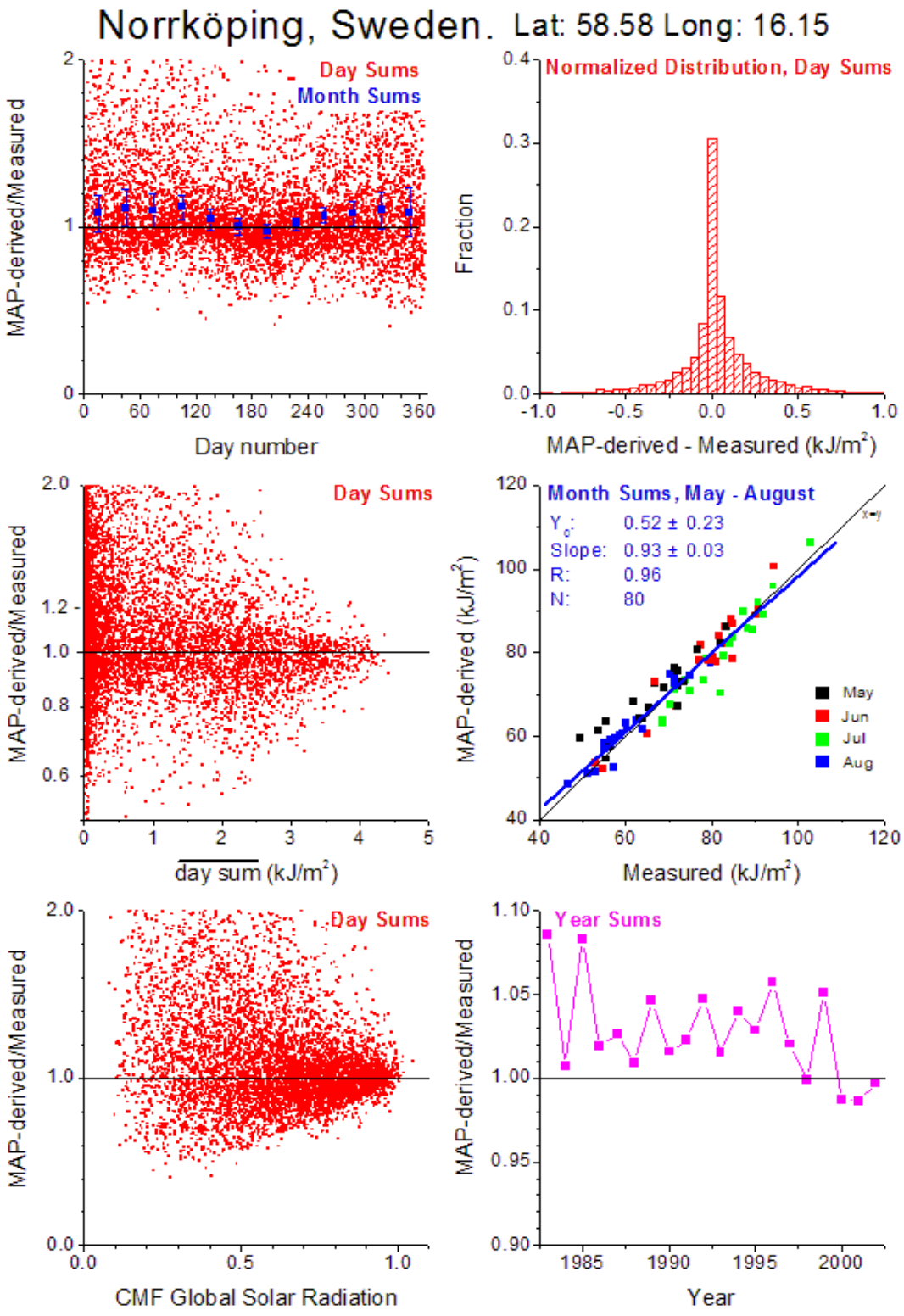

Fig. 5.1.5: Same as figure 5.1.2 for Norrköping, Sweden.

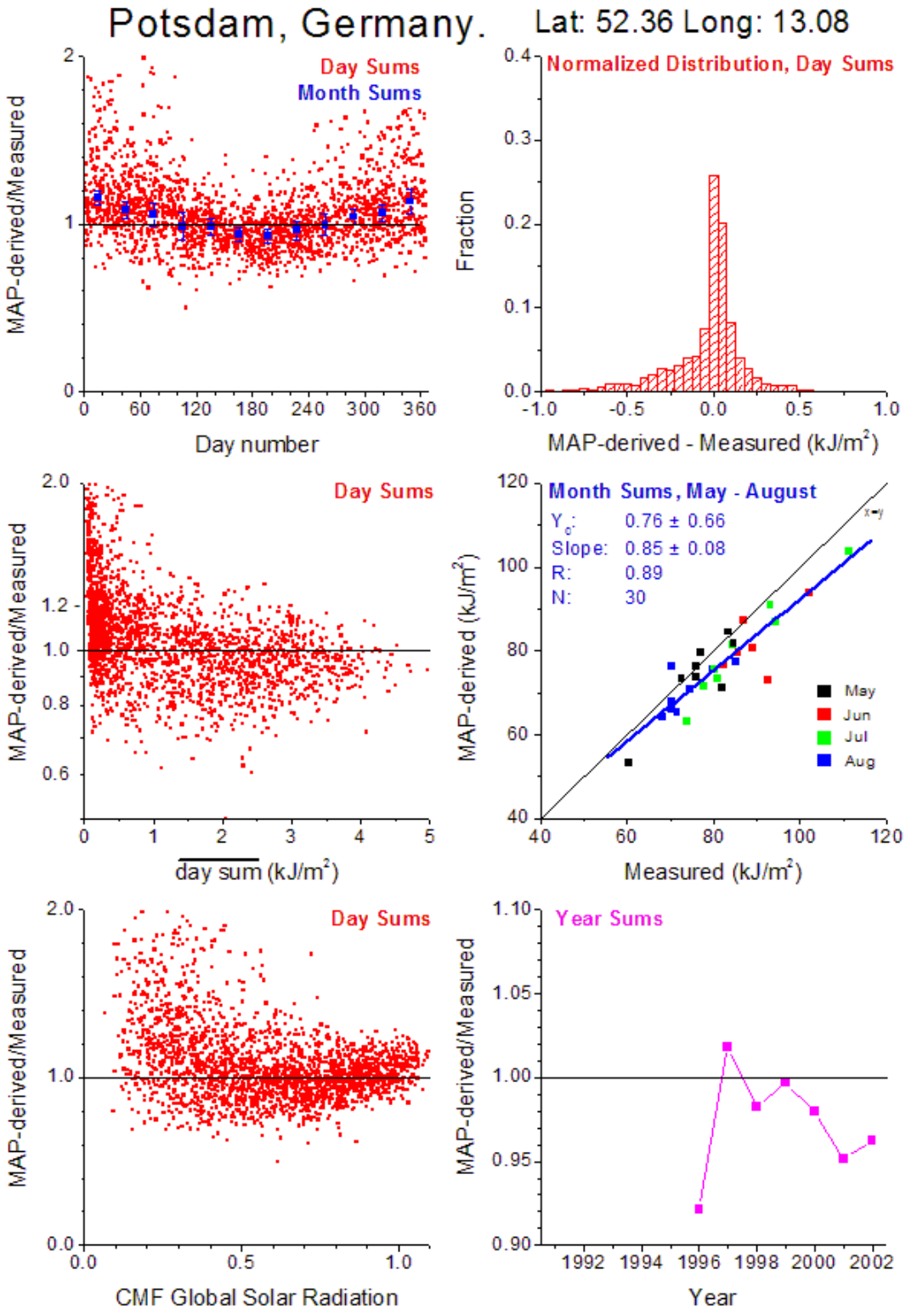

Fig. 5.1.6: Same as figure 5.1.2 for Potsdam, Germany.

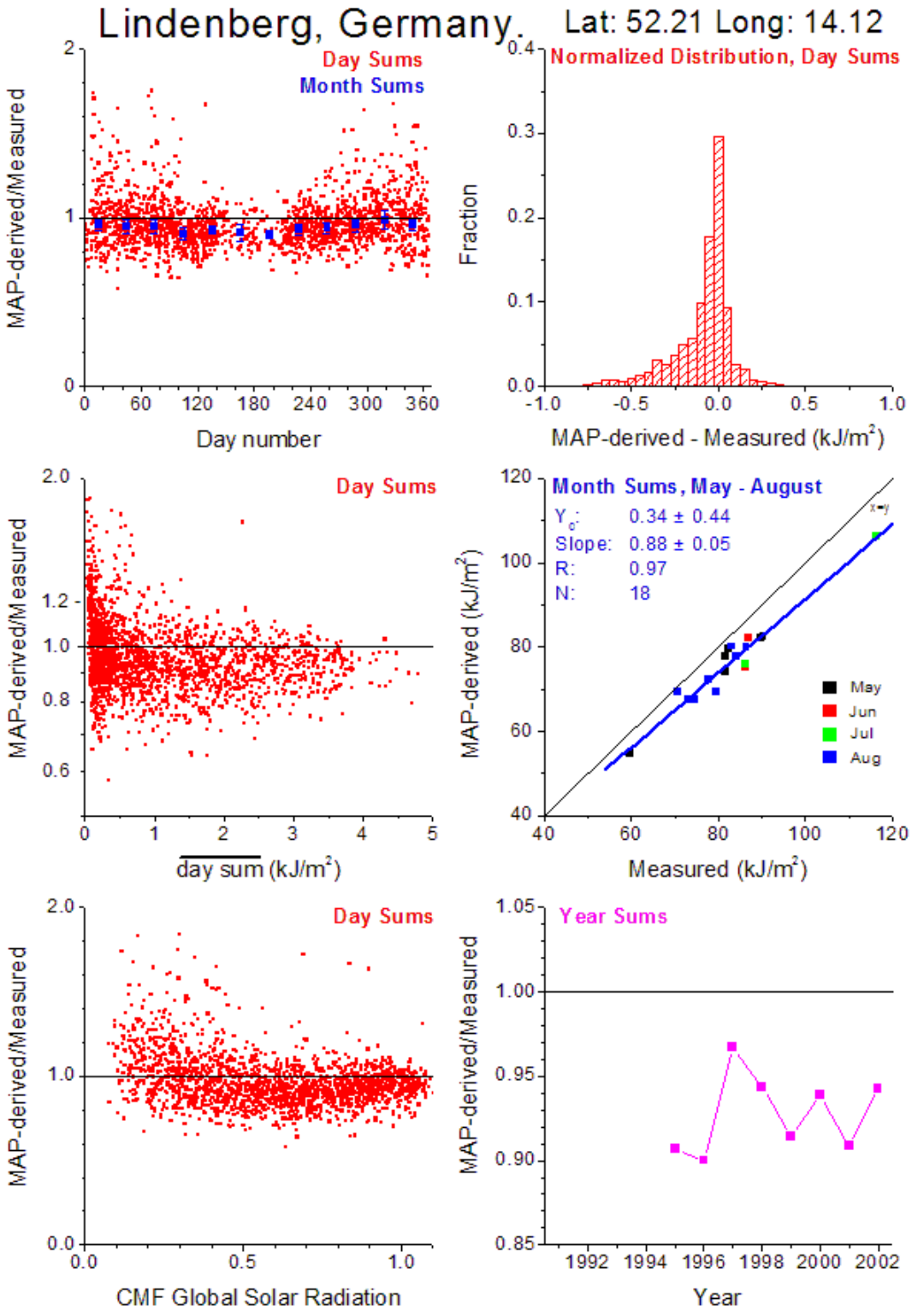

Fig. 5.1.7: Same as figure 5.1.2 for Lindenberg, Germany.

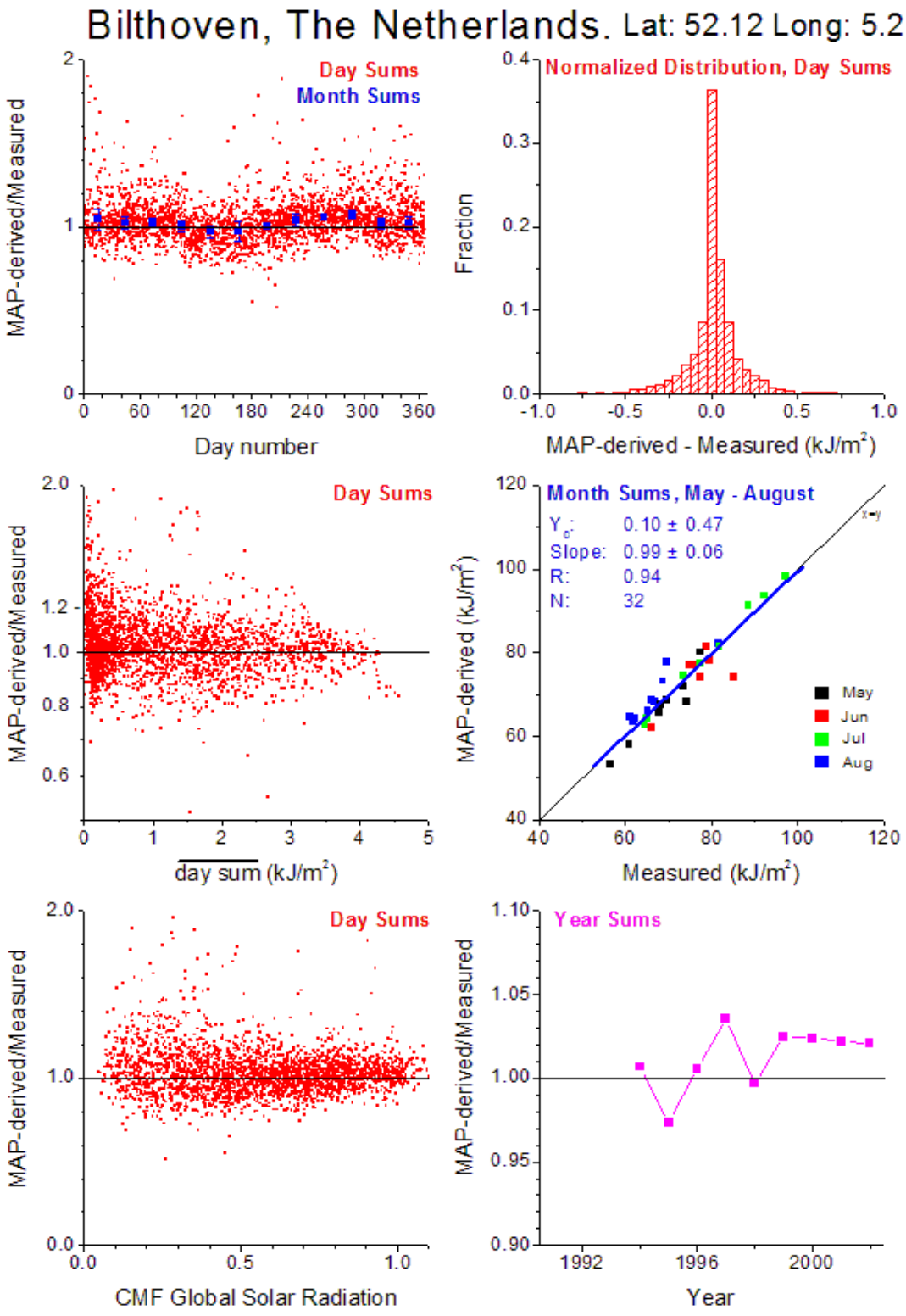

Fig. 5.1.8: Same as figure 5.1.2 for Bilthoven, The Netherland.

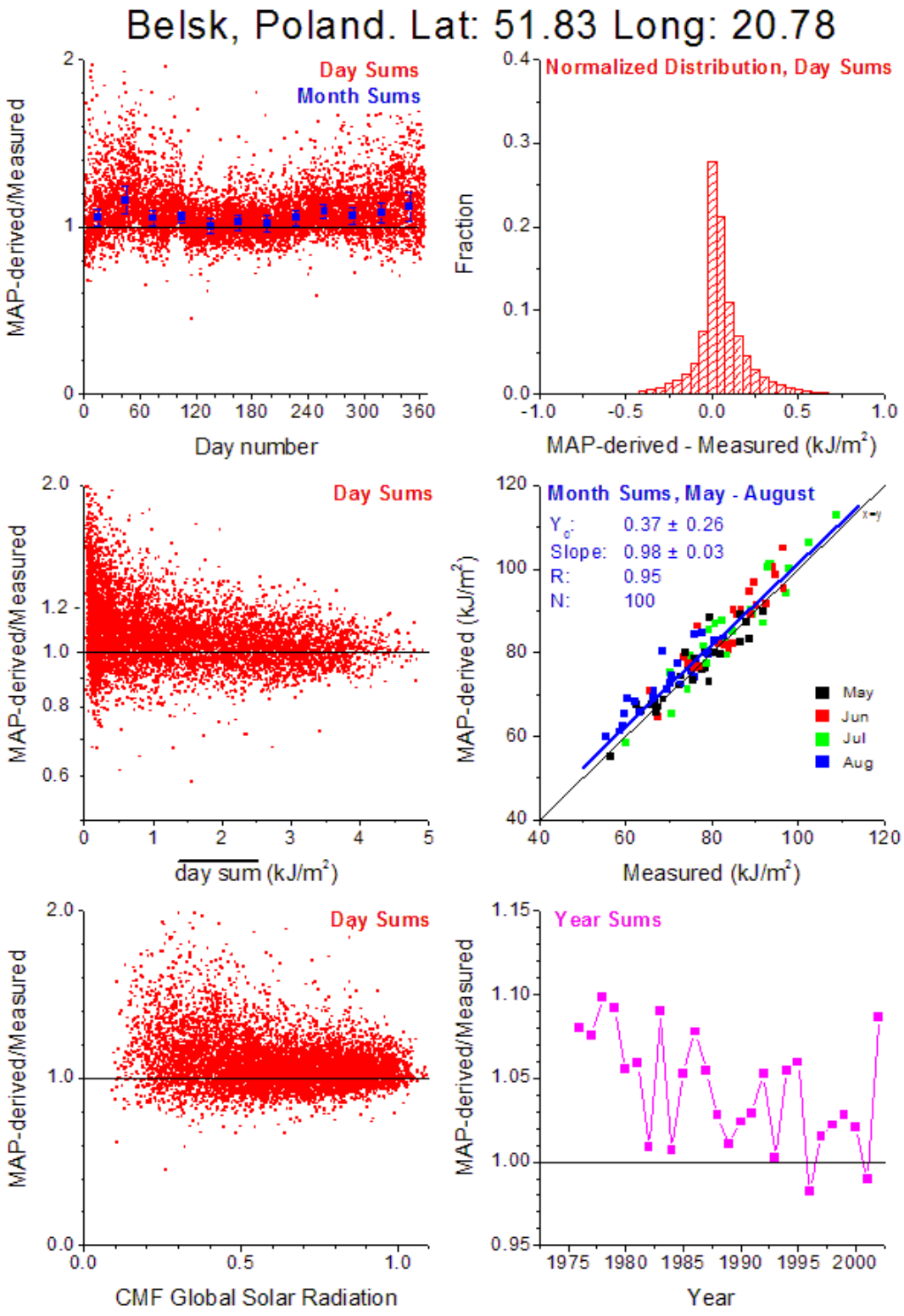

Fig. 5.1.9: Same as figure 5.1.2 for Belsk, Poland.

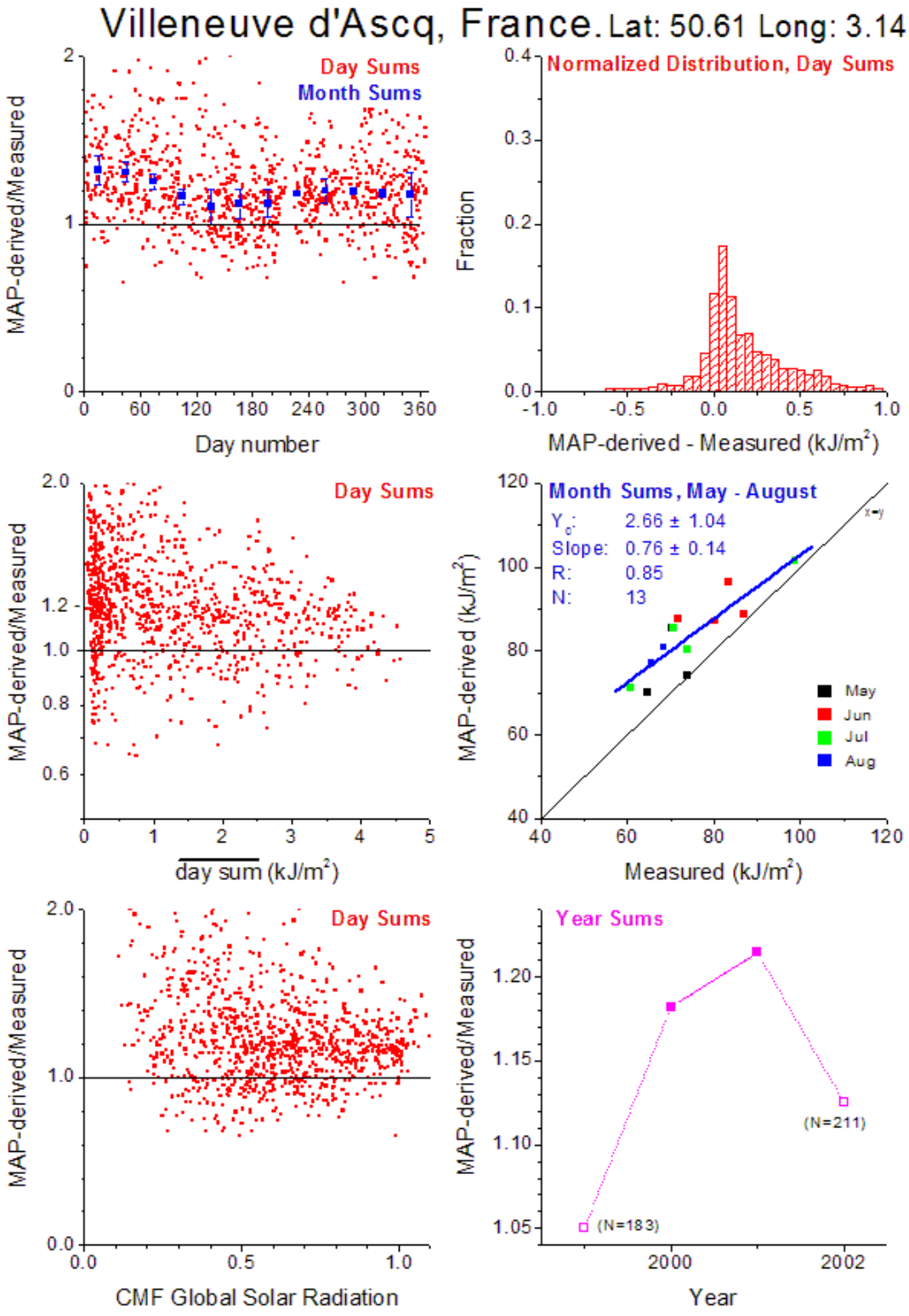

Fig. 5.1.10: Same as figure 5.1.2 for Villeneuve d'Ascq, France.

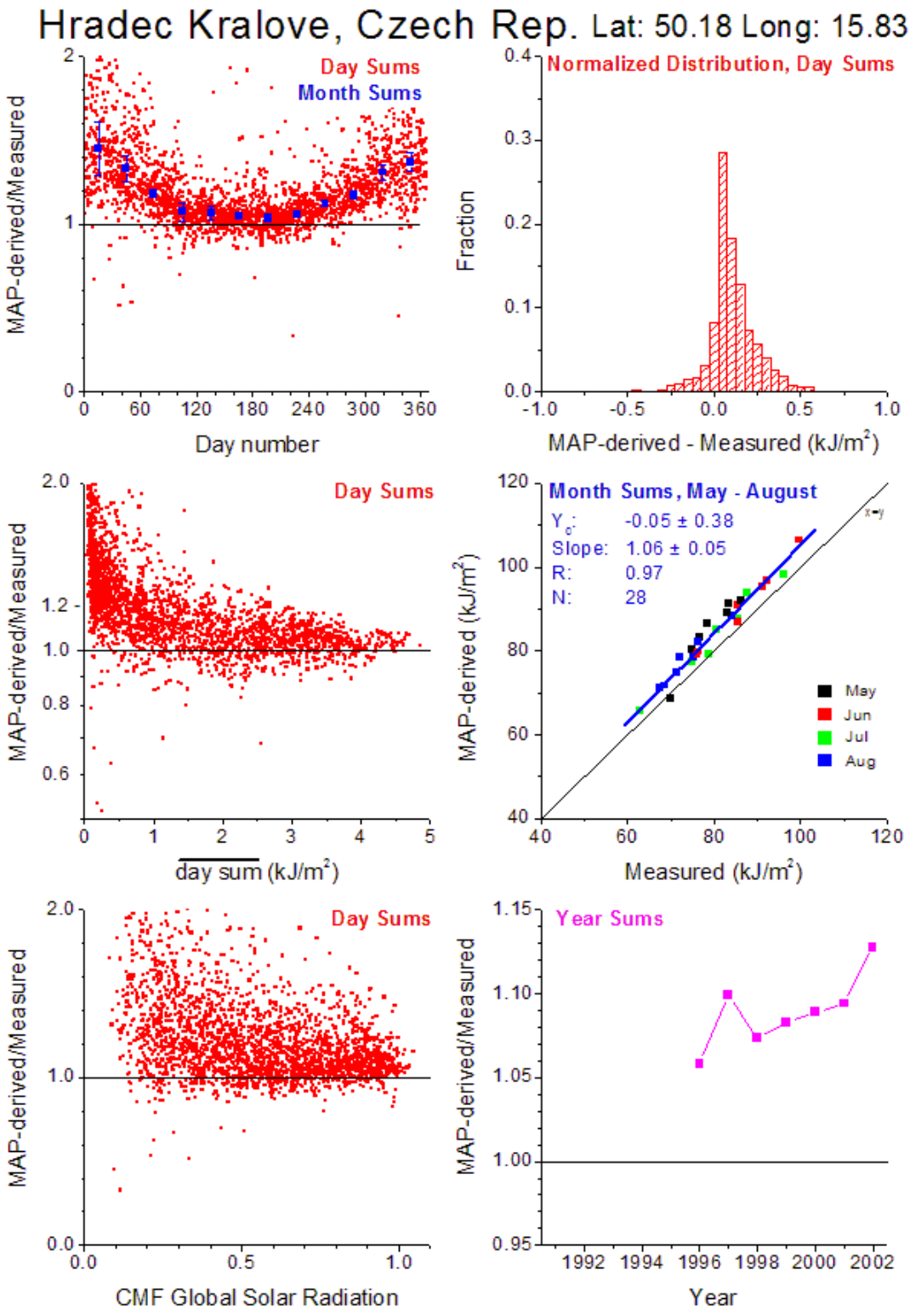

Fig. 5.1.11: Same as figure 5.1.2 for Hradec Kralove, Czech Republic.

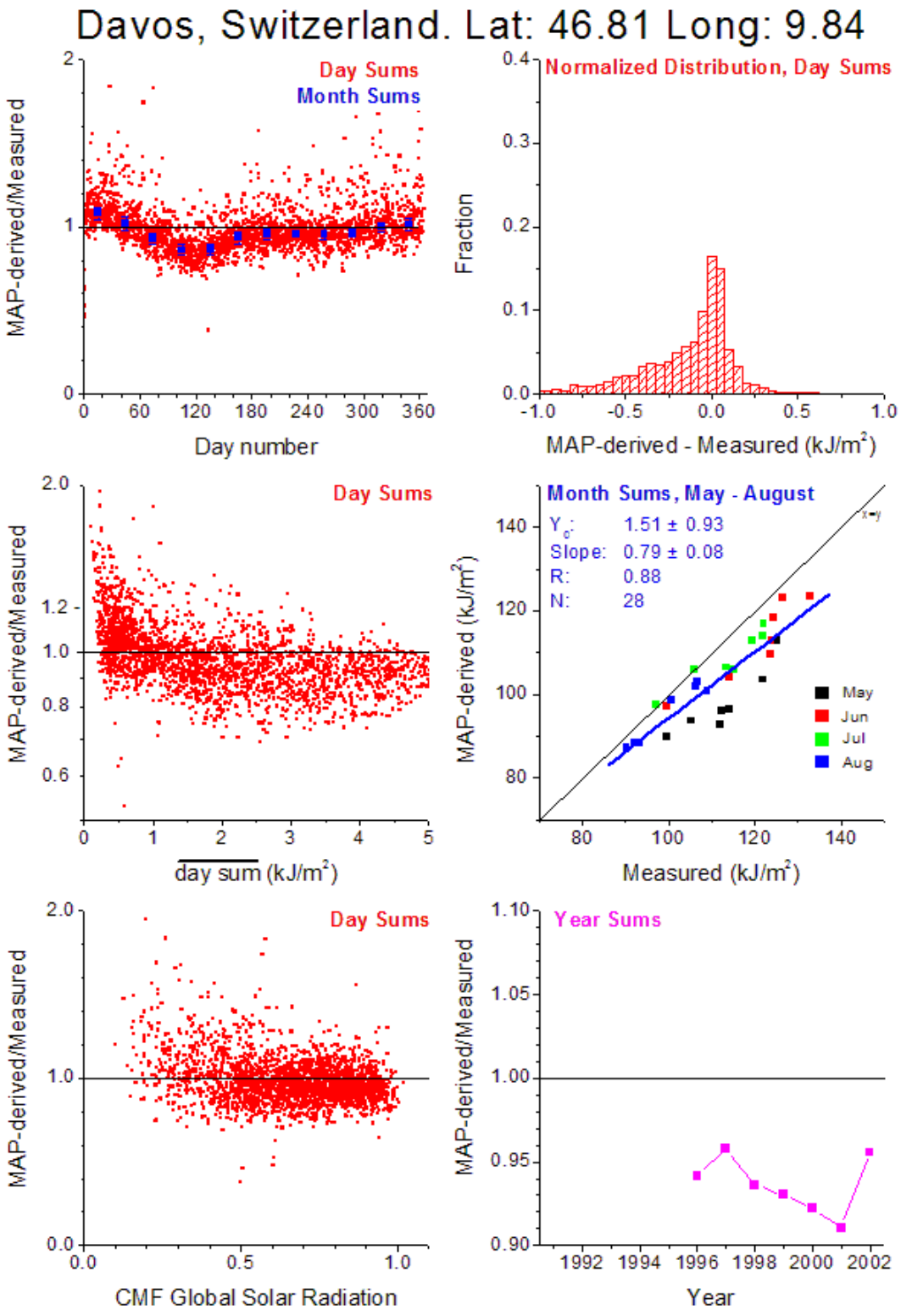

Fig. 5.1.12: Same as figure 5.1.2 for Davos, Switzerland.

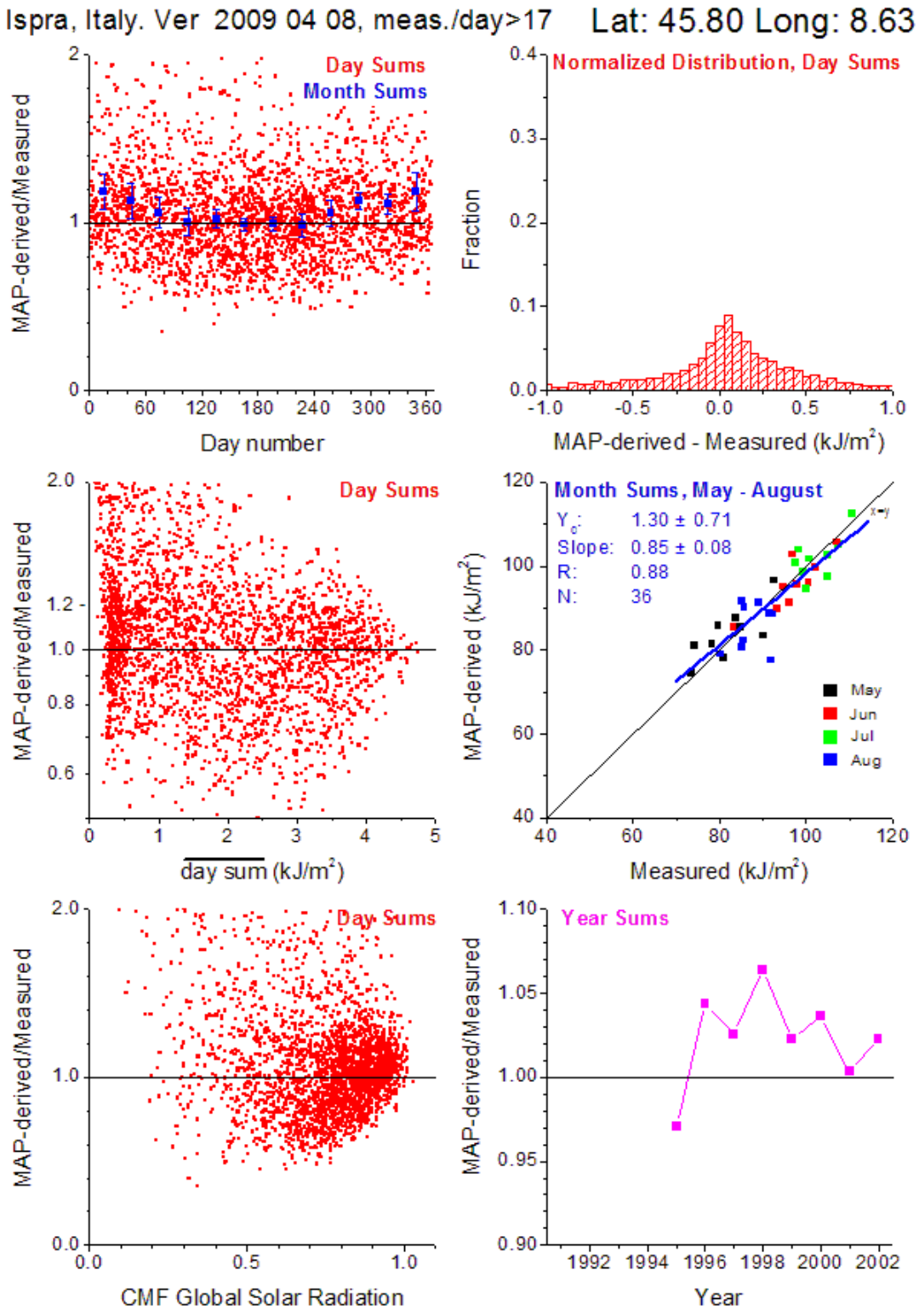

Fig. 5.1.13: Same as figure 5.1.2 for Ispra, Italy.

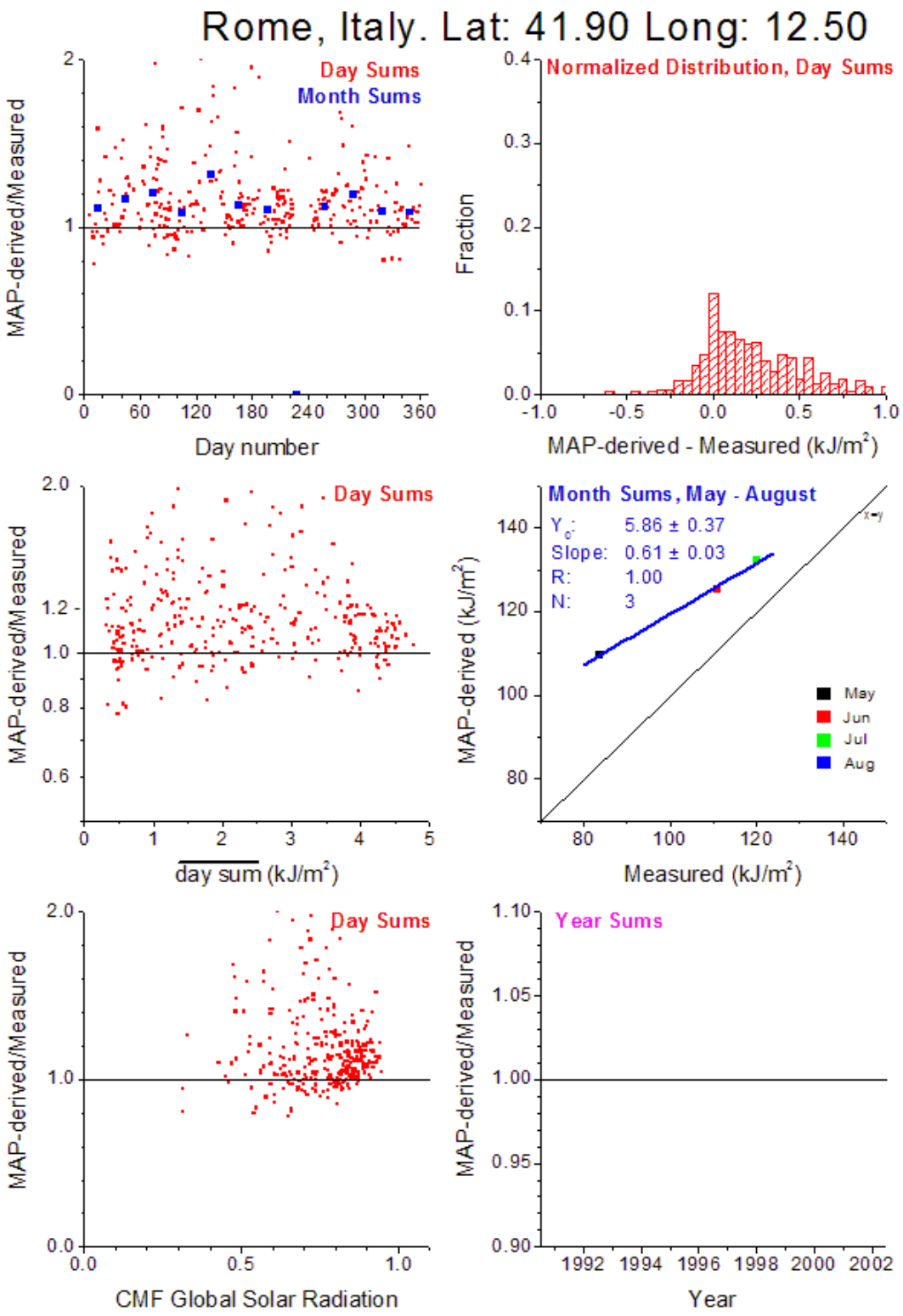

Fig. 5.1.14: Same as figure 5.1.2 for Rome, Italy.

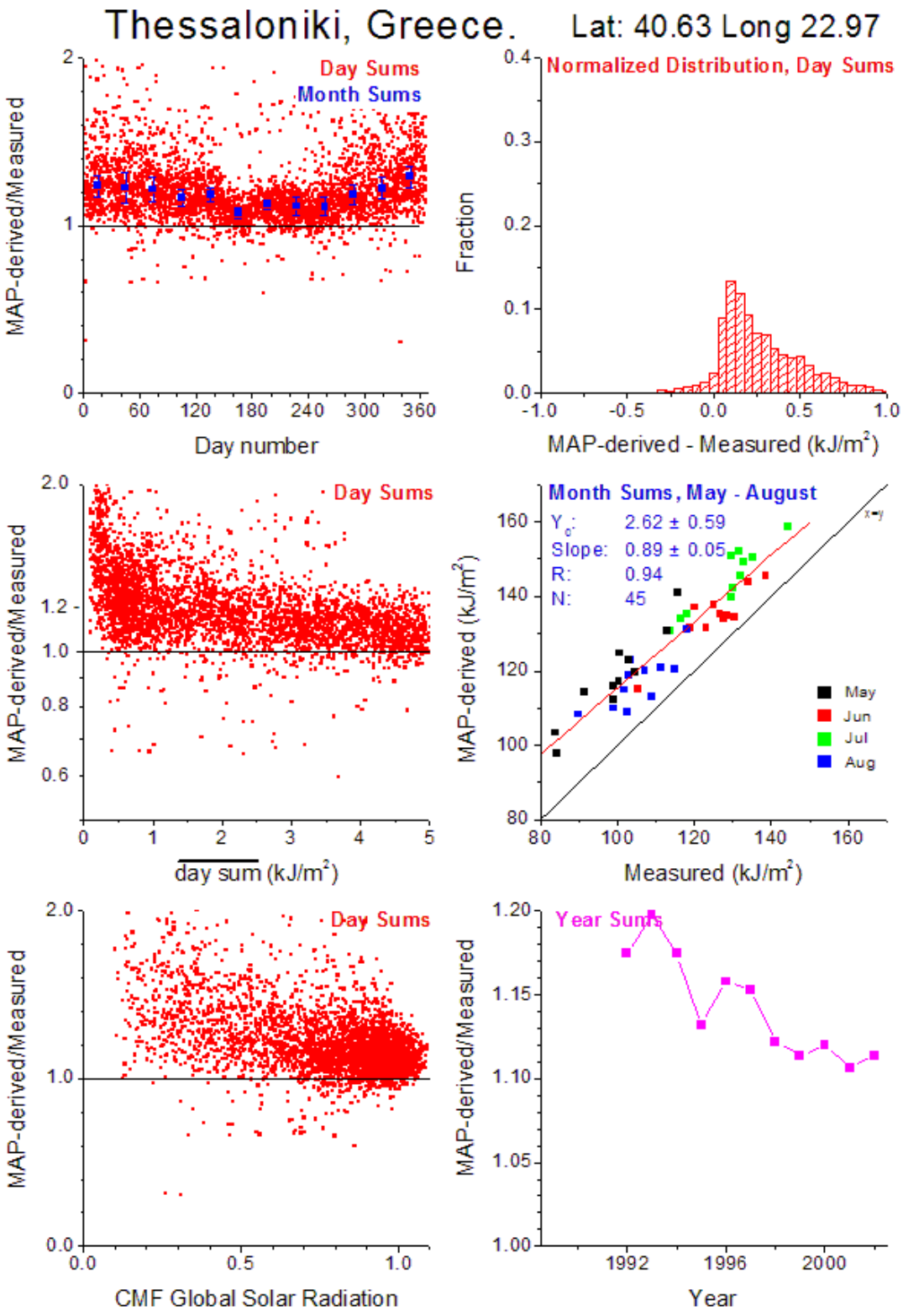

Fig. 5.1.15: Same as figure 5.1.2 for Thessaloniki, Grece

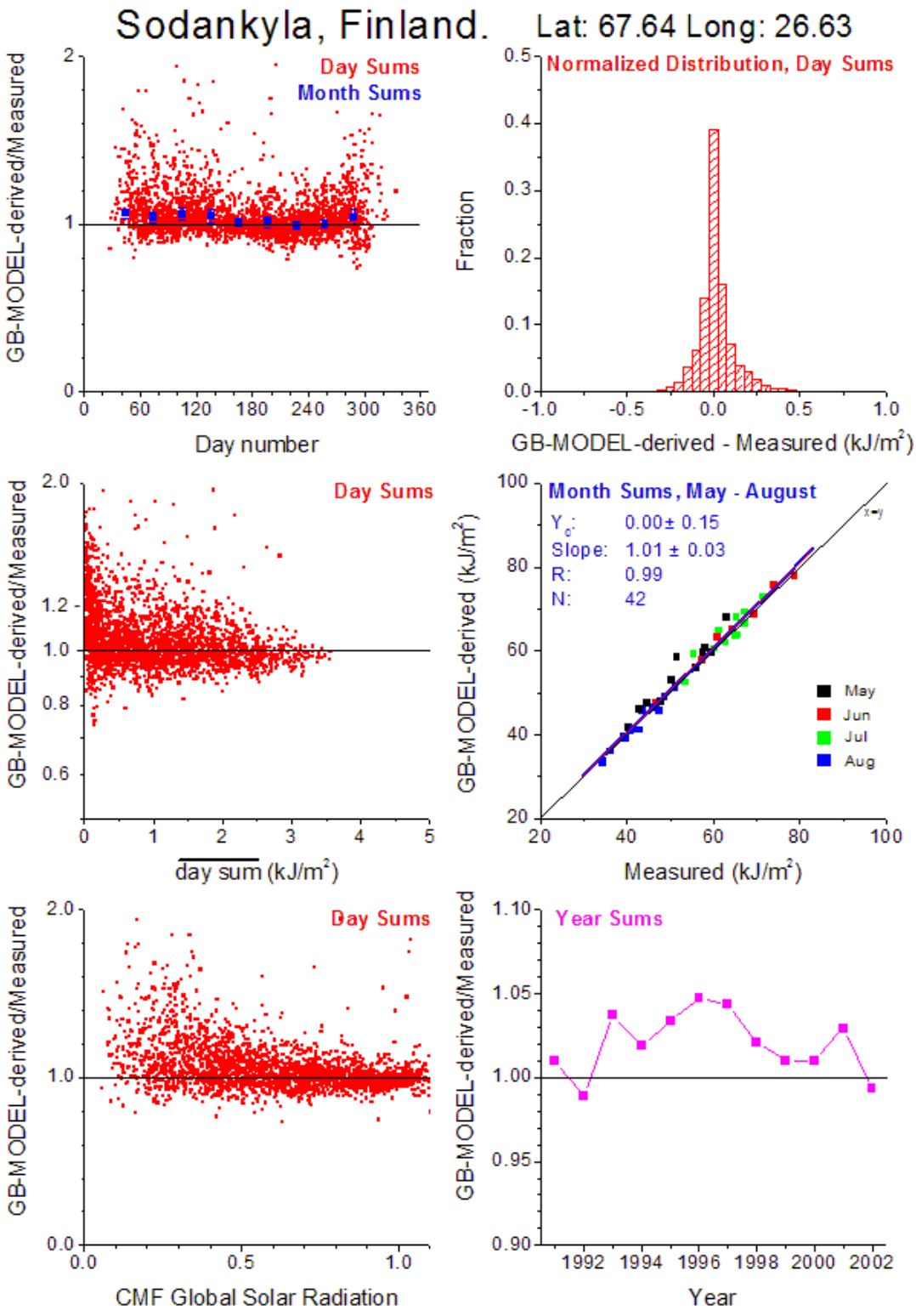

Fig. 5.1.16: Detailed results for the comparison of measured and modelled UV-doses. Results are for ground based modelling using the RIVM model technique (den Outer, 2005) for Sodankyla, Finland.

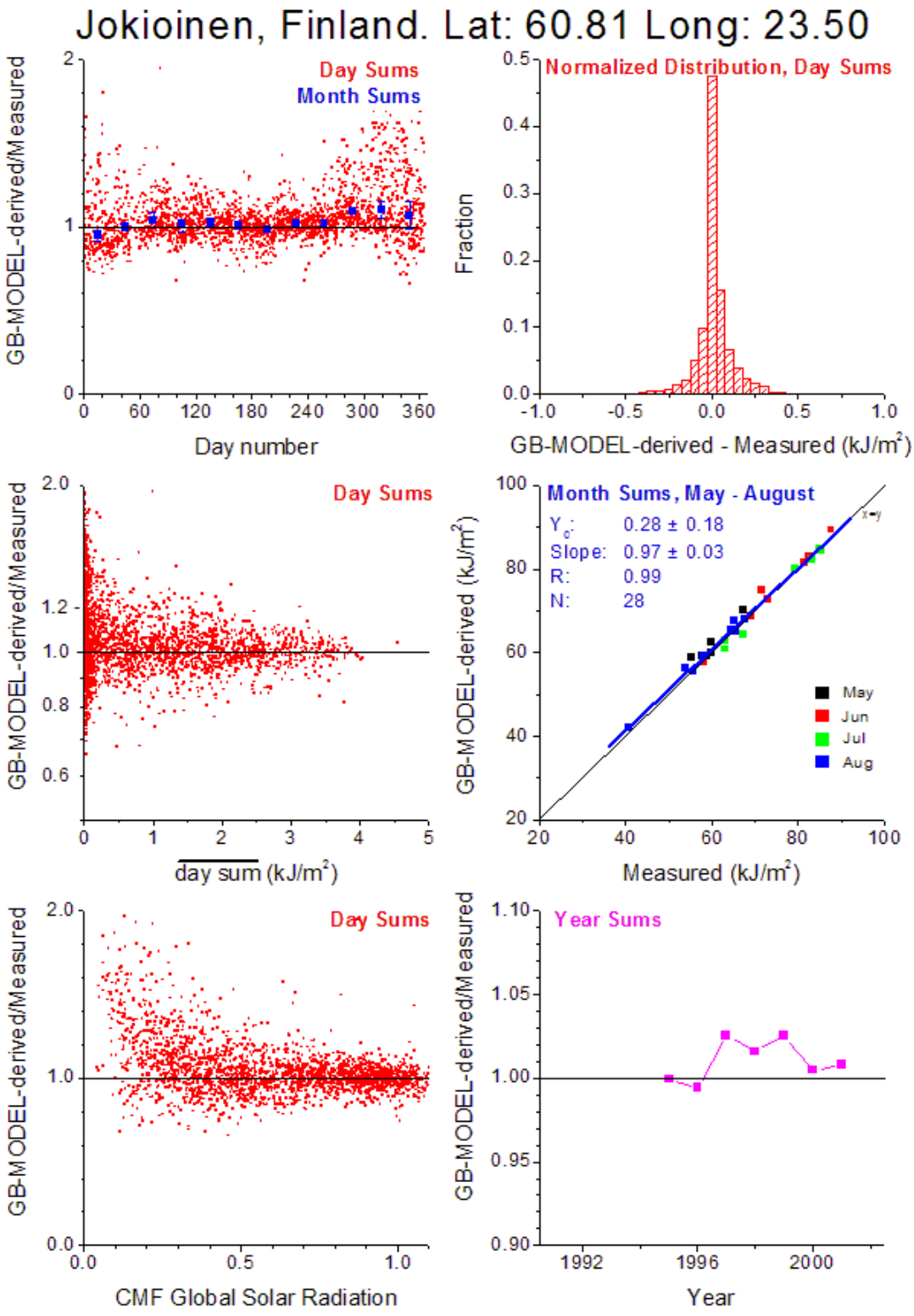

Fig. 5.1.17: Same as figure 5.1.16 for Jokioinen, Finland.

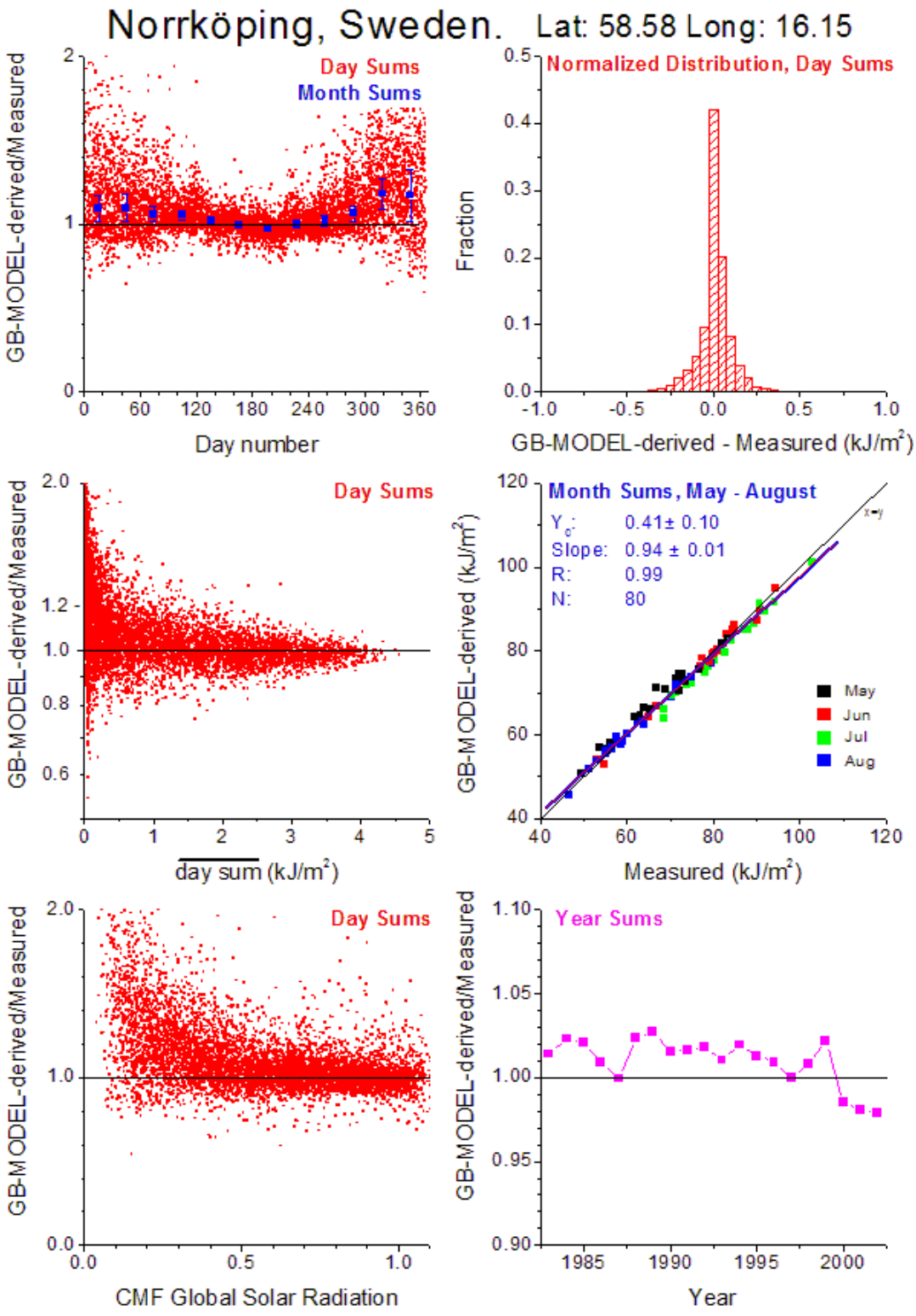

Fig. 5.1.18: Same as figure 5.1.16 for Norrköping, Sweden.

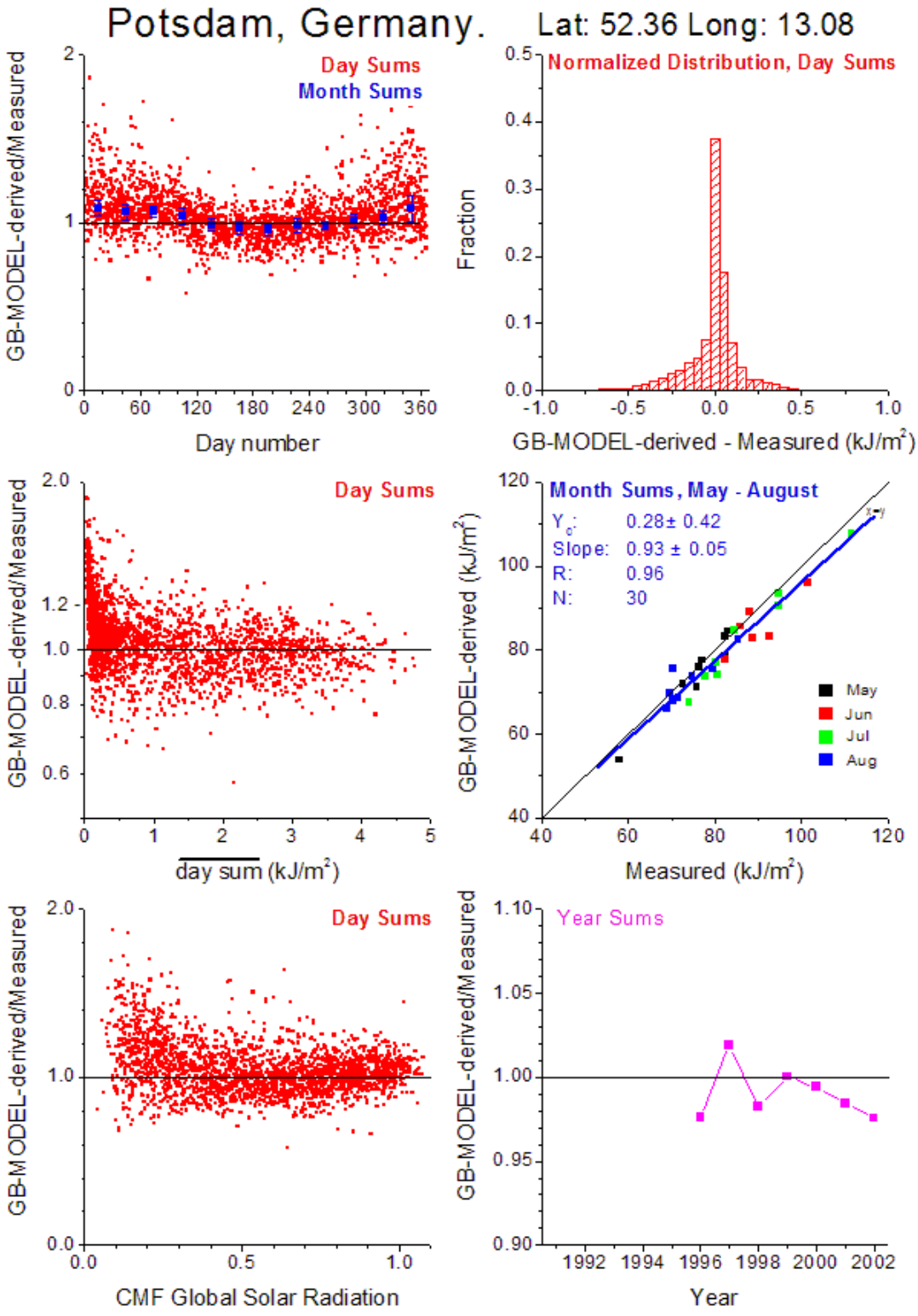

Fig. 5.1.19: Same as figure 5.1.16 for Potsdam, Germany.

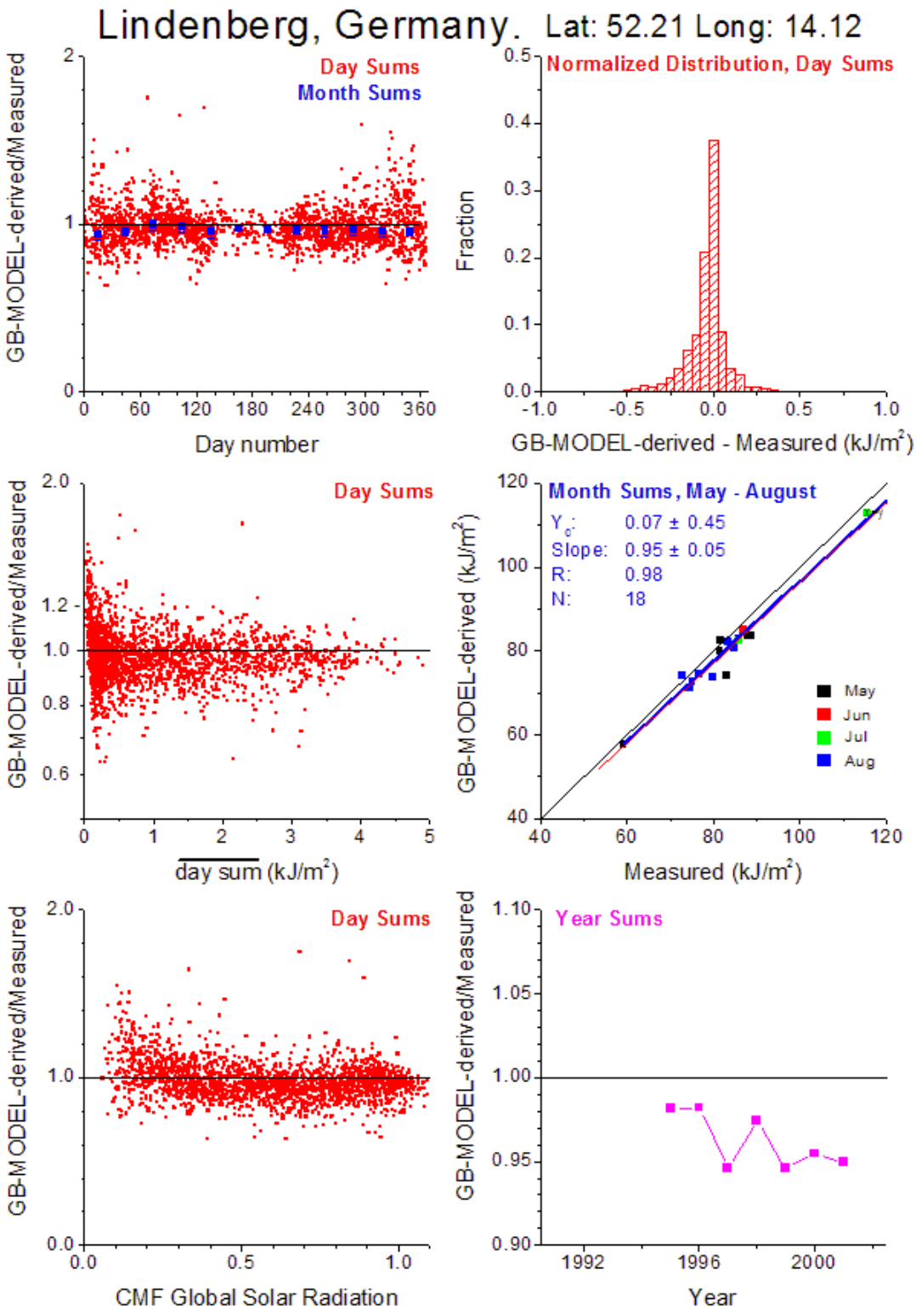

Fig. 5.1.20: Same as figure 5.1.16 for Lindenberg, Germany.

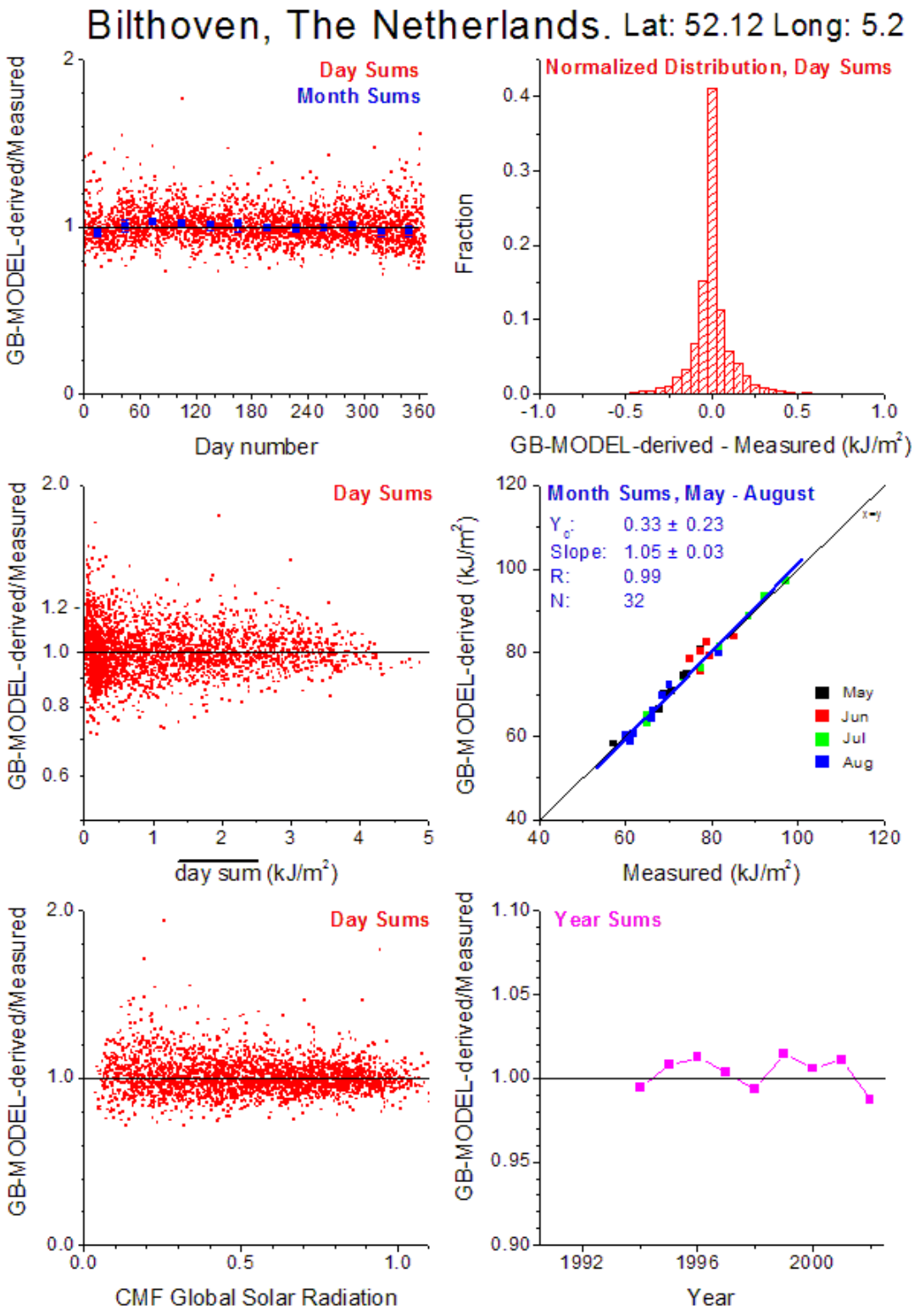

Fig. 5.1.21: Same as figure 5.1.16 for Bilthoven, The Netherland.

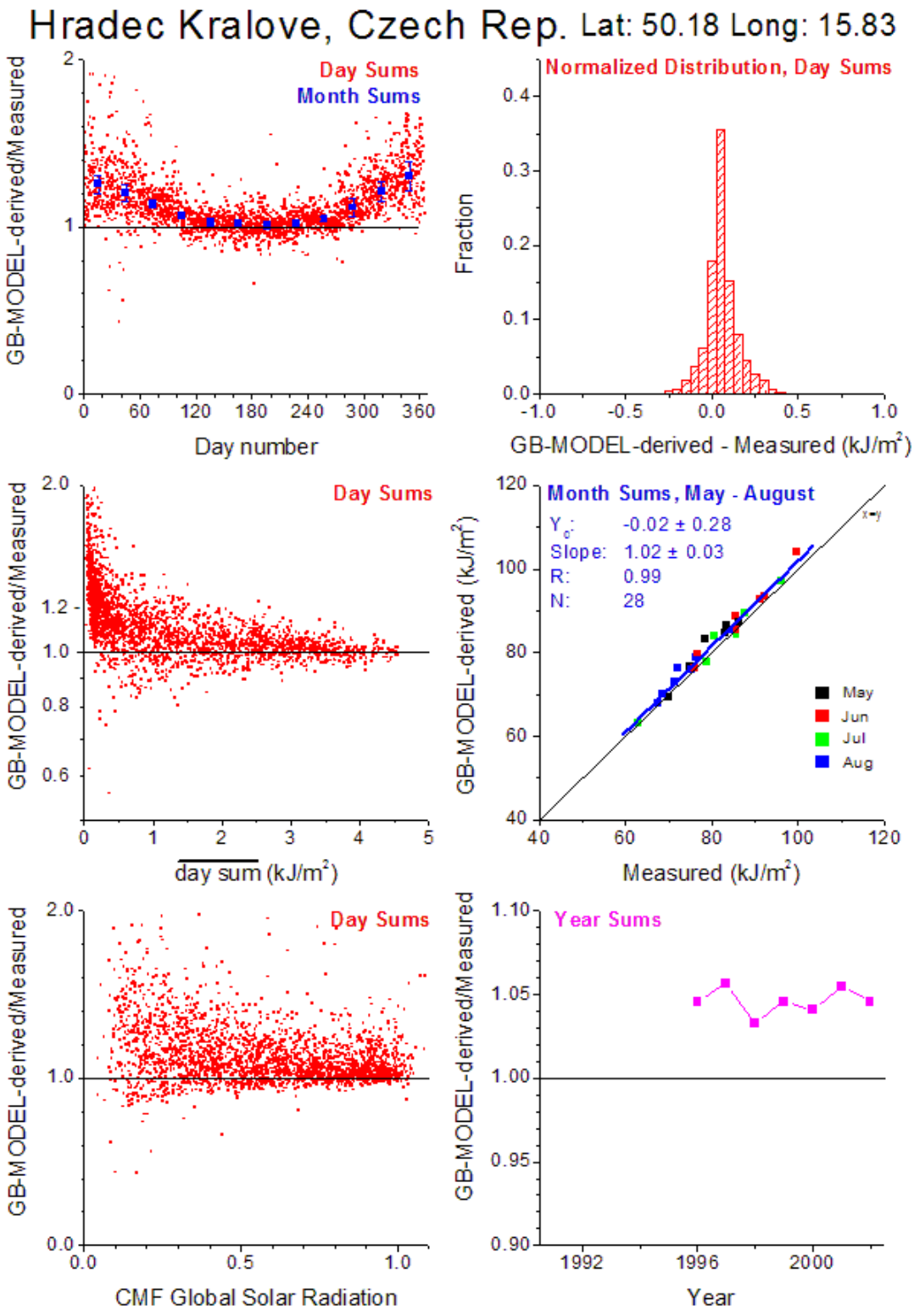

Fig. 5.1.22: Same as figure 5.1.16 for Hradec Kralove, Czech Republic.

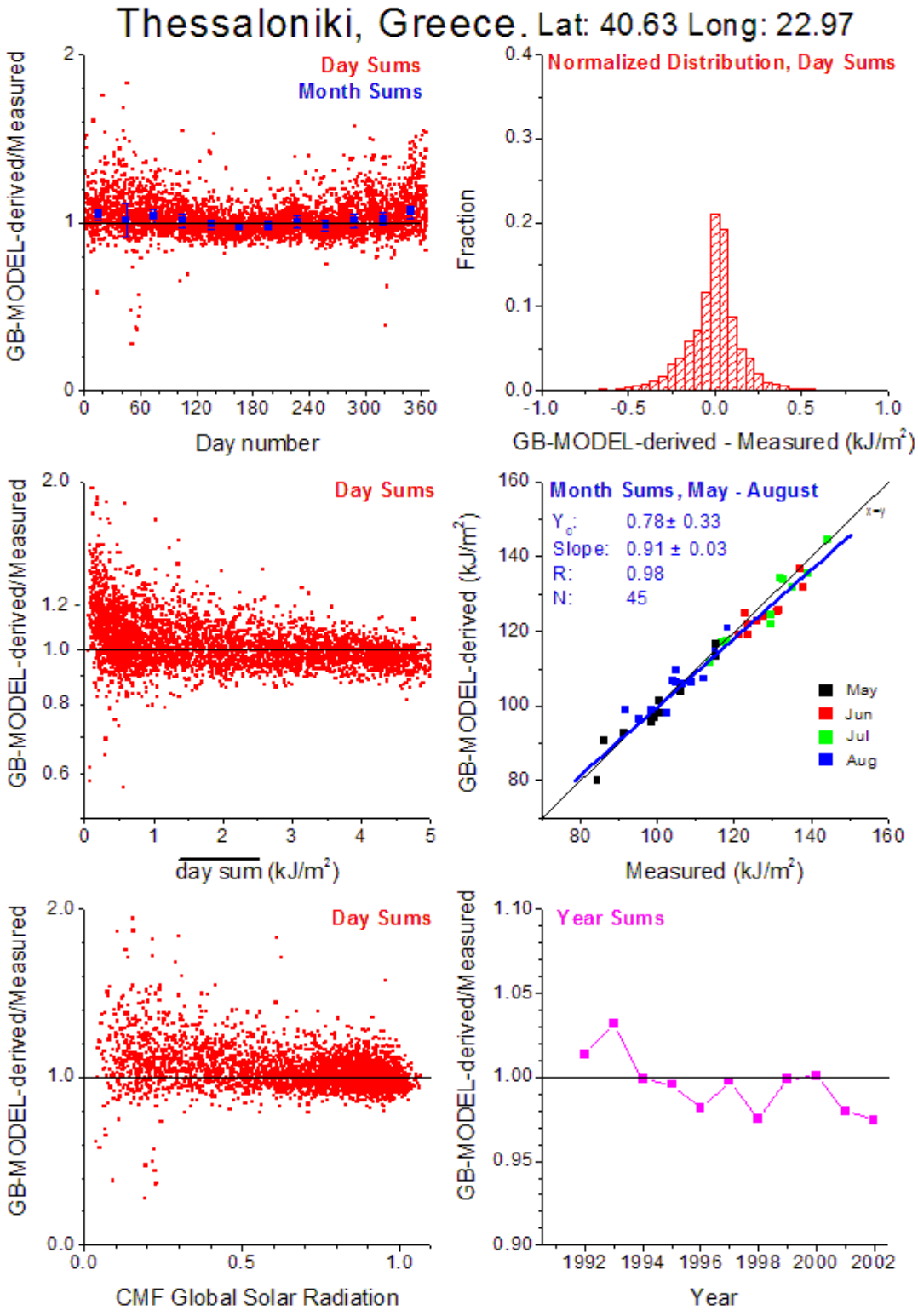

Fig. 5.1.23: Same as figure 5.1.16 for Thessaloniki, Greece.

The results of this section show that the COST 726 UV-mapping method is providing adequate results for the twelve sites especially for monthly and yearly UV-doses. The uncertainty in daily values can be up to 40–50 % under low irradiation conditions.

5.2 UNCERTAINTY DUE TO UNCERTAIN INPUT DATA

Henning Staiger [a]

a) German Meteorological Service.

The accuracy of modelled daily UV doses depends on the accuracy of the parameterisation, and on uncertainty of input used in modelling. The uncertainty due to the available input is estimated for erythemally weighted (ERY) UV, and at the wavelength 310 nm. The evaluation uses an error term in DWD's operational UV modelling algorithm. The algorithm calculates UV irradiation as a basic quantity valid for mean sea level, clear-sky conditions, and set values for aerosol properties, and for UV surface albedo. The basic quantity accounts for solar zenith angle (SZA), total ozone column (TOC), and profiles of ozone, temperature and pressure varying with season and latitude. It is adjusted by factors to current aerosol properties, albedo, altitude, and modification by clouds. These factors are constructed to be linearly independent, and thus, allow an error to be assessed representing the propagation of relative uncertainties via the individual component "i" impacting the modelled UV irradiation: uncertainty factor = $\exp(\pm\mathrm{sqrt}(\Sigma\, e_i^2))$, $e_i = \ln(1 + \mathrm{RMSE}_i / \mathrm{mean}_i)$. A latitudinal and seasonal dependency of inaccuracies must be assumed. The assessed uncertainty in UV due to uncertain input is valid for an individual daily UV dose derived from COST 726 fields.

The influence of uncertain TOC on the basic UV dose is estimated using the exponential proportionality for ozone-related UV changes (Madronich et al., 1998), and an appropriate radiation amplification factor, 1.10 for ERY, and 1.25 for 310 nm, respectively. In the satellite period (since 1979) the inaccuracy in TOC input for the COST 726 area is given versus ground based measurements (Bodeker et al. 2005). For the pre-satellite period it has additionally to be accounted for modelling inaccuracies (Krzyscin, 2008). According to Schwander et al. (1997) the inaccuracy in clear-sky UV modelling is less than 3 %, if monthly mean profiles are used. This coincides with the finding of den Outer et al. (2005), that the accuracy of clear-sky modelling is within ±2 % compared to measurements.

Table 5.2.1: Long-term uncertainty (RMSE_i / mean_i) of input variables.

		35° N – 45° N 10° W – 35° E	45° N – 55° N 05° W – 35° E	55° N – 70° N 05° E – 35° E
TOC uncertainty: Since 1979	JUL	3.16%	3.16%	3.16%
	FEB	3.16%	3.16%	3.16%
TOC uncertainty: pre-satellite:	JUL	4.49%	4.71%	5.05%
	FEB	5.86%	6.27%	6.83%
Uncertainty of AOD climatology	JUL	19.37%	24.23%	31.48%
	FEB	33.33%	41.04%	49.47%
Uncertainty of SSA at 300 nm	JUL	1.68%	1.29%	1.13%
	FEB	0.12%	1.84%	1.64%
Uncertainty in UV surface albedo	JUL	4.00%	5.35%	9.19%
	FEB	83.38%	184.18%	522.17%
Uncertainty of SOL–CMFs	JUL	14.30%	18.87%	22.59%
	FEB	27.95%	31.48%	32.99%

COST UV modelling applies a 2000 to 2008 monthly climatology of aerosol optical depth (AOD). The single scattering albedo (SSA) is set at 0.94. The impact of inaccuracy in aerosol input can be restricted to those of the climatology, because SOL–CMFs as basis of the UV–CMFs contain information on inter-diurnal variations of AOD. For the AOD climatology the relative inaccuracy is the RMSE in the individual months (Table 5.2.1). It is high in winter, because it is related to low absolute values. In the change from a low to a high turbidity atmosphere the contribution of the different aerosol optical properties to the total aerosol effect in UVB is dominated by AOD, ~55 %, and by SSA, ~30 % (Reuder

and Schwander, 1999). Hence, it has to be accounted for the inaccuracy in SSA too. Spatially covering SSA's are not available in COST 726. Alternatively, it is assumed that the inaccuracy in SSA can be estimated by the spatial variance in the Global Aerosol Data Set (Koepke et al., 1997), which is then related to the set value 0.94.

In UV, the impact of the surface albedo on the irradiation is low with the exception of snow covered surfaces. The range of inaccuracy is set at the difference between the ERA-40 derived monthly averages in case of snow and related to the mean of the snow free cases to account for inaccuracy in the ERA-40 parameterisation of water equivalent snow depths (Martin, 2004). July is free of snow, and thus, the small range of inaccuracy is taken from the inter-diurnal variations in the FMI UV surface albedo climatology (Tanskanen, 2004). The spatially high variable albedo in the Alps is not evaluated.

The inaccuracy in the SOL–CMFs is taken from the 1964 – 1993 monthly mean and accuracy (section 3.5). It is transformed to UV–CMFs applying the algorithm of den Outer et al. (2005).

Table 5.2.2 summarises the impact of uncertain input on uncertainty in individual daily UV doses for clear-sky, and all-sky conditions, respectively. The increased variability in the UV–CMFs, both spatial and temporal, dominates the impact on uncertainty for all-sky conditions. Uncertainty in ozone input has highest impact on clear-sky UV uncertainty in particular in the pre-satellite period (before 1979). High latitude winter is the exception due to the uncertain UV surface albedo. Despite the high relative variability of AOD in winter, the impact on clear-sky UV remains comparable small. The uncertainty in the UV–CMFs is slightly decreased at 310 nm compared to erythemal weighting, because of the increased diffuse irradiation at 310 nm. The exception is for high latitude winter due to high SZAs. The inaccuracy due to UV–CMFs is markedly reduced in summer compared to winter.

Table 5.2.2: Impact of uncertain input on uncertainty in individual daily erythemally weigthed (ERY), and in the daily UV doses at 310 nm, percent of mean UV dose.

			35° N – 45° N 10° W – 35° E		45° N – 55° N 05° W – 35° E		55° N – 70° N 05° E – 35° E	
			ERY	310 nm	ERY	310 nm	ERY	310 nm
clear-sky	since 1979	JUL	5.21%	5.77%	5.18%	5.50%	4.89%	5.23%
		FEB	5.33%	5.74%	7.41%	7.85%	12.95%	13.73%
	pre-satellite	JUL	6.23%	7.00%	6.51%	7.10%	6.60%	7.27%
		FEB	7.70%	8.55%	9.64%	10.54%	14.79%	15.96%
all-sky	since 1979	JUL	14.95%	12.23%	17.98%	16.74%	19.65%	19.02%
		FEB	21.97%	21.21%	22.29%	21.69%	23.64%	24.23%
	pre-satellite	JUL	15.39%	12.89%	18.48%	17.42%	20.25%	19.81%
		FEB	22.82%	22.33%	23.30%	23.00%	24.83%	25.74%

Overall, for a monthly average of an individual site the uncertainty due to uncertain input will be less than 5 %, and for 10 year monthly averages less than 1.5 %. For an individual site, it may be assumed that measured daily sums of global irradiation are available, which would reduce the uncertainty to that of clear-sky. For isolated summits the inaccuracy may increase because it could be affected by atmospheric layers below the summit, especially in case of low clouds. Moreover, the surrounding environment may show an increased variability, e.g., due to snow fields or glaciers influencing the regional albedo. There are some European sites with UV measurements showing a stronger absorbing aerosol type, e.g., Thessaloniki (Bais et al., 2005). For these sites modelled UV doses will show a higher positive bias due to a SSA set at 0.94.

5.3 COMPARISON OF UV MAPS FROM COST AND OTHER DATA SETS

Jean Verdebout [a]

a) European Commission Directorate General Joint Research Centre.

In this section, the erythemal UV maps produced by COST 726 are briefly and qualitatively compared with maps derived from METEOSAT and other data (Verdebout 2000, Arola et al. 2002, Verdebout 2004). The METEOSAT-derived maps are produced in a way very similar to the processing of COST 726 maps. The main difference resides in the cloud information used, which is derived from the visible band METEOSAT images. A parameter equivalent to the cloud optical thickness is estimated from the increase with respect to the cloudless situation of the radiance seen by METEOSAT. In this process, the presence of snow is also detected and a UV albedo inferred. This is done at the full spatial resolution of METEOSAT (~4 km in central Europe). The cloud parameter and the UV albedo are then re-sampled on a regular 0.05° × 0.05° grid and used as input into a Look Up Table to produce the surface erythemal down welling irradiance. Several images per day are used to reconstruct daily dose maps. The ozone data come from TOMS (1° × 1.25°), the aerosol are taken into account by gridding daily horizontal visibility measurements from ~1000 ground stations and the altitude is from the GOTO30 data set, as for COST 726 maps. The period covered by these METEOSAT-derived maps is from January 1st 1984 to August 31st 2003.

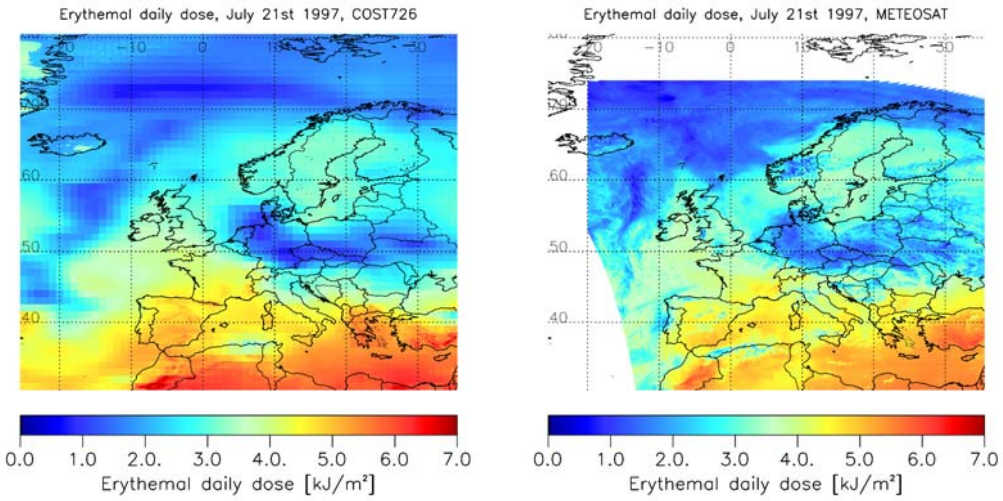

Fig. 5.3.1: Erythemal daily dose maps on July 1st 1997, COST 726 (left) and METEOSAT-derived (right).

Figure 5.3.1 shows the erythemal daily dose on July 21st 1997. It can be seen that, with respect to the METEOSAT-derived the values in the COST map are higher in the south. However, the spatial patterns and in particular those associated with clouds match fairly well. This means that, despite their lower intrinsic spatial resolution, the COST maps do document the overall distribution of the UV radiation on a single day.

Figure 5.3.2 shows the difference with respect to multi-year averages (see section 6.2) of the monthly averaged daily erythemal dose in April 1984 and in June 1991. Again the spatial patterns match reasonably well. In this case, a quantitative judgment is not really possible because the period for defining the multi-year average is different for the two data sets. In June 1984, the excess over France and southern England correspond to low ozone and low cloudiness while the deficit over Greece and Turkey is caused by high ozone and heavy cloudiness. In June 1991, the pronounced deficit over Scandinavia and Finland mostly corresponds to heavy cloudiness, the ozone being quite regular from year to year in this month.

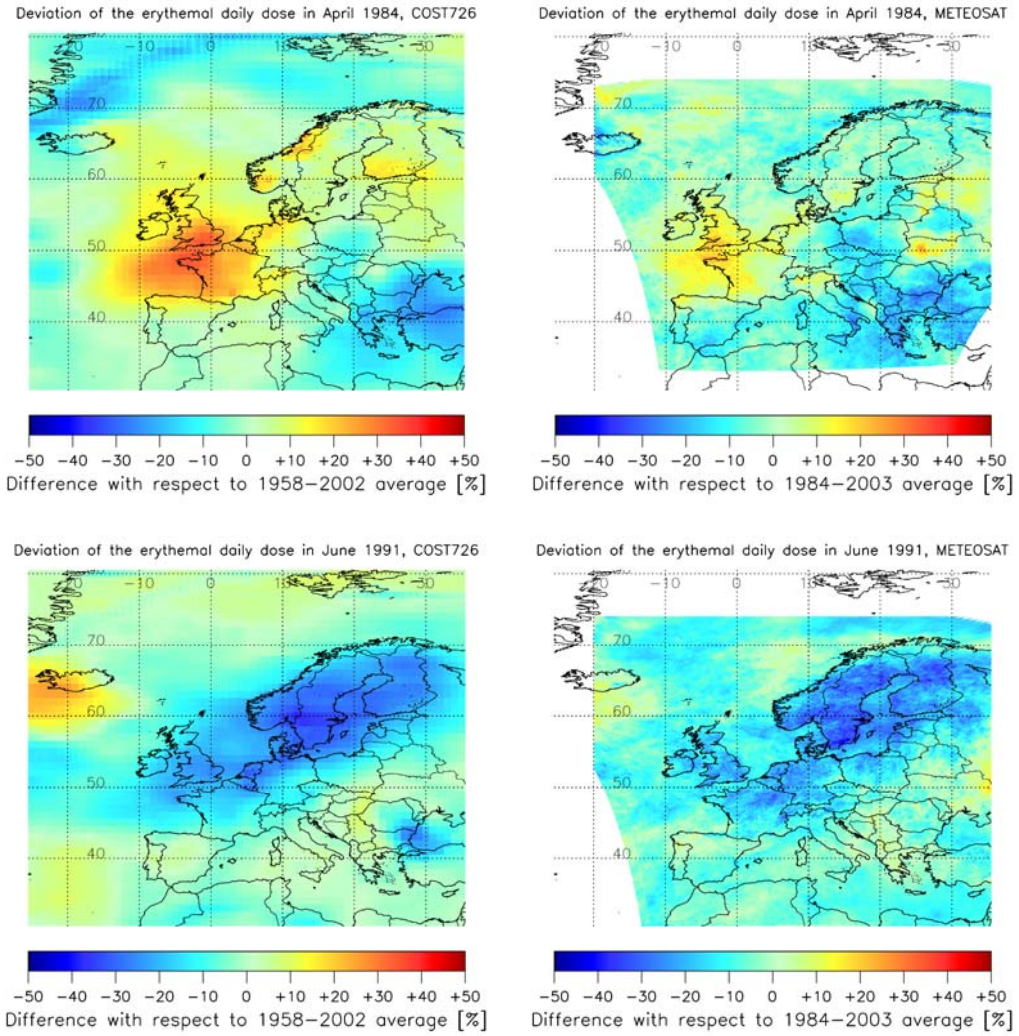

Fig. 5.3.2: Difference with respect to the multi-year averages of the monthly averaged erythemal daily dose in April 1984 (top) and June 1991 (bottom), COST 726 (left) and METEOSAT-derived (right).

6 RESULTS: UV RADIATION IN THE PAST

Jean Verdebout [a], Peter N. den Outer [b], Janusz Krzyścin [c], Alois Schmalwieser [d].

a) European Commission Directorate General Joint Research Centre; b) Dutch National Institute for Public Health and the Environment (RIVM); c) Polish Academy of Sciences, Institute of Geophysics; d) Institute of Medical Physics and Biostatistics, University of Veterinary Medicine, Austria.

Long-term assessment of the European UV-climate relevant for biological effects cannot be directly based on ground-based measurements of UV, because such measurements are not available at a sufficient number of locations and for the required long time periods. Therefore, modelling approaches are required to analyse the past UV-climate in relation to ozone, clouds and aerosols. The previous chapter provides an extensive validation of two such approaches, and in this chapter these approaches are used to analyse the past UV-climate. The approaches were a selected subset of methods that were included in a modelling exercise carried out by COST action 726. The modelling exercise demonstrated that several methods are capable of providing accurate UV-estimates, provided that the model-input data is of sufficient quality, i.e. data on ozone column, global radiation (cloud-effects) and aerosols. In section 6.1 the UV-climate is reconstructed for 8 locations using ground-based measurements and also compared with time series extracted from the COST 726 UV-maps. Section 6.2 illustrates the map data set produced by COST 726. In section 6.3 a wavelet analysis is made, identifying different time scales in the UV changes. In the last section results of a questionnaire regarding the use of photobiological weighting functions, action spectra, are presented and the influence of spectral resolution, inter and extrapolation of these action spectra of the derived effective UV is discussed.

6.1 STATION RESULTS ERYTHEMAL WEIGHTED UV

Peter N. den Outer [a], Harry Slaper [a], Jean Verdebout [b].

a) Dutch National Institute for Public Health and the Environment (RIVM); b) European Commission Directorate General Joint Research Centre.

Within this COST action 726, a modelling exercise has been carried out, where 16 different reconstruction models were tested against ground-based UV-measurements (Koepke et al., 2008). A number of models were found to have results that were in good agreement with the measurements, both in absolute and relative comparisons. We use one of those models to make an analysis of the UV radiation levels over the European Continent in the past 25–40 years using COST 726 and SCOUT-O3 datasets. The latter data sets contain ground-based ozone and pyranometer measurements accompanied with snow cover and aerosol climatology (section 3.2). These data sets were gathered within the European project SCOUT-O3. Now we present results for 8 sites covering 40–67 ° N.

This reconstruction model, which was developed at RIVM, is described by Den Outer et al. (2005). It combines effective UV-dose rates taken from a look-up table (UV as a function of ozone and SZA) pre-calculated using the TUV-model with a standard cloud-free atmosphere (Madronich et al., 1998). The RIVM-model makes use of site information of the ground-albedo and (monthly) aerosol climatology. CMFs for the UV daily sums are derived from the pyranometer measurements using an SZA-dependent empirical relationship (den Outer et al., 2005). It is the same relationship that has been used to derive CMFs for the UV maps from the corrected ERA-40 dataset. The relationship between the SOL–CMFs and UV–CMFs was initially established at Bilthoven.

The yearly erythemally weighted UV sums are shown as a function of time for the eight sites in figure 6.1.1 for the eight sites. We also show the yearly sums constructed from the time series that have been extracted from the COST 726 UV maps. The yearly sums range from 290 ± 22 kJ/m^2 for Sodankylä at 67 ° N to 720 ± 44 kJ/m^2 for Thessaloniki at 40 ° N, based on ground-based modelling. A severe overestimation by the UV map-extracted yearly sums occurs for Thessaloniki in this respect; for the UV-map-extracted result we find 792 ± 50 kJ/m^2, see also table 6.1.1. This can most likely be attributed to the heavy aerosol loading for Thessaloniki, which is not fully grasped by the aerosol climatology as included

in the COST 726 mapping method. The overall year-to-year variability does not show a distinct behaviour for one of the sites, but ranges from 6 to 8 %. The variability of the monthly UV sum (from year-to-year) was lowest at Thessaloniki during the summer months as may be expected from the usual absence of clouds (see Fig. 6.1.2). The relative variation is of the order of 5–6 % for these months while the rest of the sites show an almost season independent variability of 10–17 %.

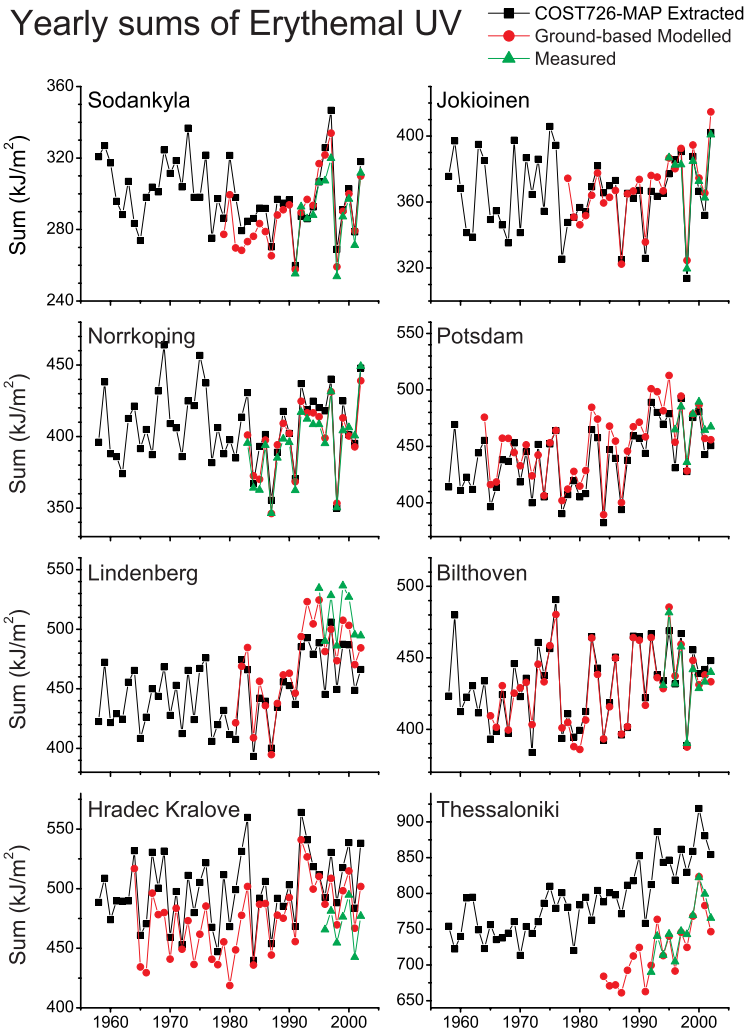

Fig. 6.1.1: Evolution of the yearly erythemally weighted UV sum for eight European sites. Different colours indicate underlying data used.

Table 6.1.1: Derived yearly sums and variability for eight European locations using ground-based modelling (GB) or the COST 726 UV-maps extracted time series (COST).

		Lat.	Yearly sum (kJ/m^2)		% Variability	
Code	Site	(deg. dec)	GB	COST	GB	COST
FIS	Sodankylä	67.36	288.1	294.3	6.7	6.5
FIJ	Jokioinen	60.81	366.8	363.4	5.7	5.6
SEN	Norrköping	58.58	398.1	405.3	6.3	6.9
DEP	Potsdam	52.36	451.0	440.0	6.8	6.7
DEL	Lindenberg	52.21	470.3	456.3	7.5	6.7
NLB	Bilthoven	52.12	428.6	430.4	6.3	6.7
CRH	Hradec Kralove	50.18	475.0	500.1	6.3	6.3
GRT	Thessaloniki	40.63	720.0	832.2	6.2	4.9

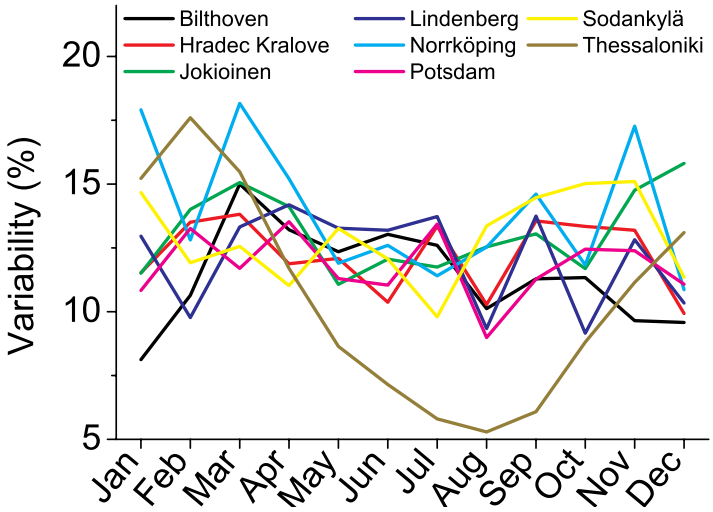

Fig. 6.1.2: Variability of the monthly erythemally weighted UV sum, using the modelled data based on ozone and pyranometer measurements. The whole available period is included.

Binning the reconstructed UV dose per decades, we derive the relative long-term changes as given in figure 6.1.3. Time window is limited to the period where both ozone and pyranometer data is available. The same type of graph is made for the clear-sky situation, and shown as figure 6.1.4. Prior to 1980 the average yearly UV sums appear to be on a stable level. An increase is seen for all sites after the eighties. Characterizing this increase by a single linear trend line yields 0.45 ± 0.05 % per year for the cloudy sky situations and 0.22 ± 0.4 % per year for the clear-sky situation. A similar behaviour is found for a number of other sites where the COST 726 ozone and COST 726 CMFs have been implemented (see Fig. 6.1.5). Additionally, a trend in the aerosol optical depth has been identified at Thessaloniki (Kazadzis et al., 2007). The result of this trend being a larger increase of the annual UV sum 14 % per decade for the all-sky situations and 10 % for the clear-sky estimates, than without this aerosol trend in that case 3 and 8 % increases per decade are found, for all- and clear-sky situations respectively. The fact that for the cloudy UV dose, a significantly larger trend is shown, compared with the clear-sky UV, suggests that part of the UV increase must be induced by a diminishing of cloud impact on the UV irradiance. In figure 6.1.6 we show the CMFs on the yearly sums as a function of the year; the cloudy sky yearly sum is divided by the corresponding clear sky yearly sum. The overall cloud impact on yearly UV is the largest in The Netherlands (CMF = 0.66), and the smallest in Greece (CMF = 0.81). But more interestingly, all sites show a diminishing of the cloud impact for years after 1979. The CMF increases with 0.020 ± 0.008 per

decade. If this can be regarded as a genuine trend in cloudiness is still to be investigated, because the number of years included in the analysis is too small.

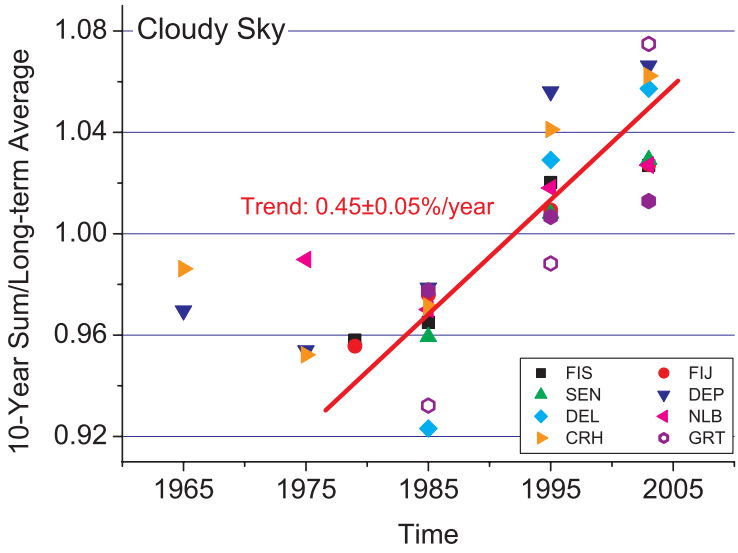

Fig. 6.1.3: Reconstructed yearly UV-sums averaged per decade using ground-based measured ozone and pyranometer data. FIS and FIJ have only one year sum for 1960–1979, i.e. 1979. The solid points for GRT are derived using constant aerosol climatology.

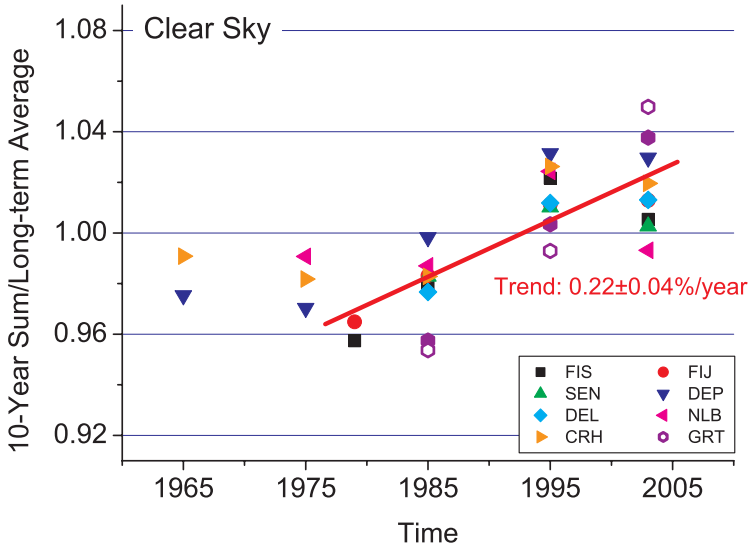

Fig. 6.1.4: Reconstructed yearly UV-sums averaged per decade using ground-based measured ozone. FIS and FIJ have only one year sum for 1960-1979, i.e. 1979. The solid points for GRT are derived using constant aerosol climatology.

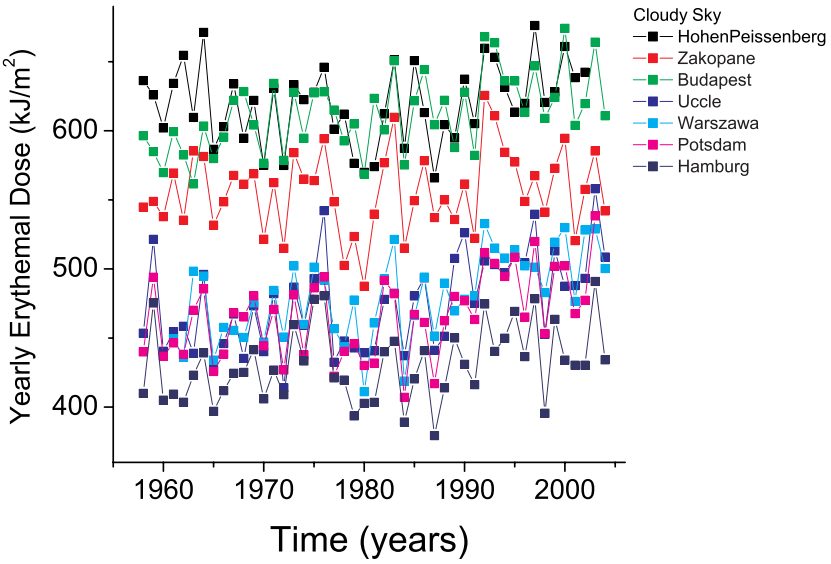

Fig. 6.1.5: Reconstructed yearly UV-sums for some Central European sites, using COST 726 ozone and CMF.

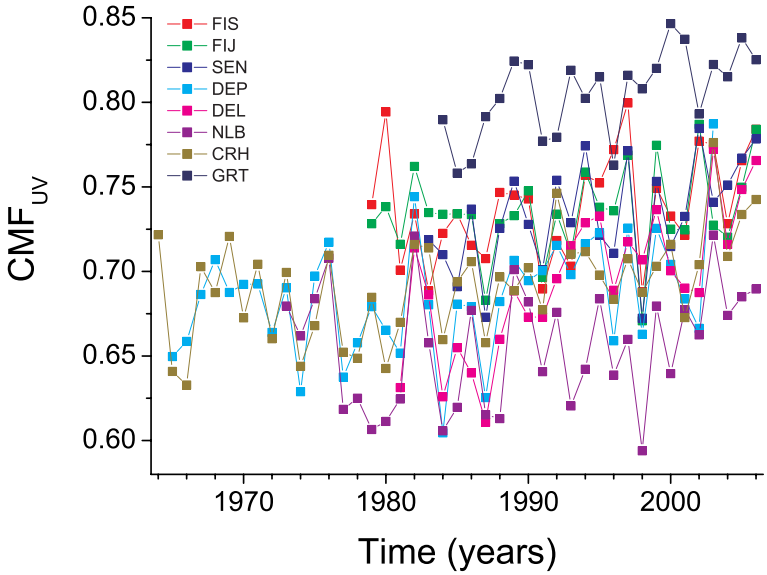

Fig. 6.1.6: Derived annual cloud impact on the yearly UV sums, expressed as yearly CMF, as function of the year for the eight European sites.

6.2 MAPS – ERYTHEMAL WEIGHTED UV

Jean Verdebout [a], Henning Staiger [b], Peter N. den Outer [c], Natalia Chubarova [d].

a) European Commission Directorate General Joint Research Centre; b) German Meteorological Service; c) Dutch National Institute for Public Health and the Environment (RIVM); d) Moscow State University, Meteorological Observatory.

The purpose of this section is to illustrate the map data set produced by COST 726. As stated before, the maps cover the area from 25.5° W to 35.5° E and 30.5 to 80.5° N with a spatial resolution of 0.05°. The basic product is made of daily dose maps with the spectral weighting corresponding to the erythemal effect and at 7 discrete wavelengths (295, 300, 305, 310, 315, 330 and 360 nm) with a 5 nm FWHM triangular slit function. This set of 8 maps has been produced for each day in the period from January 1st 1958 to August 31st 2002. Thanks to the completeness of the input data sets, there is not any missing day.

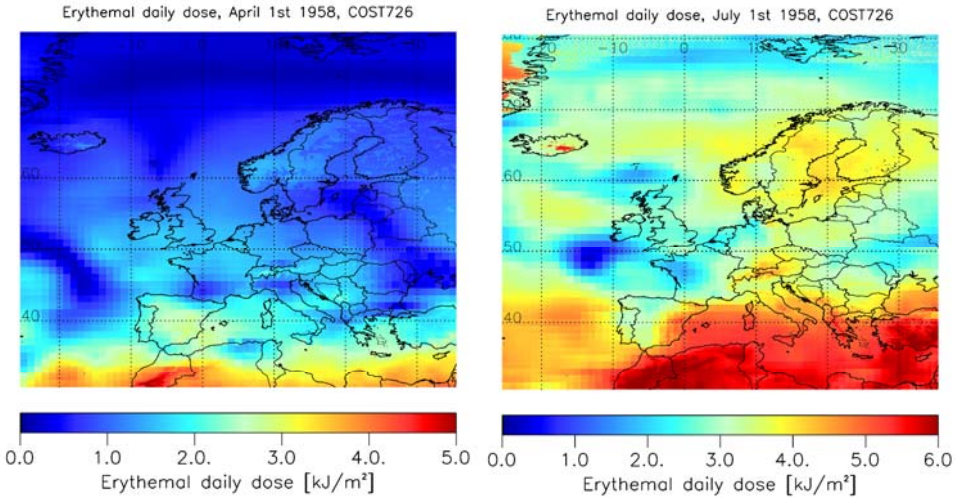

Fig. 6.2.1: Two examples of erythemal daily dose maps, respectively on April 1st 1958 and July 1st 1958.

The daily dose maps are illustrated for two days in figure 6.2.1. In addition to the latitude gradient associated with the solar zenith angle, one can distinguish patterns caused by cloudiness, snow cover and altitude. In order to document the year to year variability and to make visible systematic geographical patterns, it is useful to generate monthly averaged values (Fig. 6.2.2) and multi-year (1958–2002) averages of the monthly averaged values (Fig. 6.2.3). In these averaged maps, the cloud patterns are smoothed out but the attenuation by clouds is present.

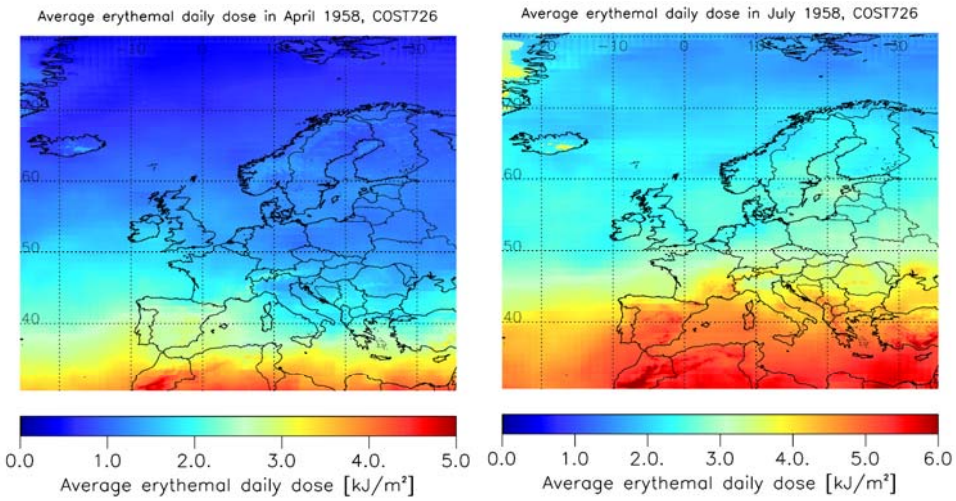

Fig. 6.2.2: Two examples of monthly averaged erythemal daily dose maps, respectively in April and July 1958.

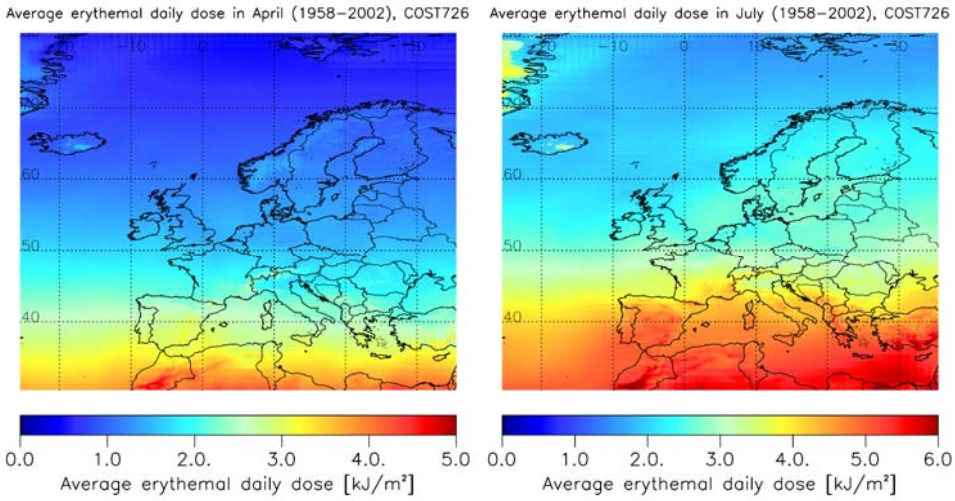

Fig. 6.2.3: Multi-year averages of monthly averaged erythemal daily dose maps for April and July.

The multi-year averages allow distinguishing systematic geographical differences. However, because of the limitations of a representation with a colour table, it is necessary to zoom in and to use an optimized scale. Figure 6.2.4 shows the multi-year average (erythemal radiation) over the Alpine arc and a large part of Italy in April (left) and in August (right). The UV radiation enhancement over the mountains is more pronounced in spring when it is caused both by the altitude and the presence of snow, in August only the altitude effect is present (except over permanent glaciers). One can also notice a lower UV intensity in the Po valley with respect to the same latitude in the Rhone valley. This feature is caused by a heavier cloudiness and larger aerosol load in Northern Italy.

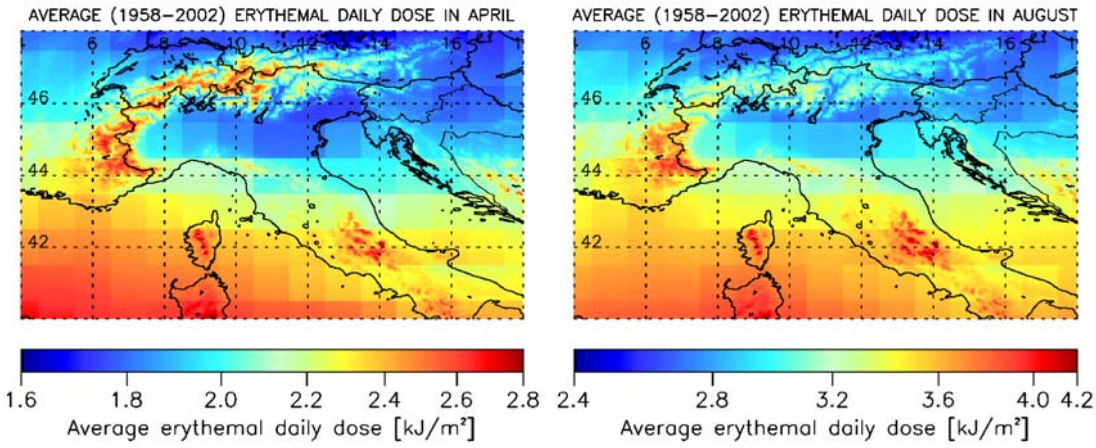

Fig. 6.2.4: Multi-year averages of the monthly averaged erythemal daily dose for April and August, over the alpine arc and a large part of Italy.

Figure 6.2.5 shows the multi-year average in the northern part of Norway, Sweden and Finland in March. Again, the effects of altitude and snow cover are visible, including over the Gulf of Bothnia, which is regularly ice covered at that time of the year. Figure 6.2.6 shows how the Cantabric Mountain system acts as a climatological barrier with a noticeably heavier cloudiness north of the range.

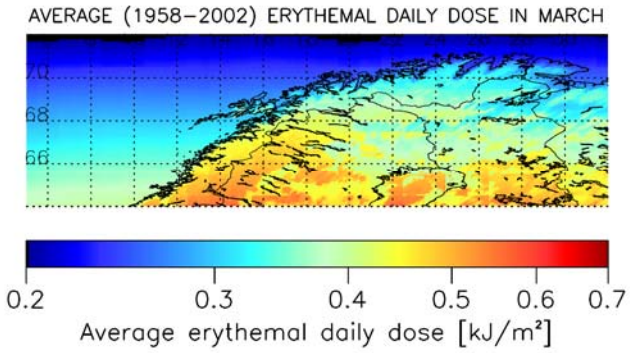

Fig. 6.2.5: Multi-year averages of the monthly averaged erythemal daily dose for March, over northern Norway, Sweden and Finland.

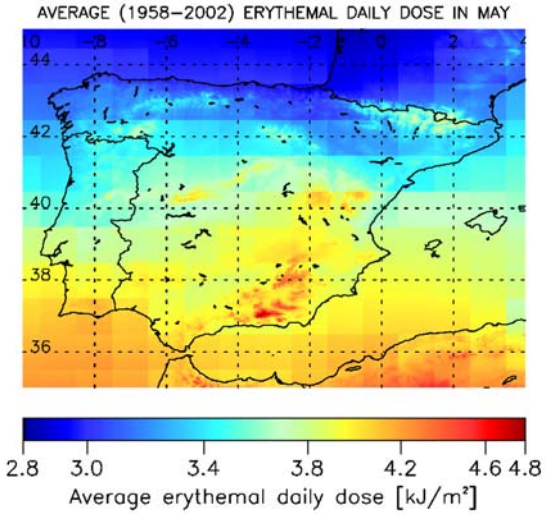

Fig. 6.2.6: Multi-year averages of the monthly averaged erythemal daily dose for May, over the Iberian Peninsula.

The main interest of the COST 726 map data set is probably to document the variability in time of the surface UV radiation. Again because of the dominant latitude gradient and the limitations of the representation by means of a colour table, it is not easy to distinguish the differences between for instance the images of figure 6.2.2 (monthly averages in 1958) and those of figure 6.2.3 (multi-year averages). Instead, figures 6.2.8 to 6.2.19 show, for each month and each year, the relative difference between the monthly averaged erythemal daily dose and its corresponding multi-year average (for the same month); the multi-year averages maps themselves are illustrated in figure 6.2.7. It then appears that the year to year variability is large, easily reaching ±50 % in spring. The two main factors responsible for this variability are cloudiness and total column ozone. All possible combinations can be found, i.e. cloudiness and ozone sometimes add their effect to produce a pronounced excess or deficit or compensate each other. The variability is less in summer because the atmospheric ozone is more regular in this season.

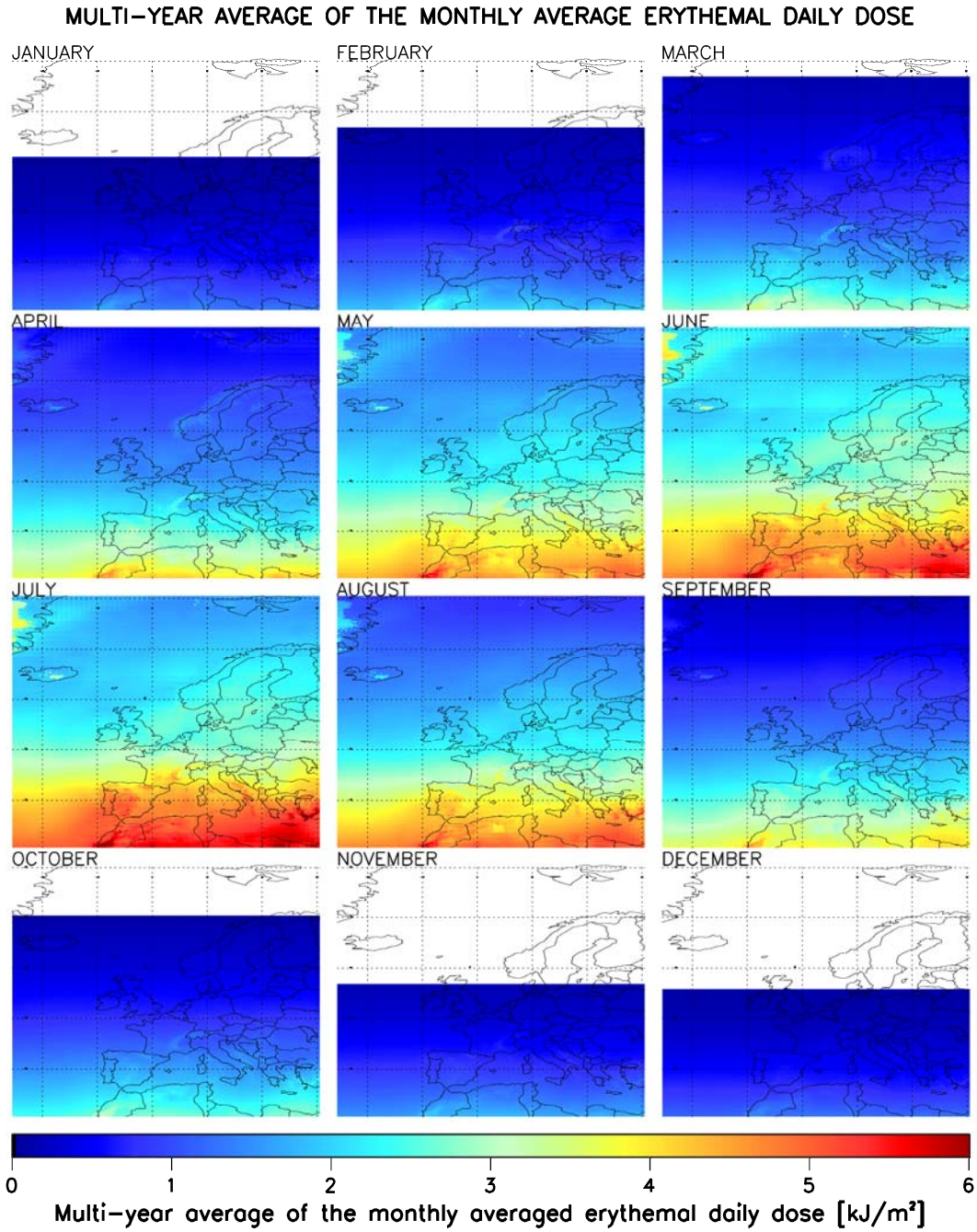

Fig. 6.2.7: Multi-year averages (Jan.-Aug.: 1958-2002, Sep.-Dec.: 1958-2001) of the monthly averaged erythemal daily dose over Europe.

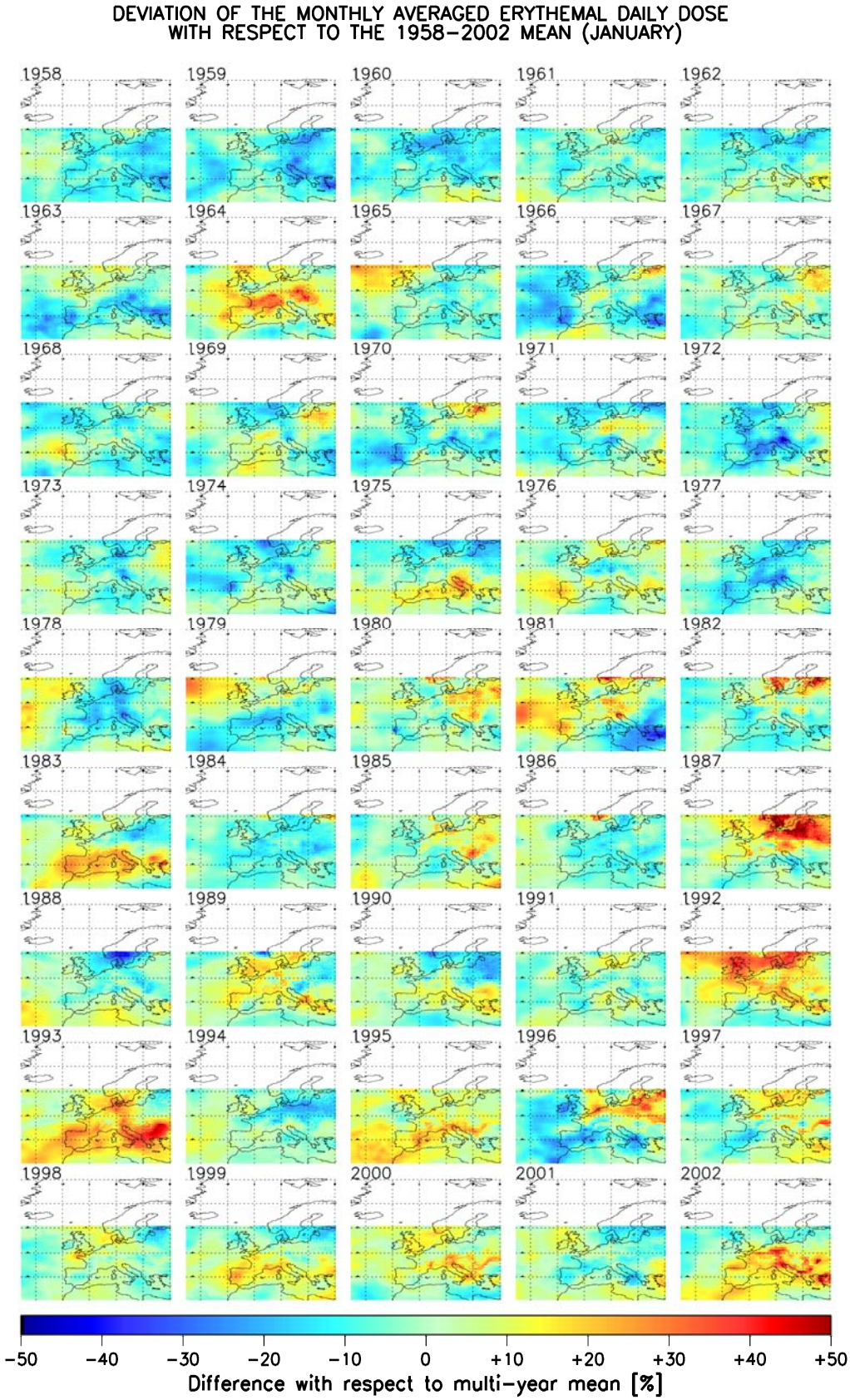

Fig. 6.2.8: Year to year variability of the monthly averaged erythemal daily dose in January.

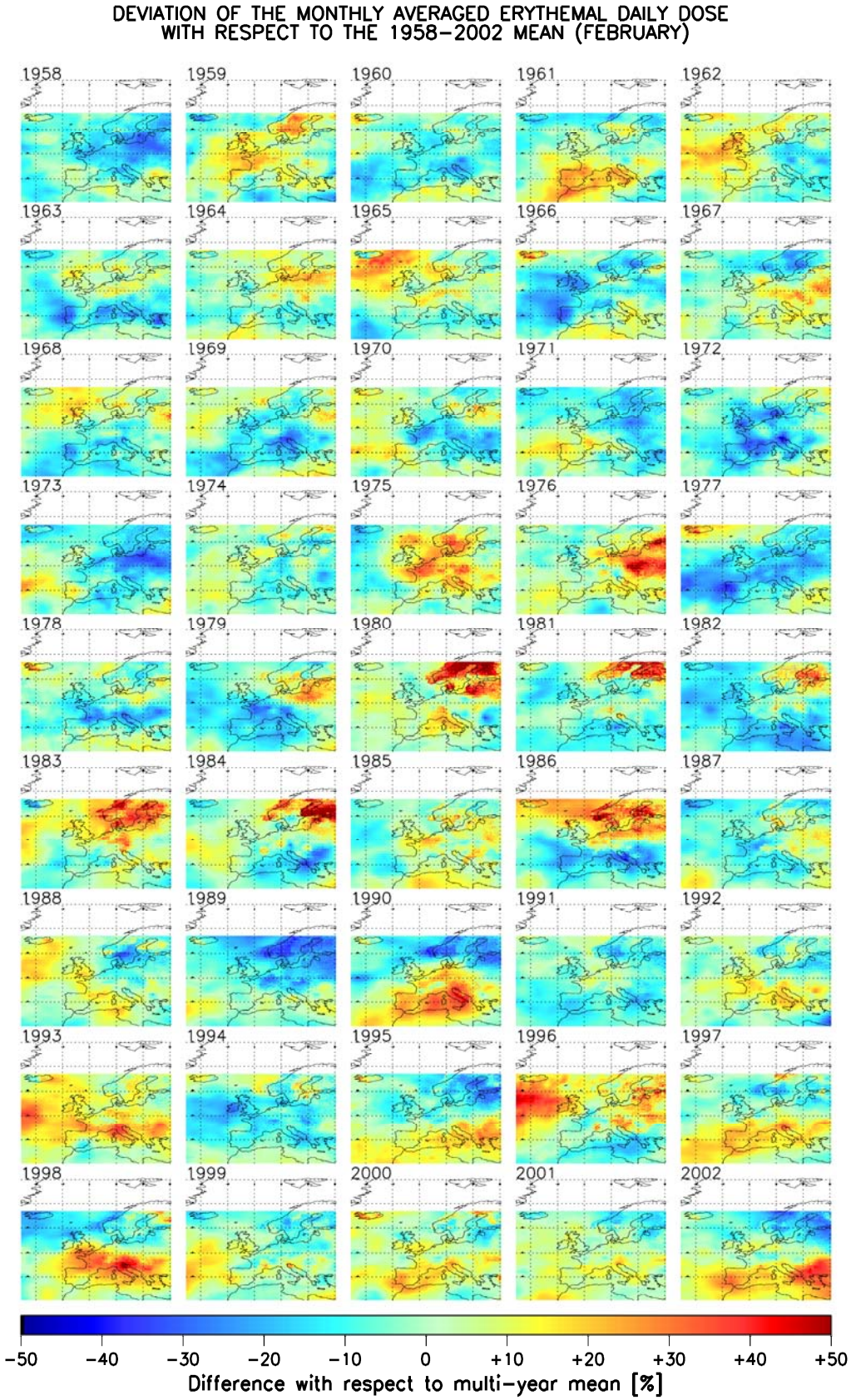

Fig. 6.2.9: Year to year variability of the monthly averaged erythemal daily dose in February.

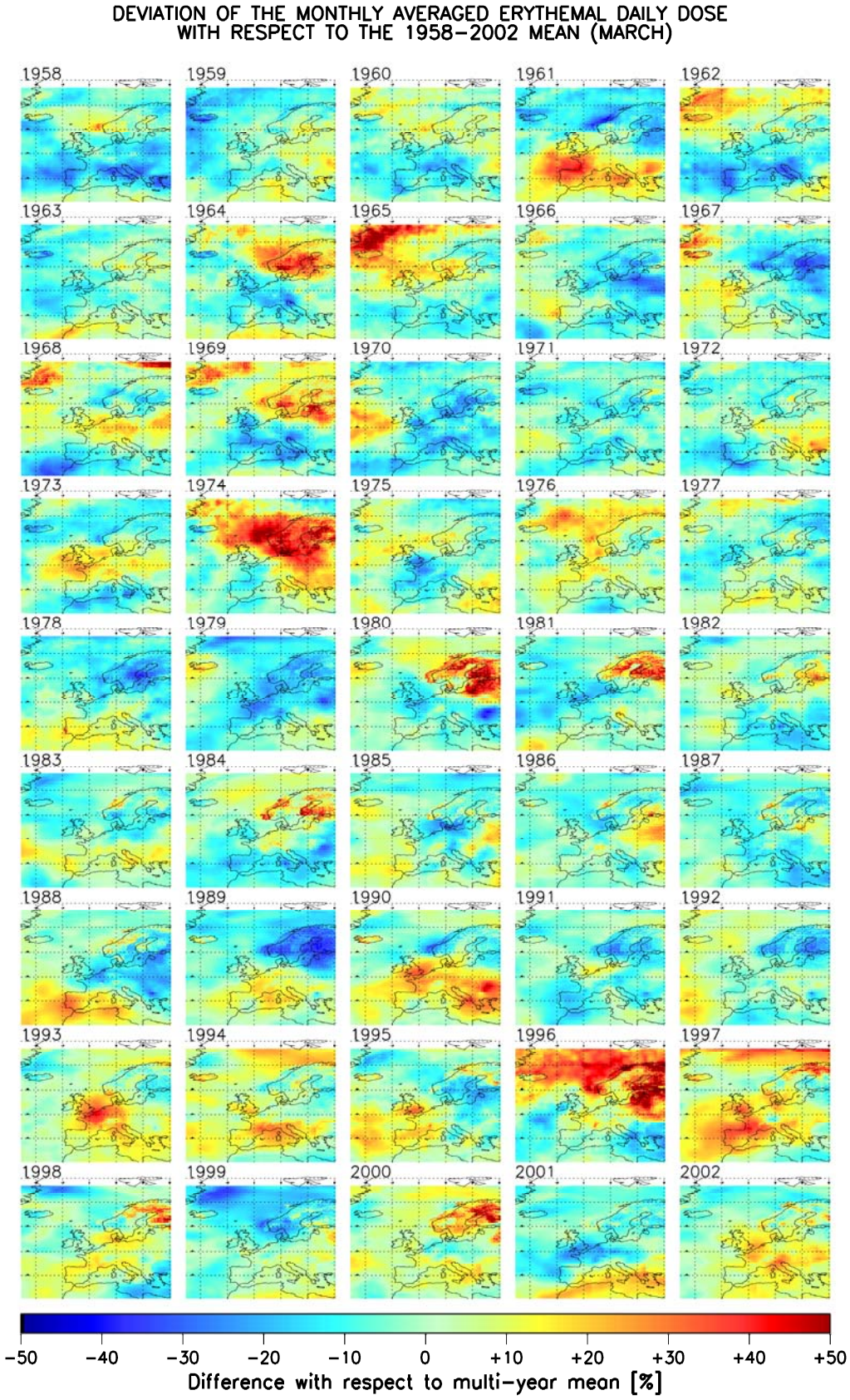

Fig. 6.2.10: Year to year variability of the monthly averaged erythemal daily dose in March.

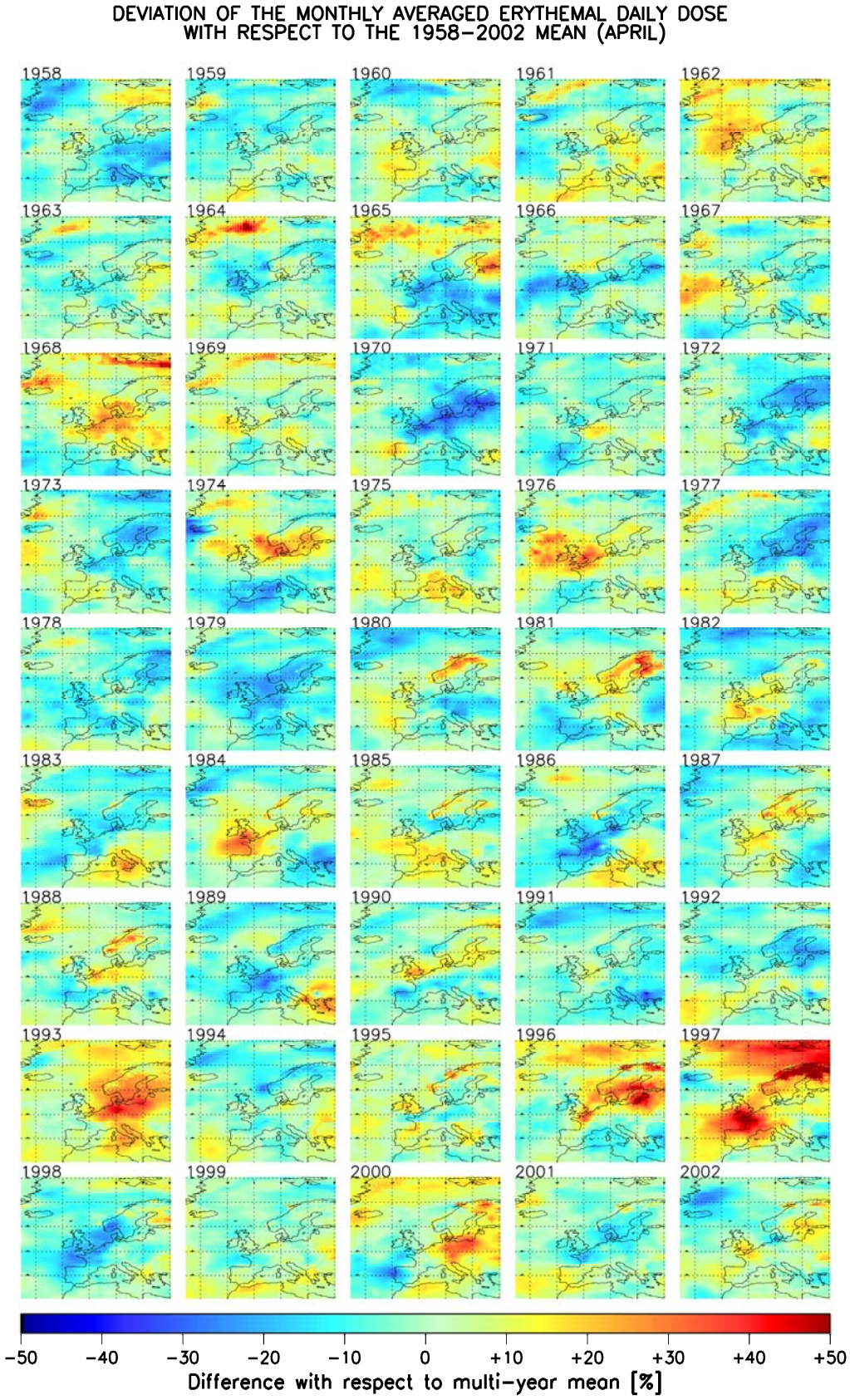

Fig. 6.2.11: Year to year variability of the monthly averaged erythemal daily dose in April.

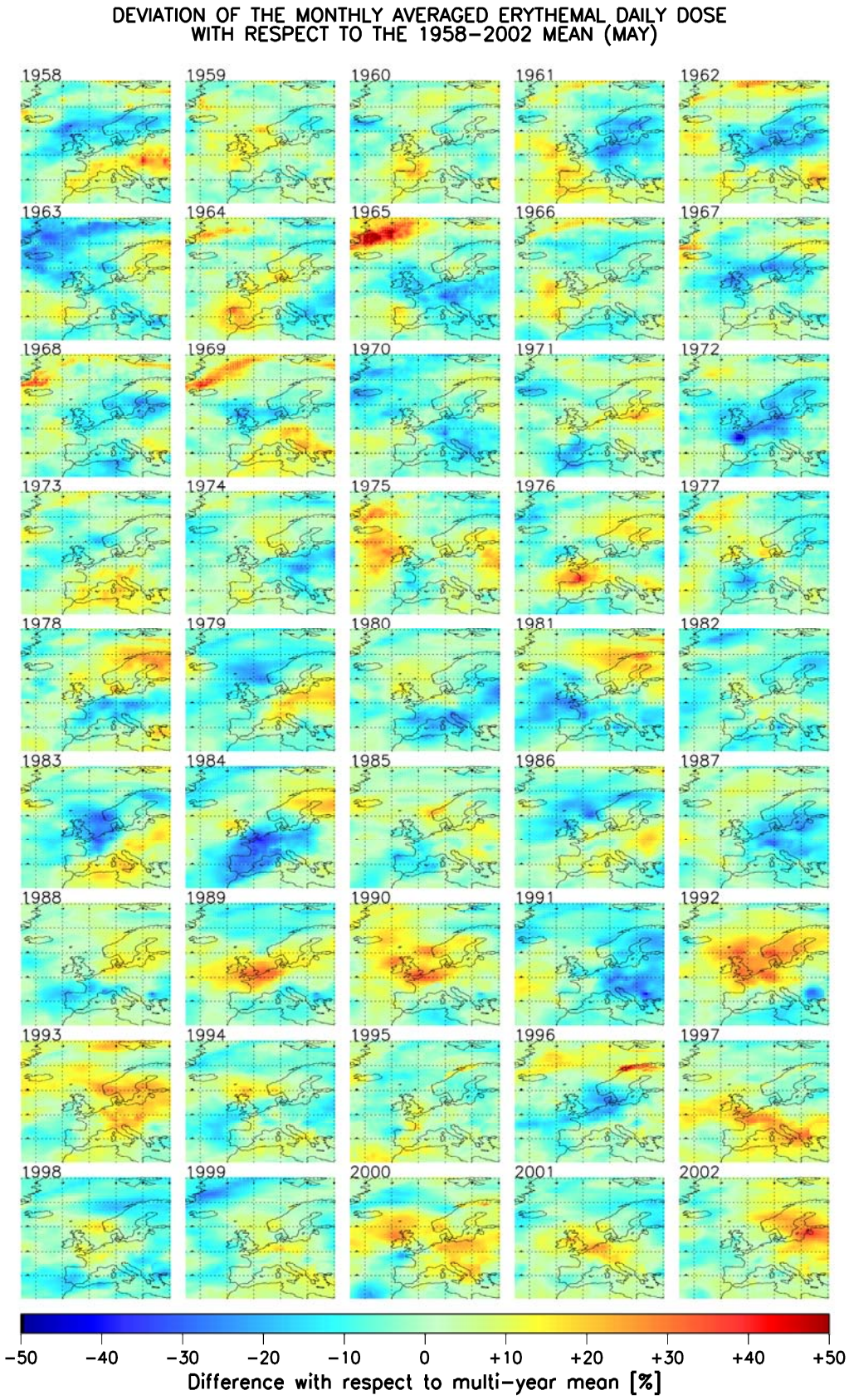

Fig. 6.2.12: Year to year variability of the monthly averaged erythemal daily dose in May.

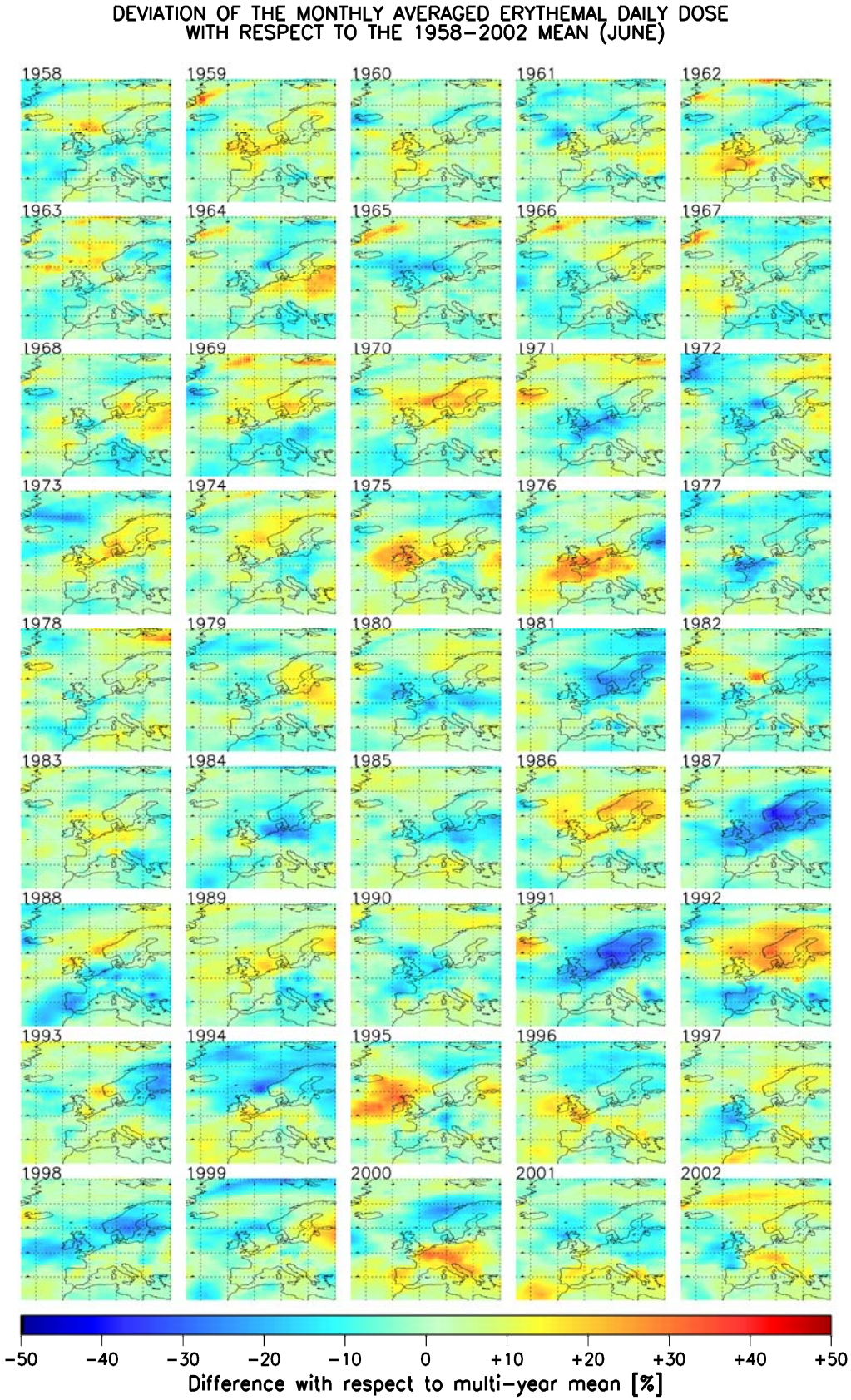

Fig. 6.2.13: Year to year variability of the monthly averaged erythemal daily dose in June.

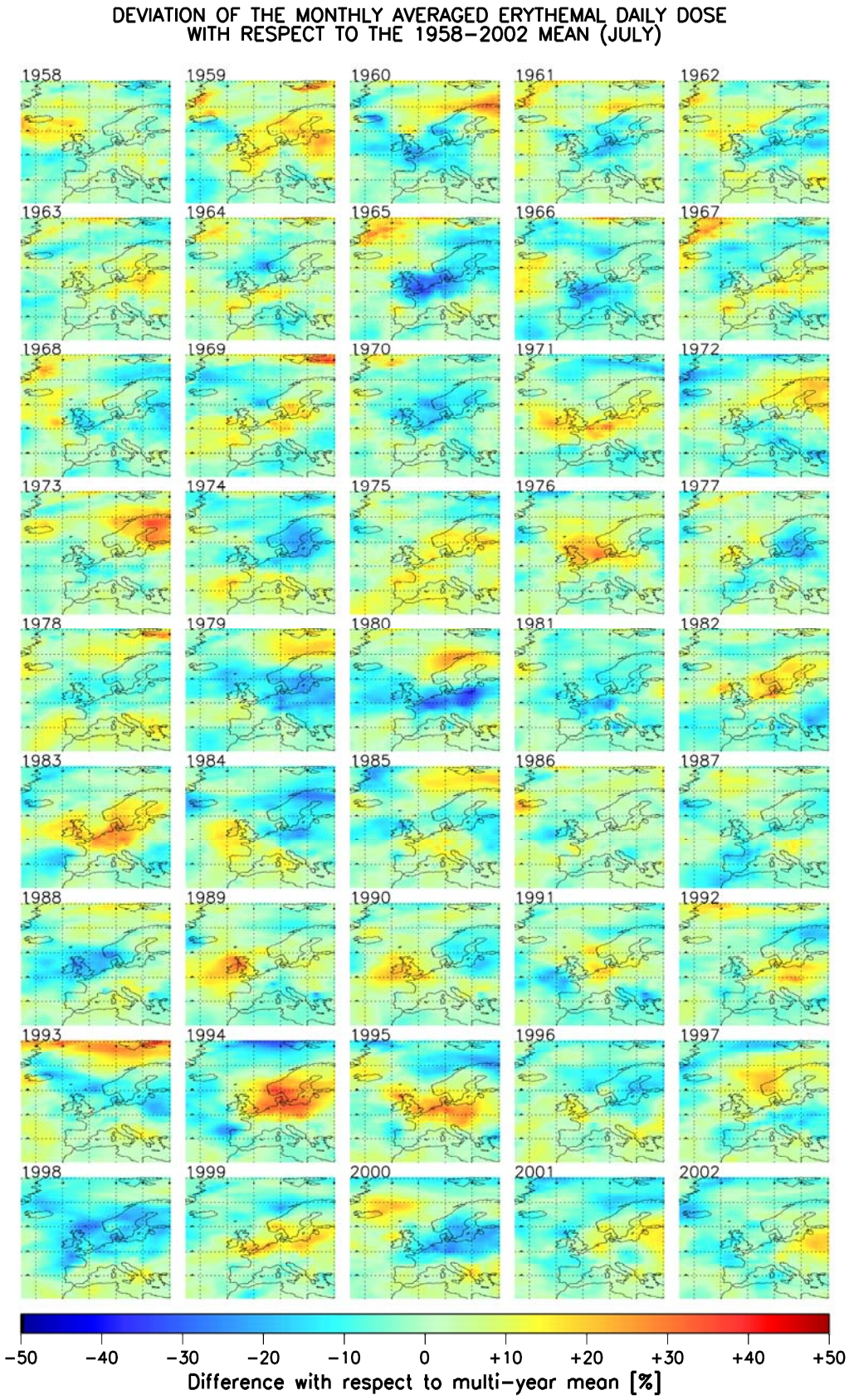

Fig. 6.2.14: Year to year variability of the monthly averaged erythemal daily dose in July.

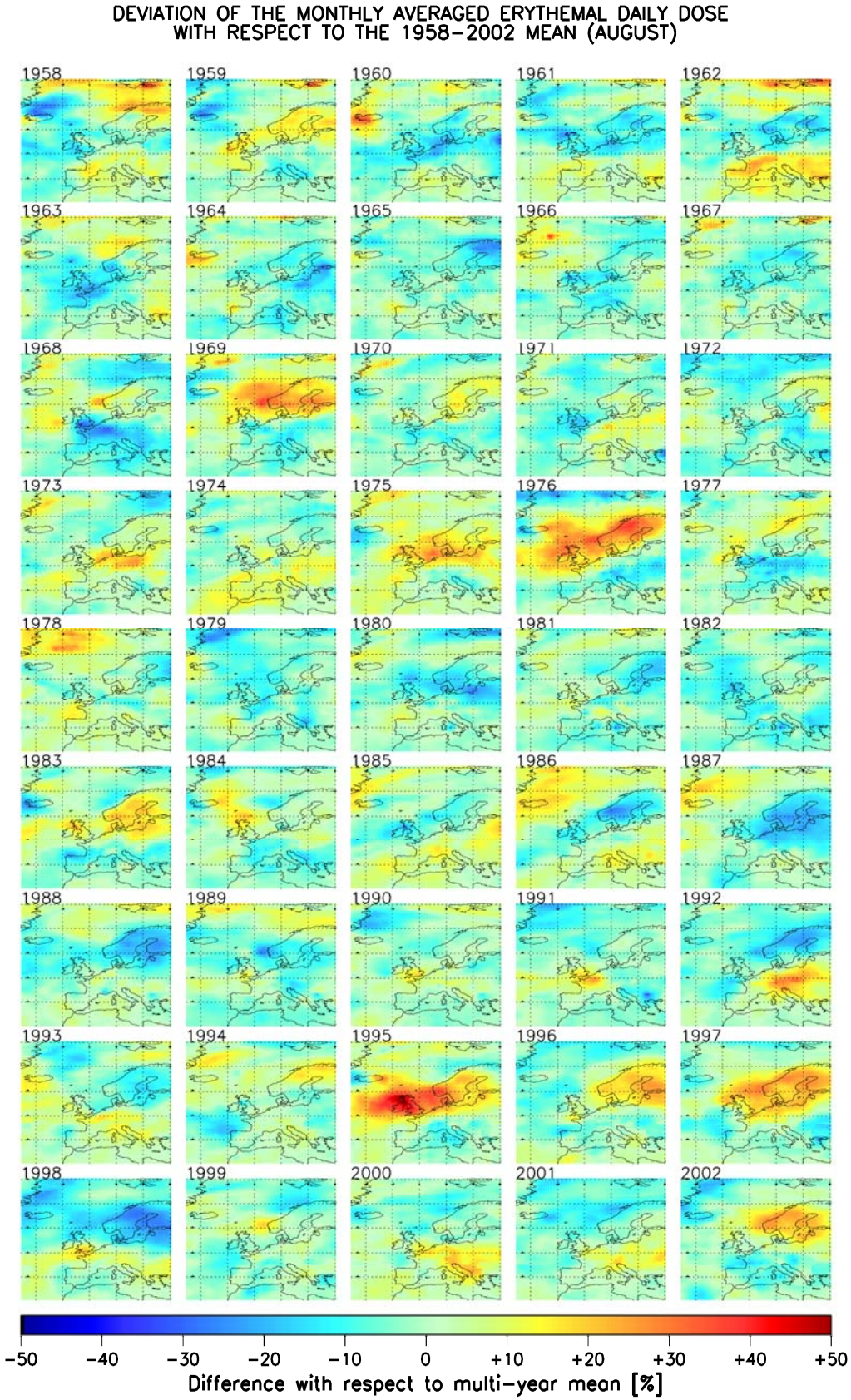

Fig. 6.2.15: Year to year variability of the monthly averaged erythemal daily dose in August.

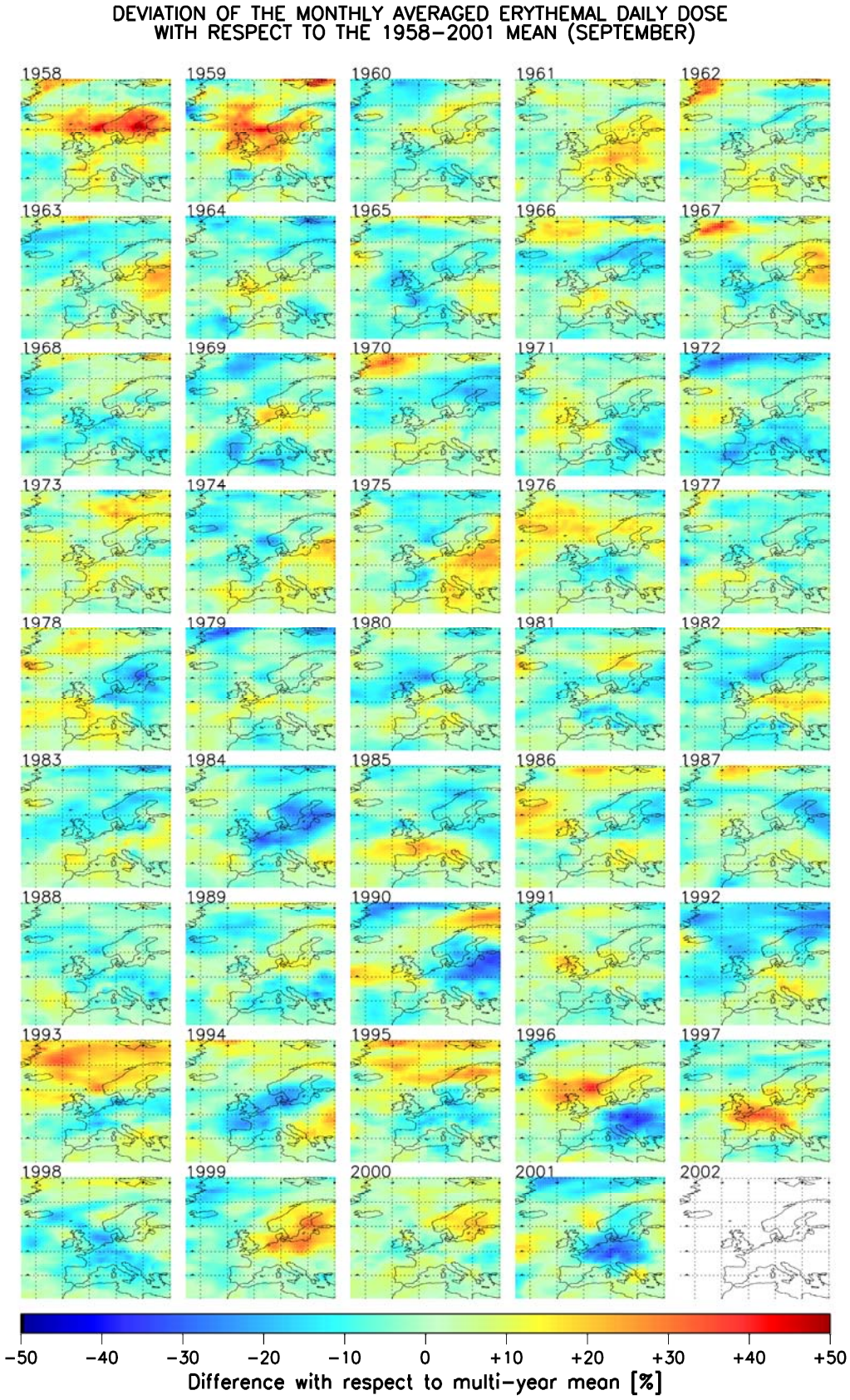

Fig. 6.2.16: Year to year variability of the monthly averaged erythemal daily dose in September.

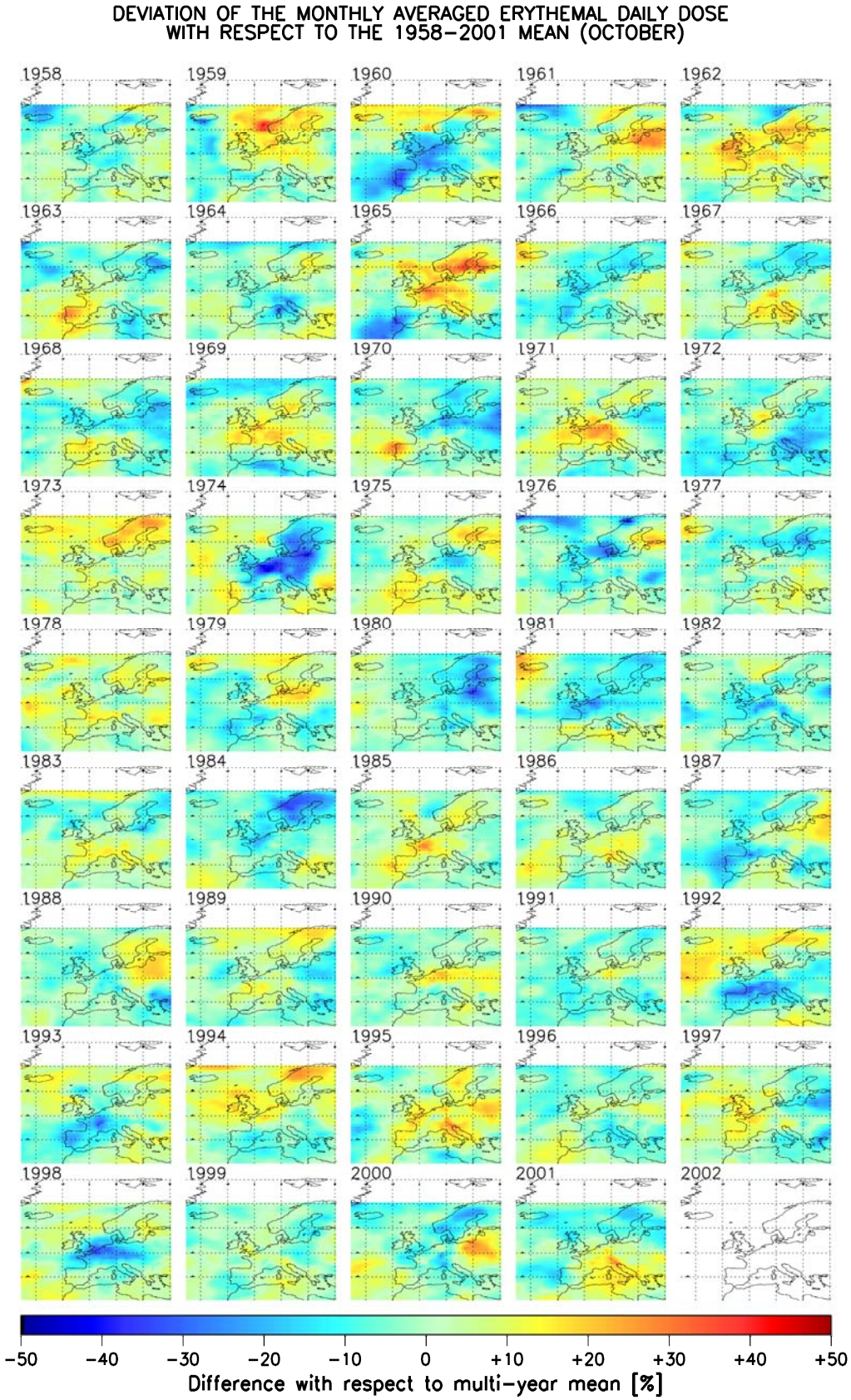

Fig. 6.2.17: Year to year variability of the monthly averaged erythemal daily dose in October.

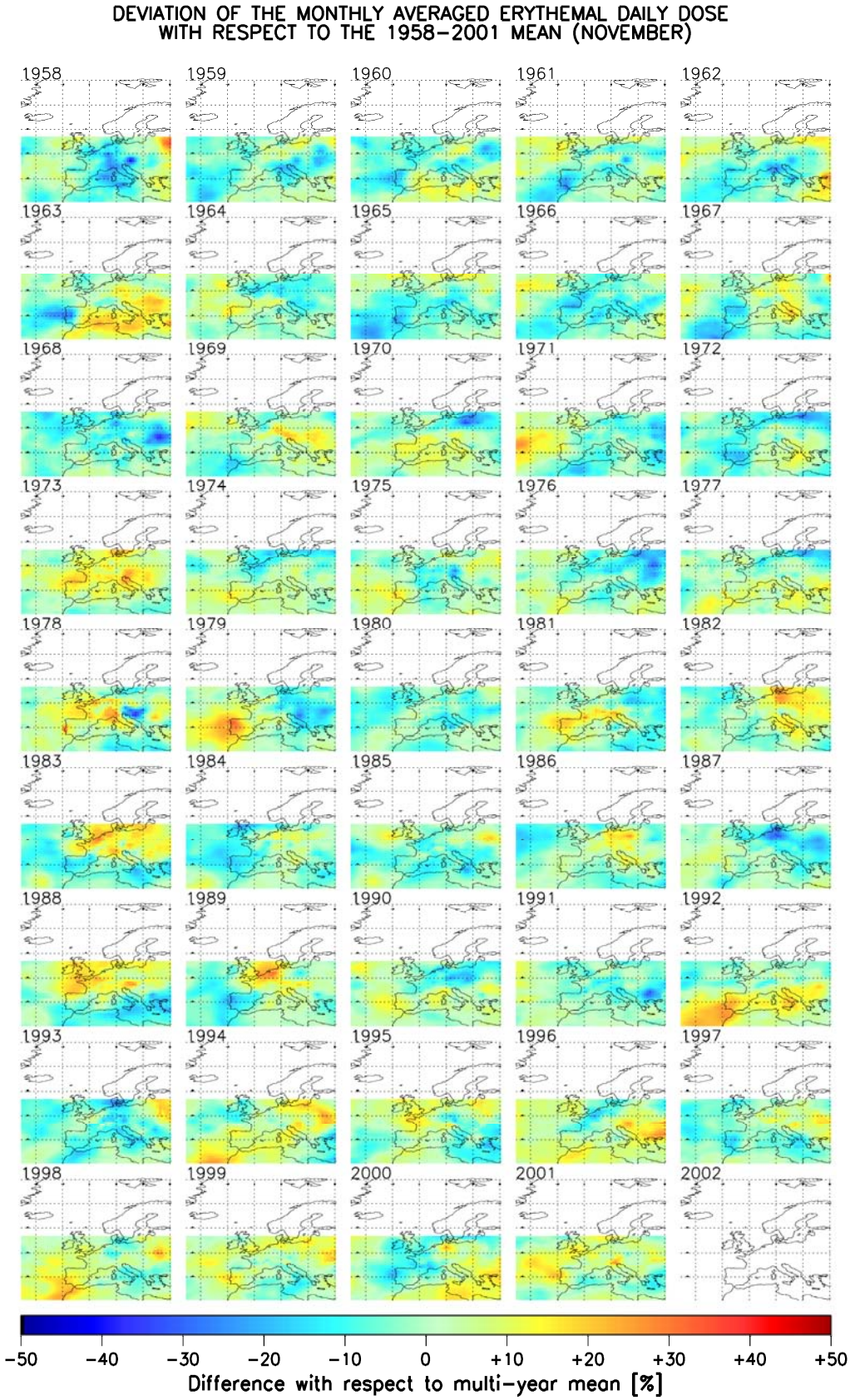

Fig. 6.2.18: Year to year variability of the monthly averaged erythemal daily dose in November.

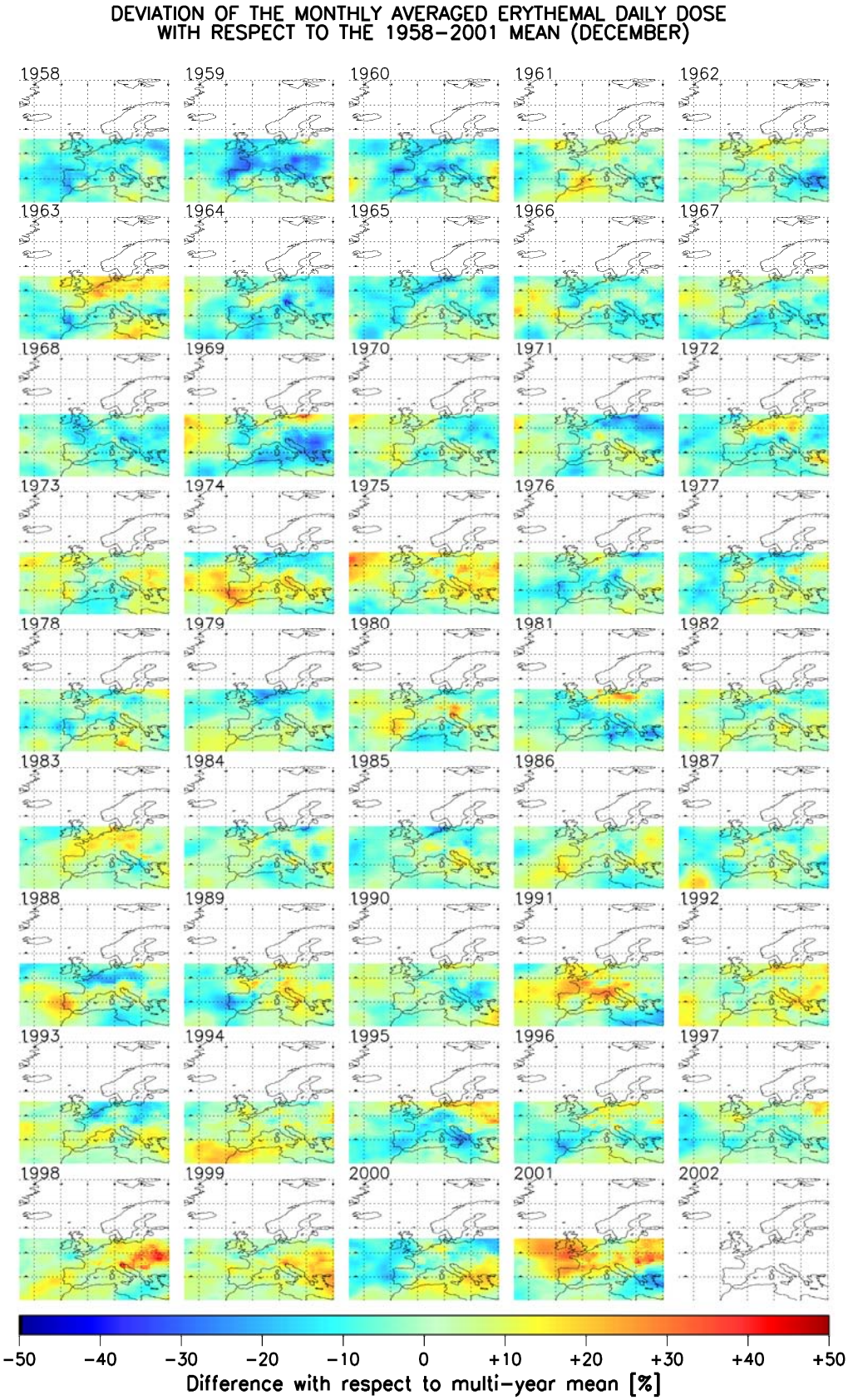

Fig. 6.2.19: Year to year variability of the monthly averaged erythemal daily dose in December.

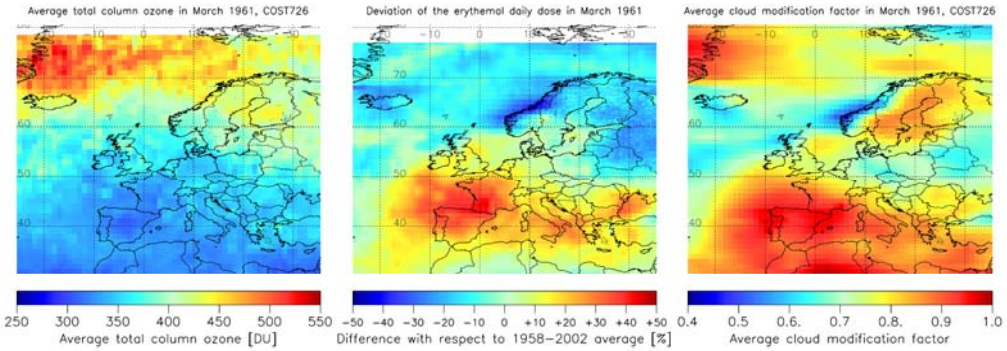

Fig. 6.2.20: March 1961, average total column ozone (left), deviation of the erythemal UV (centre) and average cloud modification factor (right).

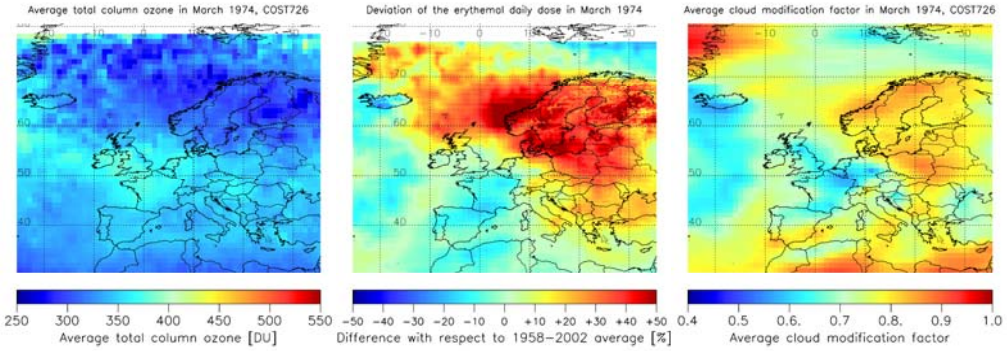

Fig. 6.2.21: March 1974, average total column ozone (left), deviation of the erythemal UV (centre) and average cloud modification factor (right).

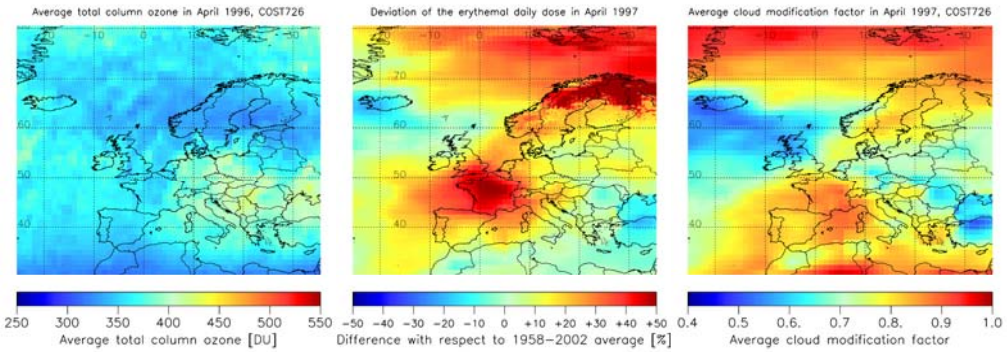

Fig. 6.2.22: April 1996, average total column ozone (left), deviation of the erythemal UV (centre) and average cloud modification factor (right).

The figures above show three cases extracted from the full series, accompanied by the corresponding total column ozone (on the left) and the average cloud modification factor (on the right). In March 1961 (Fig. 6.2.20) the ozone was exceptionally abundant in the North, leading to a deficit in the erythemal radiation, even if the cloudiness was relatively low in the same area. The large excess over Scandinavia and Finland in March 1974 (Fig. 6.2.21) results from the combination of low ozone and low cloudiness. So is the case in April 1996 (Fig. 6.2.22) while the excess over France is caused by low cloudiness, the ozone being close to normal at this latitude.

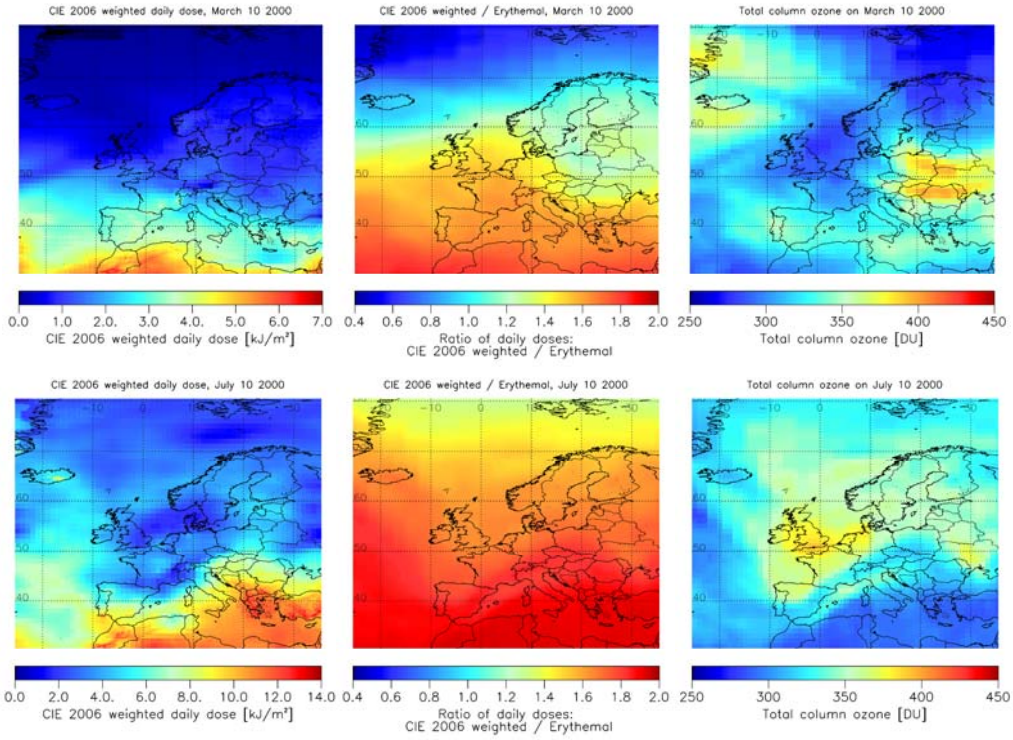

Fig. 6.2.23: March 10 (top) and July 10 2000 (bottom), CIE 2006 weighted daily dose (left), ratio of CIE 2006 weighted to erythemal daily dose (centre) and total column ozone field (right).

As previously mentioned, the data set also contains daily maps at 7 discrete wavelengths. The purpose of these additional maps is to enable the reconstruction of daily doses corresponding to other effects of UV radiation. An important and beneficial one is the photosynthesis in the skin of pre-vitamin D3. Figure 6.2.23 illustrates the UV radiation spectrally weighted for its efficiency with regard to this process. The action spectrum used is the one endorsed by the International Committee on Illumination (CIE 2006). The two images on the on the left represent the CIE 2006 weighted daily dose on March 10 (top) and July 10 2000 (bottom) respectively. The influencing factors are the same as for the erythemal radiation: cloudiness, altitude, surface albedo, aerosols, solar zenith angle and total column ozone. However, the "vitamin D efficient UV" is more sensitive to absorption by ozone than the erythemal radiation. With respect to the erythemal action spectrum, the CIE 2006 action spectrum indeed puts a larger relative weight on shorter wavelengths and is close to zero in the UVA. As a consequence, the "vitamin D efficient UV" decreases with high solar zenith angle more rapidly than the erythemal UV, as the effective path of the photons through ozone gets longer. This shows in the centre images of the panel representing the ratio of CIE 2006 weighted to erythemal daily doses on the two days. In July and at low latitude, this ratio is close to two while it drops below one in the North in March. Obviously this ratio also decreases with the amount of total column ozone itself. One can see that the patterns in the ratio images correspond to the patterns of total column ozone on the corresponding days (images on the right).

6.3 TEMPORAL CHANGE, TREND ANALYSIS – ERYTHEMAL UV

Janusz Krzyścin [a]

a) Polish Academy of Sciences, Institute of Geophysics.

Surface UV exhibits variations in different time scales ranging from minutes up to decades. Such variability reflects many complicated processes affecting UV transmission through the atmosphere. The most pronounced periodical signal in the UV data is the daily and yearly course related to the sun elevation. The highest sun elevation at local noon corresponds usually to the UV maximum. As

reconstructed daily total ozone values are available for Europe since January 1, 1950 it becomes possible to estimate all-sky modelled UV radiation for sites providing global solar radiation from measurements that allows to estimate cloud correction of the clear-sky UV irradiances calculated on the basis of total ozone data and other variables fixed to their climatological means. There are many weather stations that measure routinely global radiation using pyranometers. Stations providing long series (~50 years) of the solar measurements are of special interest in discussion of the multi-scale UV variability. The interest on UV temporal variations encompasses mostly a prediction of next-day daily maximum (UV index) or an extraction of persistent tendency from the time series. In this chapter, we will focus on calculations of the long-term changes in the reconstructed UV data.

One of the objectives of COST 726 was examination of the European UV reconstruction models (Koepke et al., 2008). Following models have been found within the group of best performing models when compared with the measured erythemally weighted UV daily doses: Geophysical Institute, Slovak Academy of Sciences (GSAS), Bratislava, Slovakia; Institute of Meteorology and Water Management (IMGW), Warsaw, Poland; National Institute for Public Health and the Environment (RIVM), Bilthoven, the Netherlands. Here we discuss the temporal UV variability for some reconstruction sites using output of these models. For example, figure 6.3.1 shows the reconstructed (GSAS model) UV series for Budapest starting in January 1, 1950. Moreover, we examine the spatial distribution of long-term UV changes and its forcing factors over Europe using COST 726 maps with 1° × 1° resolution.

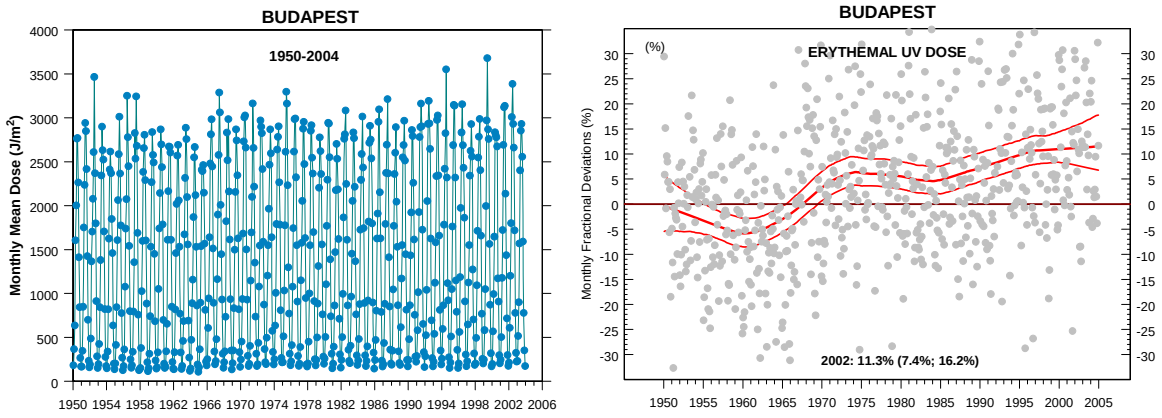

Fig. 6.3.1: Monthly mean doses from the reconstructed (GSAS model) daily erythemaly weighted doses for Budapest since January 1950 – (left), smooth curve fitted to monthly fractional deviations with 95 % uncertainty range to illustrate trend pattern and its uncertainty – (right).

In multi-scale analysis of the data it is convenient to use monthly fractional deviations, i.e., deviations of actual monthly means from the long-term monthly means expressed in percent of these long-term means. In this way, the strong yearly course is subtracted from the data. Next, a spectral analysis is performed to separate the variability in selected time scales. Wavelet decomposition allows not only identifying periodicities of the original signal but also the amplitudes of the signal multiscale components. Figure 6.3.2 shows the wavelet decomposition of the monthly fractional deviations for Budapest derived from the reconstructed UV data by the GSAS model. The low frequency components (with time scale >10 years) of the wavelet decomposition are summed to form a trend component. The trend pattern for Budapest shows two periods with positive tendency (1960–1975 and since 1985). Further in the text we will analyze the UV level in 2002 that is taken from the trend pattern extracted from various fractional deviations (individual stations, maps).

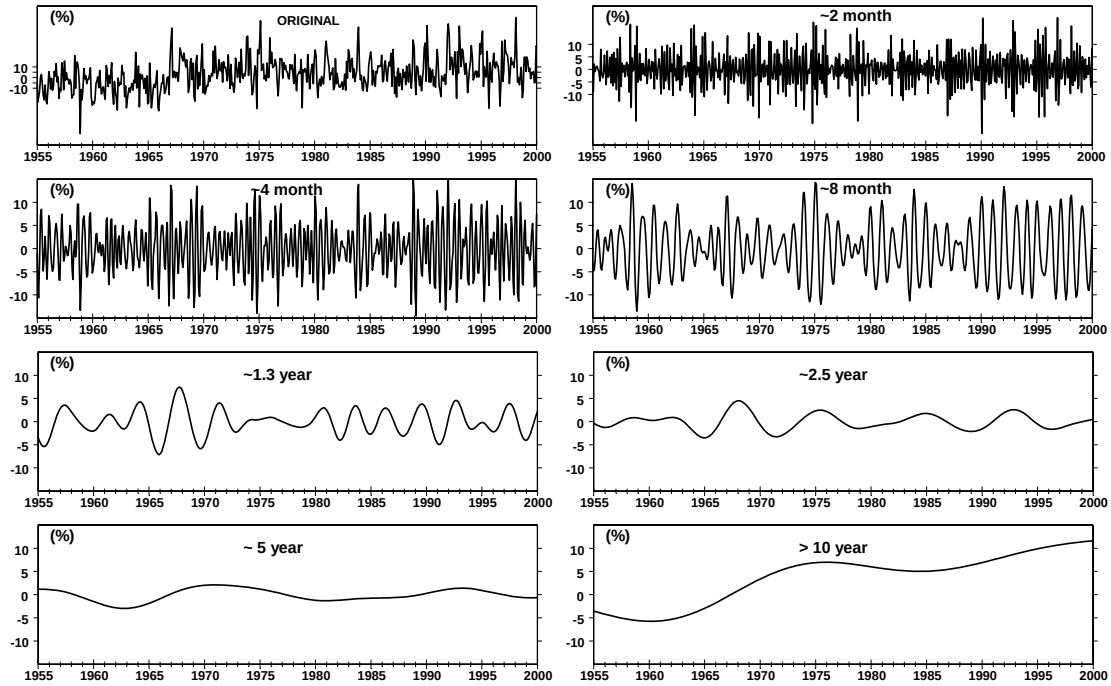

Fig. 6.3.2: Wavelet decomposition of the monthly fractional variations taken from reconstructed (GSAS model) erythemaly weighted doses for the period 1950-2004 in Budapest.

The long-term variability is usually extracted from a straight line fit to the whole analyzed time series or its subsets (e.g., Reinsel et al., 2002; WMO, 2003). A comparison of slopes of the regression lines enables to infer temporal variations of the long-term component of time series. Recently a concept of trend evaluation using a smooth curve fit to the data has been developed (Harris et al., 2003; Krzyścin et al., 2005; Oltmans et al., 2006; and Krzyścin, 2006). In such an approach, a trend component means a continuous and smooth pattern extracted from the time series, i.e., the pattern is not a priori assumed. A model using such concept is the so-called flexible trend model and it is also used here. The 95 % confidence ranges for the trend curve uncertainty are derived by block bootstrapping (Krzyścin and Borkowski, 2008).

Tables 6.3.1 and 6.3.2 show the departures of the monthly values of the erythemaly weighted UV, CMF, and ozone in 2002 relative to the base-line level of the variables (long-term monthly means before 1979) in percent of the base-line value. Table 6.3.1 presents the results obtained by GSAS and IMGW model for Budapest (reconstructed UV time series since 1950), Uccle (since 1951), and Tartu (since 1950). Table 6.3.2 contains results by RIVM model for Budapest (since 1950), Hamburg (since 1950), Hohenpeissenberg (since 1953), Potsdam (since 1950), Uccle (since 1951), Warsaw (since 1961), and Zakopane (since 1958). It can be inferred from the models output comparison for Budapest and Uccle that the results by various models are almost equivalent. The models provide the same significance of the estimated values for all sites and seasons. There are slight differences between the mean value estimates. Most of them are within the 95 % confidence interval.

Table 6.3.1: Departure of the reconstructed erythemally weighted radiation (UV), cloud modification factor (CMF_{UV}), and column amount of ozone (Ozone) in 2002 relative to the long-term mean (before 1979) in percent of the long term mean for warm sub-periods (April-September), cold periods (October-March), and the whole year (January-December). 95 % confidence ranges of the estimates are in the parentheses. Asterisks mark statistically significant results.

GSAS model

Site	UV	CMF_{UV}	Ozone
		April-September	
Budapest	6.4*(2.5, 10.5)	3.2 (-0.2, 6.3)	-2.4*(-4.0, -0.8)
Tartu	3.5 (-1.2, 8.4)	1.0 (-2.8, 4.6)	-2.6*(-4.4, -0.9)
Uccle	7.9*(2.7,13.6)	3.4 (-0.2, 8.0)	-3.4*(-5.4, -1.7)
		October-March	
Budapest	16.3*(11.4,23.1)	10.0*(5.2, 15.2)	-4.1*(-6.4, -2.1)
Tartu	-6.5*(-11.8,-1.4)	-8.5*(-12.1,-4.6)	-3.0*(-5.9, -0.7)
Uccle	6.5*(2.2, 10.5)	0.9 (-3.2, 5.0)	-4.6*(-6.9, -2.4)
		January-December	
Budapest	11.3*(7.4, 16.2)	6.6* (3.0,10.4)	-3.3*(-4.9, -1.8)
Tartu	-1.7 (-5.3, 2.3)	-3.8*(-6.6,-0.8)	-2.8*(-4.7, -1.1)
Uccle	7.2*(3.7, 11.8)	2.3 (-0.3, 5.9)	-4.0*(-5.9, -2.5)

IMGW model

Site	UV	CMF_{UV}	Ozone
		April-September	
Budapest	5.9*(1.7, 9.4)	2.6 (-0.2, 5.1)	-2.3*(-4.0, -0.8)
Tartu	4.2 (-0.9, 9.1)	1.4 (-2,1, 4.7)	-2.6*(-4.5, -0.8)
Uccle	7.9*(3.1,13.3)	3.0 (-0.3, 6.9)	-3.4*(-5.2, -1.8)
		October-March	
Budapest	21.7*(15.3,29.4)	11.8*(6.3, 17.7)	-4.1*(-6.3, -2.2)
Tartu	-6.6*(-13.4,-1.3)	-9.3*(-14.1,-4.2)	-3.0*(-5.9, -0.7)
Uccle	10.4*(5.9, 15.1)	3.5 (-0.5, 7.9)	-4.6*(-6.8, -2.5)
		January-December	
Budapest	13.6*(9.8, 18.8)	7.2* (3.6,10.8)	-3.3*(-5.0, -1.8)
Tartu	-1.3 (-5.6, 4.0)	-4.2*(-7.3,-0.8)	-2.8*(-4.9, -1.1)
Uccle	9.5*(5.8, 13.4)	3.2* (0.8, 7.1)	-4.1*(-5.9, -2.4)

Higher UV levels in 2002 by ~5-10 % than those before satellite era (pre-1979) are found over many stations. However, such increase is the most pronounced for stations located in large urban regions. The differences between the reconstructed UV levels over the stations are mainly induced by the local properties of cloud/aerosol forcing. Ozone drives a smooth increase of UV since the early 1980s. The level in 2002 is about 3–5 % higher than that before 1979 due to the ozone forcing. Long-term increase of the atmosphere transparency induced by changes in cloud/aerosol properties is especially pronounced for Budapest in cold seasons and Warsaw in all seasons. Both ozone and cloud/aerosol effects induce a high increase of the present mean UV level up to ~15 % in Budapest. Over Tartu and Zakopane we have found the opposite effects in the cold sub-periods and the mean UV level in 2002 is the lowest in the record with ~5 % deficit. The statistically significant decline of UV at the end of the time series has been found in

cold seasons only for Tartu and Zakopane. The uncertainties of the mean UV level estimates are large prohibiting discussing differences between stations with a UV positive trend.

Table 6.3.2: The same as table 6.3.1, but the results are from RIVM model and for additional stations.

	RIVM model		
Site	UV	CMF_{UV}	Ozone
	April-September		
Budapest	5.7*(1.9, 9.7)	2.4 (-0.7, 5.5)	-2.5*(-4.1, -0.9)
Hamburg	5.0*(0.6, 10.9)	0.8 (-2.5, 4.8)	-3.2*(-4.7, -1.7)
Hohenpeissenberg	8.0*(2.4, 13.7)	3.1 (-1.1, 7.5)	-4.3*(-6.1, -2.2)
Potsdam	6.2*(2.4, 13.7)	3.1 (-1.3, 7.6)	-2.8*(-4.7, -1.0)
Uccle	8.1*(2.7, 14.7)	3.3 (-0.6, 8.0)	-3.4*(-5.3, -1.7)
Warsaw	11.2*(6.9, 15.2)	7.1*(3.9, 10.1)	-2.9*(-4.6, -1.4)
Zakopane	-0.7 (-4.7, 4.0)	-4.0*(-8.0,-0.8)	-2.7*(-4.2, -1.3)
	October-March		
Budapest	10.8*(6.4, 16.3)	7.0*(2.5,11.3)	-4.2*(-6.5, -2.2)
Hamburg	5.3*(1.5, 9.3)	-0.2 (-2.5, 4.8)	-4.7*(-6.9, -2.5)
Hohenpeissenberg	0.4 (-4.7, 5.9)	-5.8*(-9.8,-1.7)	-5.5*(-8.7, -2.7)
Potsdam	11.7*(6.7, 16.1)	6.4*(2.4,10.2)	-4.7*(-7.5, -2.3)
Uccle	9.0*(5.0, 12.7)	3.4 (-0.3, 7.1)	-4.6*(-6.7, -2.7)
Warsaw	10.3*(5.5, 14.1)	8.3*(3.8,11.8)	-2.9*(-4.8, -1.5)
Zakopane	-3.6*(-7.6, -0.5)	-5.6*(-8.6,-1.7)	-3.1*(-4.6,-1.9)
	January-December		
Budapest	8.3*(4.9,12.1)	4.8*(1.8, 7.8)	-3.4*(-5.0, -1.9)
Hamburg	5.1*(1.6, 9.3)	0.3 (-2.4, 3.1)	-3.9*(-5.6, -2.4)
Hohenpeissenberg	4.3 (-0.3, 8.7)	-0.7 (-4.4, 2.3)	-4.6*(-6.8, -2.7)
Potsdam	9.2*(6.7,16.1)	4.9*(0.7, 8.1)	-3.9*(-5.9, -1.9)
Uccle	8.5*(5.0,12.9)	3.4*(0.9, 6.7)	-4.0*(-5.9, -2.5)
Warsaw	10.7*(7.3,13.9)	7.7*(4.6,10.2)	-3.1*(-4.7, -1,9)
Zakopane	-2.1 (-5.1, 1.4)	-4.5*(-7.2,-1.5)	-3.1*(-4.6, -1.9)

Maps provide a different category of the reconstructed UV data. The reconstructed UV time series is for the period 1958-2002. The cloud effects on UV radiation are derived from the corrected ERA-40 daily sum of global solar radiation representing the cloud pattern averaged over the grid area (1° × 1°) rather than local cloud properties. Both reconstructed UV models for the selected sites with the pyranometric measurements and the grid points use the COST 726 total ozone database. Table 6.3.3 shows the UV departures averaged over the latitudinal bands in 2002. The positive deviations in the UV field relative to the long-term mean level before 1979 are mostly found in the European mid-latitudes in the extended winters (October-April) and the whole year data. For the higher latitudes and extended summers (May-September) the UV departure at the end of time series is not statistically significant. Also worth mentioning is the occurrence of a statistically significant negative departure found in the warm sub-periods for the uppermost band (75°–80° N).

Table 6.3.3: Departure of reconstructed (COST 726 map) erythemaly weighted radiation in 2002 relative to the long-term mean (before 1979) in percent of the long term mean for extended summer (May–September), extended winter (October–March), and the whole year (January–December). 95 % confidence ranges of the estimates are in the parentheses. Asterisks mark statistically significant results.

Band	Warm	Cold	Year
35° – 40° N	2.1 (-0.3, 4.9)	6.3*(2.8, 9.5)	4.7*(2.2, 7.5)
45° – 50° N	0.8 (-2.3, 3.8)	6.5*(3.5, 9.6)	4.5*(1.5, 7.1)
55° – 60° N	1.8 (-1.7, 6.1)	1.3 (-2.0, 4.6)	1.2 (-1.2, 4.3)
65° – 70° N	-1.2 (-4.0, 1.6)	-0.7 (-4.6, 4.6)	-1.4 (-4.4, 2.2)
75° – 80° N	-4.8*(-7.8,-1.3)	1.9 (-4.1, 9.2)	-2.4 (-6.2, 2.0)

Figure 6.3.3 shows maps of the deviations of erythemaly weighted UV level in 2002 over Europe and surroundings relative to the base line level (1958-1978) expressed in percent of the base line level. Positive (negative) departure means overall increasing (decreasing) UV levels in the period 1979-2002. The UV increase over the continental Europe and western part of North Africa, and Svalbard is disclosed in the extended winter sub-periods. The hot spots are: Slovenia, East-Northern part of Greece, eastern part of Ukraine. The UV level at these areas is ~10–15 % higher than that before 1979. The estimates for these regions are highly statistically significant. The same hot spots, excluding Ukraine, exist also in the extended summers. The UV increase over the continental Europe approaches 10 % in extended summers and it is slightly lower than that in the extended winters. Statistically significant UV increases are found only in some isolated areas in continental Europe during the summer sub-periods. The UV increase over Greece is still very strong. Regions with whole year UV increase appear over continental Europe and the western part of Africa but the change is statistically significant mostly over the mentioned hot spots. A UV decrease is identified over seas (the Greenland Sea, the Bay of Biscay and the Norwegian Sea), but the results for these regions should be treated with caution as the cloud variability over these regions is not supported by real measurements of global solar radiation.

To identify the sources of the UV changes we draw similar maps illustrating spatial variability of the departure for UV forcing variables at the end of time series relative to the base-line level before 1979. Figure 6.3.4 shows the cloud transparency (in UV range) and the total ozone variability is illustrated in figure 6.3.5. The pattern of ozone decline is quite smooth over the whole analyzed area. The UV increase due to ozone changes in the cold sub-periods of the year is at most of about 5 % being only slightly more negative than that in the warm sub-periods. The appearance of the UV hot spots discussed earlier in this section is due to the cloud transparency increases. The cloud transparency increases ~5–10 % in the mentioned UV hot spots. It seems that the atmospheric brightening found over these sites is a local phenomenon. For example, it is worth noting a difference between the cloud transparency tendency found for two sites relatively close to each other, Greece (brightening) and Ukraine (diming) in the warm sub-periods. Declining tendency in the cloud transparency (atmospheric dimming) is the most pronounced over the Bay of Biscay. However, it cannot be excluded that it is partially artificial effect caused by the ERA-40 cloud model deficiency in that region as the model is not trimmed by global solar radiation measurements there.

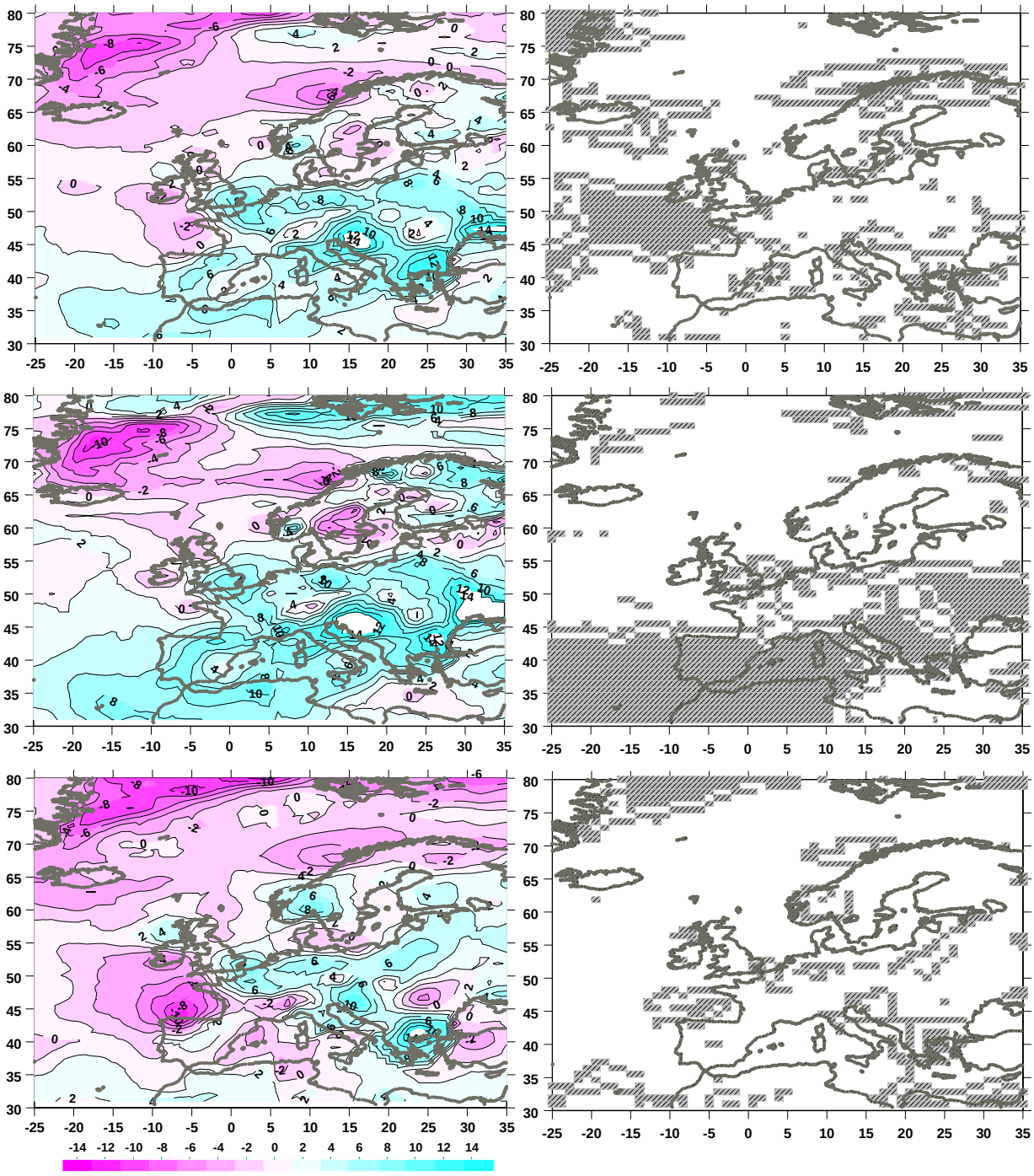

Fig. 6.3.3: Departure of erythemaly weighted UV in 2002 relative to the base-line (1958–1978) UV level expressed in percent of the base-line value: whole year data (top), extended winter October-April (middle), extended summer May-September (bottom). The dashed areas (on the right) show the region where the change is statistically significant at 95 % confidence level.

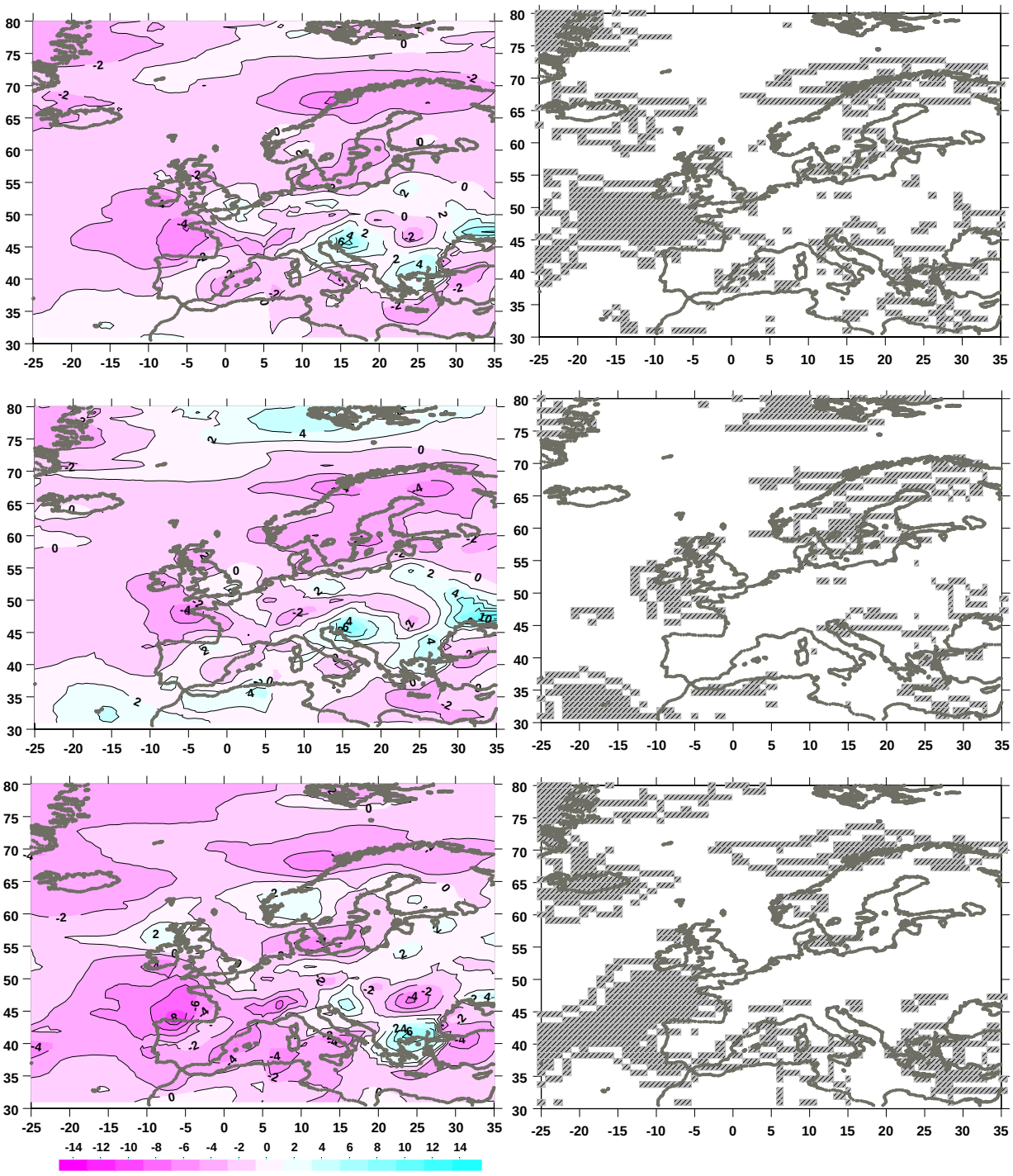

Fig. 6.3.4: Departure of Cloud Modification Factor in the UV range (CMF_{UV}) relative to the base-line (1958–1978) CMF_{UV} level: whole year data (top), extended winter October-April (middle), extended summer May-September (bottom). The dashed areas (on the right) show regions with statistically significant results.

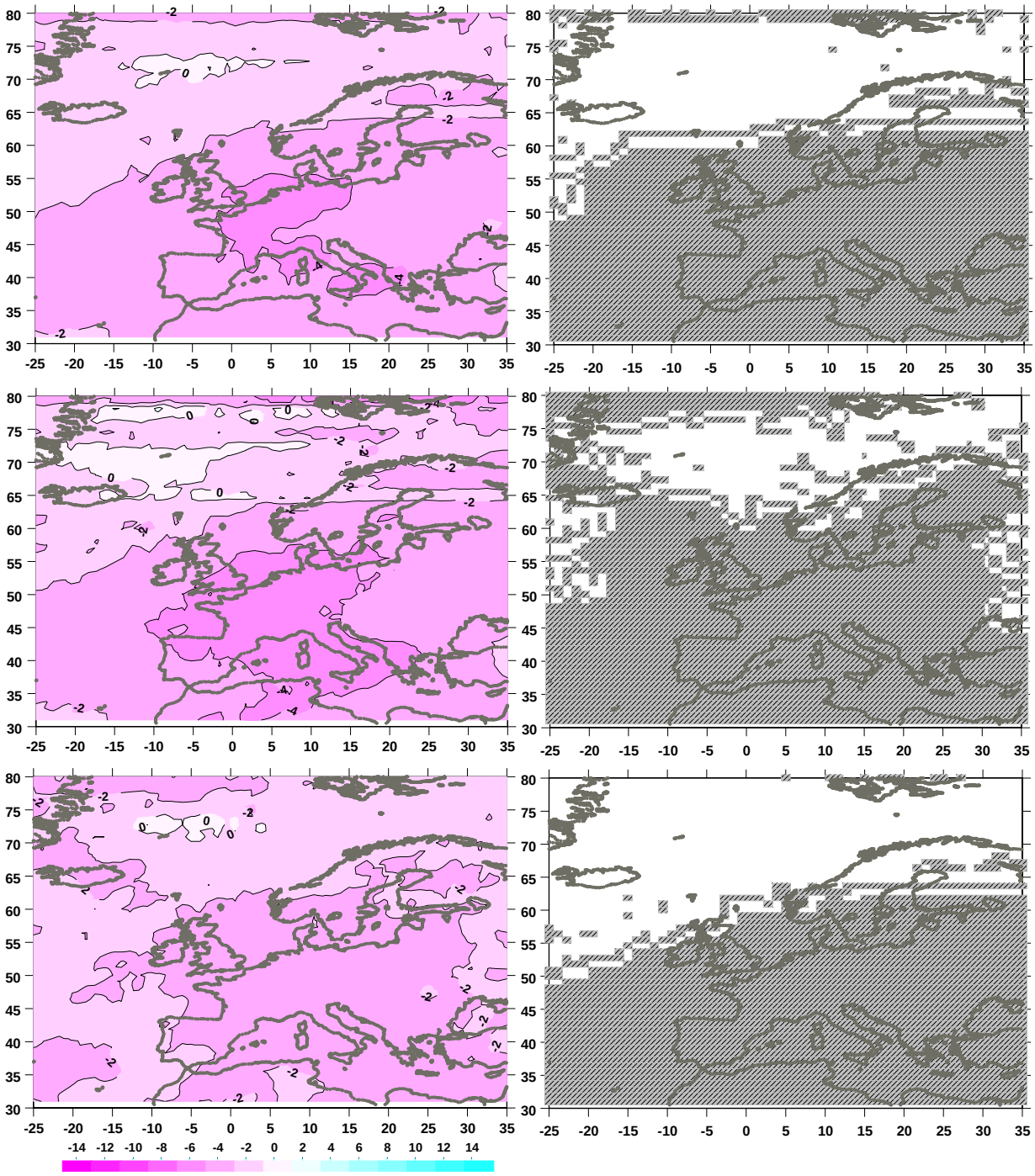

Fig. 6.3.5: Same as figure 6.3.3, but for the column amount of ozone.

It was not possible to identify long-term tendency in other important factors responsible for UV changes, i.e., aerosols and albedo. It is suggested that the appearance of decreasing trend in the aerosol optical depth (in the visible range) over the western continental Europe is a result of the environment protection (Ruckstuhl et al., 2008). The COST 726 model uses fixed aerosol properties. Global solar radiation could account for such changes only partially and the aerosol impact on UV is overwhelmed by the cloud variability. Thus the discussed pattern of the long-term UV variability over Europe is mostly driven by the ozone and cloud transparency changes and may differ from real pattern of UV changes as

the aerosol and albedo effects are only roughly included in the COST 726 reconstruction model. It is worth mentioning that the recent UV changes from COST 726 maps over Europe are not dramatic. The present (2002) smoothed UV level is approximately within ±10 % range relative the base-line (before 1979) UV level and for large European areas we could not find a statistically significant UV change due to large year-to-year variability of the forcing factors.

6.4 UV RADIATION FOR OTHER BIOLOGICAL PROCESSES

Alois Schmalwieser [a]

a) Institute of Medical Physics and Biostatistics, University of Veterinary Medicine, Austria.

A UV climatology is of interest not only for erythemal UV, but also for other biological effects. Spectral modelling allows one to calculate the biological effective radiation for any photobiological effect, if the biological weighting function (action spectrum) is known. A hundreds of action spectra were published in the past. That is the reason why within this COST action we have spread out a questionnaire (within COST 726 countries) to find out which photobiological weighting functions are applied for modelling or to weight measurements. It was found that the most frequently applied action spectrum is that for erythema as standardised by CIE in 1987. But several others are in use as well. All action spectra contemplated in the answered questionnaires are listed in table 6.4.1 and shown in figures 6.4.5 and 6.4.6 over the range from at least 280 nm to 400 nm and generally normalised at 300 nm.

Table 6.4.1: Reference Action Spectra

Spectra	Reference
DNA-Damage	Setlow (1974)
Photoconjunctivitis	CIE (1986a)
Photokeratitis	CIE (1986b)
Human Erythema	CIE (1987)
Skin Lipid peroxidation	Morliere et al. (1995)
Skin elastosis	Wulf et al. (1989)
Photoisomerization	Gibbs et al. (1993)
Photoinmunosupression	De Fabo et al. (1990)
Non-melanoma skin cancer	de Gruijl and van der Leun (1994)
Vitamin D	CIE (2006)
General human risk	ACGIH (1990)
General human risk	ICNIRP (2004)
Photosynthesis	Caldwell (1971)
Generalized plant damage	Caldwell et al. (1986)
GPD in higher plants	Flint and Caldwell (2003)
Microbicidal / Disinfection	OENORM M5873-2 Prestandard (2003)

Modelling of the biologically effectiveness of radiation needs action spectra with high spectral resolution over the whole solar UV range.

However, most of the experimentally derived action spectra deliver the effectiveness only at certain wavelengths. Therefore interpolation and also extrapolation is necessary to get spectrally high resolved effectiveness values over the whole solar UV range.

Just a few action spectra are derived from laser applications (e.g. erythema from Anders et al. 1995) with high spectral resolution. Some of the most important action spectra are already standardised with high resolution like Vitamin D photosynthesis (CIE 2006) or microbicidal effectiveness (OENORM

2003). Others were provided as functions (e.g. erythema by CIE1987). However most action spectra are only available for certain wavelengths and interpolation is necessary.

In most cases action spectra are not derived over the whole solar UV range because research is mainly focused on the identification of the responsible chromosphore and only seldom on the application as weighting function.

Within Working Group 3 an exercise (Zipoli and Grifoni 2007) was undertaken to estimate the uncertainty on the biologically effective radiation which comes from spectral resolution. In this exercise 3 different action spectra were applied to spectral measurements at 3 different Italian stations (using a spectroradiometer Macam SR9910-v7 with a bandwidth of 2 nm, a wavelength resolution up to 0.25 nm and a wavelength accuracy of ±0.5 nm) using different spectral resolutions: 1 nm, 2 nm, 3 nm, 5 nm and 10 nm. For each station and each action spectrum the differences due to a lower spectral resolution than 1 nm were calculated. Quite different results may be obtained using data obtained from instruments with different specifications.

Figure 6.4.1 shows the effect on the erythemally (CIE 1987, see Fig. 6.4.5) effective radiation. As it can be seen the error increase rapidly. Using a spectral resolution of 4 nm may lead already to an error around 5 %. Figure 6.4.2 shows the effect on the keratitis (CIE 1986, see Fig. 6.4.6) effective radiation. Work with a spectral resolution of 4 nm possesses an error larger than 5 %. Figure 6.4.3 shows the effect on the plant damaging (Flint and Caldwell 2003, see Fig. 6.4.6) effective radiation. In this case the spectral resolution of 5 nm causes an error around 5 %. These case studies indicate that, for all three action spectra, only a spectral resolution of at least 3 nm keeps the error below 5 %.

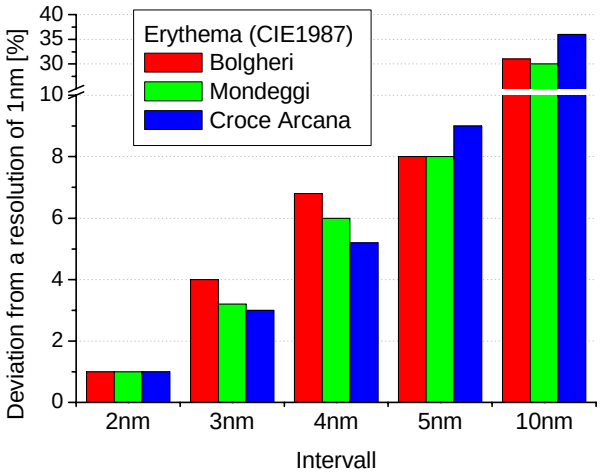

Fig. 6.4.1: Differences from different spectral resolutions compared to a spectral resolution of 1 nm for the erythemally effective radiation (scale break between 11 % and 25 %).

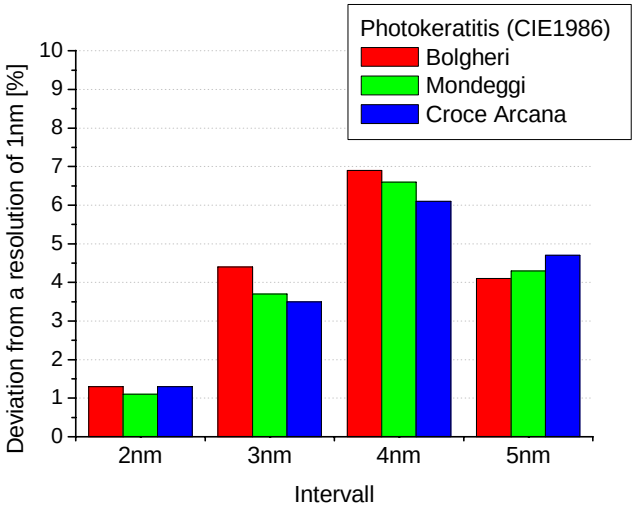

Fig. 6.4.2: Differences from different spectral resolutions compared to a spectral resolution of 1 nm for the keratitis-effective radiation.

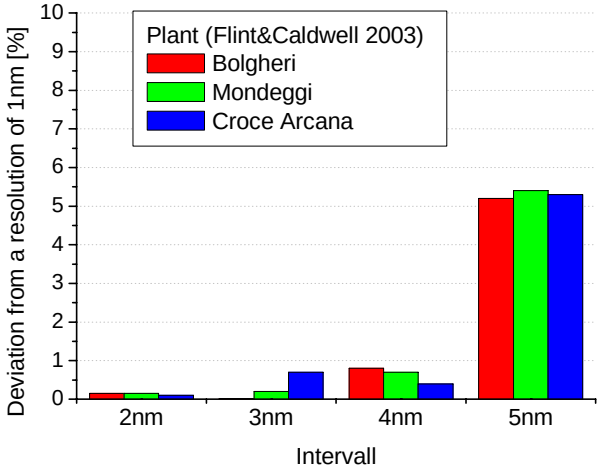

Fig. 6.4.3: Differences from different spectral resolutions compared to a spectral resolution of 1 nm for plant damaging effective radiation.

Interpolation of action spectra has to fulfil some basic requirements:

- High spectral resolution (1 nm);
- The shape gained by interpolation must be continuous as expected for photobiological and photochemical processes;
- Interpolation must pass all effectiveness values;
- Interpolation may not deliver values which are in contrary to the nature of the effect (e.g. negative values);
- Fitting an interpolation function must be reproducible.

Neither linear nor logarithmic interpolation fulfils these requirements since there are not continuous at the node points.

Approximation of the effectiveness values by a function would deliver a smooth shape. However the resulting shape does not pass all the effectiveness values. Additionally the approximated function is not unique. Different function can have the same value for a chosen error indicator (e.g. root mean square error).

A method that delivers a smooth shape which passes all the effectiveness values and delivers an error of zero is cubic spline interpolation (e.g., Stoer and Bulrisch 1980). Cubic spline interpolation provides a formula that is smooth in the first derivative, and continuous in the second derivative, both within an interval and at its boundaries. Spline interpolation can deliver positive but also negative values independently if all effectiveness values are higher or lower than zero. This is a serious disadvantage of spline interpolation, especially at a steep decrease, like over one magnitude, between two effectiveness values. Spline interpolation prolongs the decrease leading to values below zero. Afterwards the spline function comes back with positive values to match the next effectiveness value. If all effectiveness values are positive, such an interpolation delivers an unacceptable shape since completely misinterpreting the photoeffect. More details on cubic spline interpolation as well as a guide for numerical calculation can be found in Press et al. (1987). Cubic spline interpolation is nowadays included in many analysing software.

But how to solve the dilemma with action spectra having only positive values and having steep slopes? The solution comes from a logarithmic scale which inhibits negative values. If the effectiveness values are transformed to the logarithmic scale only negative values appear since the maximum is log(1) respectively zero. The application of spline interpolation is done for these logarithmic values. Afterwards the interpolated values are transferred back to the original scale. Logarithmic cubic spline interpolation fulfils all the above requirements.

One of nowadays most frequently applied action spectra is that for pro-Vitamin D photosynthesis (e.g., CIE 2003). This action spectrum was derived by McLaughlin et al. (1982). Effectiveness values are only available in the UVB. For the UVA there is no information available although relative effectiveness is still 0.01 around 315 nm (where the AS stops) (see Fig. 6.4.4).

Within the work of COST 726 we made an attempt to estimate the influence of this assumed cut-off. If one expends this AS by assuming that the effectiveness value is around 10^{-4} at 400 nm (see dotted line in Fig. 6.4.4), then a noticeable contribution comes from the UVA. For Central Europe (48° N) the difference between the Vitamin D effective irradiance from an AS that stops at 320 nm or a prolonged AS (as described) is in the order of 30 % in spring and autumn. The difference is somewhat lower in summer and off course higher in winter. The relative difference increases also with latitude.

Vitamin D is a positive effect. Underestimation of vitamin D effective irradiance is less critical since there is no Vitamin D overdose from solar exposure. In the case of a deleterious effect such negligence in the UVA may be critical because than the hazard is underestimated.

Practically the problem of extrapolation is more critical in the UVA than in the UVB since solar UVB is much lower than UVA.

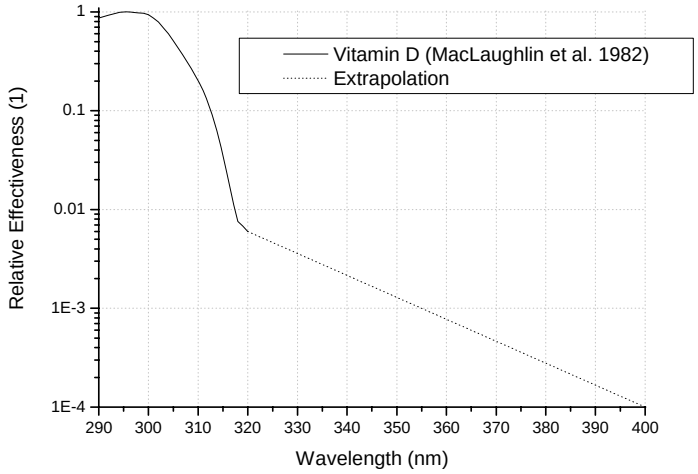

Fig. 6.4.4: Action spectrum for photosynthesis of pre-vitamin D after MacLaughlin et al. (1982). The dotted line shows a prolongation of this action spectrum into the UVA.

As already stated, UV modelling needs action spectra which cover the whole solar UV range (280 nm to 400 nm). This is a challenge. There are at least 3 possibilities for extrapolation:

- Extrapolation by using the absorption curve of the corresponding chromosphore,
- Extrapolation by expanding the last slopes,
- Set to Zero where the slope of the action spectrum is so steep that no contribution from further wavelengths can be expected.

In any case there remain uncertainties.

The following paragraph describes how the action spectra (as quoted by the questionnaire) were prepared to become appropriate for modelling.

a) Interpolation and extrapolation needed

- Photoconjunctivitis: interpolated between 220 nm and 310 nm; extrapolated by setting at 400 nm to 0.00000001 (expending last slope).
- Photokeratitis: interpolated between 240 nm to 316 nm, extrapolated by setting at 400 nm to 0.00000001 (expending last slope).
- Photoisomerization: Interpolated between 240 nm to 340 nm, extrapolated by setting at 400 nm to 0.00000001 (expending last slope).
- Photoinmunosupression: Interpolated: 280 nm to 330 nm, extrapolated by setting at 400 nm to 0.00001 (expending last slope).

b) Only interpolation needed

- Skin Lipid peroxidation: interpolated between 250 nm to 427 nm.
- Skin elastosis: Interpolated between 280 nm to 410 nm.

c) Used as published

- Human Erythema (CIE 1987), Non-melanoma skin cancer (CIE 2000), Vitamin D
- CIE 2003), ACGIH-General human risk (ACGIH 1992), ICNIRP-General human risk (ICNIRP 2004), Microbicidal / Disinfection (OENORM M5873-2).

d) Used as provided by the authors

- DNA-Damage (R.B. Setlow priv. comm.),
- Photosynthesis, Induction of flavonoid synthesis in higher plants, Generalized plant damage, and GPD in higher plants all by Flint and Caldwell priv. comm.

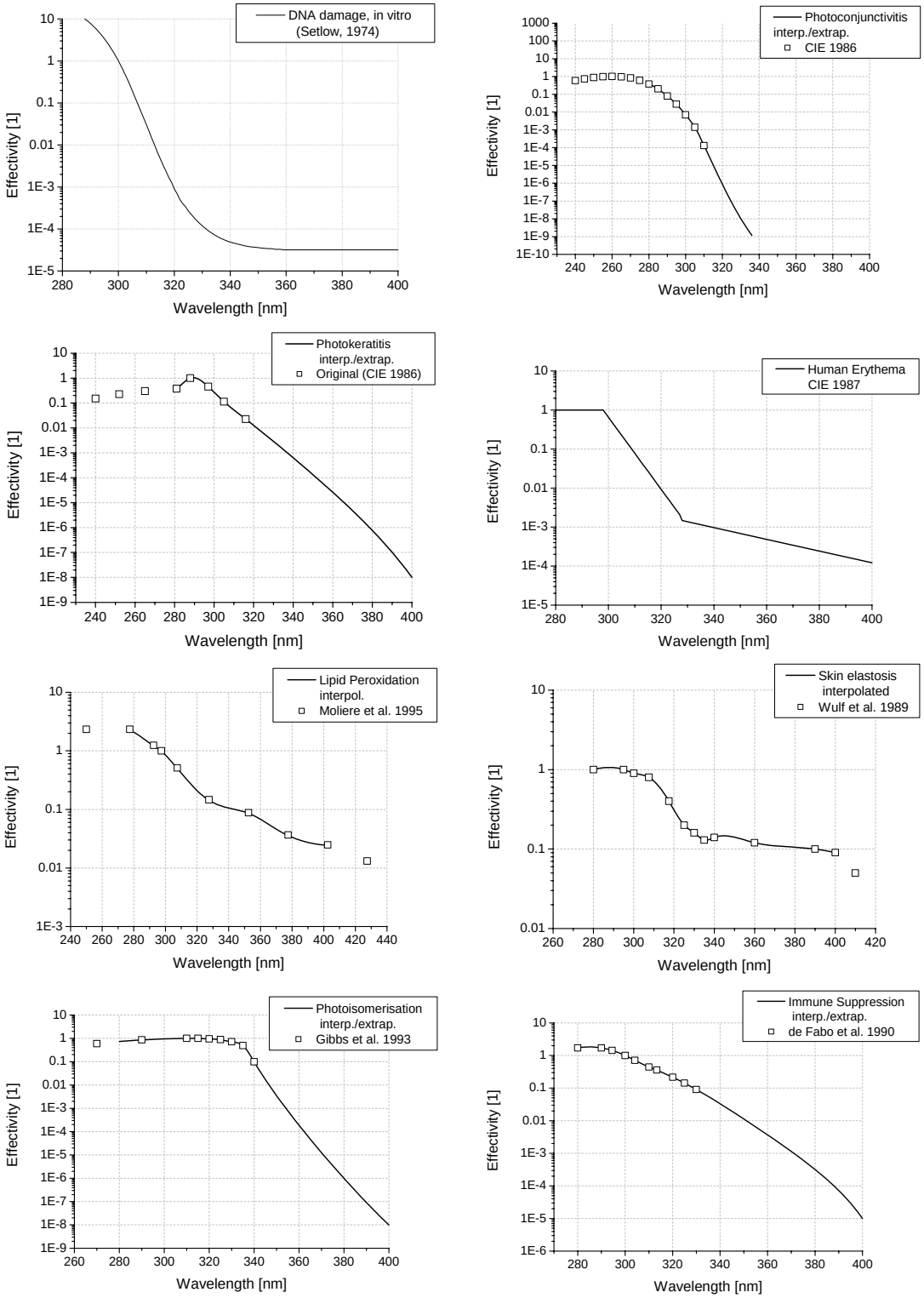

Fig. 6.4.5: Action spectra prepared for modelling. Values of action spectra represent only as lines are provided at a spectral resolution of 1 nm by the author. Action spectra shown as squares and lines are action spectra which had to be prepared for modelling whereas the squares give the original values from reference.

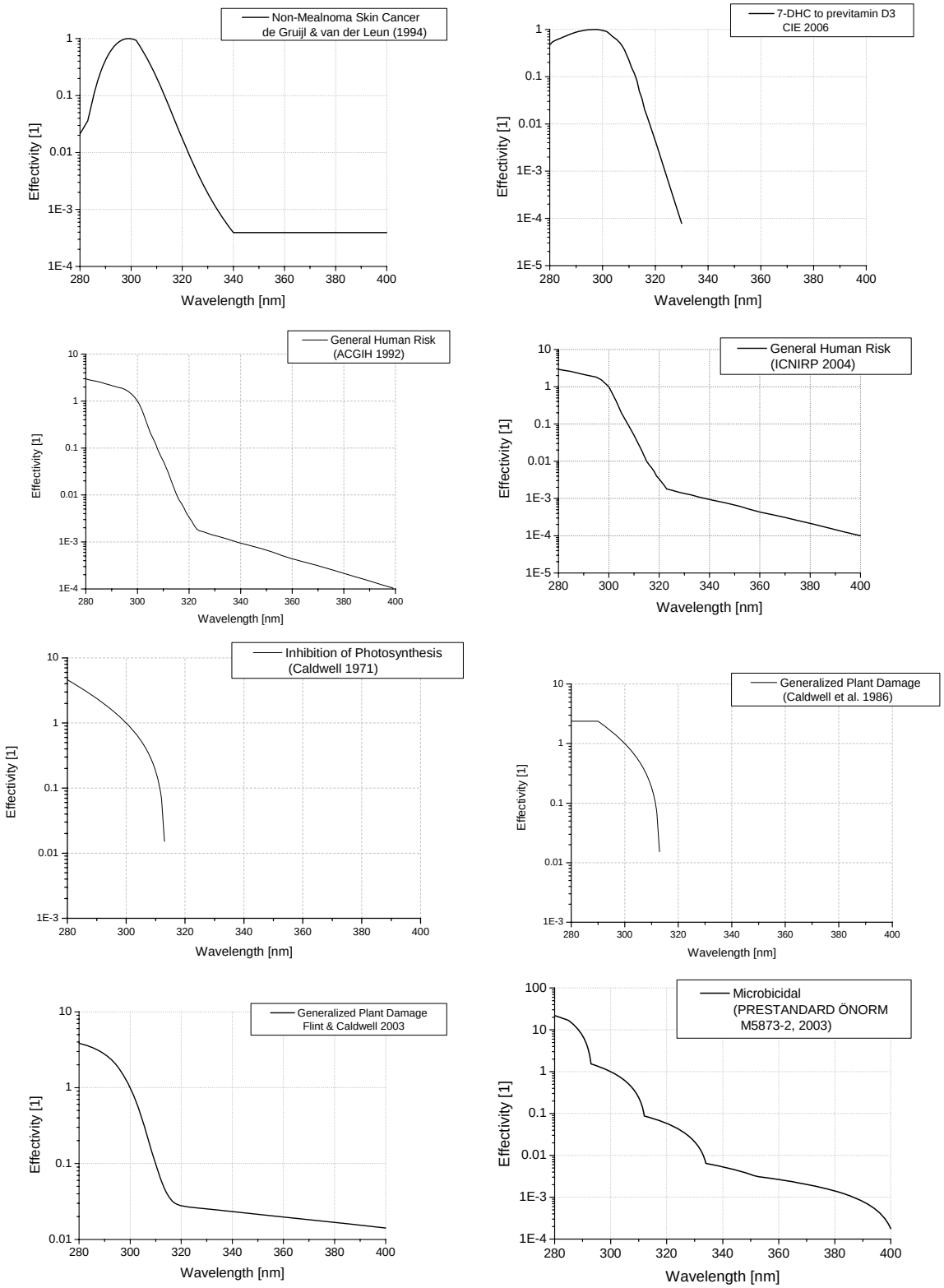

Fig. 6.4.6: Action spectra prepared for modelling. Values of action spectra represent only as lines are provided at a spectral resolution of 1 nm by the author. Action spectra shown as squares and lines are action spectra which had to be prepared for modelling whereas the squares give the original values from reference.

7 CONCLUSION

Peter Koepke [a]
a) Meteorological Institute, L.-M.-University Munich.

Studies of the impact of UV radiation on the environment, with various biological systems and especially humans, require knowledge of UV climatology and changes that have occurred in the past. It is necessary to have the estimates of average and extreme characteristics of the UV impact as well as doses over different time periods, for long time in the past. Since the climatic conditions in Europe are highly variable, a UV climatology for Europe has to be made for the whole area with high spatial resolution.

To meet these demands a European coverage of scientists is necessary, with the capability to activate the various relevant national stakeholders across different disciplines and institutional remits. The same holds for the flexibility in adapting methodologies to existing know-how and the cooperation of scientist who are coming from different disciplines, but all strongly interested in the basic questions. These problems clearly can best be solved by a COST action, and the successful realisation of the demands of the actual action again shows the high effectiveness of COST.

Result of the action is the climatology of UV daily doses for erythemal weighted UV, as it is of relevance for human health. These results are visualised in maps that give a clear overview of variability of UV daily dose depending on location and time.

However, many more achievements result from the action. To get UV irradiances in the past, modelling of UV irradiances is the only possibility, using adequate data for the atmospheric parameters which are of relevance for the UV. Since such data were not available at the beginning of the action, additional activities have been performed by the members of the COST action. The results now are available for the use in very different scientific questions besides UV irradiance.

These results are e.g. a spatially resolved ozone climatology for Europe for the last 50 years and monthly mean values of the aerosol optical depth in the UV over Europe, using different sources. Spatially resolved global solar irradiance data of ERA-40 have been adapted to measured high quality solar irradiance data, with a method regarding the distance of variable information to each specific point. The approach to convert cloud modification factors from the solar to the UV spectral range has been improved with respect to spectral dependencies. A method has been developed to get the snow albedo as function of easily available data. UV irradiances modelled by different methods and databases have been compared among each other and against measured data.

The long term series of reconstructed UV radiation have been used for trend calculations and analyses. A separation for the reasons of the determined trend change of the UV radiation, as change of total zone or cloudiness has been examined to reveal sources of temporal variations of the UV trend patterns over Europe.

The basic climatology is the erythemal weighted UV, as it is of relevance for the human health. However, a lot of additional biological UV effects exist, for which the relevant biological action spectra have been collected in the COST action. Moreover, a method has been developed and made available that gives the possibility to get UV data, and thus European UV climatology, for all these different action spectra on the basis of a 7 wavelengths algorithm.

The major goal of the Action, a geographically broader and scientifically deeper knowledge of the climatology of UV radiation and of selected biologically effective UV radiation doses across Europe, has been reached with high quality. The results will give, among others, the basis for research of skin cancer development, since this has such a long incubation period with the consequence that measured instantaneous UV data are not meaningful.

The Climatology was derived based on modelling studies since reliable measurements were not available for the past 50 years. Nevertheless, a few selected measurement sites were used for the validation of the UV Climatology. The current COST action has put large efforts into assuring future reliable UV measurements across European networks so that future UV climatologies can be based on accurate measurements of solar UV radiation. Thus, common quality control and maintenance procedures were established. Several large scale intercomparison and calibration campaigns were organized to

calibrate reference radiometers used in national and regional networks. Through direct bi-lateral intercomparisons, six European calibration laboratories were compared showing excellent agreement between the majority of these laboratories. The outcome of this COST action has produced a baseline for accurate and reliable UV Measurements for future studies of UV Radiation based on quality assured and harmonized measurements from UV monitoring networks across Europe.

To make the results of the COST action 726 "Long term changes and climatology of UV radiation over Europe" available to a broader audience, a booklet has been published, specially designed for the public and medical authorities. Additionally an action web-site has been established (www.cost726.org), which gives free access to general information on the action, on proceedings of seminars, and moreover to actual reports and publications. Data generated by this action are available too. For the atmospheric science community an electronic atlas has been prepared (see Appendix E). Thus the public, researchers in atmospheric and medical sciences as well as authorities and policy makers are beneficiaries of the action.

REFERENCES

ACGIH (1990), "Threshold limit values and biological exposure indices for 1990-1991", *American Conference of Industrial Hygienists*, Cincinnati, Ohio, USA.

Ambach, W., and H. Eisner (1986), "Albedo verschiedener Schneeoberflächen für erythemalwirksame solare Strahlung", *Wetter und Leben*, **38**, 1-4.

Anders, A., H.-J. Altheide, M. Knälmann, and H. Tronnier (1995), "Action spectrum for erythema in humans investigated with dye lasers", *Photochem. Photobiol.*, **61**(2), 200–205.

Arola, A., Kalliskota, S., den Outer, P.N., Edvardsen, K., Hansen, G., Koskela, T., Martin, T. J., Matthijsen, J., Meerkötter, R., Peeters, P., Seckmeyer, G., Simon, P., Slaper, H., Taalas, P., and Verdebout, J. (2002), "Four UV mapping procedures using satellite data and their validation against ground-based UV measurements", *J.Geophys. Res.*, **107**, ACL 11 1-11.

Bais, A. F., Kazantzidis, A., Kazadzis, S., Balis, D. S, Zerefos, C. S., and Meleti, C. (2005), "Deriving an effective aerosol single scattering albedo from spectral surface UV irradiance measurements", *Atmos. Environ.*, **39**, 1093-1102.

Balk, B., and K. Elder (2000), "Combining binary decision tree and geostatistical methods to estimate snow distribution in a mountain watershed", *Water Resour. Res.*, **36**(1), 13–26.

Bener, P (1950), "Beiträge zur Strahlungsmeßmethodik III: Untersuchungen über die Wirkungsweise des Solarigraphen MOLL-GORCZYNSKI", *Arch. Meteor. Geophys. Biokl.*, **B 2**, 188-249.

Blumthaler, M., and W. Ambach (1988), "Solar UVB-albedo of various surfaces", *Photochem. Photobiol.*, **48**(1), 85-88.

Bodeker, G. E., J. Scott, K. Kreher, and R. McKenzie (2001), "Global ozone trends in potential vorticity coordinates using TOMS and GOME intercompared against the Dobson network: 1978–1998", *J. Geophys. Res.*, **106**, 23,029–23,042.

Bodeker, G. E., H. Shiona, and H. Eskes (2005), "Indicators of Antarctic ozone depletion", *Atmos. Chem. Phys.*, **5**, 2603– 2615.

BSRN (2004), World Climate Research Programme. Baseline Surface Radiation Network (BSRN), Operations Manual, Version 2.1. L. J. B. McArthur, pp 176.

Caldwell, M. M. (1971), "Solar ultraviolet radiation and the growth and development of higher plants", *Photophysiology*, **6**, 131–177.

Caldwell, M. M., W. G. Gold, G. Harris, and C.W. Ashurst (1983), "A modulated lamp system for solar UV-B (280-320 nm). Supplementation studies in the field", *Photochem. Photobiol.*, **37**(4), 479–485

Caldwell, M. M., L. B. Camp, C. W. Warner, and S. D. Flint (1986), "Action spectra and their key role in assessing biological consequences of solar UV-B radiation change", In: Worrest, R.C., and M. M. Caldwell (eds) *Stratospheric Ozone Reduction, Solar Ultraviolet Radiation and Plant Life*. Springer, Berlin, pp 87–111, ISBN 3-540-13875-7.

Chubarova N. Y., N. G. Prilepsky, A. N. Rublev and A. R. Riebau (2009), "A Mega-Fire Event in Central Russia: Fire Weather, Radiative, and Optical Properties of the Atmosphere, and Consequences for Subboreal Forest Plants". In *Developments in Environmental Science*, **8 249**. A. Bytnerowicz, M. Arbaugh, A. Riebau and C. Andersen (Editors). Elsevier B.V. pp. 249-267.

CIE 1986a: Steck, B. (1986), "Photoconjunctivitis", CIE Research Note, *CIE-Journal*, **5**(1), 19–23.

CIE 1986b: Steck B. (1986), "Photokeratitis", CIE Research Note, *CIE-Journal*, **5**(1), 19–23.

CIE 1987: McKinlay, A.F., and B.L. Diffey (1987) "A reference action spectrum for ultraviolet induced erythema in human skin", CIE Research Note, *CIE-Journal*, **6**(1), 17–22.

CIE 2006, "Action spectrum for the production of previtamin D3 in human skin", CIE, **174**.

Curylo, A., Krzyscin, J., and Bogdanska, B. (2007), "UV reconstruction with long time series global radiation measurements", in Gröbner, J. (ed), *Proceedings of the UV Conference "One centuary of Solar UV Radiation Research"*, 18–20 September 2007, Davos, Switzerland, 211–212.

De Fabo, E.C., F.P. Noonan, and J.E. Frederick (1990), "Biologically effective doses of sunlight for immune suppression at various latitudes and their relationship to changes in stratospheric ozone", *Photochem. Photobiol.*, **52**(4), 811–817.

de Gruijl, F.R. and J.C. van der Leun (1994), "Estimate of the wavelength dependency of ultraviolet cacinogenesis in humans and its relevance to the risk assessment of stratospheric ozone depletion", *Health Physics*, **67**, 319–325.

DeBacker, H., P. Koepke, A. Bais, X. de Cabo, T. Frei, D. Gillotay, C. Haite, A.. Heikkilä, A.. Kazantzidis, A. Koskela, T. Kyrö, B. Lapeta, J. Lorente, K. Masson, B. Mayer, H. Plets, A. Redondas, A. Renaud, G. Schauberger, A. Schmalwieser, H. Schwander, and K. Vanicek (2001) "Comparison of measured and modelled UV indices for the assessment of health risks", *Meteorol. Appl.*, **8**, 267 – 277.

Den Outer, P. N., Slaper, H., and Tax, R. B. (2005), "UV radiation in the Netherlands. Assessing long-term variability and trends in relation to ozone and clouds", *J. Geophys. Res.*, **110**, D02203, 1-11, doi: 10.1029/2004JD004824.

Dubovik O., King M. D. (2000), "A flexible inversion algorithm for retrieval of aerosol optical properties from Sun and sky radiance measurements". *J. of Geophys. Res.*, **105**(D16), 20673-20696.

Dubovik, O., A. Smirnov, B. N. Holben, M. D. King, Y. J. Kaufman, T. F. Eck and I. Slutsker (2000), "Accuracy assessment of aerosol optical properties retrieval from AERONET sun and sky radiance measurements". *J. Geophys. Res.*, **105**, 9791-9806.

Eck, T., B. Holben, J. Reid, O. Dubovik, A. Smirnov, N. O'Neill, I. Slutsker, and S. Kinne (1999), "Wavelength dependence of the optical depth of biomass burning, urban, and desert dust aerosols". *J. Geophys. Res.*, **104**(D24), 31333-31349.

Erxleben, J., K. Elder, and R. Davis (2002), "Comparison of spatial interpolation methods for estimating snow distribution in the Colorado Rocky Mountains", *Hydrol. Process.*, **16**, 3627–3649, doi:10.1002/hyp.1239

Feister, U., Junk, J., Woldt, M., Bais, A., Helbig, A., Janouch, M., Jsefsson, W.,Kazantzidis, A., Lindfors, A., den Outer, P. N., and Slaper, H. (2008), "Long-term solar UV radiation reconstructed by ANN modelling with emphasis on spatial characteristics of input data", *Atmos. Chem. Phys.*, **8**, 3107–3118.

Fioletov, V. E., G. E. Bodeker, A. J. Miller, R. D. McPeters, and R. Stolarski (2002), "Global and zonal total ozone variations estimated from groundbased and satellite measurements: 1964–2000", *J. Geophys. Res.*, **107**, 4647(D22), doi:10.1029/2001JD001350.

Flint, S.D., and M. M. Caldwell (2003), "A biological spectral weighting function for ozone depletion research with higher plants", *Physiologia Plantarum*, **117**,137–144.

Foppa, N., A. Stoffel, and R. Meister (2007), "Synergy of in situ and space borne observation for snow depth mapping in the Swiss Alps", *Int. J. Appl. Earth Obs. Geoinf.*, **9**(3), 294-310, doi:10.1016/j.jag.2006.10.001

Foppa, N., S. Wunderle, A. Hauser, D. Oesch, and F. Kuchen (2004), "Operational sub-pixel snow mapping over the Alps with NOAA AVHRR data", *Annals of Glaciology*, **38**(1), 245-252, doi:10.3189/172756404781814735

Friedman, J. H. (1991), "Multivariate adaptive regression splines", *Ann. Stat.*, **19**, 1–50.

Fröhlich, C. (1991), "History of solar radiometry and the World Radiation Reference", *Metrologia*, **28**, 111-115, doi: 10.1088/0026-1394/28/3/001.

Gibbs, N. K., M. Norval, N. Traynor, M. Wolf, B.E. Johnson, and J. Crosby (1993), "Action spectra for the trans to cis photoisomerization of urocanic acid in vitro and in mouse skin", *Photochem. Photobiol.*, **57**, 584–590.

Gröbner, J., M. Blumthaler, S. Kazadzis, A. Bais, A. Webb, J. Schreder, G. Seckmeyer, and D. Rembges (2006), "Quality Assurance of spectral solar UV measurements: results from 25 UV monitoring sites in Europe, 2002 to 2004", *Metrologia*, **43**, 66-71. doi: 10.1088/0026-1394/43/2/S14.

Gröbner J., G. Hülsen, L. Vuilleumier, M. Blumthaler, J.M.Vilaplana, D. Walker, and J.E. Gil (2007), "Report of the PMOD/WRC-COST calibration and intercomparison of erythemal radiometers", ftp.pmodwrc.ch/pub/publications/PMOD_COST726_BBreport.pdf

ICNIRP (2004), "Guidelines on Limits of Exposure to Ultraviolet Radiation of Wavelengths between 180 nm and 400 nm (Incoherent Optical Radiation)", *Health Physics*, **87**(2), 171–186.

Harris, J. M., S. J. Oltmans, G. E. Bodeker, R. Stolarski, R. D. Evans, and D. M. Quincy (2003), "Long-term variations in total ozone derived from Dobson and satellite data", *Atmos. Environ.*, **37**, 3167–3175.

Holben B. N., Eck T. F., Slutsker I., Tanre D., Buis J. P., Setzer A., Vermote E., Reagan J. A., Kaufman Y. J., Nakajima T., Lavenu F., Jankowiak I., Smirnov A. (1998), "AERONET - A federated instrument network and data archive for aerosol characterization". *Rem. Sens. Environ.*, **66**, 1-16

Hülsen, G., and J. Gröbner (2007), "Characterisation and Calibration of UV Broadband Radiometers Measuring Erythemally Weighted Irradiance", *Applied Optics*, **46**, 5877-5886.

Hülsen, G., Gröbner, J., Bais, A., Blumthaler, M., Disterhoft, P., Johnsen, B., Lantz, K. O., Meleti, C., Schreder, J., Vilaplana Guerrero, J. M., and Ylianttila, L. (2008), "Intercomparison of erythemal broadband radiometers calibrated by seven UV calibration facilities in Europe and the USA", *Atmos. Chem. Phys.*, **8**, 4865-4875.

Ineichen, P. (2006), "Comparison of eight clear sky broadband models against 16 independent data banks", *Solar Energy*, **80**, 468-478.

Janowiak, J. E. and P. Xie (1999). "CAMS_OPI: A Global Satellite-Rain Gauge Merged Product for Real-Time Precipitation Monitoring Applications". *J. Climate*, **12**, 3335-3342.

Johnsen, B., et al. (2008), "Intercomparison and harmonization of UV Index measurements from multiband filter radiometers", *J. Geophys. Res.*, **113**, D15206, doi:10.1029/2007JD009731.

Johnsen, B. et al (2008), "Intercomparison of Global UV Index from Multiband Filter Radiometers: Harmonization of global UVI and spectral irradiance" WMO/TD, DRAFT GAW Report No. 179, www.wmo.int/pages/prog/arep/gaw/gaw_home_en.html

Kalnay, E., M. Kanamitsu, R. Kistler, W. Collins, D. Deaven, L. Gandin, M. Iredell, S. Saha, G. White, J. Woollen, Y. Zhu, A. Leetmaa, B. Reynolds, M. Chelliah, W. Ebisuzaki, W. Higgins, J. Janowiak, K. C. Mo, C. Ropelewski, J. Wang, R. Jenne, and D. Joseph (1996), "The NCEP/NCAR 40-Year Reanalysis Proct". *Bulletin of the American Meteorological Society*.

Kazadzis S., A. Bais, V. Amiridis, D. Balis, C. Meleti, N. Kouremeti, C. S. Zerefos, S. Rapsomanikis, M. Petrakakis, A. Kelesis, P. Tzoumaka, and K. Kelektsoglou (2007), "Nine years of UV aerosol optical depth measurements at Thessaloniki, Greece". *Atmos. Chem. Phys.*, **7**, 2091–2101.

Koepke, P., Hess, M., Schult, I., and Shettle, E. P. (1997), "Global Aerosol Data Set", Max-Planck-Institut für Meteorologie, Report No. 243, 1-44.

Koepke, P., A. Bais, D. Balis, M. Buchwitz, H.D. Backer, X.D. Cabo, P. Eckert, P. Erikson, D. Gillotay, A. Heikkilä, T. Koskela, B. Lapeta, Z. Littynska, J. Lorente, B. Mayer, A. Renaud, A. Ruggaber, G. Schauberger, G. Seckmeyer, P. Seifert, A. Schmalwieser, H. Schwander, K. Vanicek, and M. Weber (1998), "Comparison of models used for UV Index calculations", *Photochem. Photobiol.*, **67**, (6), 657-662.

Koepke, P., de Backer, H., Bais, A., Curylo, A., Eerme K., Feister, U., Johnsen, B., Junk, J., Kazantzidis, A., Krzyscin, J., Lindfors, A., Olseth, J. A., den Outer, P., Pribullova, A., Schmalwieser, A., Slaper, H., Staiger, H., Verdebout, J., Vuilleumier, L., and Weihs, P. (ed.) (2008), "EUR 23338 – COST action 726 – Modelling solar UV radiation in the past: Comparison of algorithms and input data", COST Earth System Science and Environmental Management, Luxembourg: Office for Official Publications of the European Communities, 94 pp.

Koukouli M. E., S. Kazadzis, V. Amiridis, C. Ichoku and D. S. Balis, (2007). "Comparisons Of Satellite Derived Aerosol Optical Depth Over A Variety Of Sites In The Southern Balkan Region As An Indicator Of Local Air Quality". In Remote Sensing of Clouds and the Atmosphere XII, edited by

Adolfo Comerón, Richard H. Picard, Klaus Schäfer, James R. Slusser, Aldo Amodeo, *Proc. of SPIE* **6745**, 67451V-1. doi: 10.1117/12.737681

Krzyscin, J. W., Jaroslawski, J., and Sobolewski, P.S. (2003) "Effects of clouds on the surface erythemal UV-B irradiance at northern midlatitudes: estimation from the observations taken at Belsk, Poland (1999 – 2001)", *J. Atmos. Solar-Terrestr. Phys.*, **65**, 457-467.

Krzyścin, J. W., J. Jarosławski, and B. Rajewska-Więch (2005), "Beginning of the ozone recovery over Europe? – Analysis of the total ozone data from ground-based observations, 1964–2004", *Ann. Geophys.*, **23**, 1685–1695.

Krzyścin, J. W. (2006), "Change in ozone depletion rates beginning in the mid 1990s: trend analyses of the TOMS/SBUV merged total ozone data, 1978–2003", *Ann. Geophys.*, **24**, 493–502,.

Krzyścin, J. W. (2008), "Statistical reconstruction of daily total ozone over Europe 1950 to 2004", *J. Geophys. Res.*, **113**, D07112, doi:10.1029/2007JD008881.

Krzyścin, J. W., and J. L. Borkowski (2008), "Variability of the total ozone trend over Europe for the period 1950–2004 derived from reconstructed data", *Atmos. Chem. Phys.*, **8**, 2847–2857.

Lenoble, J., A. Kylling, and I. Smolskaia (2004), "Impact of snow cover and topography on ultraviolet irradiance at the Alpine station of Briançon", *J. Geophys. Res.*, **109**, D16209, doi:10.1029/2004JD004523.

Lenoble, J. (2000), "Influence of the environment reflectance on the ultraviolet zenith radiance for cloudless sky", *Appl. Opt.*, **39**(24), 4247-4254.

Lindfors, A., Kaurola, J., Arola, A., Koskela, T., Lakkala, K., Josefsson, W., Olseth, J. A., and Johnsen, B. (2007), "A method for reconstruction of past UV radiation based on radiative transfer modeling: Applied to four stations in northern Europe", *J. Geophys. Res.*, **112**, D23201, 1-15, doi: 10.1029/2007JD008454.

López-Moreno, J. I., and D. Nogués-Bravo (2006), "Interpolating local snow depth data: an evaluation of methods", *Hydrol. Process.*, **20**, 2217–2232, doi: 10.1002/hyp.6199

MacLaughlin, J. A., R. R. Anderson, and M. F. Holick (1982) "Spectral character of sunlight modulates photosynthesis of previtamin D3 and its photoisomers in human skin", *Science*, **216**, 1001–1003.

Madronich, S., McKenzie R. L., Björn, L. O., Caldwell, M. M. (1998), "Changes in biologically active ultraviolet radiation reaching the Earth's surface", *J. Photochem. Photobiol.*, **46**, 5-19.

Martin, E. (2004), "Validation of Alpine Snow in ERA-40." ECMWF ERA-40 Project Report Series, No.14, pp. 21.

Mayer, B. and Kylling, A. (2005), "Technical note: The libRadtran software package for radiative transfer calculations - description and examples of use", *Atmos. Chem. Phys.*, **5**, 1855-1877.

Molotch, N. P., M. T. Colee, R. C. Bales, and J. Dozier (2005), "Estimating the spatial distribution of snow water equivalent in an alpine basin using binary regression tree models: the impact of digital elevation data and independent variable selection", *Hydrol. Process.*, **19**, 1459–1479, doi: 10.1002/hyp.5586

Morliere, P., A. Moysan, and I. Tirache (1995), "Action spectrum for UV-induced lipid peroxidation in cultured human skin fibroblasts", *Free Radical Biology & Medicine*, **19**(3), 365–371.

Norris, J. R. and Wild, M. (2007), "Trends in aerosol radiative effects over Europe inferred from observed cloud cover, solar "dimming," and solar "brightening"", *J. Geophys. Res.* **112**, D08214, doi: 10.1029/2006JD007794.

OENORM M5873-2 Prestandard (2003), "Plants for the disinfection of water using ultraviolet radiation – Requirements and testing Part 2: Medium pressure mercury lamp plants", Österreichisches Normungsinstitut, Vienna, Austria.

Oltmans, S. J., A.S. Lefohn, and J.M. Harris (2006), "Trends of ozone in the troposphere", *Atmos. Environ.*, **40**, 3156–3173.

Persson, T. (2000), "Measurements of solar radiation in Sweden 1983 – 1998", *SMHI Rep. Meteorol. and Climatol.*, **RMK 89**, Swedish Meteorological and Hydrological Institute, Norrköping, Sweden.

Peterson, T., C., Easterling, D. R., Karl, T. R., Groisman, P., Nicholls, N., Plummer, N., Torok, S., Auer, I., Boehm, R., Gullett, D., Vincent, L., Heino, R., Tuomenvirta, H., Mestre, O., Szentimrey, T., Salinger, J., Forland, E., J., Hanssen-Bauer, I., Alexandersson, H., Jones, P., and Parker, D. (1998), "Homogeneity Adjustments of In Situ Atmospheric Climate Data: A Review", *Int. J. Climatol*, **18**, 1493-1517.

Press, W. H., S. A. Teukolsky, W. T. Vetterling, and B. P. Flannery (1992), "Numerical Recipes", Cambridge University Press, Cambridge, UK.

Pribullova, A., and Chmelik, M. (2008), "Typical distribution of the solar erythemal UV radiation over Slovakia", *Atmos. Chem. Phys.*, **8**, 5393–5401.

Reinsel, G. C., E. C. Weatherhead, G. C. Tiao, A. J. Miller, R. M. Nagatani, D. J. Wuebbless, and L. E. Flynn (2002), "On detection of turnaround and recovery in trend for ozone", *J. Geophys. Res.*, **107**(D10), 4078, doi:10.1029/2001JD000500.

Remer, L. A., et al. (2008), "Global aerosol climatology from the MODIS satellite sensors". *J. Geophys. Res.*, **113**(D14) S07, doi:10.1029/2007JD009661.

Remund, J., Wald, L., M. Lefevre, M., and Ranchin, T. (2003), "Worldwide Linke Turbidity Information", *Proceedings of ISES Solar World Congress*, 16-19 June 2003, Göteborg, Sweden, CD-ROM published by the International Solar Energy Society.

Reuder, J., and Schwander, H. (1999), "Aerosol effects on UV radiation in nonurban regions", *J. Geophys. Res.*, **104**, D4, 4065-4077.

Rieder, H. E., Holawe, F., Simic, S., Blumthaler, M., Krzyscin, J. W., Wagner, J. E., Schmalwieser, A. W., and Weihs, P. (2008), "Reconstruction of erythemal UV-doses for two stations in Austria: a comparison between alpine and urban regions". *Atmos. Chem. Phys.*, **8**, 6309–6323.

Rigollier, C., Bauer, O., and Wald, L. (2000), "On the Clear Sky Model of the ESRA - European Solar Radiation Atlas - With Respect to the HELIOSAT Method", *Sol. Energy*, **68**, 33-48.

Ruckstuhl, C., R. Philipona, K. Behrens, M. Collaud Coen, B. Dürr, A. Heimo, C. Mätzler, S. Nyeki, A. Ohmura, L. Vuilleumier, L., M. Weller, C. Wehrli, and A. Zelenka (2008), "Aerosol and cloud effects on solar brightening and recent rapid warming", *Geophys. Res., Lett.*, **35**, L12708, doi: 10.1029/200GL034228.

Schaap, M., Sauter, F., Timmermans, R.M.A., Roemer, M.,Velders, G., Beck, J., Builtjes, P.J.H. (2007), "The LOTOSEUROS model: description, validation and latest developments". *International Journal of Environmental Pollution,* in press.

Scharmer, K., and Greif, J. (ed.) (2000), "The European Solar Radiation Atlas, Vol. 2: Database, Models and Exploitation Software", École des Mines de Paris, 1-296, France.

Schieldrup Paulsen, H. (1968), "A study of the radiation climate of southern Norway; Part II: On the calibration of radiation instruments", *Arbok for Univ. i Bergen Mat. Naturw. Serie* **2**, pp. 74.

Schwander, H., Koepke, P., and Ruggaber, A. (1997) "Uncertainties in modeled UV irradiance due to limited accuracy and availability of input data", *J. Geophys. Res.*, **102**, D8, 9419-9429.

Schwander, H., B. Mayer, A. Ruggaber, A. Albold, G. Seckmeyer, and P. Koepke (1999), "Method to determine snow albedo values in the ultraviolet for radiative transfer modelling", *Appl. Opt.*, **38**(18), 3869-3875.

Seckmeyer G., A. F. Bais, G. Bernhard, M. Blumthaler, C. R. Booth, R. L. Lantz, R. L. McKenzie, P. Disterhoft, and A. Webb, (2007) "Instruments to measure solar ultraviolet radiation. Part 2: Broadband instruments measuring erythemally weighted solar irradiance," WMO#GAW 164, World Meteorological Organization, Geneva.

Setlow, R.B. (1974), "The Wavelengths in Sunlight Effective in Producing Skin Cancer: A Theoretical Analysis", *Proc. Nat. Acad. Sci. USA*, **71**(9), 3363–3366.

Skaugen, T., S. Beldring, and H.-C. Udnæs (2003), "Dynamical properties of the spatial distribution of snow", *Hydrol. Earth Syst. Sc.*, **7**(5), 744-753

Smolskaia, I., D. Masserot, J. Lenoble, C. Brogniez, and A. de la Casinière (2003), "Retrieval of the ultraviolet effective snow albedo during 1998 winter campaign in the French Alps", *Appl. Opt.*, **42**, 9, 1583-1587.

Sonntag, D. (1975), "Pyranographen bzw. Effektivpyranographen mit galvanisch erzeugter Thermosäule und ihre Erprobung in Berlin, Potsdam, Stockholm, Leningrad und Bergen". *Abh. Meteorol. Dienst DDR*, **Nr. 115**, pp 80.

Staiger, H., den Outer, P., Bais, A., Feister, U., Johnsen, B., and Vuilleumier, L. (2008), "Hourly resolved cloud modification factors in the ultraviolet", *Atmos. Chem. Phys.*, **8**, 2493–2508.

Stoer, J. and R. Bulirsch (1980) "Introduction to Numerical Mathematics", Springer, Berlin, Germany.

Tanskanen, A. (2004) "Lambertian Surface Albedo Climatology at 360 nm from TOMS Data Using Moving Time-Window Technique". In: *Proceedings of the XX Quadrennial Ozone Symposium*, 1-8 June 2004, Kos, Greece.

Uppala, S. M., Kallberg, P. W., Simmons, A. J., Andrae, U., Da Costa Bechtold, V., Fiorino, M., Gibson, J. K., Haseler, J., Hernandez, A., Kelly, G. A., Li, X., Onogi, K., Saarinen, S., Sokka, N., Allan, R. P., Andersson, E., Arpe, K., Balmaseda, M. A., Beljaars, A. C. M., Van De Berg, L., Bidlot, J., Bormann, N., Caires, S., Chevallier, F., Dethof, A., Dragosavac, M., Fisher, M., Fuentes, M., Hagemann, S., Holm, E., Hoskins, B. J., Isaksen, L., Janssen, P. A. E. M., Jenne, R., McNally, A. P., Mahfouf, J.-F., Morcrette, J.-J., Rayner, N. A., Saunders, R. W., Simon, P., Sterl, A., Trenberth, K. E., Untch, A., Vasiljevic, D., Viterbo, P., and Woollen, J. (2005), "The ERA-40 re-analysis", *Q. J. R. Meteorol. Soc.*, **131**, 2961-3012, doi: 10.1256/qj.04.176.

Verdebout, J. (2000), "A method to generate surface UV radiation maps over Europe using GOME, Meteosat, and ancillary geophysical data", *J. Geophys. Res.*, **105**:D4, 5049-5058.

Verdebout J. (2004), "A European satellite-derived UV climatology available for impact studies", *Radiation Protection Dosimetry*, **111**:4, 407-411.

Wackernagel, H. (2003), "Multivariate Geostatistics", 3. Edition, Springer-Verlag, Berlin, Heidelberg, New York, pp. 387.

Walker, D., L. Vuilleumier, C. Marty, U. Lohmann and S. Broennimann (2009), "Regional Snow Distribution and Evolution in Switzerland between 1980 and 2008", Submitted to *J. Appl. Meteor. Climatol.*

Webb A. F., J. Gröbner, and M. Blumthaler (2006), "A practical guide to operating broadband instruments measuring erythemally weighted irradiance", EUR 22595, ISBN 92-898-0032-1, European Commission, 2006.

Weihs, P., et al. (2001), "Modeling the effect of an inhomogeneous surface albedo on incident UV radiation in mountainous terrain: determination of an effective surface albedo", *Geophys. Res. Lett.*, **28**(16), 3111–3114.

World Meteorological Organization (WMO) (2003), "Scientific assessment of ozone depletion: 2002", Global Ozone Research and Monitoring Project- Rep. No. 47, Geneva, Switzerland, 498 pp.

WMO (2003 a), "Guidelines on Climate Metadata and Homogenization", WCDMP-No. 53, WMO-TS No. 1186, Geneva.

WMO (ed.) (2003 b), "Fourth Seminar for Homogenization and Quality Control in Climatological Databases (Budapest, Hungary, 6-10 October 2003)", WCDMP-No. 56, WMO-TD No. 1236.

WMO (2006), "Guide to Meteorological Instruments and Methods of Observation". Seventh edition. WMO-No. 8. Chapter 7: Measurements of Radiation. World Meteorological Organization – Geneva – Switzerland.

World Meteorological Organization (WMO) (2007), "Scientific assessment of ozone depletion: 2006", Global Ozone Research and Monitoring Project - Rep. No. 50, Geneva, Switzerland, 572 pp.

Wulf, H. C., T. Poulsen, R. E. Davies, and F. Urbach (1989), "Narrow-band UV radiation and induction of dermal elastosis and skin cancer", *Photodermatology*, **6**(1), 44–51.

Zelenka, A., Czeplak, G., Josefsson, W., Maxwell, E., Perez, R., Noia, M., Ratto, C., and Festa, R. (1992), "Technique for supplementing solar radiation network data", Vol. 1-3, International Energy Agency, Report No. IEA-SHCP-9D-1.

Zipoli, G., and D. Grifoni (2007), "The role of action spectra in determining the biologically effective UV radiation", In: ESP 2007 - 12th Conference European Society of Photobiology Bath England 1st-6th September - Programme and Book of Abstracts, p. 97–98.

APPENDIX A. ACRONYMS

AERONET	Aerosol Robotic Network (NASA Goddard Space Flight Center)
AOD / AOT	Aerosol optical depth / thickness
BSRN	Baseline Surface Radiation Network (of WMO / WCRP)
CAMS_OPI	Climate Anomaly Monitoring System ("CAMS") and OLR Precipitation Index (“OPI”)
CIE	International Commission on Illumination
CIMEL	Sun / sky photometer (http://www.cimel.fr/index_us.html)
CMF	Cloud Modification Factor: All-sky to clear-sky down-welling irradiation
COST	Cooperation in the field of Science and Technical Research
CPC	Climate Prediction Center (US government NOAA)
DWD	German Meteorological Service
ECMWF	European Centre for Medium-Range Weather Forecast
ERA-40	ECMWF 45-year Re-Analysis, here: 01 Jan 1958 to 31 Aug 2002
ERY	Erythemally weighted UV
ESRA	European Solar Radiation Atlas
EUVC	European UV Reference Centre
FMI	Finnish Meteorological Institute
FWHM	Full Width at Half Maximum
GCM	General Circulation Model
GTOPO30	Global 30 arc-second digital elevation data set (USGS)
LUT	Lookup table
METEOSAT	Meteorological Satellite (EUMETSAT)
MODIS	Moderate Resolution Imaging Spectrometer (NASA)
NCEP/NCAR	National Centers for Environmental Prediction / National Center for Atmospheric Research (US government, NOAA/ National Weather Service)
NRPA	Norwegian Radiation Protection Authority
NIWA	National Institute of Water and Atmosphere Research, Lauder, New Zealand
NMHS	National Meteorological and Hydrological Services
NREL	National Renewable Energy Laboratory (US Department of Energy)
QASUME	Quality Assurance of Spectral Ultraviolet Measurements in Europe through the development of a transportable unit
RAF	Radiation amplification factor
RMS / RMSE	Root mean square error
SCOUT-O3	EU project: Stratospheric-Climate Links with Emphasis on the Upper Troposphere and Lower Stratosphere
SOL-CMF	Solar Cloud Modification Factor, short-wave spectral range
SSA	Single scattering albedo
SZA	Solar zenith angle
TOC	Total column ozone
USGS	U.S. Geological Survey
UV	Ultraviolet (spectral range)
UV-CMF	Cloud Modification Factor in the UV spectral range
WCRP	World Climate Research Programme (WMO)
WMO	World Meteorological Organization, Geneva
WRDC	World Radiation Data Centre, St. Petersburg, Russian Federation (WMO)

APPENDIX B. DISCLAIMER AND DATA USAGE

The results of COST action 726 “Long term changes and climatology of UV radiation over Europe” are free for non-commercial use.

The COST action does not guaranty for error-free information, results or data. Neither the COST Office nor any person acting on its behalf is responsible for the use which might be made of the information contained in this publication. The COST Office is not responsible for the external websites referred to in this publication.

If data of the COST action 726 are used for a scientific publication send an electronic copy of the paper to A. Schmalwieser, Vienna, so that it can be mentioned on the action's website, and give as reference:

COST action 726 “Long term changes and climatology of UV radiation over Europe”.

APPENDIX C. REFERENCE INSTITUTIONS IN THE COST 726 COUNTRIES

Austria

Institute of Medical Physics and Biostatistics, University of Veterinary Medicine, Veterinaerplatz 1, A-1210 Vienna
Mr. Alois W. Schmalwieser, Tel: +43 1 250774324

Institute of Meteorology, University of Natural Resources and Applied Life Sciences, Peter Jordan Strasse 82, A-1190 Vienna
Mr. Philipp Weihs, Tel: + 43 1 470582822

Belgium

Royal Meteorological Institute of Belgium (R.M.I.B.), Ringlaan 3, B-1180 Ukkel
Mr. Hugo de Backer, Tel: + 32 2 37305 94

Cyprus

Cyprus Meteorological Service, Nikis 28, CY- 1418 NICOSIA
Mr. Marios Theophilou, Tel: + 35 7 22332878
Ms. Sophia Louca, Tel: + 35 7 22802926

Czech Republic

Solar and Ozone Observatory of the Czech Hydrometeorological Institute, Hvezdarna 456, 500 08 Hradec Kralove 8
Mr. Michal Janouch, Tel: + 42 0 495260352

Department of Dermatology, Medical Faculty Hradec Kralove, Charles University Prague, Sokolska 581, 500 05 Hradec Kralove
Mr. Karel Ettler, Tel: + 42 0 495836357

Denmark

Danish Meteorological Institute, Lyngbyvej 100, 2100 Copenhagen
Mr. Paul Eriksen, Tel: + 45 39157500

Estonia

Tartu Observatory, 61602, Tõravere, Tartumaa
Mr. Kalju Eerme, Tel: +37 2 7410 258

Finland

Finnish Meteorological Institute, Meteorological Research Division, Ozone and UV-radiation Research Group, POB 503 (Vuorikatu 19), FIN-00101 Helsinki
Mr. Jussi Kaurola, Tel. + 358 9 19294181
Mr. Anders Lindfors, Tel: + 358 9 19294170

 **France**

Laboratoire d'Optique Atmosphérique, Université des Sciences et Technologies de Lille, 59655 Villeneuve d'Ascq
Ms. Colette Brogniez, Tel: + 33 3 20436643

Météo-France, 42 avenue G. Coriolis, F-31057 Toulouse Cedex 1
Ms. Aline Peuch, Tel: + 33/0 5 61 07 80 84

 **Germany**

Ludwig-Maximilians-Universität, Meteorological Institute, Department of Physics, L.-M.-University Munich, Theresienstr. 37, 80333 Muenchen
Mr. Peter Koepke, Tel: +49 89 21804367

Deutscher Wetterdienst, Meteorologisches Observatorium – Richard-Aßmann-Observatorium Lindenberg, Am Observatorium 12, 15848 Lindenberg
Mr. Uwe Feister, Tel: + 49 33677 60143

Universität Hannover, Institut für Meteorologie und Klimatologie, Herrenhauser Str. 2, D-30419 Hannover
Mr. Gunther Seckmeyer, Tel: +49 51 17624022

 **Greece**

Aristotle University of Thessaloniki, Physics Department, Laboratory of Atmospheric Physics, Campus Box 149, 54124 – Thessaloniki
Mr. Alkiviadis Bais, Tel: + 30 2310 998184

University of Patras, Physics Department, Laboratory of Atmospheric Physics, 26500 – Patras
Mr. Andreas Kazantzidis, Tel: + 30 2610 997549

 **Hungary**

Hungarian Meteorological Service, Measurement Techniques and Methodology Division, Gilice tér 39, H-1181 Budapest
Mr. Zoltan Toth, Tel: + 36 1 3464857
Mr. Zoltan Nagy, Tel: + 36 1 3464857

 **Italy**

C.N.R. IBIMET, Via Caproni 8, 50144 Firenze
Mr. Gaetano Zipoli, Tel: + 39 055 3033711

Univesità di Roma 'La Sapienza', Physics Department, P.le A. Moro 2, 00185 Rome
Ms. Anna Maria Siani, Tel: + 39 064 9913479

 **Netherlands**

Royal Netherlands Meteorological Institute (KNMI), P.O. Box 201, 3730 AE De Bilt
Mr. Michiel van Weele, Tel: + 31 30 2206410

Laboratory of Radiation Research National Institute of Public Health and the Environment (RIVM), P.O. Box 1, 3720 BA Bilthoven
Mr. Harry Slaper, Tel: + 31 30 2743488

 **Norway**

Norwegian Radiation Protection Authority (NRPA), P.O.Box 55, N-1332 Oesteraas
Mr. Bjorn Johansen, Tel: + 47 67 162549

Norwegian University of Science and Technology (NTNU), Department of Physics, N-7491 Trondheim
Ms. Berit Kjeldstat, Tel: + 47 73 591995

 **Poland**

Centre of Aerology, Institute of Meteorology and Water Management, Zegrzynska 38, 05-119 Legionowo
Ms. Zenobia Litynska, Tel: + 48 22 7673100

Satellite Research Department, Institute of Meteorology and Water Management, Piotra Borowego 14, 40-045 Krakow
Ms. Bozena Lapeta, Tel: + 48 12 6398194

Institute of Geophysics, Polish Academy of Sciences, Ksiecia Janusza 64, 01-452 Warsaw
Mr. Janusz Krzyscin, Tel: + 48 22 6915874

 **Portugal**

Instituto de Meteorologia de Portugal, Delega¹Ño Regional dos Azores, Observatorio Afonso Chaves Rua MÑe de Deus – RelvÑo, 9500-321 Ponta Delgada, Azores
Ms. Fernanda do Rosario da Silva Carvalho, Tel: +351 296650210

 **Romania**

National Institute Meteorology, Hydrology and Water Administration
Mr. Constantin Rada, Tel: + 40 21 2303116
Ms. Laura Manea, Tel: + 40 21 2303116

 **Slovakia**

Slovak Hydrometeorological Institute, Poprad-Ganovce 178, 05 801 Poprad-Ganowce
Mr. Miroslav Chmelik, Tel: + 421 527731097

Slovak Academy of Sciences, Geophysical Institute, Dubravska cesta 9, 845 28 Bratislava
Ms. Anna Pribullova, Tel: + 420 527879146

 **Spain**

Instituto Nacional de Técnica Aeroespacial – INTA, Ctra. San Juan del Puerto-Matalascañas Km 33, SP-21130 Mazagón, Huelva
Mr. Jose Manuel Vilaplana Guerrero, Tel: + 34 959 208858

Instituto Nacional de Meteorología, Izaña Atmospheric Observatory, C/ La Marina 20, 6º Planta, SP-38071 Santa Cruz de Tenerife, PO-BOX 880
Mr. Alberto Redondas Marrero, Tel: + 34 922 373878

 **Sweden**

Swedish Radiation Safety Authority (SSM), Solna strandvag 96 SE-17116 Stockholm
Mr. Ulf Wester, Tel: + 46 8 7297171

Swedish Meteorological and Hydrological Institute, SE-601 76 Norrköping
Mr. Weine Josefsson, Tel: + 46 11 4958000

 **Switzerland**

MeteoSwiss, C.P 316, CH-1530 Payerne
Mr. Laurent Vuilleumier, Tel: + 41 26 6626306

Physikalisch-Meteorologischews Observatorium Davos/World Radiation Center (PMOD/WRC), Dorfstrasse 33, CH-7260 Davos Dorf
Mr. Julian Groebner, Tel: + 41 81 4175157

 **United Kingdom**

University of Manchester, SEAES, Sackville Street Building, P.O.Box 88, Manchester M60 1QD
Ms. Ann R. Webb, Tel: + 44 (0) 1613063917

 **EC JRC**

European Commission, Joint Research Centre, Institute for Environment and Sustainability, via Enrico Fermi 2749, 21020 Ispra (VA)
Mr. Jean Verdebout, Tel: + 39 0332 785034

 **WMO**

World Radiation Data Centre (WRDC), Voeikov Main Geophysical Observatory, Karbyshev Str. 7, 194021, St. Petersburg
Mr. Anatoly Tsvetkov, Tel: + 812 2474390

 **Russia** – non-COST country

Geographical Faculty, Moscow State University, GSP-1, Leninskie Gory, Moscow, 119991
Ms. Natalia Chubarova, Tel: +7495 9392337

APPENDIX D. LIST OF WEB PAGES WITH UV INFORMATION

 **Austria**

http://www.uv-index.at
http://www-med-physik.vu-wien.ac.at/uv/uv_online.htm

 **Belgium**

http://www.meteo.be/meteo/view/en/522044-UV.html
http://www.meteo.be/meteo/view/en/65239-Home.html
http://ozone.meteo.be/meteo/view/en/1351412-OzoneC+UV+and+Aerosol+studies.html
http://www.aeronomie.be/en/topics/interplanetary/uv_live_belgium.htm

 **Cyprus**

http://lap.physics.auth.gr/uvnet.gr

 **Czech Republic**

http://www.chmi.cz/meteo/ozon/UV_online.html

 **Denmark**

http://www.dmi.dk/dmi/index/danmark/solvarsel.htm
http://www.dmi.dk/dmi/index/verden/uv_idag.htm
http://promote.dmi.dk

 **Estonia**

http://sputnik.aai.ee/koduleht

 **Finland**

http://www.fmi.fi/uvi

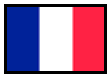 **France**

http://www.soleil.info/uv-meteo/

 **Germany**

http://www.uv-index.de
http://orias.dwd.de/promote/index.jsp
http://www.suvmonet.de
http://www.dwd.de/mol/

 **Greece**

http://www.uvnet.gr

 Italy

http://www.uv-index.vda.it

 **Netherlands**

http://www.temis.nl/uvradiation/index.html
http://www.knmi.nl/kodac/weer_en_gezondheid/zonkracht.html
http://www.rivm.nl/milieuportaal/onderwerpen/straling-en-EM-velden/ultraviolette-straling/

 **Norway**

http://www.nrpa.no/uvnett/default_en.aspx
http://retro.met.no/varsel/index.html
http://uv.nilu.no/index.cfm?fa=uv.main
http://www.fys.uio.no/plasma/ozone/

 **Poland**

http://www.pogodynka.pl/polskauv.php
http://www.igf.edu.pl/pl/zaklady_naukowe/fizyki_atmosfery/ozon_uv

 **Portugal**

http://www.meteo.pt/en/ambiente/uv

 **Slovakia**

http://www.shmu.sk/sk/?page=73

 **Spain**

http://www.aemet.es/es/eltiempo/observacion/radiacionuv

 **Sweden**

http://www.smhi.se/cmp/jsp/polopoly.jsp?d=5626&l=sv
http://www.smhi.se/cmp/jsp/polopoly.jsp?d=7850&l=en
http://produkter.smhi.se/strang/
http://produkter.smhi.se/strang/omna/
http://www.stralsakerhetsmyndigheten.se/Allmanhet/UV--laser/

 **Switzerland**

http://www.uv-index.ch/de/home.php
http://www.meteoswiss.admin.ch/web/en/weather/health/uv-index.html
http://www.meteoswiss.admin.ch/web/en/weather/health/uv-index/uv_measurement.html
http://www.meteoswiss.admin.ch/web/en/weather/health/uv-index/uv_radiation.html
http://www.meteoswiss.admin.ch/web/en/research/projects/cost_726.html

 **United Kingdom**

http://www.hpa.org.uk/webw/HPAweb&HPAwebStandard/HPAweb_C/1195733761671?p=1158934607746

 **WHO** Intersun, World Health Organization
http://www.who.int/uv/en/

APPENDIX E. HOW TO USE THE E-ATLAS

This program enables to extract reconstructed erythemally weighted daily dose values for a certain location and a certain period.
Data are available from 1.1.1958 to 31.8.2002 for longitudes from 25° E to 35° W and latitudes from 30° N to 80° N. These data are mean values over an area of 1° x 1°.
It is possible to extract daily values, monthly sums and calculate a simple annual statistics.
On next page, an illustration shows the program interface buttons and fields to be used for completing the steps described below.

Step 1: After starting the program select the period. Please note that data are available from 1.1.1958 to 31.8.2002.

Step 2: Select the geographical coordinates (latitude and longitude). Please note that coordinates are integer numbers. The UV radiation values are mean values over the corresponding pixel of 1°x 1°

Step 3: To get the data out of the database press one of the "Read" buttons
- **3a)** Use this button if you would like to store the data year by year. Using this button it is not necessary to change the end date of the period.
- **3b)** Use this button if you would like to store the data over the whole period.

Step 4: During reading this bar shows you the progress of reading. It is filled blue when finished. Below the bar the year is shown.

Step 5: After the data are read out a simple analysis appears in Statistic-Window

Step 6: Saving data: Data are saved as *.csv. First of all select the "Separator" between data columns. You can choose either ";" or ","

Step 7: Saving data: you have the possibility to choose one of three options
- **7a)** Monthly statistic: This stores the data as shown in the Statistic-Window (5). Columns are separated as selected.
- **7b)** Daily sums: by pressing this button the data a stored day by day.
- **7c)** Monthly sums: by pressing this button the data a stored as monthly sums.

If you would like to store the data also in another format just click the corresponding button. It is not necessary to repeat reading (Step 3-5).

Step 8: The "Open last exp."-button opens a text editor where you can see the latest data as ASCII-text.

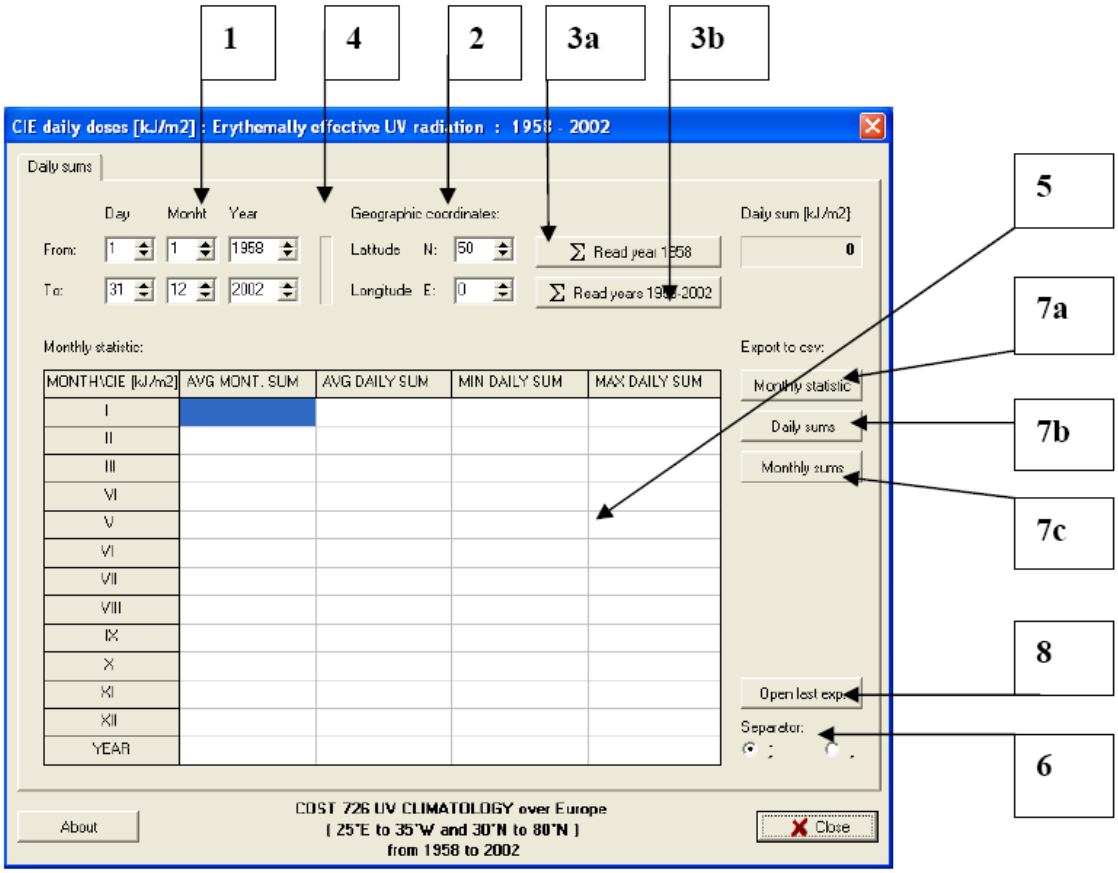
1
4
2
3a
3b
5
7a
7b
7c
8
6
CIE daily doses [kJ/m2] : Erythemally effective UV radiation : 1958 - 2002
Daily sums
Day
Monht
Year
From:
To:
Geographic coordinates:
Lattitude N:
Longitude E:
Read year 1958
Read years 1958-2002
Daily sum [kJ/m2]
Monthly statistic:
Export to csv:
Monthly statistic
Daily sums
Monthly sums
Open last exp
Separator:
MONTH\CIE [kJ/m2]
AVG MONT. SUM
AVG DAILY SUM
MIN DAILY SUM
MAX DAILY SUM
I
II
III
VI
V
VI
VII
VIII
IX
X
XI
XII
YEAR
About
COST 726 UV CLIMATOLOGY over Europe
(25°E to 35°W and 30°N to 80°N)
from 1958 to 2002
Close

APPENDIX F. ACKNOWLEDGEMENTS

The management committee of COST 726 would like to thank the previous TC Meteorology and its chair Professor Joze Rakovek, its Scientific Secretary Dr Pavol Nejedlik, and the Rapporteur Dr Peter Havranek for the friendly and fruitful cooperation.

We also thank the DC ESSEM and its chair Professor Sylvain Joffre, its Senior Science Officer Dr Carine Petit, the Administrative Officer Chandrasa Sjamsudin, and the Rapporteur Professor Michal Marek.

The Action benefited from the fact that the Institute of Meteorology and Water Management (IMWM) in Poland agreed to act as Grant Holder. Thus we would like to express our gratitude to the director of IMWM for the period 2005-2007 Professor Jan Zielinski, for the period 2008-2009 Dr Mieczyslaw Ostojski, and especially to the Grant Holders Secretariat, its Science Officer Bozena Lapeta and its Administrative Officer Magda Malinska.

Special thanks go to Dr Alois Schmalwieser from the University of Veterinary Medicine in Vienna, Austria, who built and is managing the web site of the action (www.cost726.org) and to the Federal Ministry of Transport, Building and Urban Affairs (BVBS) in Germany for providing us the opportunity of using the BSCW data server for storage and dissemination of data and documents within the COST 726 project.

We are also grateful to Dr Alois Schmalwieser (University of Veterinary Medicine in Vienna), Dr Jean Verdebout from the Joint Research Centre, Ispra, Itlay, and Dr Michal Janouch and Dr Martin Stanek from the the Czech Hydrometeorological Institute, Hradec Kralove, Czech Republic, for developing an electronic atlas and an associated computer code that will facilitate the dissemination of the results of COST action 726.

We acknowledge the support of the Meteorological Services of all the member states of the action, by making UV and meteorological data available, and especially EUMETSAT for providing very many METEOSAT images, as well as ECMWF for ERA40 data on global irradiance. Global irradiance data were also provided by Dr Anatoly Tsvetkov, the Director of the WMO World Radiation Data Centre in St. Petersburg, Russia, whose support we strongly appreciate.

Three UV radiometer comparisons have been performed during the life of the action, which improved the quality of the measurement results that were used. Since all comparisons required additional man power and the infrastructure of the hosting institutions, we want, last but not least, to express our gratitude to the Physikalisch-Meteorologisches Observatorium Davos / World Radiation Center, Davos, Switzerland, to the Norwegian Radiation Protection Authority and the Norwegian Research Council, Oslo, Norway, to the WMO, and to the Instituto Nacional de Técnica Aeroespacial, “El Arenosillo” Observatory, Huelva, Spain.